Froth across the Universe Dynamics and Stochastic Geometry of the Cosmic Foam

Weygaert, R. van de

Published in:
ArXiv

Publication date:
2002

FROTH ACROSS THE UNIVERSE

DYNAMICS AND STOCHASTIC GEOMETRY OF THE COSMIC FOAM

Rien van de Weygaert
Kapteyn Institute, University of Groningen, Groningen, the Netherlands
weygaert@astro.rug.nl

Abstract The interior of the Universe is permeated by a tenuous space-filling frothy network. Welded into a distinctive foamy pattern, galaxies accumulate in walls, filaments and dense compact clusters surrounding large near-empty void regions. As borne out by a large sequence of computer experiments, such weblike patterns in the overall cosmic matter distribution do represent a universal but possibly transient phase in the gravitationally propelled emergence and evolution of cosmic structure. We discuss the properties of this striking and intriguing pattern, describing its observational appearance, seeking to elucidate its dynamical origin and nature and attempting to frame a geometrical framework for a systematic evaluation of its fossil content of information on the cosmic structure formation process.

An extensive discussion on the gravitational formation and dynamical evolution of weblike patterns attempts to put particular emphasis on the formative role of the generic anisotropy of the cosmic gravitational force fields. These tidal fields play an essential role in shaping the pattern of the large scale cosmic matter distribution. A profound investigation of their role will be a key element in understanding the implications of the observed cosmic foam for the very process of cosmic structure formation.

The apogee of this contribution is reached in the specific attention for the geometric and stochastic aspects of the cosmic fabric. Its distinct geometric character – linking various distinct anisotropic morphological elements into a global all-encompassing framework – and the stochastic nature of this assembly provides the cosmic web with some unique and at first unexpected properties. The implications for galaxy clustering and its potential as discriminating of the galaxy distribution are discussed on the basis of its relevant branch of mathematics, stochastic geometry. Central within this context are Voronoi tessellations, which have been found to represent a surprisingly versatile model for spatial cellular distributions, whose flexibility and efficient exploitation warrant a central role in systematic assesments of the *cosmic foam*.

Keywords: Large-scale structure of the Universe, Methods: statistical, numerical

1. ACROSS THE UNIVERSE ...

Over the past two decades we have witnessed a paradigm shift in our perception of the Megaparsec scale structure in the Universe. As increasingly elaborate galaxy redshift surveys charted ever larger regions in the nearby cosmos, an intriguingly complex and salient foamlike network came to unfold and establish itself as thé quintessential characteristic of the cosmic matter and galaxy distribution.

In a great many physical systems (see Fig. 55), the spatial organization of matter is one of the most readily observable manifestations of the forces and processes forming and moulding them. Richly structured morphologies are usually the consequence of the complex and nonlinear collective action of basic physical processes. Their rich morphology is therefore a rich source of information on the combination of physical forces at work and the conditions from which the systems evolved. In many branches of science the study of geometric patterns has therefore developed into a major industry for exploring and uncovering the underlying physics (see e.g. Balbus & Hawley 1998).

The vast Megaparsec cosmic web is undoubtedly one of the most striking examples of complex geometric patterns found in nature. Revealed through the painstaking efforts of redshift survey campaigns, it has completely revised our view of the matter distribution on these cosmological scales. Figure 1 forms a telling testimony of the gradual unfolding of the cosmic foam patterns in the galaxy distribution by a sequel of ever deeper probing galaxy redshift surveys. It depicts a compilation of the CfA2/SSRS survey (courtesy, L. da Costa), the Las Campanas redshift survey (courtesy: LCRS team), the 2dF survey (courtesy 2dF Galaxy Redshift Survey team) and the first impression of the Sloan SDSS redshift survey (with thanks to M. Strauss).

In its own right, the vast dimensions and intricate composition of the cosmic foam make it one of the most imposing and intriguing patterns existing in the Universe. Its wide-ranging importance stems from its status as a cosmic fossil. On the typical scale of tens up to a few hundred Megaparsecs it is still relatively straightforward to relate the configuration at the present cosmic epoch to that of the primordial matter distribution from which it has emerged. With the cosmic foam seemingly representing this phase, it assumes a fundamental role in the quest for understanding the origin of all structures in the Universe. It represents a key element in the search for a compelling theoretical framework

[1]Lennon & McCartney, 1970, Let it Be (EMI records)

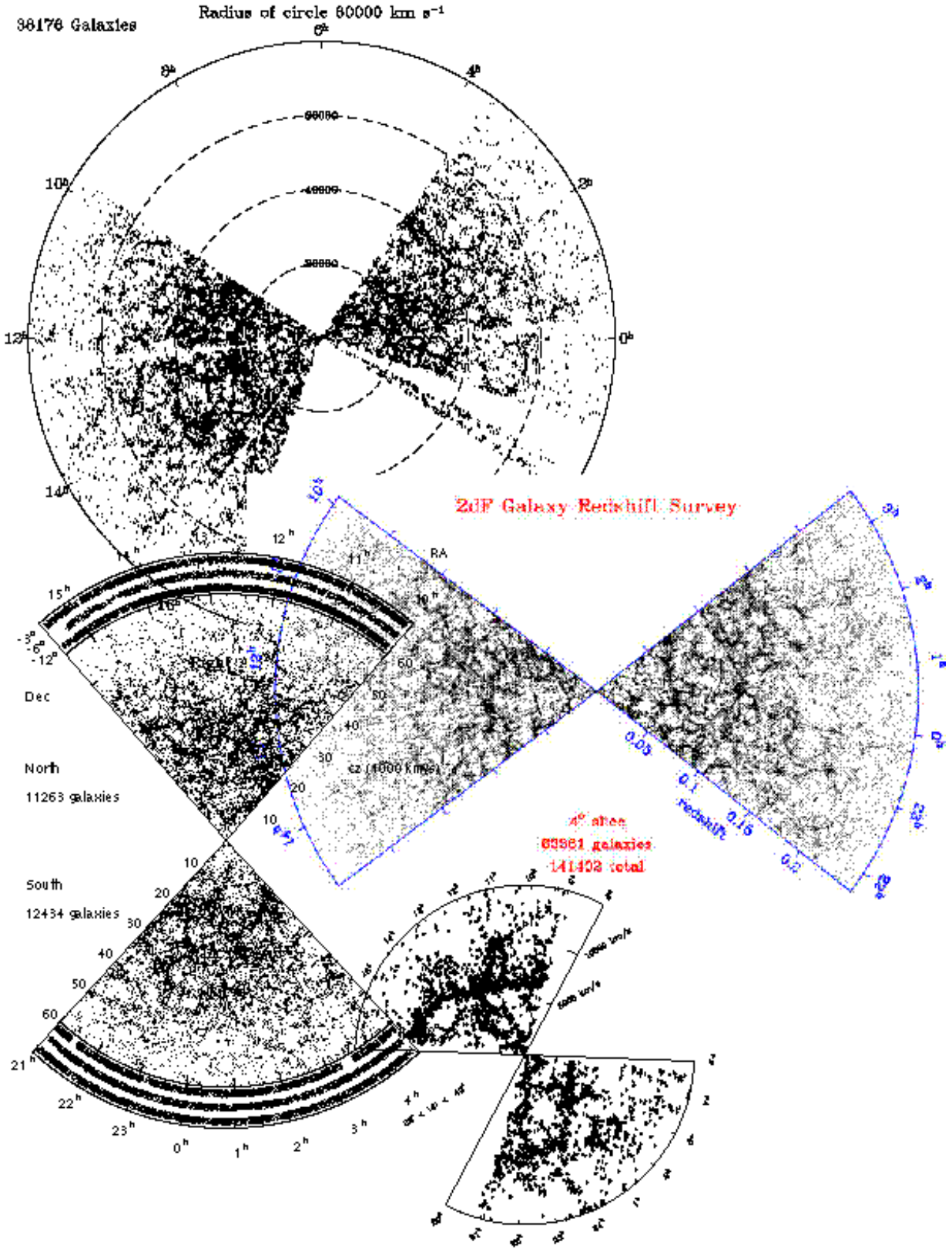
Radius of circle 60000 km s⁻¹
98176 Galaxies
2dF Galaxy Redshift Survey
RA
Dec
North
11263 galaxies
South
12434 galaxies
cz (1000 km/s)
redshift
4° slice
99981 galaxies
141422 total

Figure 1. The development of our Megaparsec cosmos worldview over the past two decades. A compilation of the galaxy distribution charted in four major galaxy redshift survey campaigns. The CfA2/SSRS survey (bottom righthand figure, courtesy L. da Costa) formed the first stage in disclosing the existence of a complex spatial pattern in the cosmic galaxy distribution. The Las Campanas redshift survey (bottom lefthand figure, courtesy LCRS team) confirmed the ubiquity and reality of these foamy patterns over vast reaches of our Universe. Moreover, it also provided evidence for sizes of the corresponding inhomogeneities not to surpass scales of $100 - 200h^{-1}$Mpc. With the arrival of the major and uniformly defined galaxy redshift campaigns of the 2dF survey (central frame, courtesy 2dF Galaxy Redshift Survey team) and the overwhelming 1 million galaxy redshift Sloan SDSS survey (top lefthand frame: preliminary galaxy redshift map, kindly provided by M. Strauss, with courtesy of the SDSS consortium) the fabric and the kinematics of the local Universe will get firmly established and provide a major resource for systematic scientific studies of all aspects of cosmic structure formation. Courtesy: L. da Costa; LCRS team (Shectman, S., Schechter, P., Oemler, G., Kirshner, B., Tucker, D., Landy, S., Hashimoto, Y. & Lin, H.); the 2dF consortium, with special thanks to J. Peacock; the SDSS consortium, with special gratitude to M. Strauss.

that offers and self-consistent explanation and description for the breathtaking variety and wealth of structures and objects that populate the present-day Universe, making it such a fascinating world to live in.

The emergence and formation of structure out of the almost perfectly smooth, virtually featureless, pristine Universe still remains one of the major unsettled issues in astrophysics. Ultimately, the intention is the framing of a theory that not only concerns the global cosmological aspects embodied in the FRW models but also includes a fully self-consistent explanation for the configuration and evolution of its interior mass distribution is. At present, the search for the necessary extension of the Friedmann-Robertson-Walker models towards such an all-embracing cosmological theory figures as of the most active branches of modern astrophysical research.

The Friedmann-Robertson-Walker models – based on the premise of a homogenous and isotropic Universe whose gravitationally driven evolution is drafted in terms of General Relativity theory – have proven to provide a remarkably succesfull description of the structure, evolution and thermal history of the global Universe. The gradual accumulation of an impressive array of observational evidence has been so compelling that we have come to regard the "Hot Big Bang" model as a central tenet of our scientific worldview.

Yet, the FRW cosmological framework cannot be considered complete, as it suffers from a fundamental deficiency. It does not comprise an implicit explanation for what is after all one of its most visible characteristics, the state of its material content. The bare FRW cosmology

is fundamentally incapable of addressing the question of why matter has condensed into a hierarchy of distinct objects and a variety of more or less coherent structures – planets, stars and galaxies, as well as the vast clusters and Megaparsec superclusters.

Indeed, while in itself one of the most fundamental issues in astrophysics, appealing to one of the most profound questions occupying mankind since the dawn of civilization – the quest for the origin of our world and that of its constituents – it is also a prominent issue for a variety of additional reasons. The study of geometry, structure, evolution and dynamics of our Universe would be an idle and unyielding enterprise if we would not have the full arsenal of astronomical objects (ranging from stars, gas clouds to galaxies and clusters) to function as basic probes enabling the measurement of the relevant physical quantities. Yet, lacking a precise understanding of their position and origin within the grander cosmological context, interpreting the measured information will always involve an element of uncertainty and arbitrariness. Moreover, perhaps the most essential of all conditions for advancements in answering these questions at all, the formation of structure paved the road for the rise of an inquiring intelligence, ...

This contribution revolves around the central position of the cosmic web in the investigations intent to solve the remaining riddles of the structure formation process. Particular attention is directed towards the stochastic and geometric properties of the cosmic web. While its complex cellular morphology involves one of the most outstanding and evident aspects of the cosmic foam, it has also remained one defying simple definitions which may be the cause of it having remained one of the least adressed aspects. The geometry of the cosmic foam may be described as a nontrivial stochastic assembly of various anisotropic and asymmetric elements. A major deficiency in the vast majority of studies on the large scale distribution of galaxies has been the lack of suitable quantitative and statistical characterizations of the truely fundamental aspects of the cosmic foam geometry, and the subsequent description in mere qualitative and not very decisive terms. Such patterns escape descriptions by appropriate simplified approximations. A statistical description in terms of a few conventional parameters will almost certainly fail, after all its highly nonlinear pattern implicates significant values for a range of higher order correlation functions. The limited mathematical machinery, in turn, has been a major obstacle in exploiting the potentially large information content of the cosmic web.

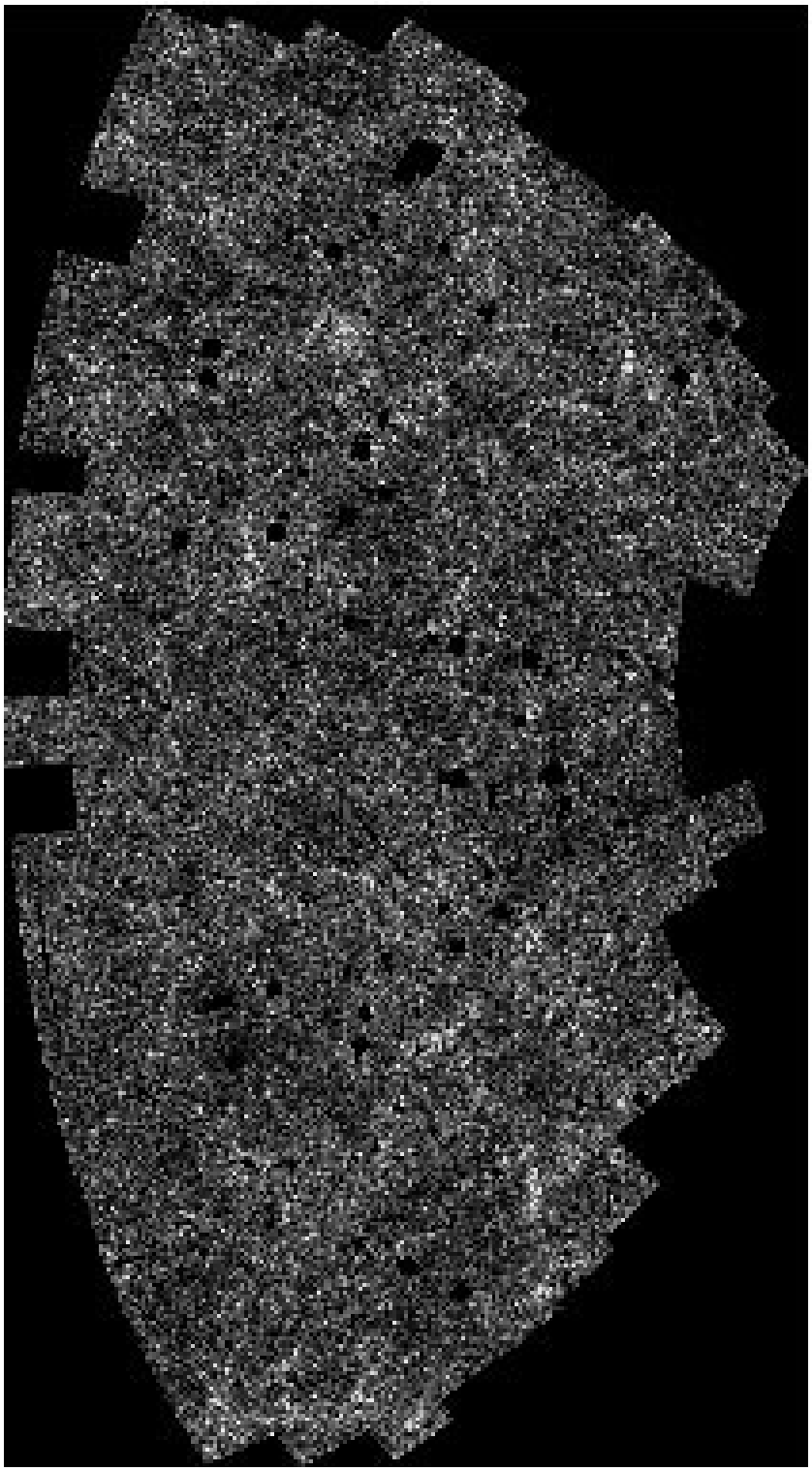

Figure 2. The sky distribution of galaxies in the APM survey. This uniformly defined galaxy map comprises $\approx$ 2 million galaxies with a magnitude in between $m = 17$ and $m = 20.5$, located within an angular region of 4300 square degrees on the southern sky. The survey is based on objective machine scans of 185 UK Schmidt plates, each of $6^\circ \times 6^\circ$. The resulting projected galaxy distribution provides ample evidence f0r the existence of large inhomogeneities. However, although superior for the large number of objects, for an overall impression of topology and morphology of the spatial galaxy distribution galaxy redshift surveys remain instrumental. See Maddox et al. 1990a,b. Courtesy: S. Maddox, G. Efstathiou, W. Sutherland, en D. Loveday

Hence we attempt to lay the foundations for a compelling geometrical framework enabling us to analyze the cosmic foam to a more profound and substantial extent than hitherto customary. For the appropriate concepts and instruments, we have delved into the mathematical field of stochastic geometry. This branch of mathematics deals with a stochastic context of geometric objects and concepts. By implication it is also the field adressing the issues of spatial point clustering, a prominent point of attention in the study of the galaxy distribution. In particular, we emphasize the virtues of one of stochastic geometry's basic concepts, Voronoi tessellations. The phenomological similarity of Voronoi foams to the cellular morphology seen in the galaxy distribution is suggestive for its further exploration. Indeed, we will indicate that such similarity is a consequence of the tendency of gravity to shape and evolve structure emerging from a random distribution of tiny density deviations into a network of anisotropically contracting features. The application of Voronoi tessellations gets firmly vindicated by a thorough assessment of its spatial clustering properties. They provide us with a succesfull, surprisingly versatile geometrical model for spatial cellular distributions. Its high flexibility and applicability to a large variety of situations, enables us to systematically study the consequences of the existence of a cellular network for spatial clustering of galaxies and other cosmic objects. Indeed, we will show that some well-known spatial clustering properties of galaxies may indeed ultimately and intricately stem from the very network geometry of the cosmic galaxy distribution itself. It is within the context of these spatial statistical tests that unexpected profound 'scaling' symmetries were uncovered, shedding new light on the intricacies of spatial clustering.

The path of delving into the secrets of cosmic structure by means of such cellular geometries is following a tradition almost as old as mankind has come to realize that the elevated realm of mathematics paves the road towards understanding the workings of the world of 'necessity'. It was Plato who saw a world of geometric forms underlying the manifes-

tations of the 'Becoming' (Plato, ≈ 355-350 B.C.). Most purely he was succeeded by Descartes (Fig. 33, Descartes 1664), combining geometric objects into a tessellating pattern in an unsuccesfull and not fully appreciated attempt for explaining the causal action propelling our solar system. We think the world at large may be the proper sphere in which to to pursue these momentous ventures of inquiry.

2. WORLDWIDE WEB: ... the Foamy Distribution of Galaxies

One of the most impressive examples of a physical system displaying a salient geometrical morphology, and the largest in terms of sheer size, is the one we have encountered on Megaparsec scales in the Universe. Although at hindsight the projections of the spatial galaxy distribution in the form of galaxy sky maps contained ample hints for the existence of a complex spatial pattern (see the APM galaxy position sky map in Fig. 2, see Maddox et al. 1990a,b), it was the seminal publication of the first redshift slice by de Lapparent, Geller & Huchra (1986, see Fig. 3) which offered the first direct panorama onto the cosmic tapestry. Their "Slice of the Universe" may rightfully be regarded as the turning point for our view of the cosmic matter distribution. It changed it from an undefined amorphous, be it clumped, point process into one of a complex intriguing pattern. Since then, through ever more substantial and sophisticated observational campaigns enabled by large technological advances, the reality of foamlike structural arrangements has been proven to be a fundamental characteristic of the Universe. As we may infer from Figure 1, the past few decades have more than substantiated the early impression that on scales of a few up to more than a hundred Megaparsec, galaxies conglomerate into intriguing cellular or foamlike patterns pervading throughout the observable cosmos.

A dramatic illustration of the accompanying advance in our perception of the "cosmic foam" is that in Figure 4 (courtesy 2dF Galaxy Redshift Survey team), the recently published map of the distribution of more than 150,000 galaxies in a narrow region on the sky yielded by the 2dF – two-degree field – redshift survey. Instead of a homogenous distribution, we recognize a sponge-like arrangement, with galaxies aggregating in filaments, walls and nodes on the periphery of giant voids. Outlined by galaxies populating huge *filamentary* and *wall-like* structures woven into an intriguing *foamlike* tapestry permeating the whole of the explored Universe, this frothy geometry of the Megaparsec universe evidently represents one of the most prominent aspects of the cosmic fabric (also see Fig. 14 and 15). Indeed, as we may infer from the preliminary map

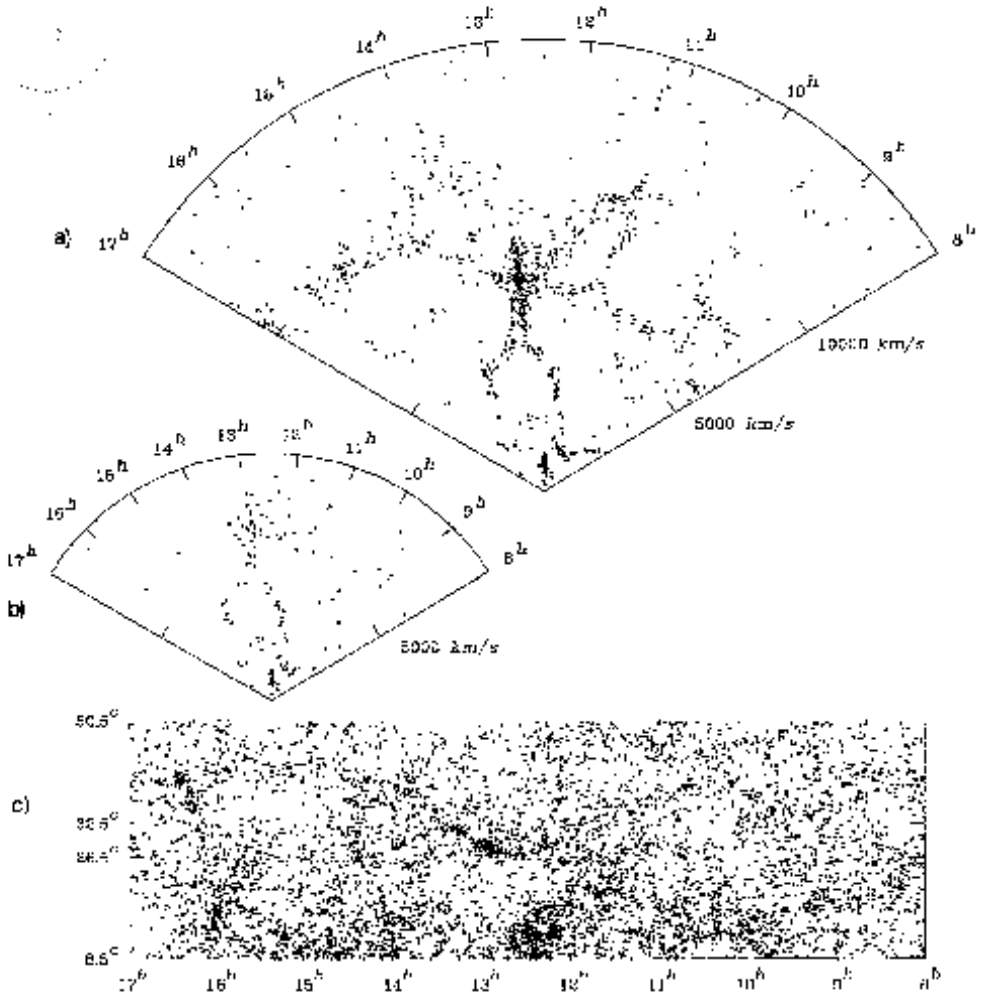

Figure 3. The revelation of the cosmic foam. The first published "Slice of the Universe" from the CfA2 survey, by de Lapparent, Geller & Huchra (1986). It comprises all galaxies with an apparent magnitude $m \leq 15.5$ in a narrow 6° slice in a region towards the Coma Cluster $((\alpha, \delta) \approx (13^h, 27°), seec)$. This stereological sampling of the galaxy distribution represents a highly efficient method to obtain an impression of the overall spatial pattern. The result was the at first surprising finding of the apparently idiosyncratic cellular galaxy distribution. Note that the shallower CfA1 survey (cf. b), probing to $m < 14.5$ at hindsight contained a hint for these nontrivial patterns, be it not yet sufficiently convincing. Rightfully, this slice may be seen as a historic document, being a turning point for our view of the Universe's structure. Courtesy: V. de Lapparent, M. Geller & J. Huchra. Reproduced by permission of the AAS.

of the currently ongoing one-million galaxy redshift survey of the SDSS consortium (Fig. 1, topleft figure, kindly provided by Michael Strauss), as we probe deeper and deeper into space, the better we can appreciate the global ubiquity of the foamlike galaxy arrangement.

2.1. Worldwide Web: Chains and Walls

The closest and best studied of these massive anisotropic matter concentrations can be identified with known supercluster complexes, enor-

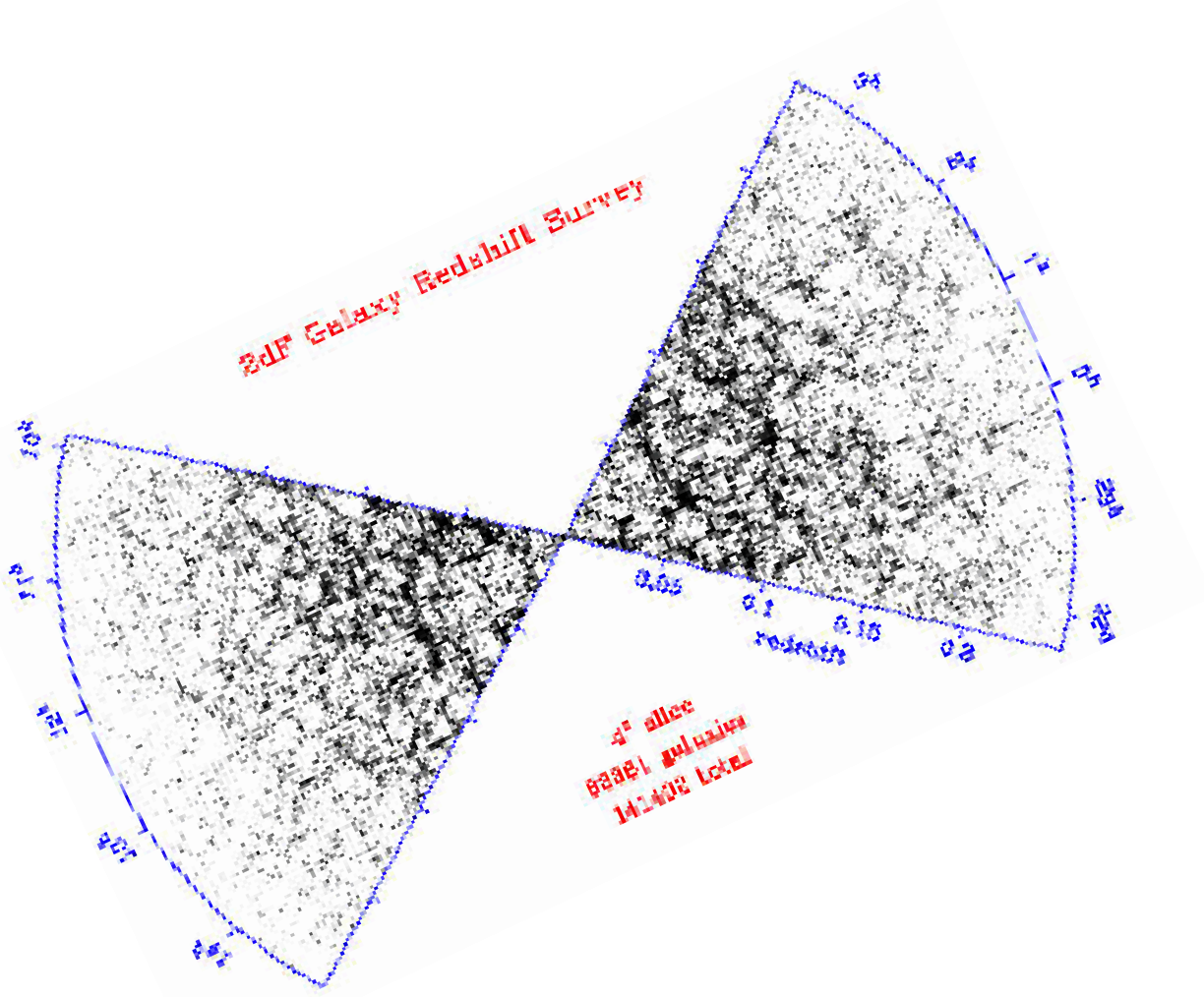

Figure 4. The 2dF galaxy redshift survey. Here confined to a narrow 4° slice, comprising 63361 out of a total of 141402 galaxies, out to a redshift $z \approx 0.25$, the universality, complexity and intricacy of the cosmic web is strikingly displayed. Picture courtesy of the 2dF Galaxy Redshift Survey team, kindly provided by J. Peacock.

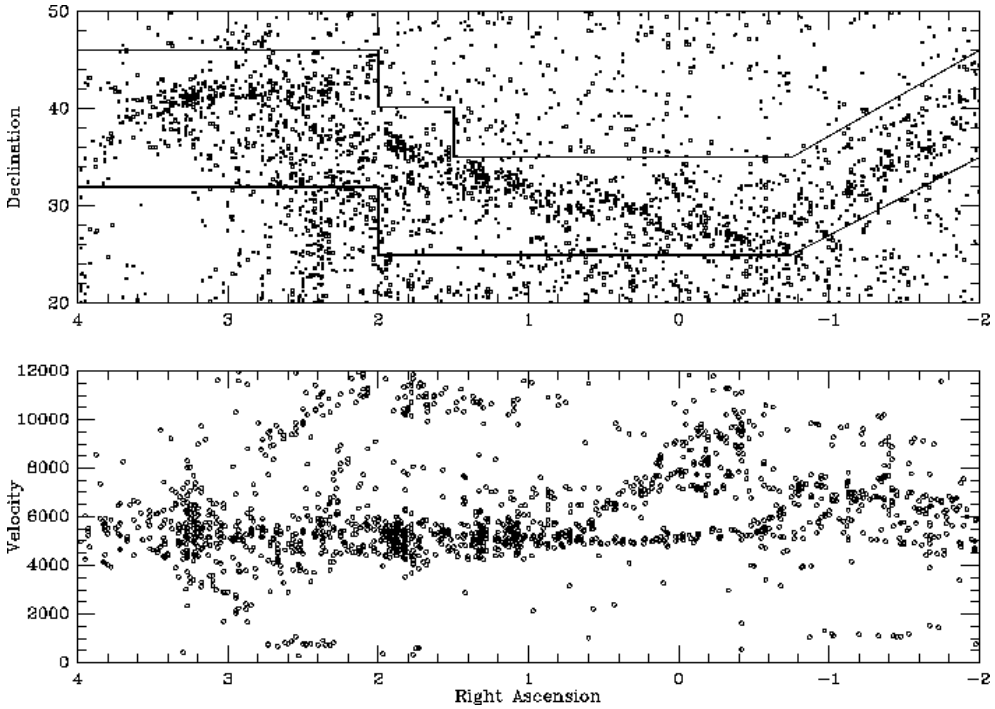

Figure 5. The Perseus-Pisces supercluster chain of galaxies. Separate two-dimensional views of the galaxy distribution in the northern region of the Pisces-Perseus region: sky-projected (top) and in depth (redshift, bottom). From Giovanelli & Haynes 1991, 1996, kindly provided by M. Haynes.

mous structures comprising one or more rich clusters of galaxies and a plethora of more modestly sized clumps of galaxies. The sizes of the most conspicuous one regularly exceeding $100\mathrm{h}^{-1}$ Mpc. They are mostly dynamically youthful structures, not yet having reached a stage of contraction, and whose prominence is due to the more than average deceleration of its initial expansion as a consequence of its mere moderate overdensity. Both our Local Group and the Virgo cluster are members of such a supercluster complex, the Local Supercluster, a huge flattened concentration of about fifty groups of galaxies in which the Virgo cluster is the dominating and central agglomeration. The Local supercluster is but a modest specimen of its class, counting only one rich cluster amongst its "subjects".

A far more prominent nearby representative is the Perseus-Pisces supercluster (Fig. 5). Its relative proximity ($\approx 55h^{-1}$ Mpc), its characteristic and salient filamentary morphology and its favourable orientation have made it into one of the best mapped and meticulously studied superclusters. It is a huge conglomeration of galaxies that clearly stands

out on the sky. The boundary of the supercluster on the northern side is formed by the filament running southwestward from the Perseus cluster. This majestic chain of galaxies has truely impressive proportions, a $5h^{-1}$ wide ridge of at least $50h^{-1}$ Mpc length, possibly extending out to a total length of $140h^{-1}$ Mpc. Along this major ridge we see a more or less continuous arrangement of high density clusters and groups, of which the most notable ones are the Perseus cluster itself (Abell 462), Abell 347 and Abell 262.

In addition to the presence of such huge filaments the galaxy distribution also contains vast planar assemblies. A striking example is the *Great Wall*, a huge planar assembly of galaxies with dimensions that are estimated to be of the order of $60 \times 170 \times 5$ h^{-1}Mpc, which has the Coma cluster of galaxies as its most prominent density enhancement (Geller & Huchra 1989).

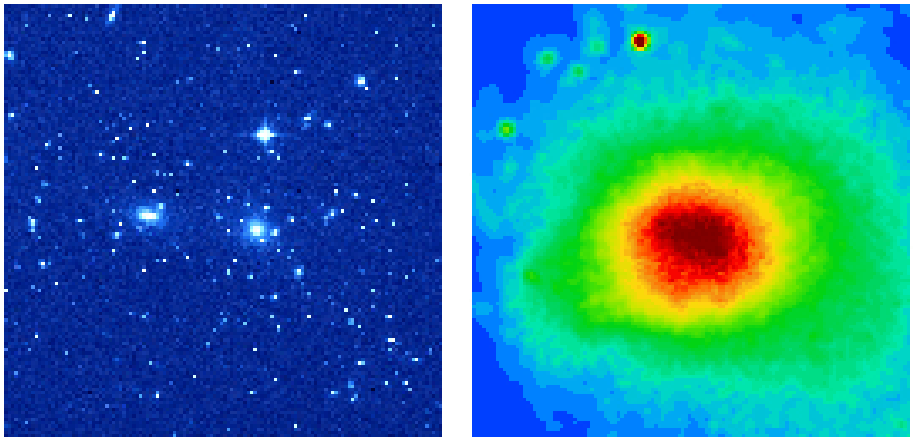

Figure 6. Comparison of optical and X-ray images of Coma cluster. Left: optical image; right: X-ray image (ROSAT). Courtesy: Chandra X-Ray Observatory Center.

2.2. Worldwide Web: Junctions, Galaxy Clusters

Rather than smooth and featureless features, filaments and walls appear to be punctured by a variety of internal structure and density condensations. These can range from modest groups of a few galaxies up to massive compact *galaxy clusters*, residing at the interstices of the cosmic network. The latter stand out as the most massive – and likely most recent – fully collapsed and (largely) virialized objects in the Universe. The richest of them contain many thousands of galaxies within a relatively small volume of only a few Megaparsec size. For instance, in the nearby

Virgo and Coma clusters more than a thousand galaxies have been identified within a radius of a mere $1.5h^{-1}$ Mpc around their core (see Fig. 6). The cluster galaxies are embedded in deep gravitational wells that have been identified as a major source of X-ray emission, emerging from the diffuse extremely hot gas trapped in these wells, possibly representing the most abundant state of baryonic matter in our Universe (Fig. 6, right). The clusters may be regarded as a particular population of cosmic structure beacons as they typically concentrate near the interstices of the cosmic web, *nodes* forming a recognizable tracer of the cosmic matter distribution (e.g. Borgani & Guzzo 2001).

Containing many hundreds to thousands of galaxies within a compact region, rich clusters of galaxies are highly luminous objects at optical wavelengths and can be seen out to large cosmic depths. Even more conspicuous is their X-ray brightness, the result of the emission by the diffuse extremely hot intracluster gas trapped in their gravitational potential wells. The X-ray emission represents a particularly useful signature, an objective and clean measure of the potential well depth, directly related to the total mass of the cluster (see e.g. Reiprich & Böhringer 1999). A potentially very promising and objective measure for the mass content of clusters is based on the shearing alternative measure of the cluster mass may be deduced from the deformation of the light path of background objects. However, mass determinations by gravitational lensing still involve very elaborate procedures, and as yet it is not feasible to use these as a basis for survey selections.

Through their high visibility clusters can be traced out to vast distances in the Universe. Hence, we can study their spatial distribution within large volumes of the cosmos. Thus, even though they represent a sparse mapping of the underlying large scale matter distribution, they are an ideal means of assessing its characteristics in very large volumes and over large scales, in particular when they relate to the underlying matter distribution in a direct and uncontrived fashion. This makes clusters into an efficient and time-saving probe for mapping the matter distribution over very large scales. A large range of observational studies, mainly based on optically selected samples, still display a substantial level of clumping on scales where clustering in the galaxy distribution has diminished below detectability levels. Be that due to the absence of genuine galaxy correlations or the fact that the clustering signal is so weak that it drowns in the noise, this turns out to be not so for cluster samples. It is in particular the Abell catalogue of optically identified galaxy clusters (Abell 1958; Abell, Corwin & Olowin 1989) which has fulfilled a central role for the study of the large scale matter distribution on scales of several tens of Megaparsec (see Bahcall 1988). A wide

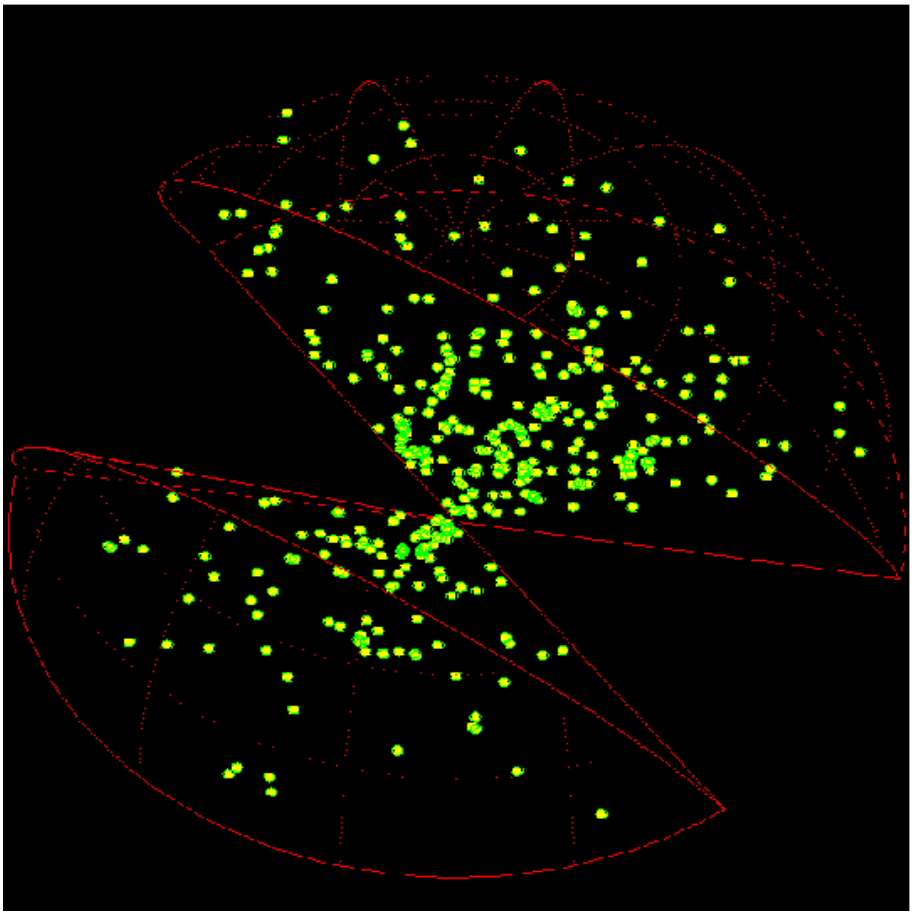

Figure 7. The spatial cluster distribution. The full volume of the X-ray REFLEX cluster survey within a distance of $600h^{-1}$Mpc. The REFLEX galaxy cluster catalogue (Böhringer et al. 2001), contains all clusters brighter than an X-ray flux of 3×10^{-12}ergs^{-1}cm^{-2} over a large part of the southern sky. The missing part of the hemisphere delineates the region highly obscured by the Galaxy. Courtesy: Borgani & Guzzo (2001). Reproduced by permission of Nature.

range of observational studies on the basis of such optically selected samples have shown that the clustering of clusters is significantly more pronounced. Their two-point correlation function has a shape similar to that of galaxies, yet with a substantially higher amplitude and detectable out to distances of at least $\sim 50h^{-1}$Mpc. Mainly on instigation of these results, theoretical arguments were put forward motivating a simple linear amplified level of clumping in the cluster population on the premise of clusters representing the high-density peaks in a properly filtered underlying mass density field (Kaiser 1984). The precise values of the constant "linear bias" factor with respect to that of the underlying

matter field will depend on both cluster mass and structure formation scenario (Mo & White 1996).

A very good impression of the spatial distribution of rich clusters can be obtained from Fig. 7 (from Borgani & Guzzo 2001). It depicts the spatial distribution of the clusters in the REFLEX galaxy cluster catalogue (Böhringer et al. 2001), containing all clusters brighter than an X-ray flux of 3×10^{-12}ergs^{-1}cm^{-2} over a large part of the southern sky. Maps such as these show that clusters themselves are not Poissonian distributed, but instead are highly clustered (see e.g. Bahcall 1988, Borgani & Guzzo 2001). They aggregate to form huge supercluster com-

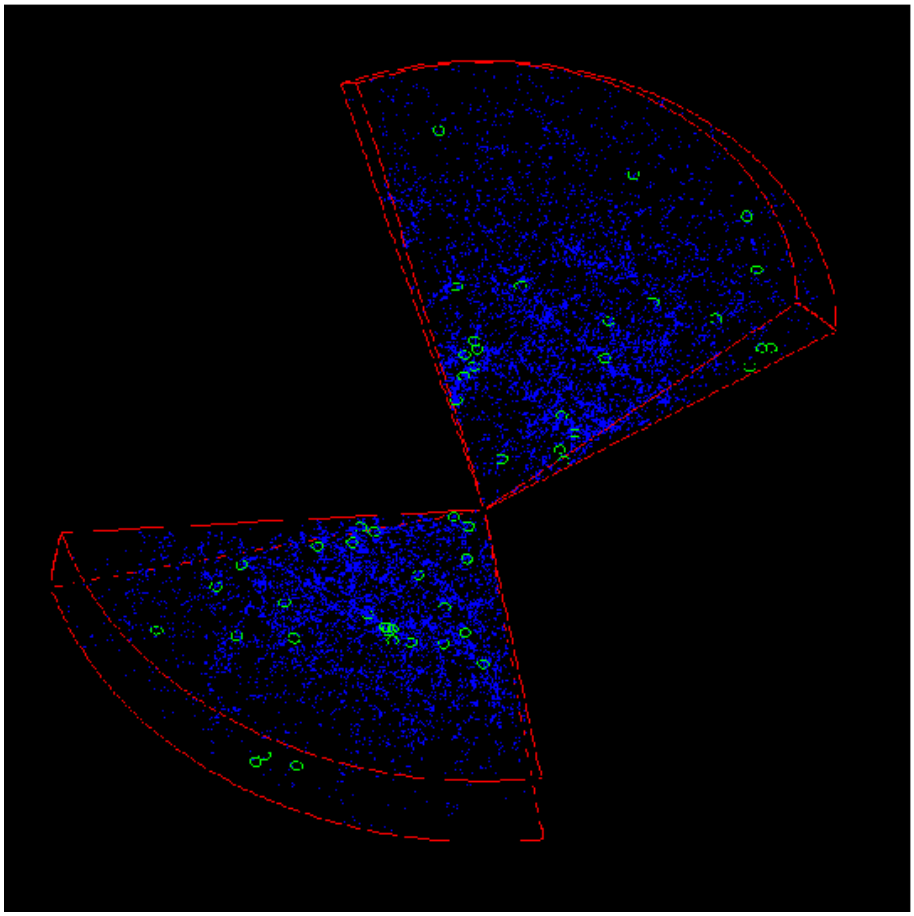

Figure 8. The spatial cluster distribution and its relation to the cosmic web. The green circles mark the positions of REFLEX X-ray clusters in the northern and southern slices of the Las Campanas redshift survey (LCRS, Shectman et al. 1996), out to a maximum distance of 600h^{-1} Mpc. Underlying, in blue, the galaxies in the LCRS delineate a foamlike distribution of filaments, walls and voids. Courtesy: Borgani & Guzzo (2001). Reproduced by permission of Nature.

plexes, coinciding with the filaments, walls and related features in the galaxy distribution. Indeed, in the case of the very highest density complexes filaments may represent such deep potential perturbations that also they may even light up in X-ray emission, as was discovered by Kull & Böhringer (1999). Most galaxies in these complexes are then located in the diffuse regions in between the clusters, which according to illuminating Dutch expression should be seen as the "currants in the porridge". Note that such superclusters are mere moderate density enhancements on scale of tens of Megaparsec, typically in the order of a few times the average density. They are still co-expanding with the Hubble flow, be it at a slightly decelerated rate, and are certainly not to be compared with the collapsed, let alone virialized, and verily pronounced entities like clusters. Instead, it is probably most apt to see them as clouds of points in a stochastic spatial point process, clouds whose boundaries are ill-defined.

What centres in our interest is the relation between the very large scale cluster distribution (Fig. 7) and the underlying matter distribution, in particular the weblike morphology of the latter. Figure 8 (Borgani & Guzzo 2001) provides a catching illustration, comparing the subset of REFLEX clusters within the region of the Las Campanas redshift survey to that of the galaxy distribution in the same region ($\sim 26,000$ galaxies, Shectman et al. 1996). From Fig. 8 we see that the cluster distribution represents a mere coarse mapping of the underlying structure. Not immediately outstanding, a thorough spatial statistical analysis will therefore be needed to establish the extent and nature of the correspondence between the two distributions.

On large scales valuable insight into the relation between the population of clusters and other cosmic residents has has been provided by the measurement, analysis and mutual comparison of large scale peculiar velocity fields of galaxies and clusters. By comparing the cluster population kinematics with the underlying matter and/or galaxy distribution, meaningful information has been obtained on the "bias" of clusters with respect to the overall matter distribution. Taking into account the vastly large cosmic region covered by cluster samples, a firmly established link between clusters and matter would provide us with the opportunity to map out the source for the peculiar motion of our own Local cosmic neighbourhood with respect to the cosmic background, as measured by the MWB dipole. For instance, Scaramella, Vettolani & Zamorani (1991) and Plionis & Valdarnini (1991) sought to establish on the basis of the cluster distribution within a distance of $r \approx 300h^{-1}$Mpc whether indeed the origin of our cosmic motion should be located within this volume, or whether there are indications for even larger cosmic struc-

tures. In a subsequent more systematic analysis, Branchini & Plionis (1996) sought to relate the dipole motion implied by the cluster distribution, in an analysis similar to that of galaxy peculiar velocity samples, to the dipole observed in the microwave background. In the meantime the availability of measured galaxy peculiar velocity samples covering large volumes of our local cosmos have allowed to perform such analyses over relevant local cosmic regions, shedding substantially more light on this important issue (see Branchini et al. 2001). The absence of major surprises, and their rough mutual agreement, is a strong argument for a systematic correlation between the cluster distribution and that of other cosmic representatives. Related numerical studies of various structure formation scenarios provided a substantial theoretical foundation for such a link (Moscardini et al. 1996). These large-scale studies, involving scales $> 10h^{-1}$Mpc, do need to be complemented by related small-scale studies. The detailed physical processes establishing a systematic relation between cluster population and the underlying matter distribution will ultimately be established on much smaller scales, unaivalable to the necessary low-resolution velocity studies. Focussing on aspects like the implied small-scale clustering patterns of clusters, and

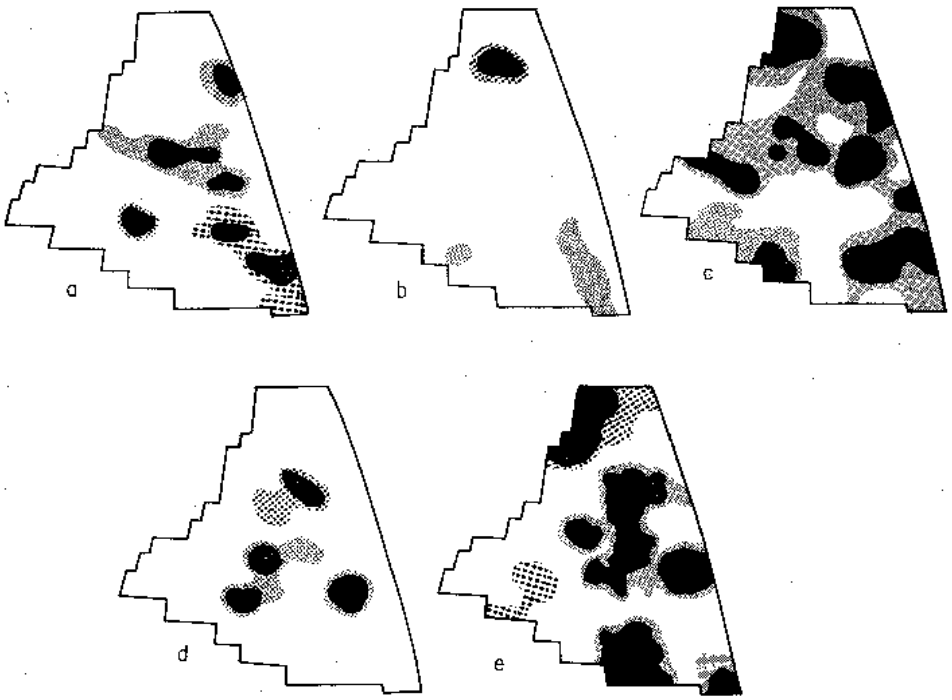

Figure 9. The Boötes void as revealed by the galaxy number space density in a sequence of five different recession velocity intervals in the direction of the Boötes constellation on the sky. The lowest contour represents a density equal to 0.7 of the cosmin mean, each higher contour represents a factor of 2 increase in density. Velocity ranges (km/s): (a) 7,000-12,000; (b) 12,000-17,000; (c) 17,000-23,000; (d) 23,000-29,000; (e) 29,000-39,000. Frame (b) clearly reveals a large void in the galaxy distribution, which turns out to be roughly spherical in outline. Figure from Kirshner et al. (1987). Reproduced by permission of the AAS.

scrutinizing their link to the anisotropic geometric patterns of the cosmic foam, and systematically adressing the processes creating such morphological connections are absolutely necessary for the ultimate unravelling of this important cosmic kinship.

2.3. Worldwide Web: the Valley of Voids

Complementing this cosmic inventory leads to the large *voids*, one of the most intriguing and unexpected findings emanating from extensive redshift surveys. They revealed that the planar, linear and compact structural elements of the galaxy distribution appear to be located on the surface of vast underdense regions. These concern vast regions of space, mostly roundish in shape, practically devoid of any galaxy, and typical sizes in the range of $20-50h^{-1}$ Mpc. The earliest recognized one, the Boötes void (Kirshner et al. 1981, 1987, see Fig. 9), a conspicuous almost completely empty spherical region (however, see Szomoru 1995) with a diameter of around $60h^{-1}$Mpc, is still regarded as the canonic example. The role of voids as key ingredients of the cosmic matter distribution has since been convincingly vindicated in various extensive redshift surveys, up to the recent results produced by Las Campanas redshift survey (Fig. 9) and the 2dF redshift survey (Fig. 4) and the Sloan redshift survey (see Fig. 1).

2.4. Worldwide Web: Monster Complexes

As our view of the spatial cosmic galaxy distribution is gradually expanding, we start to come across some truely awesome and rather uncharacteristic dense concentrations supercluster complexes. The Shapley concentration is the canonical example, by far the most outstanding complex in the Local Universe (see e.g. Raychaudhury 1989; Ettori et al. 1997; Quintana, Carrasco & Reisenegger 2000; Reisenegger etal. 2000). With the first maps of the SDSS redshift survey seeing the light, a first qualitative assessment suggests the presence of more comparable extreme supercluster complex, which appears to be in line with the claim by Batuski et al. (1999) for the existence of other comparable structures.

The most detailed impression of such "monster complexes" is offered by the Shapley concentration, first noted by Shapley (1930). It is an imposing concentration of galaxy clusters, the most massive concentration of matter at $z < 0.1$. It is located at a distance of $\sim 140h^{-1}$Mpc, beyond the Hydra-Centaurus supercluster (at $\sim 40h^{-1}$Mpc). It amasses more than 30 rich Abell galaxy clusters into a core region of $\sim 25h^{-1}$Mpc. An impression of this extraordinary concentration may be obtained from the depicted galaxy sample sky distribution in Fig. 10 (from Quintana, Carrasco & Reisenegger 2000). The central core is dominated by ACO clusters A3556, A3558 and A3562 and two poor clusters. Besides this core, one can identify an eastern part consisting of the clusters A3570, A3571, A3572 and A3575, and a western region formed by A3528, A3530 and A3532, while an elongation to the north includes A1736 and A1644. Several of these clusters are amongst the brightest X-ray clusters known (Ettori et al. 1997).

Telling for its huge mass is that the Shapley concentration is probably responsible for about $10 - 20\%$ of the optical dipole observed in the motion of the Local Group with respect to the cosmic microwave background (e.g. Raychaudhury 1989). Such is also suggested by num-

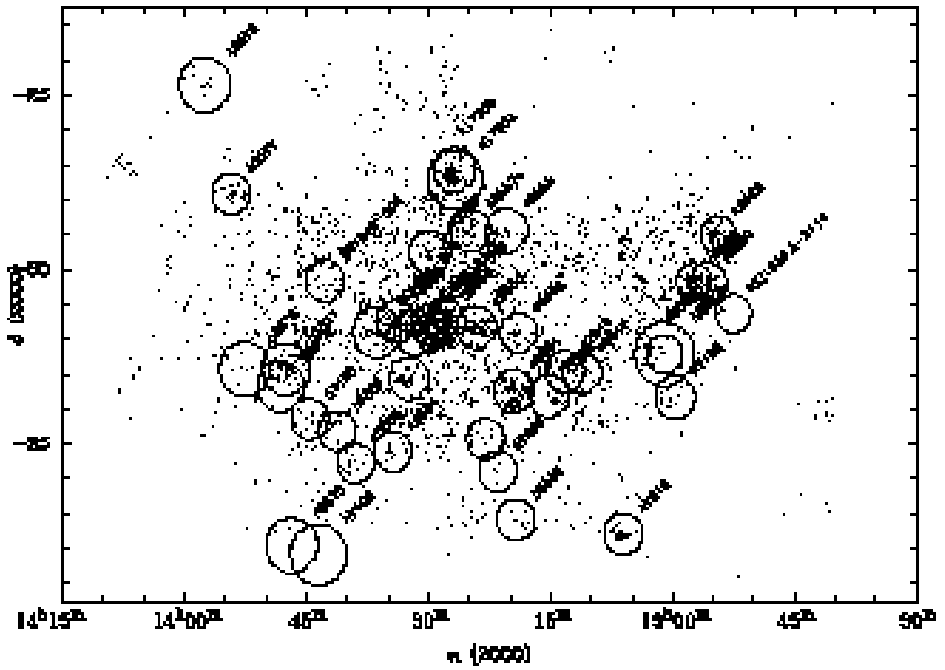

Figure 10. The Shapley Supercluster complex. Two-dimensional sky distribution of sample galaxies in Shapley concentration used in study of Quintana etal. (2000). Open circles indicate the locations of clusters within the complex. From Quintana, Carrasco & Reisenegger 2000. Reproduced with permission of the AAS.

ber counts in redshift space, which suggest that most of the supercluster has a density several times the cosmic average, while the two complexes within $\sim 5h^{-1}$Mpc of clusters A3558 and A3528 have overdensities ~ 50 and ~ 20 times, respectively. Such regions are therefore far outside the "linear" regime of small density perturbations, and have indeed started contracting, although far from having reached the stage of collapse and virialization (Bardelli et al. 2000). Such overdensities on scales of $\sim 25h^{-1}$Mpc surely do stress popular theories of hierarchical structure formation by gravitational stability to the utmost, and consequently represent a wonderful testbed for the corresponding scenarios.

Here we wish to draw special attention to these "monster complexes", as we will argue later that in fact they represent an important and natural manifestation of large scale cellular patterns. When clusters are concentrated near the junctions of the cellular network, it will induce a specific pattern of clustering in which a "geometric biasing effect" can be identified. The amplified level of clustering for the richest galaxy clusters may then be intimately linked with a concentration of such clusters in corresponding flattened or elongated superstructures defined by the distribution of the nodes of the network, the size of whom may supersede tens of Megaparsec (i.e. sizes comparable to the mean voidsize of $\sim 10 - 20h^{-1}$Mpc).

2.5. Worldwide Web: Universal Pretensions

The first impressions of a weblike galaxy distribution suggested by the first shallow CfA slices (de Lapparent et al. 1986) got continuously and increasingly convincing confirmed as larger and more ambitious surveys expanded their reach onto greater depths of our Universe. The image of a vast universal cosmic foam got firmly established through the publication of the results of the Las Campanas redshift survey (LCRS, Shectman et al. 1996). Its chart of 26,000 galaxy locations in six thin strips on the sky, extending out to a redshift of $z \sim 0.1$, until recently represented the most representative impression of cosmic structure available.

The LCRS comprised the first cosmologically representative volume of space. In the meantime, two ambitious enterprises, the 2dF and the Sloan digital sky survey, have embarked on ambitious missions to map the galaxy distribution of the Universe out to unexplored depths of cosmic territory, out to distances of $\sim 1000h^{-1}$Mpc. Up to a million galaxy redshifts will yield an unprecedented outline of the structure of our cosmic environment, for the first time a fully representative and truely uniform sample of our Universe. Indeed, the published results of the 2dF survey (Fig. 4) can only be characterized as stunning in the

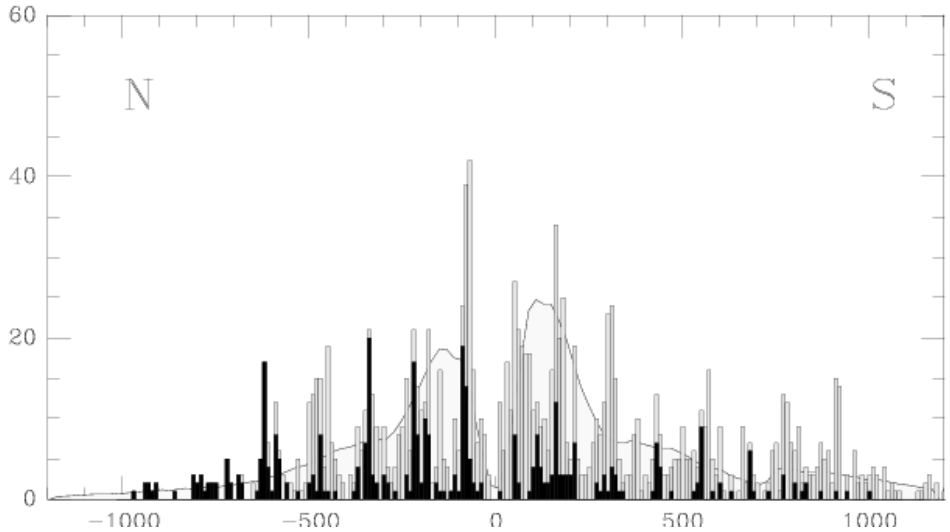

Figure 11. A pencil beam redshift survey. The redshift distribution of galaxies out to a distance of of $1200h^{-1}$Mpc towards the south Galactic pole (negative velocities) and the north Galactic pole (positive velocities). Plotted is the number of galaxies in $10h^{-1}$Mpc bins. This figure is a combination of several very narrow pencil beam redshift surveys, comprising fields of 5 to 20arcminutes. The black bars represent the number of galaxies in the original survey of Broadhurst, Ellis, Koo & Szalay (1990). The superposed dotted bars represent more recent extensions of and additions to the original (1990) survey. The continuous curve at the background is the survey selection function, which combines the effects of the different geometries and apparent magnitude limits of composite survey beams. Kindly provided by Alex Szalay.

detailed and refined rendering of the foamlike morphology traced out by the galaxy distribution. The extent and ubiquity of the foamlike patterns throughout the surveyed volume, extending out to a redshift $z \sim 0.2$, is truely perplexing. With respect to its universality, possibly most telling has been the finding that a narrow and very deep "needle-shaped" one-dimensional probe through the galaxy distribution results in a conspicuous pattern of sharp spikes separated by shallow valleys. Such pencil beam redshift surveys (Broadhurst et al. 1990) clearly conjure up the idea of piercing through a foamlike structure of walls and filaments (see e.g. van de Weygaert 1991a), which suggest the cosmic foam to extend at least up to a redshift of $z \sim 0.5$.

All, involve a strong confirmation of the existence of foamlike galaxy distributions out to large cosmic distances. It has made us realize that the cosmic foam is a truely universal phenomenon, extending over a vast realm of the observable Universe.

2.6. Worldwide Web: Gravitational Signature

Having observed its pronounced features reflected in the spatial distribution of galaxies, we should naturally wonder whether the foamlike network is indeed also the spatial arrangement of the (full) matter distribution. Given the fact that we still do not understand properly how and where galaxies did form during the evolution of the Universe the foamlike galaxy distribution may represent a biased reflection of the underflying matter distribution. In principal the specific foamlike features may therefore be as much be a consequence of the processes involved with the forming of galaxies as a result of the spatial matter distribution. The issue is even more pressing since we know that probably more than 80% of the matter in the Universe consists of a collisionless, weakly interacting matter. It is certainly not self-evident that the distribution of baryonic matter, be it the galaxies or the diffuse intergalactic medium, does form a faithful representation of the spatial properties of the dominant species of matter. Nonetheless, substantial evidence for the universal presence of the cosmic foam, not merely confined to the galaxy distrubition, has been inferred from the properties of the absorption of radiation by the intergalactic medium of neutral hydrogen, specifically at the Lyα transition. The observed Lyα forest of absorption lines in the spectra of background quasars has provided a rich source for exploring the spatial and thermal characteristics of the intergalactic medium. Interpreting them with the help of cosmohydrodynamic simulations of structure formation the evidence is quite compelling that the forest should be interpreted in terms of lines of sight piercing through a medium confined within a foamlike diffuse gas distribution.

However, as far as its genuine material distribution, the most unbiased test for the reality of the cosmic foam is by means of its gravitational impact. Through meticulous work the gravitational influence of the matter distribution has indeed been opened to a more profound study. Two major physical effects provide us with a means to probe the material content of the Universe.

Within the commonly accepted view of structure formation through gravitational instability (see section 3), we know that the the peculiar velocities of galaxies are induced by the residual gravity stemming from the inhomogenous matter distribution (see Dekel 1994 and Strauss & Willick 1995 for excellent over- and reviews). Hence, we may use these deviations of galaxies' velocities from the global Hubble flow as a means to explore the underlying matter distribution. This has indeed developed into a major industry. A major complicating factor is that as yet galaxy distance estimates are still rather coarse, their accuracy rarely

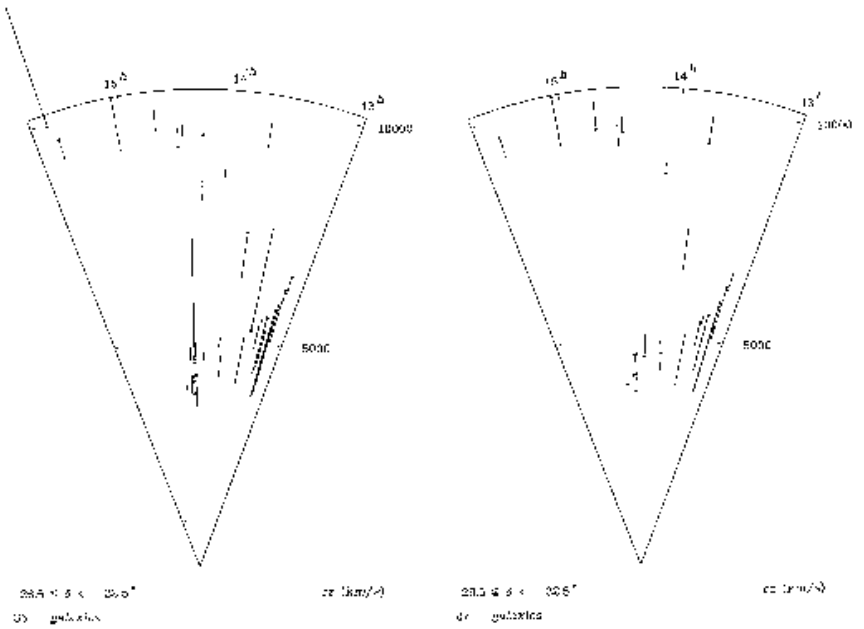

Figure 12. Velocity field for galaxies on the edge of the largest void in first CfA2 slice. The velocities of the galaxies were estimated on the basis of I-band Tully Fisher measurements. Left: all 35 galaxies with I-band TF measurements. Right: the 27 galaxies with reliable I-band TF distances. The tip of each galaxy velocity vector is indicated by a small circle. Notice the infall pattern towards the Coma cluster for the galaxies along the edge of the void. From Bothun etal. 1992. Reproduced by permission of the AAS.

lower than 20%, which usually restricts the interpretation of the measured velocity fields to scales exceeding $\approx 10h^{-1}$Mpc. On those scales, where structure is still residing in the linear stage of development, the velocities are expected to be linearly proportional to the exerted peculiar gravitational force. While this has lead to succesfull reconstructions of the matter distribution in the Local Universe, and included the discovery of a nearby huge matter concentration, the Great Attractor, it also implies that it is very difficult to see whether we see traces of a foamlike matter distribution. After all, typical are its anisotropic elements, elongated along one or two directions, yet of a small extent in at least one other direction. The smoothing operations involved with these studies of cosmic flows therefore tend to abolish the distinctly anisotropic marks of a foamlike matter distribution.

Yet, a few indications have been uncovered and appear to indicate the reality of a foamlike matter distribution. One strategy is to study in

more detail the velocity field around salient filamentary features. The other smartly adresses the effects of voids within the matter distribution. Some studies have indeed been focussing on peculiar velocity fields near some outstanding filamentary features and appear to indicate faster velocities than would be expected on the basis of a more "spherical" matter distribution. Such is to be expected in the case of anisotropic features.

In an early study, Bothun et al. (1992) studied the peculiar velocities of galaxies on the edges surrounding the largest void in the first lice of the CfA redshift survey (de Lapparent, Geller & Huchra 1986). They found indications for significantly higher infall velocities into Coma than expected on the basis of merely the gravitational influence of Coma itself (see Fig. 12). Upon close inspection of the velocity pattern in the slice (Fig. 12), we can clearly recognize a flow along the filament connecting onto the Coma cluster. On the basis of these (coarse) data one could therefore suspect the gravitational (pushing) influence of the void to indeed represent a significant contribution to the overall gravitational field. Additional analyses of the velocity fields in other superclusters, in particular the Perseus-Pisces supercluster filament, also do suggest a clear signature of a anisotropic infall pattern along the ridge of the complex (see e.g. Baffa et al. 1993).

The indication for the dynamical influence of voids was further substantiated by the far more extensive and systematic analysis of peculiar galaxy velocities in the Local Universe. Through the application of the POTENT procedure (Dekel, Bertschinger & Faber 1990, Bertschinger et al. 1990) the observed radial peculiar velocities of galaxies can be used to recover the full three-dimensional field, smoothed on scales of $\sim 10h^{-1}$Mpc. On linear scales reconstructed 3-D velocity maps on the basis of the Mark III catalogue (Willick et al. 1997) can subsequently be applied towards reconstructing the density field in the corresponding region of the Local Universe. On the basis of such reconstructions, the gravitational impact of voids in the Local Universe can clearly be recognized (also see Dekel & Rees 1994). Indeed, the POTENT reconstructions show that is necessary to invoke the dynamical influence of these voids to obtain a fully selfconsistent reconstruction of the dynamics in the Local Universe. Most interesting was therefore the suggestion by Dekel & Rees (1994) to use the pushing influence of voids to set limits on the value of the cosmological density parameter Ω. Probably most promising for investigating the dynamical impact of the cosmic web is through its influence on the trajectories of light, i.e. its gravitational lensing effect. While clusters of galaxies form by far the most outstanding sources of lensing on large Megaparsec scales, there has been a major effort towards detecting the signature of the more generic large

scale structures. Theoretical evaluations by e.g. Jain, Seljak & White (2000) have shown this to be a feasible and promising technique. Since the presence of a significant signal of cosmic shear has been inferred for by meticulous statistical analysis of wide field sky images (Van Waerbeke et al. 2000), we know it must indeed be possible to probe the signal of individual features such as those of filaments. However, despite its great promise, instrumental complications are still preventing the first significant reconstruction of such features on the basis of weak lensing

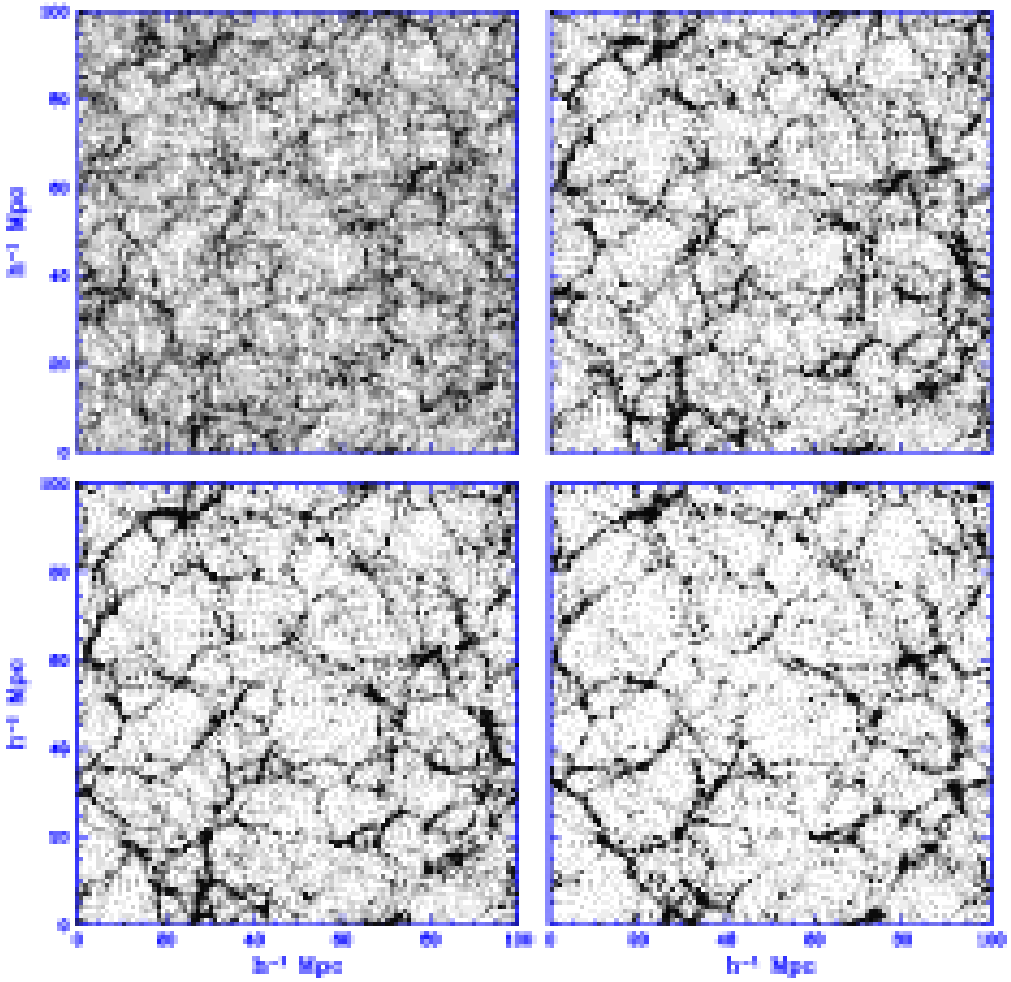

Figure 13. Evolution of structure and development of a cellular morphology in a scenario of structure formation through gravitational instability. Illustrated are 4 slices, at $a = 0.2, 0.3, 0.5$ and $a = 0.7$ in SCDM scenario ($\Omega_0 = 1.0, H_0 = 50\,\mathrm{km/s/Mpc}$) from a $\mathrm{P^3M}$ N-body simulation following the clustering of 128^3 particles in a $100\mathrm{h}^{-1}$ Mpc box.

measurements (there has been a claim of the detection of a filamentary bridge by Kaiser et al. 1998). Despite its pristine status, we may therefore look forward to a major amount of information on the dynamics of the cosmic web in the coming years.

2.7. Worldwide Web: the Filigree of Fantasy

Foamlike patterns have not only been confined to the cosmos of reality. Equally important has been the finding that foamlike patterns do occur quite naturally in a vast range of structure formation scenarios within the context of the generic framework of gravitational instability theory. Prodded by the steep increase in computing power and the corresponding proliferation of ever more sophisticated and extensive simulation software, a large range of computer models of the structure formation process have produced telling images of similar foamlike morphologies (Fig. 13).

They reveal an evolution proceeding through stages characterized by matter accumulation in structures with a pronounced cellular morphology, involving large anisotropic clustering structures such as filaments and walls. Whether or not these stages form a transient stage or a more permanent aspect of the matter distribution is not yet entirely clear, but will certainly depend on the scenario, the cosmological density parameter Ω, and possibly various other factors. Evidently, the observation that numerical models seem to display the idiosyncratic tendency of forming foamlike patterns provides us with a firm ground for a gaining a more substantial insight into its formation mechanisms and conditions.

2.8. Worldwide Web: the Cosmic Symbiosis

Of utmost significance for our inquiry into the issue of cosmic structure formation is the fact that the prominent structural components of the galaxy distribution – clusters, filaments, walls and voids – are not merely randomly and independently scattered features. On the contrary, we have noticed them to have arranged themselves in a seemingly highly organized and structured fashion, the *cosmic foam*. The voids are generically associated with surrounding density enhancements. In the galaxy distribution they represent both contrasting as well as complementary components, the vast under-populated *voids* being surrounded by *walls* and *filaments* with the most prominent and massive cosmic matter concentrations, the *clusters* of galaxies, at the intersections of the latter.

A major challenge will be to quantify the intricacies and cohesiveness of this cosmic foam geometry in a fashion befitting its rich information

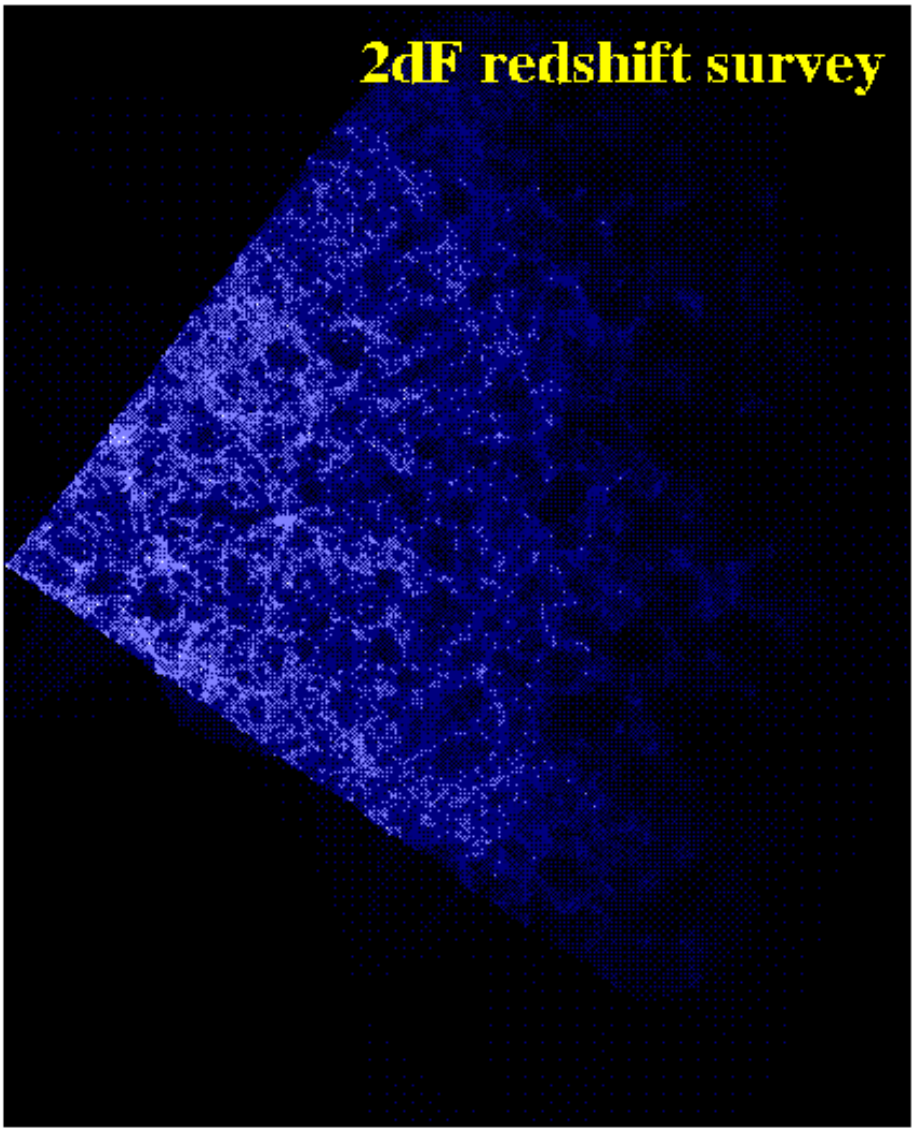

Figure 14. The Delaunay Field Estimator reconstruction of the 2dF survey field south. The DFE reconstruction more clearly than the galaxy distribution itself shows the coherence of the cosmic foam discretelt "sampled" by the galaxy distribution. Notice the detailed and refined structure which appears to be specifically strengthened by this fully adaptive method (from Schaap & van de Weygaert 2002b). Data courtesy: the 2dF consortium.

content. Such analysis should be able to yield a meaningful quantification of the structural content of the foamlike network, on the basis of which it will be possible to define distinct discriminating measures

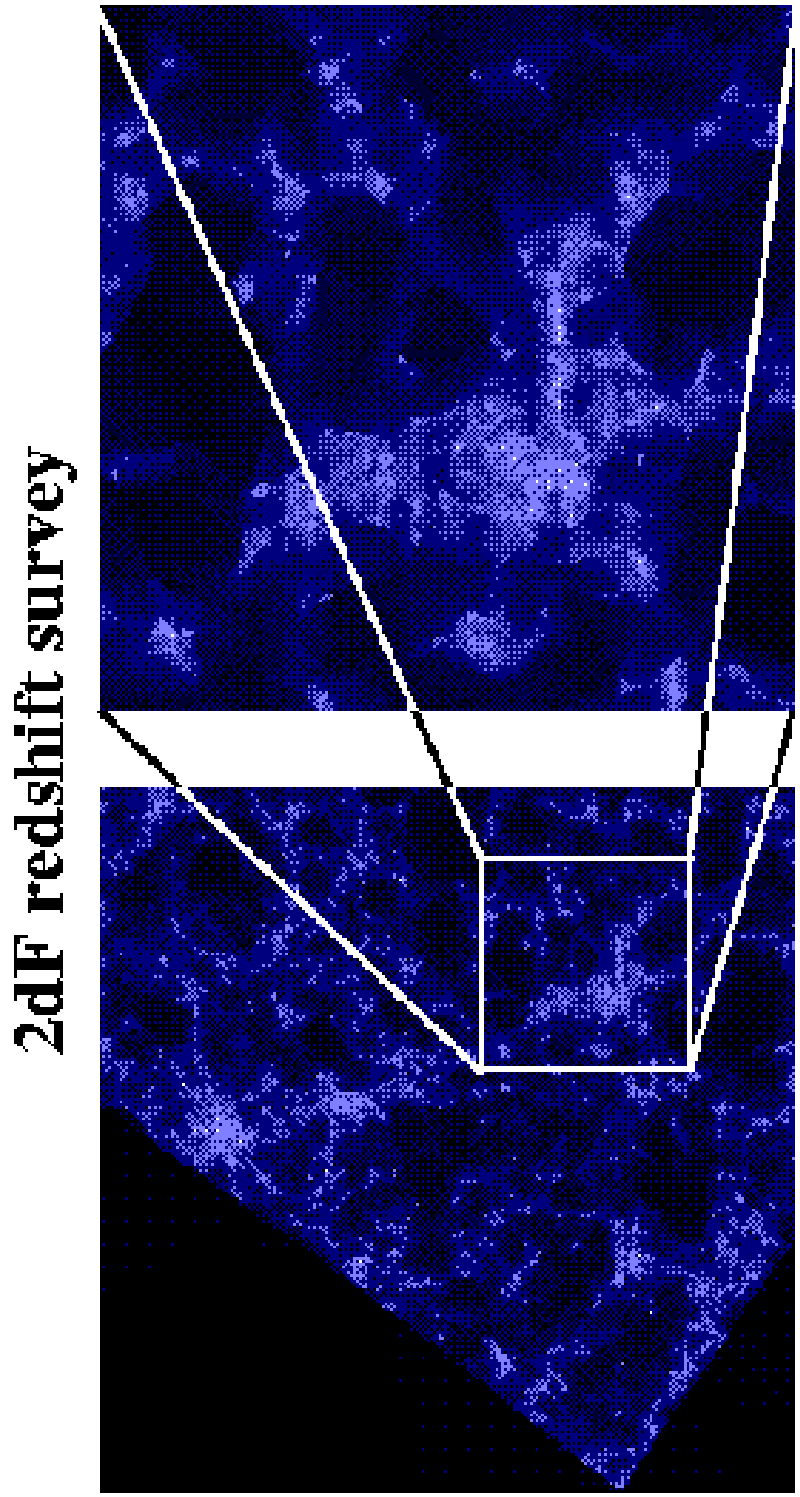
2dF redshift survey

Figure 15. The Delaunay Field Estimator reconstruction of the 2dF survey field south. In particular focussing in on a high-density junction point within the weblike structure, a massive matter concentration. Not only do we clearly recover the filamentary extensions emanating from the massive "core", but we can also observe the internal structure of these various elements (from Schaap & van de Weygaert 2002b). Data courtesy: the 2dF consortium.

enabling a comparison between the various viable structure formation scenarios.

The recent development of a fully adaptive method based on the Delaunay tessellation of the corresponding spatial point process, the *Delaunay Tessellation Field Estimator* (DTFE, see Schaap & van de Weygaert 2000), appears to hold great promise. Based on the earlier work by Bernardeau & Van de Weygaert (1996) to reconstruct a complete volume-covering and volume-weighted velocity field from a set of point-sampled velocities – which proved to yield a significant improvement in reproducing the statistics of the underlying continuous velocity field – it reconstructs the full and cohesive density field of which the discrete galaxy distribution is supposed to be a sparse sample. Without invoking any artificial and often structure diluting filter it is able to render both the *anisotropic* nature of the various foam elements as well as the *hierarchical* character of the distribution in full contrast (see Schaap & van de Weygaert 2002a).

The potential promise of the DTFE may be amply appreciated from its succesfull reconstruction of a density field from the galaxy distribution in the southern part of the 2dF survey (Fig. 14, cf. Fig. 4). Evidently, it manages to bring out any fine structural detail of the intricate and often tenuous filamentary structures. Notice the frequently razor-sharp rendition of thin edges surrounding void-like regions. Hence, it defines a volume-covering density field reconstruction that retains every structural detail, which will enable us to study in a much improved fashion the statistical and geometric properties of the foam. Indeed, it even appears to "clean" the original discrete galaxy distribution map by suppressing its shot noise contribution.

To underline its capacity to dissect the internal structure of the various structural components, in Fig. 15 we focus in on one of the major mass concentrations. It nicely illustrates its location at a junction point within the cosmic foam. Various filamentary extensions emanate from the high-density core. Not only does the DTFE method elucidate the filamentary anisotropic structures and their mutual spatial relationship, but as well it manages to highlight automatically the complex internal structure of the various connected elements.

3. POWER THAT BE: ...
Gravity Rules the Waves

The fundamental cosmological importance of the *cosmic foam* is that it comprises features on a typical scale of tens of Megaparsec, scales at which the Universe still resides in a state of moderate dynamical evolution. Structures have only freshly emerged from the almost homogeneous pristine Universe and have not yet evolved beyond recognition. Therefore they still retain a direct link to the matter distribution in the primordial Universe, and thus still contain a wealth of direct information on the cosmic structure formation process.

3.1. Power That Be: Gravitational Instability

The generally accepted theoretical framework for the formation of structure is that of gravitational instability. The gravitational instability scenario assumes the early universe to have been almost perfectly smooth, with the exception of tiny density deviations with respect to the global cosmic background density and the accompanying tiny velocity perturbations from the general Hubble expansion. For a general density fluctuation field $\delta(\mathbf{r}', t) = (\rho(\mathbf{r}') - \rho^b)/\rho^b$ (Fig. 16, top lefthand panel), this results in a corresponding total peculiar gravitational acceleration $\mathbf{g}(\mathbf{r})$ (Fig 16, top righthand panel) field which at any cosmic position $\mathbf{r}$ can be written as the integrated effect of the peculiar gravitational attraction exerted by all matter fluctuations throughout the Universe,

$$\mathbf{g}(\mathbf{r}, t) = \frac{3\Omega H^2}{8\pi} \int \mathrm{d}\mathbf{r}' \, \delta(\mathbf{r}', t) \, \frac{(\mathbf{r}' - \mathbf{r})}{|\mathbf{r}' - \mathbf{r}|^3} \; . \qquad (1)$$

Here Ω is the cosmological density parameter quantifying the mean density ρ^b of the Universe via the relation $4\pi G\rho^b = \frac{3}{2}\Omega H^2$. The above relation between density field and gravitational field $\mathbf{g}$ is in essence established through the Poisson equation,

$$\nabla^2\phi = 4\pi G\rho^b(t)a(t)^2 \; \delta(\mathbf{x}, t) = \frac{3}{2}\Omega H^2 a^2 \; \delta(\mathbf{x}, t) \; , \qquad (2)$$

relating density contrast $\delta(\mathbf{r}', t)$ and gravitational potential perturbation $\phi(\mathbf{r}, t)$, from which we obtain $\mathbf{g} = -\nabla\phi/a$. The formation and moulding of structure is then ascribed to the gravitational growth of these primordial density- and velocity perturbations. Gravity in slightly overdense regions will be somewhat stronger than the global average gravitational deceleration, as will be the influence they exert over their immediate

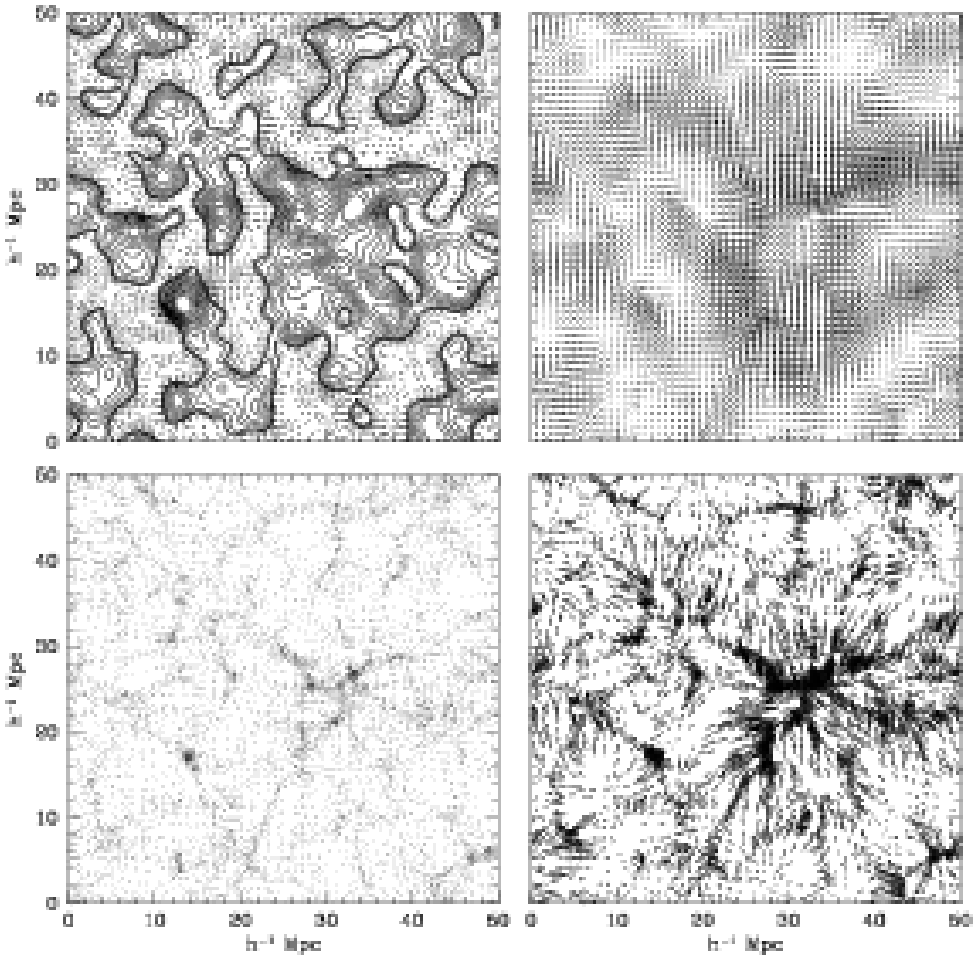

Figure 16. Gravitational Instability: schematic presentation of process. Top lefthand: contour map of a (Gaussian) stochastic density field. Top righthand: the resulting gravitational force field. Lower lefthand: resulting (nonlinear) particle distribution. Lower righthand: vector map corresponding velocity field

surroundings. In these regions the slow-down of the initial cosmic expansion is correspondingly stronger and, when the region is sufficiently overdense it may even come to a halt, turn around and start to contract. If or as long as pressure forces are not sufficient to counteract the infall, the overdensity will grow without bound, assemble more and more matter by accretion of matter from its surroundings, and ultimately fully collapse to form a gravitationally bound and virialized object. In this way the primordial overdensity finally emerges as an individual recognizable denizen of our Universe, their precise nature (galaxy, cluster, etc.)

and physical conditions determined by the scale, mass and surroundings of the initial fluctuation.

For a pressureless medium, the full evolution of this system of coupled cosmic density-, velocity- and gravity fields is encoded in three coupled fluid equations. Schematically, the essential aspects of this process of gravitational growth of structure, starting from a field primordial matter perturbations, are rendered in Figure 16. In addition to the Poisson equation (2), connecting the matter distribution to the gravitational field (left and right top panel Fig. 16), these are the *Euler equation* and the *continuity equation*. The Euler equation is the equation of motion describing the induced and corresponding matter flows (see bottom right panel Fig. 16),

$$\frac{\partial \mathbf{v}}{\partial t} \; + \; \frac{\dot{a}}{a}\mathbf{v} \; + \; \frac{1}{a}\,(\mathbf{v}\cdot\nabla)\mathbf{v} \; = \; -\frac{1}{a}\,\nabla\phi \;, \tag{3}$$

while the *continuity equation* guarantees the conservation of mass in this evolving system of matter migrations towards the emerging cosmic structures (see bottom left panel Fig. 16),

$$\frac{\partial \delta}{\partial t} \; + \; \frac{1}{a}\,\nabla\cdot(1+\delta)\mathbf{v} \;. \tag{4}$$

3.2. Cosmic Structure: Gaussian by descent.

Usually, the primordial density and velocity perturbation field is assumed to be a field of random fluctuations whose stochastic nature is that of a homogeneous and isotroptic spatial Gaussian process. The Gaussian nature of the random field $f(\mathbf{x})$ (for which we take a zero mean, for simplicity, as in the case of the density excess $\delta(\mathbf{r})$, the peculiar gravitational acceleration $\mathbf{g}_{pec}$ and peculiar velocity $\mathbf{v}_{pec}$) implies its set of N-point joint probabilities to be given by

$$\mathcal{P}_N \; = \; \frac{\exp\left[-\frac{1}{2}\sum_{i=1}^{N}\sum_{j=1}^{N} f_i\,(\mathsf{M}^{-1})_{ij}\,f_j\right]}{[(2\pi)^N\,(\det\mathsf{M})]^{1/2}}\;\prod_{i=1}^{N}\mathrm{d}f_i \tag{5}$$

where $\mathcal{P}_N$ is the probability that the field f has values in the range $f(\mathbf{x}_j)$ to $f(\mathbf{x}_j)+\mathrm{d}f(\mathbf{x}_j)$ for each of the $j=1,\ldots,N$ (with N an arbitrary integer and $\mathbf{x}_1,\mathbf{x}_2,\ldots,\mathbf{x}_N$ arbitrary locations in the field). The matrix M^{-1} is the inverse of the $N\times N$ covariance matrix M,

$$M_{ij} \; \equiv \; \langle f(\mathbf{x}_i)f(\mathbf{x}_j)\rangle \; = \; \xi(\mathbf{x}_i-\mathbf{x}_j) \;, \tag{6}$$

in which the brackets $\langle \ldots \rangle$ denote an ensemble average. In effect, M is the generalization of the variance σ^2 in a one-dimensional normal distribution. As the matrix M is fully determined by the autocorrelation function $\xi(r)$, the Fourier transform of the power spectrum $P_f(k)$ of the fluctuations $f(\mathbf{r})$,

$$\xi(\mathbf{r}) \;=\; \xi(|\mathbf{r}|) \;=\; \int \frac{\mathrm{d}\mathbf{k}}{(2\pi)^3}\; P_f(k)\mathrm{e}^{-\mathrm{i}\mathbf{k}\cdot\mathbf{r}}\;. \tag{7}$$

This forms a statement for the full characterization of the statistical properties of a Gaussian random field f by the power spectrum $P_f(k)$.

Notice that the identity of $\xi(\mathbf{r})$ and $\xi(|\mathbf{r}|)$ is an expression of the homogeneity and isotropy of the stochastic process. It means that the stochastic properties of the process are absolutely equivalent at every location and in every direction. If – as it appears to be – nature indeed has endowed us with this fortunate circumstance with respec to the matter distribution in our observable Universe, justified to invoke the *Ergodic Theorem*. On the basis of the latter, it is indeed a meaningful exercise to infer estimates of intrinsic *ensemble averages* of physical quantities on the basis of spatial averages of these quantities over merely one realization. The only provision is that the realization should comprise many statistically independent volumes. Given the fact that the one observable Universe in which we live is all we have access to, this is a rather welcome trait.

3.2.1 *The Power Spectrum.* Thé *prime concept* in any (Gaussian) structure formation scenario is the density power spectrum $P(k)$. It embodies the relative contribution of density fluctuations at every relevant spatial scale $\lambda_k (= 2\pi/k)$ to the full density field. Concretely, this is expressed through the Fourier integral over $P(k)$,

$$\sigma_\circ^2 \;=\; \int \frac{\mathrm{d}\mathbf{k}}{(2\pi)^3}\; P(k)\;. \tag{8}$$

which yields the total local density fluctuation $\sigma_\circ = \langle \delta(\mathbf{r})^2 \rangle$. Having specified the density power spectrum $P(k)$, it is rather straightforward to set up Gaussian realizations of the the corresponding density field. All other (gravitional) physical fields and quantities are fully linked to the density field. The gravitational potential is related to the density field via the Poisson equation, and thus also the gravitational force field (see Eqn. 2). In addition, via the continuity equation and Euler equation we can then infer the resulting field of peculiar velocities (for both, see Fig. 16). While in general not trivial, the full velocity field can be uniquely and directly inferred in the linear regime (Peebles 1980).

3.2.2 *Reality of Primordial Gaussianity.* There are both physical and statistical arguments in favour of the assumption that the primordial density field in the Universe was indeed of a Gaussian nature. If the very early Universe went through an inflationary phase, quantum fluctuations would generate small-amplitude curvature fluctuations. The resulting density perturbation field is generally a Gaussian random process with a nearly Harrison–Zel'dovich scale-invariant primordial power spectrum. But, even while inflation did not occur, the density field $\delta(\mathbf{x})$ will be nearly Gaussian in the rather general case that its Fourier components $\hat{\delta}(\mathbf{k})$ are independent and have random phases There are both physical and statistical arguments in favour of the assumption that the primordial density field in the Universe was indeed of this nature. If the very early Universe went through an inflationary phase, quantum fluctuations would generate small-amplitude curvature fluctuations. The resulting density perturbation field is generally a Gaussian random process with a nearly Harrison–Zel'dovich scale-invariant primordial power spectrum. But, even while inflation did not occur, the density field $\delta(\mathbf{x})$ will be nearly Gaussian in the rather general case that its Fourier components $\hat{\delta}(\mathbf{k})$ are independent and have random phases (cf. Scherrer 1992).

Evidently, the final verdict rests on observations of the real world. Most fascinating has been the opening up of the window onto the surface of last scattering, analyzing and dissecting the cosmic microwave background with fantastic sensitivity and resolution. The imprint of the density and velocity fluctuations at the epoch of recombination on the last scattered photons has provided a direct impression of the primordial conditions from which structure in the Universe has arisen. The COBE-DMR maps of Sachs-Wolfe temperature fluctuations, on a relatively large angular scale of $\approx 7^\circ$ (spatial scales in the order of a Gpc), appear to be primarily of Gaussian character (e.g. Smoot et al. 1994). although recently there has been a flurry of claims for a definite non-Gaussian signature (e.g. Ferreira, Magueijo & Górski 1998). However, rather than being intrinsic this may be a systematic artefact (see Banday, Zaroubi & Górski 2000). In the meantime, also skymaps of the cosmic microwave background at the astrophysically very interesting scales – those whose angular size of a few arcminutes brings them within the realm of present-day recognizable features in the cosmic matter distribution – have become available through the impressive work of balloon borne experiments like Boomerang and Máxima-1. As yet, these high resolution maps of the CMB do not seem to indicate any significant and flagrant deviations from Gaussianity (Polenta et al. 2001, Wu et al. 2001).

In spite of these strong theoretical and observational arguments in favour of an intrinsically Gaussian primordial Universe, the impact of even a tiny genuine non-Gaussian signature could be tremendous. It would involve strong repercussions for the subsequent development of structure. In particular so for the nature of the first generation of objects in the Universe.

3.3. Gravitational Instability: Progressing Complexity

The early linear stages of structure formation have been succesfully and completely worked out within the context of the linear theory of gravitationally evolving cosmological density and perturbation fields (Peebles 1980). At every cosmologically interesting scale, it aptly and succesfully describes the situation in the early eons after the decoupling of radiation and matter at recombination. It still does so at present on those spatial scales at which the landscape of spatially averaged perturbations resembles a panorama of gently sloping hills. However, linear theoretical predictions soon fail after gravity surpasses its initial moderate impact and nonlinear features start to emerge. Soon thereafter, we start to distinguish the gradual rise of the complex patterns, structures and objects which have shaped our Universe into the fascinating world of astronomy.

3.3.1 *Going Nonlinear.* Once the evolution is entering a stage in which the first nonlinearities start to mature, it is no longer feasible to decouple the growth of structure on the various involved spatial and mass scales. Rapidly maturing small scale clumps do feel the effect of the large scale environment in which they are embedded. Neighbouring structures not only influence each other by external long-range gravitational forces but also by their impact on resulting matter flows. The morphology and topology of more gradually forming large-scale features will depend to a considerable extent on the characteristics of their content in smaller scale structures that were formed earlier on. This never-ending increasing level of complexity has proved to pose a daunting challenge for developing a fully consistent theoretical framework. No cosmogenic theory as yet has managed to integrate all acquired insights and observed impressions of the world around us.

3.3.2 *Stumbling upon Asymmetric Complexities.* A major and overriding complication in the efforts to frame a complete theory of

structure formation is the nature of the cosmic matter distribution itself. To a reasonably good approximation, a large proportion of astrophysically interesting objects possess readily exploitable intrinsic symmetries. Spherical, ellipsoidal and axisymmetric morphologies are amongst the most familiar in the astrophysical world. Often these function as the key towards unlocking the dynamics and kinematics of the object, its hidden internal structure and its evolution. Even a rather superficial evaluation of the cosmic foam (see e.g. Fig. 1) reveals the lack of any such useful symmetry for the cosmic matter distribution. The foamlike pattern itself is a supreme manifestation of an inherently complex system. Such complexity stems from the assumed origin of the cosmic matter distribution, a (linear) random and Gaussian primordial density and velocity fluctuation field (see former sections), subsequently moulded by the self-enforcing action of gravity.

3.3.3 *From global to partial views.* Lacking useful symmeteries, the study of structure formation has furnished an abundance of mutually complementary descriptions. Each focuses on one or more particular aspects, sometimes isolating those deemed relevant at the cost of neglecting others. Our ideas of the workings of the gravitational instability process have therefore progressed and been shaped by a plethora of theoretical and numerical approaches and techniques.

In terms of methodology deveral attitudes can be discerned. One approach seeks to formulate approximate descriptions of the full matter distribution, valid during either a restricted cosmic period or in the case of a few particular scenarios. The well-known Zel'dovich approximation, and its extensions, is the best example of this strategy. Others try to follow the full nonlinear evolution in a few conceptually simple configurations, hoping to isolate the mechanisms that appear to be the most crucial, and henceforth seeking to trace the possible imprint in the more complex world of reality. Still of enormous importance, representing the foundation on which most of our theories and descriptions are ultimately based, are the spherical model and the homogeneous ellipsoidal model (see section 4.2).

Following the Eulerian view of an evolving physical system, there have been impressive advances in following the nonlinear evolution of systems. This has produced a huge complex of advanced and complicated nonlinear perturbation analyses (for an extensive review, see Bernardeau et al. 2002). Although, these have proven to be particularly apt in uncovering and highlighting important statistical clues and signatures, thus defining essential tools for discriminating between viable formation scenarios, they are not so succesfull in guiding our physical intuition concerning

the unfolding of the complex patterns we have been discussing. These can hardly be characterized by the first orders of a full Eulerian perturbation series. The dynamical development accelerates so rapidly that any serious advance, in terms of the revelant timescales of the physical system, is posing an almost unsurmountable amount of effort.

Lagrangian approaches have proven to be the most fruitful approach in developing a physical intuition of the structural evolution during the more advanced stages. By following the matter elements on their path through the evolving cosmic matter field it is easier to appreciate the various forces and deformation tendencies acting on them. Mathematically, the conversion involves a transformation from an Eulerian to a Lagrangian time derivative,

$$\frac{d}{dt} \;=\; \frac{\partial}{\partial t} \;+\; \mathbf{v}\cdot\nabla \;, \tag{9}$$

where $\mathbf{v}$ is the velocity of the displacing fluid element.

The translation of self-gravitating systems into N-body computer simulations – the visibly most appealing, informative and widely employed technique – is the most widely known and exploited Lagrangian formulation for the issue of structure formation. In addition, they have undoubtedly been the most succesfull in capturing and shaping the imagination of a wide public, both of professional astronomers as well as of lay people. If we wish to appreciate the information and insights they can convey and, equally essential, appreciate their limitations it is beneficial to discuss them within a more general context.

3.4. Cosmic Equipment: N-body simulations

Arguably the most visible – scientifically as well as PR-wise – Lagrangian technique for studying cosmic structure formation is the use of computer models and calculations to simulate the evolution of cosmic structure through the force of gravity. They are unique in their ability to deal with the evolution of a system through the full range of linear up to highly nonlinear stages, in principal unconstrained and for any feasible configuration, independent of structural complexities and lack of helpful symmetries. Equally important is that the N-body approach is not principally restricted to purely gravitationally evolving systems. As evidenced by an array of computer codes developed over the past decade, it is rather straightforward to incorporate the influence and workings of a range of complicating (often dissipational) physical effects and processes. Sophisticated computer codes have been able to succesfully incorporate gravity, gasdynamical processes, atomic processes and a range of other

complicating factors into codes simulating the formation and evolution of cosmic structures.

With the exception of a few attempts towards an Eulerian implementation (e.g. Peebles 1987), efforts which gradually gain more ground with the inclusion of gas-dynamical and radiative processes, computational efforts have concerned N-body computer simulations. By nature, this involves a translation of the evolution of a system into a Lagrangian formulation, in which the computer gets instructed to follow the path of each particle into which the initial density field had been broken up. Fully nonlinear N-body computer simulations have produced the most readily visible, and directly appealing and accessible, descriptions of the way into which the gravitational instability process manages to mould the primordial universe into rich structural patterns.

Truely giant technological advances over the past decades have provided us with a comprehensive, physically justified and badly needed visual impression of the way into which the mutual influence of the combined gravitational forces unleashed by the matter perturbations throughout the cosmos works its way towards the emergence of structure. It has allowed the recognition of some basic mechanisms during the full nonlinear evolution of self-gravitating systems. The spatial patterns in the resulting particle distributions, as well as their kinematics and dynamics, provide us with an excellent testbed for testing and comparing quantitatively a large range of viable structure formation scenarios. However, they suffer from a variety of restricting effects, and we should be anxious not to overinterpret and/or overestimate the results of their performance.

Firstly, they can only go as far as allowed by the physics implemented into them. They will and cannot reveal basic new science to us. The full array of relevant physics, in particular when we get below scales of clusters of galaxies, is not confined to merely gravitational influences. Radiative processes, a complex interplay of various hydrodynamic processes, star formation processes, and the full impact of involved feedback interactions should make us realize the limitations of the outcome of the calculations. A large industry of new complex computer codes attempt to deal with at least a selection of these influences. They, however, also illustrate the daunting and possible unsurmountable challenges awaiting us in formulating a fully and uniquely defined scenario of structure formation, incorporating every necessary aspect of relevant physics.

Even when restricting ourselves to purely gravitational systems, strictly only applicable to scales at which nongravitational dissipation can be fully discarded as irrelevant, their results should still be considered as merely approximate and indicative. Their dynamic range is usually very

limited. This is true for the feasible spatial resolution, for the attainable mass resolution, as well as for the range of timescales that can be covered by them. As available computer memory will always restrict these, the full spatial range of fluctuations – even influential ones – can never be properly represented within a given cosmic region. A representation of the full primordial power spectrum of density fluctuations is beyond the grasp of any conceivable piece of equipment. It is therefore important that claims of validity of specific formation scenarios can never be fully justified. In addition, the limited dynamic range will also restrict the force resolution during the nonlinear evolution, which is particularly cumbersome on the smallest scales which produce the first nonlinear entities. In addition, we see a rapid increase in computational expense as we try to improve the resolution. Even though the availability of ultrafast computing machinery with ever growing huge memory capacity has expanded the achievements of cosmological N-body computer simulations to truely dramatic levels, the demands grow along with them, a pace not necessarily followed equally fast by the insights going along with them.

An additional restriction for N-body codes is that they can strictly only be applied to initial value problems (see section 3.5.3). For pure theoretical purposes, this does not pose a restriction. For a given cosmological and structure formation model the initial density and velocity field are specified and subsequently evolved and analyzed. However, when turning to the observed world, we may recognize that we are usually dealing with analyzing situations in which most information is available for the present epoch. In most cases this involves nonlinear structures for which we are not able to extrapolate in a straightforward and direct fashion towards the initial conditions. Hence we are unable to use N-body techniques towards analyzing the implications for the dynamics and evolution of the observed structures.

Possibly the most important limitation of computer calculations may be that the understanding of the dynamics and physics of the simulated systems is not significantly increased. *Simulations will not increase our understanding of dynamics without guidance from analytical approaches*, and therefore analytical approximations will be absolutely essential for that purpose. Along one direction, these do provide us with a handle to interpret the outcome of the computer experiments. Equally important, they direct us in defining the best possible computer models and configurations.

Even more important it is to be aware that full understanding involves the formulation of analytical descriptions, which should embody our insights into the systematics and regularities of a system, the true

purpose of scientific inquiry. Analytical descriptions should therefore be the preferred endgoal, the computer experiments, along with the ever growing body of available observations, are there to guide and sharpen our insight and intuition.

3.5. Cosmic Equipment:

Analytical Lagrangian schemes

While N-body simulations are the most popular specimen of Lagrangian description of gravitationally evolving systems, we may also attempt to mould our physical understanding into analytical Lagrangian formulations and approximations. For the study of gravitational pattern formation these have proven to be of overriding importance.

It is in particular the formulation of the first-order Zel'dovich approximation (Zel'dovich 1970) which has been of eminent importance in the study of cosmological structure formation. First and foremost, it did elucidate and explain qualitatively the basic tendencies of gravitational contraction in an evolving cosmos, in particular the tendency to do so anisotropically. In addition to its conceptual significance, it assumed extensive influence by providing computational cosmologists with the machinery to set up the initial conditions of cosmological N-body simulations for a wide variety of structure formation scenarios.

3.5.1 *the Zel'dovich Approximation.* By means of a Lagrangian perturbation analysis Zel'dovich (1970) proved, in a seminal contribution, that to first order – typifying early evolutionary phases – the reaction of cosmic patches of matter to the corresponding peculiar gravity field would be surprisingly simple, expressing itself in a plain ballistic linear displacement set solely by the initial (Lagrangian) force field. This framed the well-known *Zel'dovich approximation*.

In essence, the Zel'dovich approximation is the solution of the Lagrangian equations for small density perturbations ($\delta^2 \ll 1$). The solution is based upon the first-order truncation of the Lagrangian perturbation series of the trajectories of mass elements,

$$\mathbf{x}(\mathbf{q},t) \;=\; \mathbf{q} \;+\; \mathbf{x}^{(1)}(\mathbf{q},t) \;+\; \mathbf{x}^{(2)}(\mathbf{q},t) \;+\; \ldots \qquad (10)$$

when considering succesive terms of $|\partial(\mathbf{x}-\mathbf{q})/\partial\mathbf{q}|$. The truncation at the $\mathbf{x}^(1)$ term, then involves a simple linear prescription for the displacement of a particle from its initial (Lagrangian) comoving position $\mathbf{q}$ to an Eulerian comoving position $\mathbf{x}$, solely determined by the initial gravitational potential field,

$$\mathbf{x}(\mathbf{q},t) \;=\; \mathbf{q} \;-\; D(t)\nabla\Psi(\mathbf{q})\,. \qquad (11)$$

In this mapping, the time dependent function $D(t)$ is the growth rate of linear density perturbations, and the time-independent spatial function $\Psi(\mathbf{q})$ is related to the *linearly extrapolated* gravitational potential $\underline{\phi}$[2],

$$\Psi \;=\; \frac{2}{3Da^2\Omega H^2}\;\underline{\phi}\,. \tag{12}$$

This immediately clarifies that what represents the major virtue of the Zel'dovich approximation, its ability to assess the evolution of a density field from the primordial density field itself, through the corresponding linearly extrapolated (primordial) gravitational potential. While in essence a local approximation, the Lagrangian description provides the starting point for a far-reaching analysis of the implied density field development,

$$\begin{aligned}\frac{\rho(\mathbf{x},t)}{\rho^b} \;&=\; \left\|\frac{\partial\mathbf{x}}{\partial\mathbf{q}}\right\|^{-1} \;=\; \left\|\delta_{mn}-a(t)\psi_{mn}\right\|^{-1} \\ &=\; \frac{1}{[1-a(t)\lambda_1][1-a(t)\lambda_2][1-a(t)\lambda_3]}\,,\end{aligned} \tag{13}$$

where the vertical bars denote the Jacobian determinant, and λ_1, λ_2 and λ_3 are the eigenvalues of the Zel'dovich deformation tensor ψ_{mn},

$$\psi_{mn} \;=\; \frac{D(t)}{a(t)}\;\frac{\partial^2\Psi}{\partial q_m\partial q_n} \;=\; \frac{2}{3a^3\Omega H^2}\;\frac{\partial^2\underline{\phi}}{\partial q_m\partial q_n}\;, \tag{14}$$

which also implies the deformation matrix ψ_{mn} and its eigenvalues to evolve as $\psi_{mn}\propto D(t)/a(t)$. On the basis of above relation, it is then straightforward to find the intrinsic relation between the Zel'dovich deformation tensor ψ_{mn} and the tidal tensor T_{mn},

$$\psi_{mn} \;=\; \frac{1}{\frac{3}{2}\Omega H^2 a}\Big(\;\underline{T}_{mn} \;+\; \tfrac{1}{2}\Omega H^2\;\underline{\delta}\;\delta_{mn}\;\Big)\;, \tag{15}$$

where $\underline{\delta}$ and $\underline{T}_{mn}$ are the respective *linearly extrapolated* values of these quantities, i.e. $\underline{\delta}(t)\propto D(t)$ and $\underline{T}_{mn}\propto D/a^3$. Notice that, without loss of generality, we can adopt a coordinate system where the tidal tensor matrix T_{mn} is diagonal, from which we straightforwardly find a relation between the linearly extrapolated $\underline{\delta}$ and the deformation tensor, $\underline{\delta}(t)=a(t)\sum_m\lambda_m$.

[2]the *linearly extrapolated* gravitational potential is defined as the value the gravitational potential would assume in case the field would evolve according to its linear growth rate, $D(t)/a(t)$)

For appreciating the nature of the involved approximation, one should note that the continuity equation (by definition) is always satisfied by the combination of the Zel'dovich approximation and the mass conservation, yet that they do not, in general, satisfy the Euler and the Poisson equations (Nusser et al. 1991). Only in the case of purely one-dimensional perturbations does the Zel'dovich approximation represent a full solution to all three dynamic equations. Indeed, as we will emphasize in section 3.5.2, the core and essential physical significance of the Zel'dovich approximation can be traced to this implicit assumption of the tidal tensor T_{ij} being linearly proportional to the deformation tensor, and hence the velocity shear tensor.

The central role of the Zel'dovich formalism (for a review, see Shandarin & Zel'dovich 1989) in structure formation studies stems from its ability to take any arbitrary initial random density field, not constrained by any specific restriction in terms of morphological symmetry or seclusion, and mould it through a simple and direct operation into a reasonable approximation for the matter distribution at later nonlinear epochs. It allows one to get a rough qualitative outline of the nonlinear matter distribution solely on the basis of the given initial density field. While formally the Zel'dovich formalism comprises a mere first order perturbative term, it turned out to represent a surprisingly accurate description up to considerably more advanced evolutionary stages, up to the point where matter flows would start to cross each other.

3.5.2 *Local Lagrangian Approximations.* The Zel'dovich approximation (1970) belongs to a class of Lagrangian approximation schemes in which the nonlinear dynamics of selfgravitating matter is encapsulated into an approximate "local" formulation (Bertschinger & Jain 1994, Hui & Bertschinger 1996). In these approaches, the density, velocity gradient, and gravity gradient for each mass element behaves as if the element evolves independently of all the others once the initial conditions are specified. For instance, the evolution of a given mass element under the Zel'dovich approximation is completely determined once the initial expansion, vorticity, shear and density at this mass element are specified. The influence of other mass elements on the subsequent evolution of these quantities at this particular mass element is then assumed to be *fully encoded in the initial conditions*, and unaffected by the subsequent evolution of these other mass elements. Such a presumption may seem implausible in view of the unrestrained long-range gravitational force, yielding a noticeable influence from all other mass elements in the Universe. Yet, the success of the Zel'dovich approximation, having provided

a great deal of insight into the essentials of nonlinear evolution of density fluctuations, demonstrates how useful such schemes in fact can be.

The *locality* of these approximation schemes implies the evolution to be described by a set of *ordinary differential equations* for each mass element, with no coupling to other mass elements aside from those implied by the initial conditions. Note that N-body simulations are distinctly *non-local* Lagrangian descriptions. At every timestep the full gravitational potential set by the full cosmic matter distribution needs to be evaluated at the location of every mass element.

Assessing the basic Lagrangian fluid equations readily illuminates the character of these local approximations and elucidates the nature of some basic tendencies in the evolution of the matter distribution. The deformation of the evolving mass element at comoving location $\mathbf{x}$ is most straightforwardly encoded in the decomposition of the gradient of its velocity field $\mathbf{v}$ (the rate-of-strain tensor) into the expansion θ, the shear σ_{ij} and vorticity ω_{ij},

$$\frac{\partial v_i}{\partial x_j} \;=\; \frac{1}{3}\,\theta\delta_{ij} \;+\; \sigma_{ij} \;+\; \omega_{ij}\;, \tag{16}$$

in which the expansion θ is the trace of the velocity field gradient, $\sigma_{ij} = \sigma_{ji}$ the traceless symmetric part and $\omega_{ij} = -\omega_{ji} = \epsilon_{ijk}\omega^k$ the antisymmetric part (and ϵ_{ijk} the Levi-Civita symbol),

$$\theta \;=\; \nabla\cdot\mathbf{v} \quad\equiv\quad \frac{\partial v_1}{\partial x_1} + \frac{\partial v_2}{\partial x_2} + \frac{\partial v_3}{\partial x_3}\;, \tag{17}$$

$$\sigma_{ij} \quad\equiv\quad \frac{1}{2}\left(\frac{\partial v_i}{\partial x_j} + \frac{\partial v_j}{\partial x_i}\right) - \frac{1}{3}(\nabla\cdot\mathbf{v})\,\delta_{ij}\;, \tag{18}$$

$$\omega_{ij} \quad\equiv\quad \frac{1}{2}\left(\frac{\partial v_i}{\partial x_j} - \frac{\partial v_j}{\partial x_i}\right)\;, \tag{19}$$

in which $2\vec{\omega} = \nabla\times\mathbf{v}$. Under the assumption that the fluid is pressureless and irrotational (i.e. $\omega_i = 0$), the evolution of a fluid element, whose comoving trajectory is described by $\mathbf{x}(t)$ is specified by four first order differential equations. The first is the Lagrangian continuity equation, concerning the evolution of the density contrast δ,

$$\frac{d\delta}{d\tau} \;+\; (1+\delta)\;\theta \;=\; 0\;. \tag{20}$$

in which we have been following the formulation by Bertschinger & Jain (1994) and use the conformal time τ ($d\tau = dt/a$) as time coordinate, with the velocity $\mathbf{v}$ define as $\mathbf{v} = d\mathbf{x}/d\tau$.

The second and third equation describe the evolution of the trace and the traceless symmetric components of the velocity gradient tensor. The evolution of the trace of $\nabla_i v_j$, the expansion θ, is described by the *Raychaudhuri equation*,

$$\frac{d\theta}{d\tau} + \frac{\dot{a}}{a}\theta + \frac{1}{3}\theta^2 + \sigma^{ij}\sigma_{ij} = \ -4\pi G a^2 \rho^b \delta \ , \tag{21}$$

which follows from an evaluation of the Euler fluid equation (eqn. 3) in combination with the Poisson equation (eqn. 2). Similarly evaluating the symmetric part of the Euler equation we find that the shear σ_{ij} evolves according to

$$\frac{d\sigma_{ij}}{d\tau} + \frac{\dot{a}}{a}\sigma_{ij} + \frac{2}{3}\theta\sigma_{ij} + \sigma_{ik}\sigma^k_j - \frac{1}{3}\delta_{ij}(\sigma^{kl}\sigma_{kl}) \ = \ -T_{ij} \ , \tag{22}$$

where $T_{ij} \equiv \nabla_i\nabla_j\phi - (1/3)(\nabla^2\phi)$ is the gravitational tidal field (see Eqn. 19). Within the context of general relativity T_{ij} is the electric part of the Weyl tensor in the fluid frame. Evidently, as expected this equation is an expression of how the gravitational tidal field acts as a source term for inducing a shear component in the flow field.

The final "closure" relation is that relating the gravitational field ϕ and the density contrast δ, the Poisson equation (see Eqn. 2).

An interesting observation follows from evaluating the combination of the continuity and Raychaudhuri equation. This leads to a second order ordinary differential equation describing the evolution of the density contrast δ of a fluid element:

$$\frac{d^2\delta}{d\tau^2} + \frac{\dot{a}}{a}\frac{d\delta}{dt} = \frac{4}{3}(1+\delta)^{-1}\left(\frac{d\delta}{d\tau}\right)^2 + (1+\delta)\left(\sigma_{ij}\sigma_{ij} + 4\pi G\rho^b\delta\right) \ . \tag{23}$$

As Bertschinger & Jain (1994) noted by means of the *collapse term*, this equation shows that in the absence of vorticity the presence of a nonzero shear increases the rate of growth of density fluctuations (vorticity will inhibit this process). In other words, the rate of growth of δ gets amplified in the presence of shear. This conclusion holds independently of assumptions about the evolution of shear or tides and is due to the simple geometrical fact that shear increases the rate of growth of the convergence ($\propto -\theta$) of fluid streamlines. With zero shear and vorticity the velocity gradient tensor is isotropic, corresponding to uniform spherical collapse with radial motions towards some centre. Equation (23) then reduces to the exact equation for the evolution of the mean density in the spherical model. This evidently implies the growth of uniform spherical perturbations to be more slowly than more generic anisotropic configurations with a nonzero shear term.

Possibly the most telling illustration of this phenomenon can be found in the evolution of collapsing homogeneous ellipsoids. As can be found in section 4.2 (see Fig. 20) collapsing ellipsoids tend to slow down their collapse along the longest axis while they evolve far more rapidly along the shortest axis. Starting from a near spherical configuration, the net result is a rapid contraction into a highly flattened structure as the short axis has fully collapsed. When considering the complete (homogenous) ellipsoid as a "fluid" element, the correspondence with the reasoning above is straightforward.

The one remaining complication for transforming these Lagrangian fluid equations into *local* descriptions involves the development of the driving shear term σ_{ij}. Evidently, its evolution depends on the behaviour of the gravitational tide T_{ij}. Obviously, its value is generically determined by the full matter distribution throughout the cosmic volume. From a detailed evaluation of the issue in its Lagrangian context, its complexity may be seen as one relating to a highly complicated ánd *non-local* expression involving H_{ij}, the Newtonian limit of the magnetic part of the Weyl tensor in the fluid frame (see Bertschinger & Jain 1994).

Hui & Bertschinger (1996) demonstrated how the Zel'dovich approximation can be incorporated within this context of reducing the problem to a local one by invoking a specific approximation. In essence it involves an implicit decision to discard H_{ij} and the full evolution equation for T_{ij} altogether and replace it by the explicit expression for the evolution of the tidal tensor T_{ij} in the linear regime of clustering, in which T_{ij} is linearly proportional to the shear σ_{ij},

$$T_{ij} \;=\; -\frac{3\Omega H^2}{2Hf(\Omega)}\;\sigma_{ij} \tag{24}$$

where $f(\Omega) \approx \Omega^{0.6}$. From this consideration we can straightforwardly appreciate that the Zel'dovich approximation does not obey the Poisson equation. As a consequence, it does represent an exact approximation in the case of a plane-parallel density disturbance as long as the corresponding particle trajectories have not yet intersected others, but breaks down in the case of two- or three-dimensional perturbations and in general as soon as the particle tracks have crossed. One well-known implication is that the Zel'dovich approximation gives incorrect results for spherical infall.

With the Zel'dovich approximation basically concerning the first order solution in Lagrangian perturbation theory, various extensions and elaborations were formulated attempting to extend the theory to a higher order, futhering its range of applicability towards more evolutionary more progressive situations. As can be appreciated from Eqn. (24),

the Zel'dovich approximation essentially involves a truncation of the set of Lagrangian fluid equations through an implicit choice for T_{ij}, equating it linearly proportional to σ_{ij}. This implies a tinkering with the Raychaudhury and shear evolution equations. In the Zel'dovich approximation one therefore need not integrate the tidal evolution equation, the gravity field on a mass element given by a simple extrapolation of initial conditions.

Pursuing along the same track, Bertschinger & Jain (1994) and Hui & Bertschinger (1996) extended this to higher-order schemes, both approximations involving the integration of the exact Raychaudhuri and shear evolution and shifting the approximation to the level of the tidal evolution equation. Bertschinger & Jain (1994) tried to make the very specific assumption of setting the magnetic part of the Weyl tensor $H_{ij} = 0$, thus characterized as the "nonmagnetic" approximation. Subsequent work showed that this does not adhere to a well-defined or easily recognizable generic situation. Along the same lines, Hui & Bertschinger (1996) defined another approximate scheme, the "local tidal" approximation. This they showed to followed more accurately the predictions of the homogeneous ellipsoidal model than the "nonmagnetic" approximation (Bertschinger & Jain 1996) and the Zel'dovich approximation. Interestingly, while the "nonmagnetic" approximation implied collapse into "spindle" like configurations as the generic outcome of gravitational collapse, the more accurate "local tidal" approximation appears to agree with the Zel'dovich approximation in that "planar" geometries are more characteristic.

A range of additional approximate schemes, mostly stemming from different considerations, were introduced in a variety of publications. Most of them try to deal with the evolution of high-density regions after the particle trajectories cross and self-gravity of the resulting matter assemblies assumes a dominating role. Notable examples of such approaches are the adhesion approximation (Kofman, Pogosyan & Shandarin 1990), the frozen flow approximation (Matarrese et al. 1992), the frozen potential approximation (Brainerd, Scherrer & Villumsen 1993), the truncated Zel'dovich approximation (Coles, Melott & Shandarin 1993), the smoothed potential approximation (Melott, Sathyaprakash & Sahni 1996) and higher order Lagrangian perturbation theory (Melott, Buchert & Weiss 1995). The elegant generalization of the Zel'dovich approximation by Giavalisco et al. (1993) will be described later within the context of the mixed boundary conditions problem (next section). An extensive and balanced review of the various approximation schemes may be found in Sahni & Coles (1995).

3.5.3 *Mixed Boundary Conditions.* For pure theoretical purposes, cosmological studies may be restricted to considerations involving pure *initial conditions* problems. For a given cosmological and structure formation model the initial density and velocity field are specified, and its evolution subsequently evolved, either by means of approximate schemes or by for instance by means of fully nonlinear N-body computer simulations. The outcome of such studies are then usually analyzed in terms of a variety of statistical measures. These are then compared to the outcome of the same tests in the case of the observed world.

Alternatively, we may recognize that in many specific cosmological studies we are dealing with problems of *mixed boundary conditions*. Part of the large scale structures and velocities in the universe may have been measured at the present epoch, while some in the limit of very high redshift (e.g. the CMB). Typically, one seeks to compute the velocity field consistent with an observed density structure at the present epoch. Conversely, one may wish to deduce the density from the measured peculiar galaxy velocities. Evidently, the position and velocities of objects at the present epoch are intimately coupled through the initial conditions.

In the linear regime, the problem of mixed boundary conditions is easily solved. However, in the case of the interesting features in e.g. the cosmic foam the density of galaxies can reach values considerably larger than unity, even on scales of $\sim 10h^{-1}$Mpc. The associated velocities therefore need to be computed nonlinearly. As may be obvious from the earlier discussions, the nonlinear computation of gravitational instabilities in the case of arbitrary configurations is everything but trivial.

N-body codes are rendered obsolete in such issues involving mixed boundary conditions. Their application is restricted to initial value problems. A further complication of the nonlinear problem of mixed boundary conditions is the multivalued nature of the solutions. Orbit crossing makes identification of the correct orbits difficult, and impossible after virialization has erased the memory of the initial conditions. In practice, one is therefore often restricted to laminar flow in the quasi-linear regime. Perturbations may have exceeded unity but orbit crossing has not yet obstructed a one-to-one correspondence between the final and initial positions.

Evidently, the Zel'dovich approximation forms a good first-order approach towards dealing with such issues. Indeed, it was applied to the nonlinear problem of mixed boundary conditions, tested and calibrated using N-body simulations, by Nusser et al. (1991) and Nusser & Dekel (1992). In terms of the physics of the nonlinear systems, a profound suggestion was forwarded by Peebles (1989, 1990). He noticed that mixed boundary conditions naturally lend themselves to an application

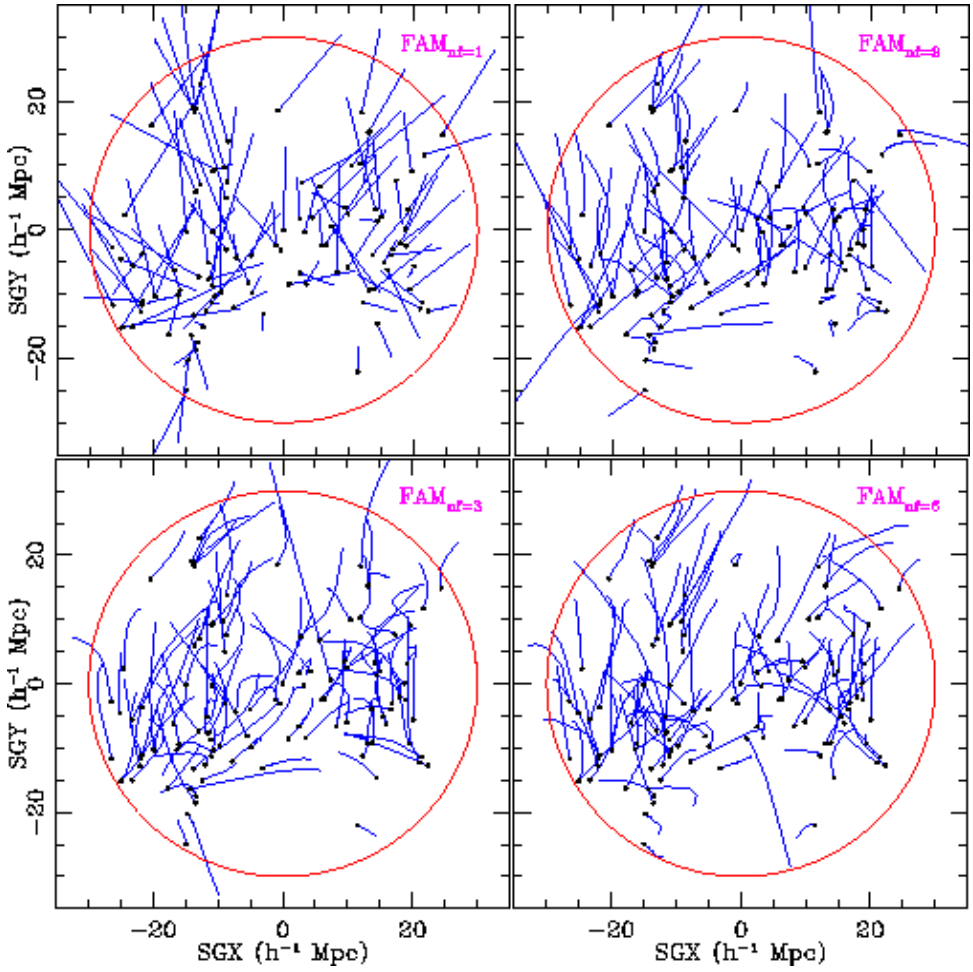

Figure 17. Projected orbits reconstructed by the Fast Action Method implementation of the Least Action Principle procdure. Four different levels of approximation are shown. The black dots represent the final (present) positions for each object. The blue lines indicate the trajectories followed by the objects as a function of time. The top-left frame shows FAM reconstructed orbits with $N_f = 1$ (Zel'dovich approximation). Subsequently shown are $N_f = 2$ (top right), $N_f = 3$ (lower left) and $N_f = 6$ (lower right). From Romano-Díaz, Branchini & van de Weygaert 2002.

of Hamilton's principle. Given the action S of a system of particles

$$S \;=\; \int_0^{t_0} L dt \;=\; \int_0^{t_0} dt \;\sum_i \,[\frac{1}{2} m_i a^2 \dot{\mathbf{x}}_i^2 - m_i \phi(\mathbf{x}_i)\;]\;, \qquad (25)$$

in which L is the Lagrangian for the orbits of particles with masses m_i and comoving coordinates x_i. The *exact* equations of motion for the

particles can be obtained from stationary variations of the action S. On the basis of Hamilton's principel one therefore seeks stationary variations of an action subject to fixed boundary conditions at both the initial and final time. Confining oneself to feasible approximate evaluation in this *Least Action Principle* approach, one describes the orbits of particles as a linear combination of suitably chosen universal functions of time with unknown coefficients specific to each particle presently located at a position $\mathbf{x}_{i,0}$,

$$\mathbf{x}_i(D) \;=\; \mathbf{x}_{i,0} \;+\; \sum_{n=1}^{N_f} \; q_n(D)\; \mathbf{C}_{i,n} \;. \tag{26}$$

In the above formulation we choose to use the linear growth mode $D(t)$ as time variable. The functions $q_n(D)$ form a set of N_f time-dependent basis functions, while $\mathbf{C}_{i,n}$ are a set of free parameters which are determined from evaluating the stationary variations of the action. The basis functions $q_n(D)$ are constrained by two orbital constraints. To ensure that at the present time the galaxies are located at their observed positions $\mathbf{x}_i(D=1) = \mathbf{x}_{i,0}$ we set the boundary constraint $q_n(1) = 0$. The other boundary condition concerns the constraint that the peculiar motions at early epochs ($D = 0$) have to vanish, which in turn ensures initial homogeneity, i.e. $\lim_{t\to 0} m_i a^2 \dot{\mathbf{x}}_i = 0$.

The choice of base functions essentially determines the approximation scheme. Originally Peebles (1989, 1990) chose the base functions $q_n(D) = f_n(t)$ to be polynomials of the expansion factor $a(t)$. For small systems this leads to a tractable problem, but for larger systems it becomes exceedingly difficult to apply because of confusions between multivalued solutions. In an elegant contribution, Giavalisco et al. (1993) merged the Zel'dovich approximation into the *Least Action Principle* (LAP) scheme by expanding the formalism into one where the base functions are higher order polynomials of the linear growth function $D(t)$. In the limit of small displacements, the LAP procedure would then reproduce the Zel'dovich approximation. The higher order terms remove the separability of the temporal and spatial dependence in the Zel'dovich approximation, and allowing arbitrary displacements so that the orbits can be determined to any accuracy. This turned out to yield a rapidly converging scheme, even for highly nonlinear perturbations.

A further improvement of the basic scheme of Giavalisco et al. (1993) was introduced by Nusser & Branchini (2000). They based their computational evaluations of the action on invoking the functions $p_n(D) \equiv dq_n/dD$ and setting them equal to conveniently defined polynomials of the growth factor D. In addition, their *Fast Action Method* (FAM)

involved a computational optimization through the evaluation of the gravitational potential by means of a gravitational TREECODE. This yielded a procedure allowing the reconstruction of the orbits of $10^4 - 10^5$ mass tracing objects back in time and reconstruct the peculiar velocities of the objects well beyond the linear regime. Its performance can be appreciated from Figure 17 (from Romano-Díaz, Branchini & van de Weygaert 2002), in which 4 panels show how the increasing levels of orbit expansion manage to probe ever deeper into the nonlinear regime. In particular, one can infer how the Zel'dovich approximation is naturally invoked as the 1st-order step (top left panel).

4. THE SHAPING FORCE OF GRAVITY: ... Pattern Formation and Anisotropic Collapse

A characteristic aspect of the gravitational formation process is its tendency to develop via stages in which the cosmic matter distribution settles into striking anisotropic patterns. Seeking to identify the cause behind this shaping tendency in the evolution of cosmic structure readily leads to the generic anisotropic nature of the gravitational force field induced by a inhomogeneous and essentially stochastic matter distribution as the ultimate culprit.

Anisotropic tidal effects are intrinsic to any cosmological scenario involving density deviations from the globally uniform Friedmann-Robertson-Walker Universe. This may be readily appreciated from considering the force field within a limited and bounded region of space, a "patch" (Bond & Myers 1996a). The spatial variation of the implied force field translates into non-zero off-diagonal elements in the tidal force tensor, so that the gravitational acceleration $\mathbf{g}(\mathbf{x})$ with respect to a position $\mathbf{x}_c$ can, to first order, be written as

$$\begin{aligned} g_i(\mathbf{x},t) &= g_i(\mathbf{x}_c,t) + \\ & a(t)\sum_{j=1}^{3}\left\{\frac{1}{3a}(\nabla\cdot\mathbf{g})(\mathbf{x}_c,t)\,\delta_{ij} - T_{ij}\right\}(x_j - x_{c,j}) \ , \end{aligned} \quad (27)$$

where $a(t)$ is the expansion factor of the universe and δ_{ij} is the Kronecker delta. Hence, in addition to the zeroth-order bulk acceleration $\mathbf{g}(\mathbf{x}_c) = -\nabla\phi/a$ within a bounded cosmic region ("patch"), the local acceleration is modified by two terms. The divergence term $\nabla\cdot\mathbf{g}$ represents the radial and thus spherically symmetric infall or outflow around $\mathbf{x}_c$. It is the principal agent in determining the collapse or expansion of the regional matter distribution, yet by virtue of its spherically symmetric character

preserves its initial shape. The latter is affected by the quadrupole tidal tensor T_{ij}, the trace-free part of $-\partial g_i/\partial r_j = \partial^2\phi/\partial r_i \partial r_j$ ($\mathbf{r}(t) = a(t)\mathbf{x}(t)$ being the physical position),

$$\begin{aligned} T_{ij}(\mathbf{x}) &\equiv -\frac{1}{2a}\left\{\frac{\partial g_i}{\partial x_i} + \frac{\partial g_j}{\partial x_j}\right\} + \frac{1}{3a}(\nabla\cdot\mathbf{g})\,\delta_{ij} \\ &= \frac{1}{a^2}\left\{\frac{\partial^2\phi}{\partial x_i \partial x_j} - \frac{1}{3}\nabla^2\phi\;\delta_{ij}\right\}\,. \end{aligned} \tag{28}$$

Usually higher order contributions to the tidal field are neglected, and attention is restricted to the quadrupolar component T_{ij}. The decisive role of the tidal field in determining the fate and final shape of an evolving structure has been most consistently and elaborately adressed in a seminal series of papers by Bond & Meyers (1996a,b,c). They developed an elaborate "peak-patch" formalism in particular focussing on cosmic regions centered on and near peaks in the primordial density field. In line with their treatment, and in order to appreciate and exploit the impact of a force field whose configuration defines a nontrivial and complex spatial pattern, it proves beneficial to introduce a (asymptotic) distinction between "internal" and "external" gravitational fields. While such a bimodal partition is rather awkward and artificial in the case of a random density fluctuation field – with density features embedded within a hierarchy of spatially larger encompassing density perturbations – and would conform to reality solely in the case of clearly distinct and spatially disjunct objects, it emphasizes fundamentally different modes in which the gravitational impact is operating and effected. The "internal" field concerns the gravitational impact of the internal matter content on an emerging structure, the "external" that of the evolving external density distribution.

4.1. *Tides in our Cosmic Backyard*

That tidal influences are indeed at work on cosmologically relevant scales has been demonstrated on the basis of what may arguably be considered their most straightforward impact. The spatial variations in gravitational force within a particular cosmic region induce a peculiar velocity field exhibiting corresponding spatial variations, manifesting itself as velocity shear. On the basis of a careful analysis of peculiar velocities of galaxies in the Local Supercluster, Lilje, Yahil & Jones (1986) estimated that at our cosmic location the velocity shear had a value in the order of $\sim 200\,\mathrm{km/s}$ with respect to the Virgo Cluster. In a bold leap of imagination they argued that the source of this shear had to be a considerable mass concentration at a distance of ~ 3 times the distance

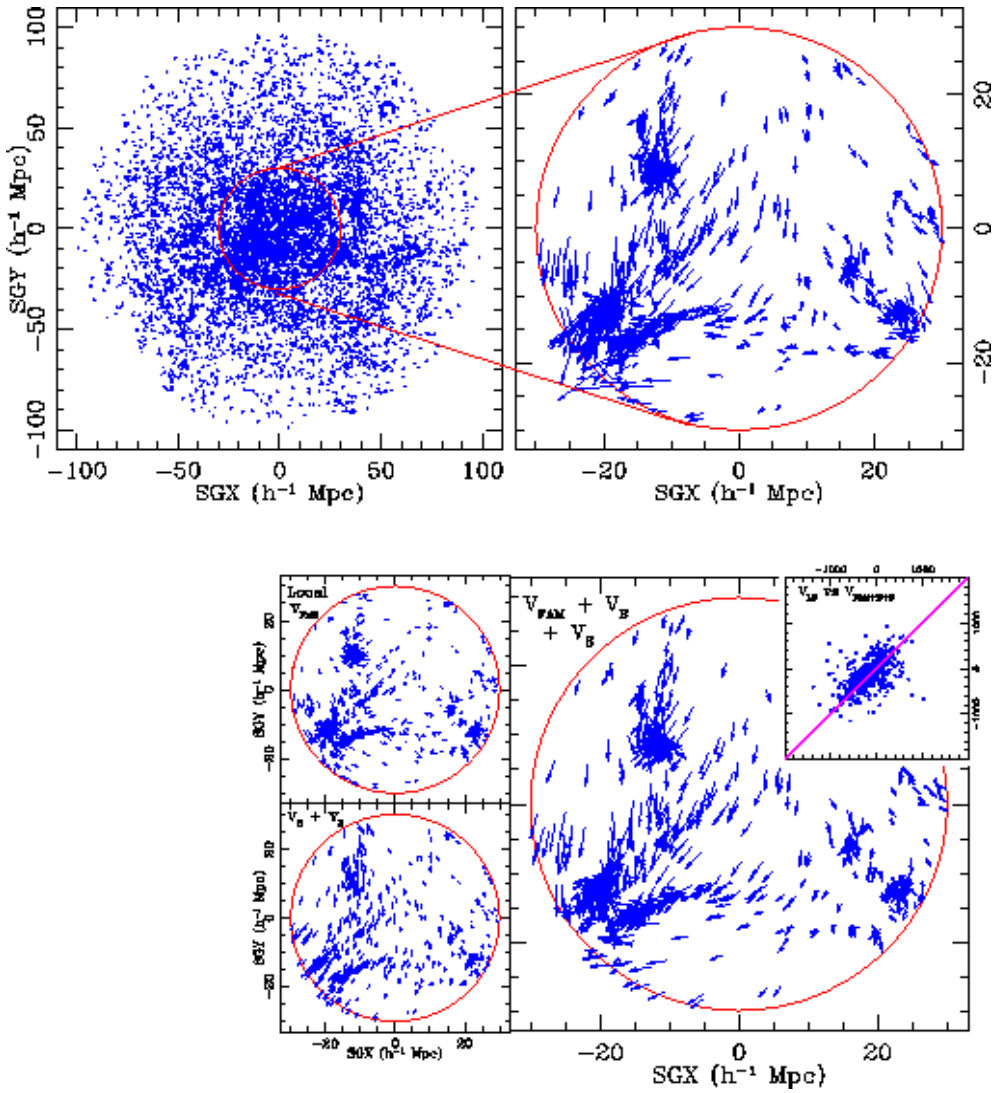

Figure 18. Left: The analyzed "mock" Local Supercluster + PSCz galaxy distribution, with the sample of "mock" measured Local Supercluster peculiar velocities. Right: FAM analysis of local velocity field: restricted to local cosmic volume (top left). Including full PSCz volume: external dipole and quadrupole components (D-Q, bottom left). Total of locally induced velocities + D-Q external contribution (right frame): agreement with full "mock" velocities illustrated by scatter plot (insert). From Romano-Díaz, Branchini & van de Weygaert 2002.

to the Virgo Cluster, soon thereafter confirmed when Lynden-Bell et al. (1988). The latter managed to uncover a local velocity flow towards a "Great Attractor" from a painstaking analysis of a sample of peculiar

velocities of galaxies within a radius of $\sim 60h^{-1}$Mpc around the Local Group. Huge efforts have since been invested into improving the quality of both the initially spatially rather limited and coarsely sampled local cosmic velocity field and the ever more sophisticated tools with which one manages to extract cosmologically meaningful information. Recently, this allowed Hoffman et al. (2001) to produce an evocative reconstruction of the tidally induced component of the cosmic velocity field out to a distance of $\sim 60h^{-1}$Mpc. The prominent dynamical role of this local field can be particularly appreciated from a closer assessment of its inferred configuration, which appears to lead to the tentative indication of the Shapley Concentration marking an immense matter concentration of $\approx 1 - 3 \times 10^{17}\mathrm{M}_{\odot}$ which apparently stretches out its dynamical clout out into our own cosmic realm (see section 2.4). Other studies involving higher quality velocity measurements, yet a less sophisticated dynamic model of the Local Universe, do not yet endorse such far-reaching conclusions (Tonry et al. 2000). However, there are strong overriding theoretical arguments for significant tidal influences stretching over scales in the order of $\approx 100h^{-1}$Mpc. For a set of viable structure formation scenarios, Romano-Díaz, Branchini & van de Weygaert (2002) assessed in how far the velocities in a local region of space would be subject to significant and noticeable tidal forces, orginating from matter concentrations enclosed within a surrounding region modelled after the sampling volume of the PSCz galaxy redshift sample (see Fig. 18). Taking into account subtle nonlinear effects in the local velocity field through the application of an advanced Least Action Principle reconstruction technique (Peebles 1989, Nusser & Branchini 2000) they managed to disentangle the "internal" influence in the local velocity from the that of "external" tidal influences induced by the outer mass concentrations, thus showing that the contribution by an external dipolar as well as a quadrupolar gravity component are necessary, yet sufficient, to account for the full velocity field in our local cosmic neighbourhood.

4.2. The Homogeneous Ellipsoidal Model

As so often, understanding the essence of a physical phenomenon – here the anisotropic patterns in the matter distribution, walls and filaments – is obtained most readily and lucidly through the assessment an asymptotic idealization of more realistic and complex configurations.

The bare essence of the driving mechanism behind the formation of cosmic walls and filaments is possibly best appreciated in terms of the dynamical evolution of homogenous ellipsoidal overdensities. In particular, the early work by Icke (1972, 1973) elucidated transparently the crucial

characteristics of their development and morphology. On the basis of an assessment of the collapse of homogeneous ellipsoids in an expanding FRW background Universe – following the formalism of Lynden-Bell (1964) and Lin, Mestel & Shu (1965) – he came to the conclusion that flattened and elongated geometries of large scale features in the Universe should be the norm. This description intrinsically involves the self-amplifying effect of a collapsing and progressively flattening isolated ellipsoidal overdensity. Quintessential was Icke's observation that gravitational instability not only involves the runaway gravitational collapse of any cosmic overdensity, but that it has the additional basic attribute of *inevitably amplifying any slight initial asphericity during the collapse*. In order to appreciate the dynamics behind the process, and be able to assess its action within more complex situations, it is insightful to focus in some detail on the evolution of homogeneous ellipsoids.

4.2.1 *Homogeneous Ellipsoidal Model: the Formalism.* The ellipsoidal approximation involves an ellipsoidal region with a triaxially symmetric geometry, described in terms of its principal axes c_1, c_2 and c_3. The matter density in the interior of the ellipsoid has a constant value of ρ^{ell}, and the ellipsoid is embedded in a background with a density ρ^b. While the basic formalism assumes an isolated ellipsoid, we seek to extend this to a more generic configuration in which the ellipsoidal object is subjected to an external tidal field induced by matter fluctuations beyond its immediate neighbourhood. It should be noted that in principle such a configuration is a contrived one, the existence of an external field implying a *contradictio in terminis* with respect to the assumption of a homogeneous background. The intention therefore is to use this as a description reasonably approximating and illuminating relevant effects. In the presence of an this external potential contribution, the total gravitational potential $\Phi^{(tot)}(\mathbf{r})$ in the interior of a homogeneous ellipsoid is given by

$$\Phi^{(tot)}(\mathbf{r}) \;=\; \Phi_b(\mathbf{r}) \;+\Phi^{(int,ell)}(\mathbf{r}) \;+\Phi^{(ext)}(\mathbf{r}) \;, \qquad (29)$$

in which (r_1, r_2, r_3) figure as the coordinates in an arbitrary Cartesian coordinate system. In this, we have decomposed the total potential $\Phi^{(tot)}(\mathbf{r})$ into three separate (quadratic) contributions,

- The potential contribution of the homogeneous background with universal density $\rho^b(t)$,

$$\Phi_b(\mathbf{r}) \;=\; \frac{2}{3}\pi G\rho^b \;(r_1^2 + r_2^2 + r_3^2) \;. \qquad (30)$$

- The interior potential $\Phi^{(int,ell)}(\mathbf{r})$ of the ellipsoidal entity, superimposed onto the homogeneous background,

$$\begin{aligned}\Phi^{(int,ell)}(\mathbf{r}) &= \frac{1}{2}\sum_{m,n}\Phi^{(int,ell)}_{mn}r_m r_n \\ &= \frac{2}{3}\pi G(\rho^{ell}-\rho^b)\ (r_1^2+r_2^2+r_3^2)\ +\ \frac{1}{2}\sum_{m,n}T^{(int)}_{mn}r_m r_n\ ,\end{aligned} \tag{31}$$

  with $T^{(int)}_{mn}$ the elements of the traceless internal tidal shear tensor,

$$T^{(int)}_{mn}\ \equiv\ \frac{\partial^2\Phi^{(int,ell)}}{\partial r_m\partial r_n}-\frac{1}{3}\nabla^2\Phi^{(int,ell)}\ \delta_{mn}\ . \tag{32}$$

- The externally imposed gravitational potential $\Phi^{(ext)}$. We assume that the external tidal field not to vary greatly over the expanse of the ellipsoid, so that we can presume the tidal tensor elements to remain constant within the ellipsoidal region (cf. Dubinski & Carlberg 1991). In this approximation, the elements $T^{(ext)}_{mn}$ of the external tidal tensor correspond to the quadrupole components of the external potential field, with the latter being a quadratic function of the (proper) coordinates $\mathbf{r}=(r_1,r_2,r_3)$:

$$\Phi^{(ext)}(\mathbf{r})\ =\ \frac{1}{2}\sum_{m,n}T^{(ext)}_{mn}r_m r_n\ . \tag{33}$$

  with the components $T^{(ext)}_{mn}$ of the external tidal shear tensor,

$$T^{(ext)}_{mn}(t)\ \equiv\ \frac{\partial^2\Phi^{(ext)}}{\partial r_m\partial r_n}\ , \tag{34}$$

  which by default, because of its nature, is a traceless tensor. Note that the quadratic form of the external potential is a necessary condition for the treatment to remain selfconsistent in terms of the ellipsoidal formalism.

As the ellipsoidal formalism does not include any self-consistent external potential, we have to impose it ourselves in an artificial way, including a specified time evolution of the tidal tensor components (see discussion in section on external tidal action, eqn. 49 to 51), In essence, we impose an artificial external tidal field based on the assumption that the background in the immediate vicinity of the ellipsoid remains homogenous and that the external structures engendering the tidal field are located

out at distances sufficiently far away from the ellipsoidal entity. This warrants the validity of the approximation by the quadratic equations, and assures that these external entities themselves are untouched themselves by the ensuing evolution of the object.

The quadratic expression for the internal ellipsoidal potential contribution $\Phi^{(int,ell)}$ can be cast into a simplified form by choosing a convenient coordinate system in which the coordinate axes coincide with the principal axes of the ellipsoid. In this case, the expression for the potential of an ellipsoid with effective density $(\rho^{ell} - \rho^b)$ and axes c_1, c_2 and c_3 reduces to (Lyttleton 1953)

$$\Phi^{(int,ell)}(\mathbf{r}) = \pi G\ (\rho^{ell} - \rho^b) \sum_m \alpha_m r_m^2\ , \tag{35}$$

where the coefficients α_m are determined by the shape of the ellipsoid,

$$\alpha_m = c_1 c_2 c_3 \int_0^\infty (c_m^2 + \lambda)^{-1} \prod_{n=1}^{3} \frac{1}{\sqrt{c_n^2 + \lambda}} \mathrm{d}\lambda\ . \tag{36}$$

As a consequence of the Poisson equation the α_m's obey the constraint: $\sum_{m=1}^3 \alpha_m = 2$. Also, we see that the components of the internal tidal shear tensor are given by,

$$T_{mn}^{(int)} \ = \ 2\pi G(\rho^{ell} - \rho^b) \left(\alpha_m - \frac{2}{3}\right)\ \delta_{mn}\ . \tag{37}$$

It is easy to appreciate that in the case of a spherical perturbation all three α_m's are equal to 2/3, reproducing the well-known fact that in such case the internal tidal tensor contributions need to vanish.

From the quadratic nature of the total potential, the acceleration of a mass at a position $\mathbf{r}$ inside the ellipsoid, $-\nabla\Phi(\mathbf{r})$, is a linear function of $\mathbf{r}$,

$$\frac{d^2 r_m}{dt^2} \ = \ -\frac{4\pi}{3} G\rho^b r_m(t) \ - \ \sum_n \Phi_{mn}^{(int,ell)} r_n(t) \ - \ \sum_n T_{mn}^{(ext)} r_n(t)\ . \tag{38}$$

This leads to a linear relation between the location $\mathbf{r}(t) = (r_1(t), r_2(t), r_3(t))$ of a mass element at time t and its initial (proper) position $\mathbf{r}_i = (r_{1,i}, r_{2,i}, r_{3,i})$,

$$r_m(t) \ = \ \sum_k R_{mk}(t) r_{k,i} \tag{39}$$

in which the matrix $R_{mn}(t)$ is a spatially uniform matrix, solely dependent on time. Notice that the initial matrix $R_{mn}(t)$ is a diagonal

matrix, $R_{mn}(t_i) = R_m(t_i)\delta_{mn}$. By combining Eqn. (38) and Eqn. (39), the evolution of the matrix elements R_{mk} is found to be described by

$$\frac{d^2R_{mk}}{dt^2} \;=\; -\frac{4\pi}{3}\pi G R_{mk} \;-\; \sum_n \Phi^{(int,ell)}_{mn} R_{nk} \;-\; \sum_n T_{mn}R_{nk} \qquad (40)$$

This also implies that similar points in concentric ellipsoidal shells behave in the same way, while the ellipsoid will remain homogeneous.

To appreciate the ramifications for the shape of an evolving ellipsoidal object, we exclude the torqueing and angular momentum inducing effects of the external tidal field. To this end, we make the simplifying assumption of the principal axes of the external tidal tensor to be aligned along the principal axes of the inertia tensor I_{ij} of the ellipsoid. Of course, in realistic situations we would not expect to find such a perfect alignment between the tidal and the inertia tensors. Yet, there is a significant correlation between orientation of tidal field and orientation of the principal axes of a peak/dip in a Gaussian random field. In particular, it implies a tendency to align the strongest tidal field component along the smallest axis (Van de Weygaert & Bertschinger 1996).

The principal axis alignment implies – when defining the coordinate system by the principal axes of the ellipsoid – that all off-diagonal (external) tidal tensor elements vanish, $T^{(ext)}_{mn} = T^{(ext)}_{mm}\delta_{mn}$. This implies $\sum_n T^{(ext)}_{mn} R_{nk} = T^{(ext)}_{mm} R_{mk}$. The resulting equation for the evolution of the matrix elements R_{mk} is then described by the second order diffential equation,

$$\frac{d^2R_{mk}}{dt^2} \;=\; -2\pi G\,\left[\alpha_m\rho^{ell} + (\frac{2}{3} - \alpha_m)\;\rho^b\;\right] R_{mk} \;-\; T^{(ext)}_{mm} R_{mk}\;. \quad (41)$$

Evidently, the coupling between the different components R_{mk} vanishes. As they are initially equal to zero this implies the non-diagonal elements $R_{mk}(t)$ to remain so, $R_{mk}(t) = R_m(t)\delta_{mn}$. At time t, a mass element initially at (proper) position $\mathbf{r}_i = (r_{1,i}, r_{2,i}, r_{3,i})$ has therefore moved to position $\mathbf{r}(t) = (r_1(t), r_2(t), r_3(t)) = (R_1(t)r_{1,i}, R_2(t)r_{2,i}, R_3(t)r_{3,i})$, in which the functions $R_m(t)$ evolve according to

$$\frac{d^2R_m}{dt^2} \;=\; -2\pi G\,\left[\alpha_m\rho^{ell} + (\frac{2}{3} - \alpha_m)\;\rho^b\;\right] R_m \;-\; T^{(ext)}_{mm} R_m\;. \qquad (42)$$

The evolution of the ellipsoid is thus fully encapsulated in terms of the the functions $R_1(t)$, $R_2(t)$ and $R_3(t)$, which in essence should be seen as scale factors of the principal axes of the ellipsoid,

$$c_m(t) \;=\; R_m(t)c_{m,i}\;. \qquad (43)$$

For any initial configuration of a homogeneous ellipsoid embedded in a FRW background Universe with current cosmic density parameter $\Omega_\circ$ and Hubble parameter $H_\circ$, specified by its initial characteristics at cosmic expansion factor a_i,

- The initial principal axes, (c_1, c_2, c_3).
- The initial ellipsoidal density ρ_i^{ell}, in terms of density contrast δ_i

$$\delta_i \equiv \frac{\rho_i^{ell} - \rho^b{}_i}{\rho^b{}_i} , \tag{44}$$

with respect to the background Universe with initial cosmic density

$$\rho^b{}_i = \frac{3}{2}\,\Omega_\circ H_\circ \left(\frac{a_\circ}{a_i}\right)^3 \tag{45}$$

the evolution of the scale factors $R_m(t)$ can be fully recovered once the boundary conditions have been set, i.e.

- The initial scale factors,

$$R_m(t_i) = 1 \tag{46}$$

for $(m = 1, 2, 3)$.

- The initial velocity perturbation,

$$\begin{aligned} v_m(t_i) = (dR_m/dt)\, r_{m,i} &= v_{Hubble,m}(t_i) + v_{pec,m}(t_i) \\ &= H_i\, R_m r_{m,i} + v_{pec,m}(t_i) , \end{aligned} \tag{47}$$

for $(m = 1, 2, 3)$, which when choosing to follow the growing mode solution of linear perturbation theory (Peebles 1980) is given by

$$\begin{aligned} v_{pec,m}(t_i) &= \frac{2f(\Omega_i)}{3H_i\Omega_i} g_{pec,m}(t_i) \\ &= -\frac{1}{2} H_i f(\Omega_i) \left[\alpha_{m,i}\delta_i + \frac{4T^{(ext)}_{mm,\circ}}{3\Omega_0 H_0^2}\, D_i\right] r_{m,i} . \end{aligned} \tag{48}$$

In the latter expression, $f(\Omega_i)$ is the corresponding linear velocity growth factor (Peebles 1980). The $\alpha_{m,i}$ are the values of the ellipsoidal shape factors α_m at expansion factor, which are yielded after evaluating the integral expression (36) for the specified initial axis ratios. For this expression, we specified the (artificially imposed) time development of the external tidal tensor through a growth factor $D(t)$, $E_{mm}/\Omega H^2 \propto D(t)$, relating the current external tidal field $T^{(ext)}_{mm,\circ}$ to its initial value.

4.2.2 *Homogeneous Ellipsoidal Model: the Approximation.* Evidently, we have to be aware of the serious limitations of the ellipsoidal model. It grossly oversimplifies in disregarding important aspects like the presence of substructure in and the immediate vicinity of peaks and dips in the primordial density field, the sites it typically deals with. Even more serious is its neglect of any external influence, whether the secondary infall or "collision" with surrounding matter or the role of nonlocal tidal field engendered by the external mass distribution. For overdensities it represents a reasonable approximation for moderately evolved features like a Megaparsec (proto)supercluster, but it will be seriously flawed in the case of highly collapsed objects like galaxies and even clusters of galaxies. Nonethelss, the concept of homogeneous ellipsoids has proven to be particularly useful when seeking to develop approximate yet advanced descriptions of the distribution of virialized cosmological objects (Bond & Myers 1996a,b,c, and Sheth, Mo & Tormen 2001).

Interestingly, in many respects the homogeneous model is a better approximation for underdense regions than it is for overdense ones. Over-

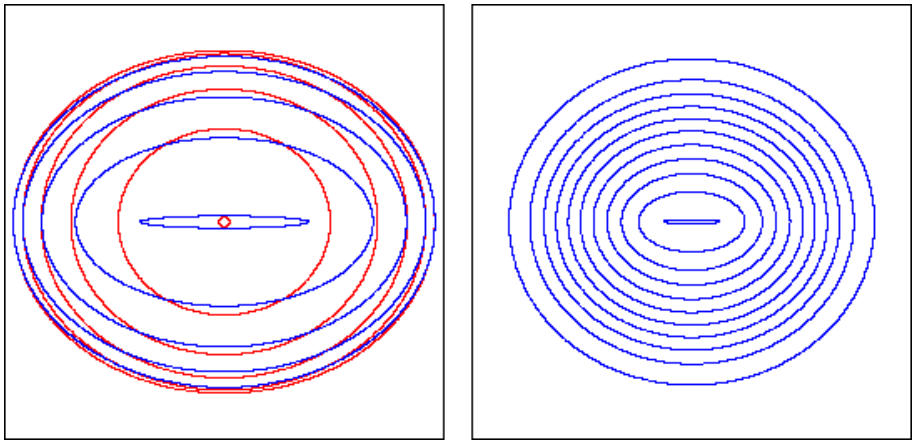

Figure 19. The evolution of an overdense homogeneous ellipsoid, with initial axis ratio $a_1 : a_2 : a_3 = 1.0 : 0.9 : 0.9$, embedded in an Einstein-de-Sitter background Universe. The two frames show a time sequel of the ellipsoidal configurations attained by the object, starting from a near-spherical shape, initially trailing the global cosmic expansion, and after reaching a maximum expansion turning around and proceeding inexorably towards ultimate collapse as a highly elongated ellipsoid. Left: the evolution depicted in physical coordinates. Red contours represent the stages of expansion, blue those of the subsequent collapse after turn-around. Right: the evolution of the same object in comoving coordinates, a monologous procession through ever more compact and more elongated configurations.

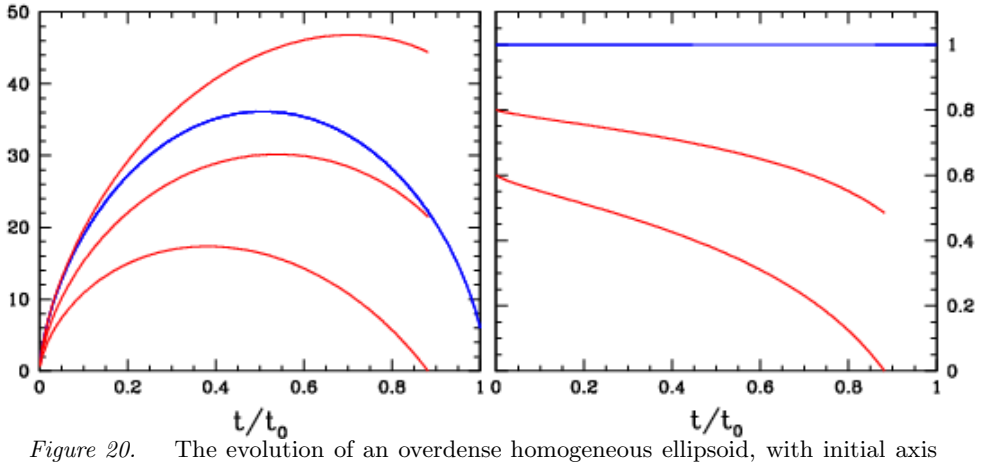

Figure 20. The evolution of an overdense homogeneous ellipsoid, with initial axis ratio $a_1 : a_2 : a_3 = 1.0 : 0.8 : 0.6$, in an Einstein-de-Sitter background Universe. Left: expansion factors for each individual axis; right: axis ratios a_2/a_1 and a_3/a_1. The ellipsoid axes are depicted as red curves. For comparison, in blue, the evolution of an equivalent homogenous spherical overdensity.

dense regions contract into more compact and hence steeper density peaks, so that the area in which the ellipsoidal model represents a reasonable approximation will continuously shrink. On the other hand, while voids expand and get drained, the density fields in the central region of the (proto)void will flatten out, so that the voids develop into regions of a nearly uniform density and the region of validity of the approximation grows accordingly. This can be readily appreciated from the conceptually simpler spherical model approximation. More significant, it was also demonstrated in the complex circumstances of voids embedded in a general cosmic density field for a set of N-body structure formation simulations (Van de Weygaert & van Kampen 1993, see Fig. 31). A direct repercussion of the flattening out of the voids is the velocity field inside them. With the exception of the ridges surrounding them, the quadratic potential approximation will be valid for most of the void's interior and therefore be characterized by a velocity field of excess Hubble expansion. The systematic study by Van de Weygaert & Van Kampen (1993) indicated how the void velocity fields in general will evolve towards a state in which they become genuine "Superhubble Bubbles" (see section 4.7). Evidently, the ellipsoidal approximation will only be useful for the interior of voids. At the outer fringes the neglect of the role of surrounding material will be rendered invalid, as the sweeping up of matter, the formation and subsequent induced 'self-interaction' and the encounter with surrounding structures will become domineering effects.

4.2.3 *Anisotropic Collapse: Shaping Force of Internal Tides.* The internal gravity field is evolving along with the evolution of the object itself, which renders it rather straightforward to account for it in a fully selfconsistent fashion. When focussing specifically on the issue of shape evolution, the obvious archetype for the intrinsic primordial flattening of an overdensity through the action of the associated "internal tidal" field is an evolving homogeneous ellipsoidal overdensity (Fig. 19). It represents the situation in which the geometry of the collapsing object is fully coupled to the anisotropy of the force field, its runaway dynamic evolution resulting from the feedback interaction between shape and force field of an object.

The basic agent behind the continuing amplification of initial asphericities of a collapsing objects is the anisotropy in the corresponding gravitational force field. The gravitational force along the shortest axis of an ellipsoid will be stronger than along the longest axis. Along the short axis it will "feel" nothing but the increased matter concentration within the enclosing sphere, while along the longest axis the effective force will be diluted by the lower density outside the object. It is self-evident that this effect becomes more pronounced as the object develops an increasingly flattened or elongated geometry.

A telling illustration of this behaviour can be observed in figures 10. It shows the evolution of a slightly overdense ellipsoid, initially almost spherical with (axisymmetric) axis ratios $a_1 : a_2 : a_3 = 1 : 0.0.9 : 0.9$, embedded in a background Einstein-de Sitter Universe. Depicted is a time sequel of attained geometric configurations (in the $x_1 - x_2$ plane) during its development from the initial small near-spherical state through its turn-around phase, after which physical collapse sets in, towards the inexorable fate of collapse as a strongly elongated spindle-like object. The evolution of the ellipsoid is computed by numerical evaluation of the corresponding second-order differential equations for homogeneous ellipsoids (Icke 1973). It is interesting to observe the contrast between its evolution in physical coordinates (lefthand frame) and that in comoving space (righthand frame). In physical space we first note the ellipsoid expanding, trailing the global expanding Universe (red contour configurations). While the initial expansion slows down more and more, the ellipsoid finally reaches a maximum volume at its "turnaround" time, after which it sets in an inexorable collapse (blue configurations). Along with this process, during both its physical expansion as well as contraction, we observe the ellipsoid to assume a continuously stronger elongated geometry, ultimately collapsing as a spindle-like object. For contrast, the same process is depicted in comoving space in the righthand frame. By removing the effect of the expanding background Universe we obtain a

better appreciation of the shape development of the object. Evidently, in comoving space it experiences a monologous contraction. Starting from its large Lagrangian volume it finally develops into the compact and fully collapsed object at the centre of the graph. It may be superfluous to note that by that stage, the simple formalism used to describe the monologous evolution of a homogeneous ellipsoid is rendered invalid as shell interactions and crossings can no longer be neglected. The latter find a partial expression in an exchange of energy as the process of virialization sets in.

Quantitatively, the systematic elongating tendency of such overdense ellipsoidal objects may be clearly appreciated from an examination of the the expansion and subsequent contraction of each of the three axes of a slightly overdense triaxial ellipsoid. Figure 20 shows a representative example, depicting the axis evolution for an ellipsoid with initial axis ratio $a_1 : a_2 : a_3 = 1 : 0.8 : 0.6$ (red curves). As in figure 19, the ellipsoid is embedded in an Einstein-de-Sitter background Universe. For contrast, the evolution of an initially equivalent homogeneous spherical overdensity has been added in the same figure (blue curve). After an initial phase of moderate expansion along all three axes we observe the successive turn-around along all 3 directions (lefthand frame), with the shortest axis being the first to turn around and with the longest one only following as last one after first having pursued its initial expansion. From the righthand frame, we can clearly see that its development is accompanied by a drastic and continuous decrease of both axis ratios. Even while the ellipsoid will collapse along all three axes, it will ultimately do so as a highly flattened object !

It may be evident, that this secular increase of aspherical perturbations provides an explanation for the *pancake-like*, and later *filamentary*, appearance of large scale structures.

4.3. Anisotropic Collapse: External Tidal Action

The internal flattening is augmented, and regularly dominated, by the anisotropy of the gravitational force field induced by the surrounding external inhomogenous matter distribution, the "external tidal " forces. The role of the internal tidal field, the expression of internally anisotropic shape and/or inhomogeneous matter distribution, is primarily that of changing – in situ – the configuration and appearance of an object. The external tidal influence proceeds almost completely independent of the emerging object itself, with the possible exception of a mostly minor backreaction on the surrounding matter configurations. The impact of these external forces is considerably more versatile than, and regularly

dominating over, the internal anisotropic force field. They play an exclusive role in spinning up a collapsing clump, making them the prime agent for the rotation of galaxies. In addition, external tides have a major influence on, and may even determine, the very outcome and fate of the gravitational collapse itself. In particular, it may hold a decisive influence on aspects such as collapse timescale and final object shape. A fully selfconsistent treatment of these effects can in principle only be achieved by following the overall matter distribution throughout the surrounding realms of the Universe. Often though, its major impact is restricted to that of the lowest two order terms of the force field, the dipolar and quadrupolar components.

4.3.1 *External Tidal Action: Composition and Development.* It has proven most difficult to get a full understanding and appreciation of the extent of the role of external tidal forces. Partly this can be ascribed to the absence of a fully selfconsistent treatment, in particular with respect to the complex nature of their temporal evolution. The external tidal field at any one location is a mixture of tidal force contributions from a diversity of inhomogeneities, spanning a wide range of spatial scales and each evolving at their own rate. Remote and coherent large-scale structures may still evolve almost linearly, while neighbouring small-scale matter concentrations may already have reached highly nonlinear stages of collapse. Moreover, the composition of the different contributions will be a function of cosmic location. Objects embedded in highly dense regions will be more affected by the short-range nonlinear tidal contributions than the ones residing in more diluted regions, which will therefore find themselves more reacting to a moderately linearly evolving force field. The external influence originating from large scale density perturbation, still evolving linearly, will therefore also grow linearly according to

$$T_{mn}^{(ext)}(t) \;\propto\; D(t)\;\Omega(t)H^2 \;\propto\; D(t)\;a(t)^{-3} \quad \begin{array}{ll} \propto & t^{-4/3} \quad (\Omega_\circ = 1) \\ \propto & t^{-3} \quad (\Omega_\circ \ll 1) \end{array} \tag{49}$$

with $D(t)$ the linear growth factor. The first line follows immediately from the well-known fact that in an $\Omega_\circ = 1$ universe $D(t) = a(t)$, implying a tidal growth of $T_{mn}^{(ext)}(t) \;\propto\; a(t)H^2 \;\propto\; 1/a(t)^2 \;\propto\; t^{-4/3}$.

On the other hand, in a low-density Universe the growth of structure grinds to a halt at a redshift of $z \;\approx\; (1/\Omega_\circ - 1)$. This implies a decline in tidal strength of $T_{mn}^{(ext)}(t) \;\propto 1/a(t)^3 \;\approx\; t^{-3}$. In essence, this is an expression of the structure being frozen in with the Hubble expansion, so

that the accompanying gravitational forces – induced by a non-evolving mass content – diminish with the accompanying expansion of physical distances and the corresponding cosmic volume. As a telling example, we may refer to Fig. 27, where the two last rows of panels depict the practically unchanging cellular pattern in an $\Omega_\circ = 0.3$ Universe.

The time dependence of the tidal field will change once the inhomogeneities enter the non-linear phase of their evolution, when the neighbouring fluctuations responsible for the major share of the tidal interactions have collapsed and virialized. It may be, in a fashion similar to that discussed for the ultimately frozen structures in a low-density Universes, that the cosmic entities recede from each other along with the general Hubble expansion of the Universe (Peebles 1969, Dubinski 1992). This gradual dilution of cosmic objects would lead to a more rapidly declining external tidal field,

$$T^{(ext)}_{mn}(t) \;\propto\; 1/a^3 \;\propto\; t^{-2}. \tag{50}$$

On the other hand, when the major share of the external tidal force is imparted by nearby small-scale highly nonlinear clumps, we may encounter a distinctly different situation. On these scales the hierarchical clustering process will usually still be in progress, so that the clumps will not move away from each other, but instead continue their congregation into ever more massive entities. One particular asymptotic example which may regarded as a reasonable approximation of the genuine situation is that of *"stable clustering"* (see e.g. Jain 1997). In essence this analytically tractable situation presumes a conglomerate of nonlinear clumps to retain the same clustering configuration in physical coordinates as the Universe is expanding along. Hence, we see a continuing contraction in comoving space, leading to a comoving density that rises along with the global Hubble expansion according to $\propto a^3$. Indeed, several N-body experiments (see e.g. Efstathiou et al. 1988, Jing 2001) have verified that this indeed appears to be a proper representation of the situation pertaining at small highly nonlinear scales. The contribution to the total tidal field originating from such tightly clustered assemblies will consequently retain its strength, i.e.

$$T^{(ext)}_{mn}(t) \;=\; \text{constant}\;. \tag{51}$$

Given their considerably different time dependences, the tidal influences from the various contributing inhomongeneities will represent continuously changing fractions of the full tidal force at any one location. Their relative contributions will be a continuously changing function of time. We may expect the large-scale linear perturbations to dominate in the early stages of evolution. This will change as nearby small-scale clumps

have reached full fruition and the process of continuing hierarchical evolution has established itself as a prominent process on relevant scales. The linearly evolving contributions will gradually become superseded by the growing weight of the nonlinear entities.

Moreover, the role of tidal fields is not solely a matter of the intrinsic evolution of the external tidal forces. Their impact as much depends on the configuration of the object over which they are exerted and the precise timing of the external forces. In early stages the external forces may still represent the dominant dynamical influence. However, as the object itself collapses and reaches a highly nonlinear phase of evolution, it largely decouples from the background and pursues its own lifetrack. Most external effects should then have made a detectable imprint. Thus, being the dominant contribution during the pristine early stages, the linear large-scale contributions may provide the only relevant external influence during an objects emergence out of the primordial density field. In the case of angular momentum generation, for instance, most studies indeed seem to indicate that most of the angular momentum should have been imparted in the early linear phase, before the object turns around and starts to contract. On the other hand, new results indicate that the nonlinear ellipsoidal collapse in the later phases may still yield a noticeable addition to the final angular momentum.

In all, it will be a daunting task, possibly not even feasible, to find globally viable prescriptions and descriptions for the influence of external tidal onto the final outcome, configuration and properties of emerging structures in the Universe. Whether the "internal" or "external" influence is dominating has not been systematically answered yet, and will most likely depend to a considerable extent on cosmological scenario and the related coherence scale in the cosmic density field. Nonetheless, on the basis of currently available work we may conclude that to no extent it is possible to neglect the impact of external tidal fields. This was clearly stated by Bond & Myers (1996a,b,c), who deemed the external tidal field of decisive importance for the final fate and morphology of collapsing patches in the cosmos, an observation on which they based their "peak-patch" formalism. Their arguments were confirmed by the succesfull improvement in predicted locations and properties of clusters of galaxies in a large cosmic volume. Additional support for this view got provided by the thorough study by Eisenstein & Loeb (1995), who systematically adressed the dynamical evolution of a large number of different homogeneous ellipsoid objects immersed in a user-specified external tidal field. Their conclusion, possibly not unequivocally relevant for and applicable to a more contrived generic world, is that on average the external tidal field would not only set the rotation of emerging ob-

jects, but would also dominate over the internal force field in determining the final shape of these homogeneous ellipsoidal overdensities.

4.3.2 *External Tidal Action: Tidal Torques and Spinning Galaxies.* That external gravitational tidal forces, effected by the inhomogenous matter distribution in the external surroundings of an evolving cosmic structure, wield a decisive role in the cosmogony of galaxies was recognized since decades for one of the most crucial physical properties of galaxies. The tidal torques which external inhomogeneities exert onto collapsing objects are an exclusive instrument for imparting angular momentum. It is the mechanism to set dark matter haloes into a spinning mode. The resulting rotation of the emerging galaxy is amongst the most distinctive and discriminative properties of galaxies, tightly coupled to their overall morphology and structure. This is the case for the conspicuously dominant rotational motion of the stellar and gaseous components of spiral galaxies, as well as for the more mixed kinematics encountered in the elliptical galaxies which seem to be supported by random motions.

Collapsing clumps of matter embedded in a global field of density fluctuations naturally acquire angular momentum through the winding action of the resulting tidal torques. Evidently, the internal gravity field is completely inept in providing any viable contribution to this important physical property, leaving the external tides as principal and exclusive agents. The torque τ imparted by an external tidal field onto the material within a Lagrangian volume V_L is

$$\tau = \int_{V_L} \rho \mathbf{r} \times \nabla\Phi \; dV \tag{52}$$

where Φ is the potential due to the external tidal field. To first order, $\Phi_{,}i \simeq T_{ij}^{(ext)} x_j$, so that the torque τ can be seen to result from the coupling between tidal field T_{ij} and inertial tensor I_{kl} of the collapsing object,

$$\tau_i \;=\; \epsilon_{ijk} T_{ji}^{(ext)} I_{kl} \;, \tag{53}$$

where ϵ_{ijk} is the Levi-Civita tensor.

An important aspect of the tidal torque scenario is that nearly all angular momentum of an evolving overdensity is imparted during the early, linear phase of formation (see e.g Peebles 1969, Dubinski 1992). We may appreciate this to some extent by observing from the previous expression that – for the case of an Einstein-de Sitter Universe – as I_{ij} grows as $t^{4/3}$ for a Lagrangian volume, and $T_{kl}^{(ext)}$ declines as $t^{-4/3}$ (see Eqn. 5), the tidal torque in the linear regime remains constant.

Therefore, the acquired angular momentum will grow linearly in time, $\mathbf{L}(t) \propto t$ (White 1984), which then would correspond to the epoch in which most angular momentum is generated.

Once an object has started to contract, self-gravity and noisy small-scale torques start to dominate over the initial coherent large-scale tidal torque. The final rotational state is therefore mostly in place by the time the object starts to collapse and finally virializes into a genuine galaxy. Even though various issues of contention remain, whether it concerns the fine-tuning issue of imparting a sufficient yet not overriding amount of angular momentum onto dissipatively collapsing baryonic galaxy disks embedded within dark matter haloes or the distorting effect of unceasing small-scale nonlinear effects such as the intermittent infall of a variety of matter clumps, the tidal torque mechanism has established itself as an essential aspect – even tenet – of the overall process of structure formation through gravitational instability.

Tidal torqueing was suggested as an explanation for the origin of galactic rotation by Hoyle (1949). The idea was more thoroughly investigated by Peebles (1969) and Doroshkevich (1970) in a linear analysis of the problem, although confusion concerning the efficiency of the mechanism remained widespread until the analytical and numerical study by White (1984). Since the early studies of this mechanism, a flurry of analytical and numerical studies (e.g. Heavens & Peacock 1988; Ryden 1988; Hoffman 1986, 1988; Quinn & Binney 1992; Dunn & Laflamme 1993; Catelan & Theuns 1996a,b) as well as extensive and more detailed N-body simulations (e.g. Efstathiou & Jones 1979; White 1984; Barnes & Efstathiou 1987; Dubinski 1992, Warren et al. 1992; Eisenstein & Loeb 1995; Sugerman, Summers & Kamionkowski 2000, Porciani, Hoffman & Dekel 2001a,b) have demonstrated its viability in a realistic cosmological setting and gradually a general consensus has been emerging on tidal torqueing as the basic mechanism for the origin of angular momentum of galaxies for structure formation scenarios based on gravitational instability.

Intriguing would be the possibility to revert the history, and exploit observed galaxy rotations in an attempt to reconstruct the very source of the galaxy rotations. Tentatively, the imprint of a large-scale generating tidal field should be reflected in the alignment of induced galaxy spins. These may constitute a significant relic the cosmic structure formation process in case the major share of the torqueing action has been assumed by large-scale coherent structures like filaments. The search for such a fossil imprint has recently been the subject of various studies. Statistically significant alignments of spin vectors of galaxies may be expected if the main source of the large-scale tidal torque would be large

spatially coherent matter concentrations, filaments and walls being the most straightforward examples, since it would lead to a roughly similar spin axis for neighbouring collapsing clumps. Assessing the prominence of such alignments would be of high interest. For one, it could potentially complicate the correct interpretation of the measurement of weak gravitational lensing effects. Particularly interesting is the suggestion by Lee & Pen (2000) that the correlated galaxy spin orientations in a particular cosmic region offer a unique and alternative way of reconstructing the cosmic gravitational shear and potential field, and hence the large-scale density field.

However, in reality the effect may be substantially clouded. Nonlinear contributions to the spin direction may totally erase the linearly predicted alignments, as the study by Porciani, Dekel & Hoffman (2001a) has indicated. Even if some level of alignment survives, any significant alignment will only be evident as a residual effect amidst a mostly random distribution of galaxy spin axes. The direction of the principal axes of protogalaxies – the peaks in the primordial density field – and that of the axes of the tidal shear at its location are each determined by random stochastic processes (see e.g. Bardeen et al. 1986) and are mutually misaligned with respect to each other. Their stochastic distributions, however, are expected to be significantly correlated (see e.g. van de Weygaert & Bertschinger 1996, Lee & Pen 2000).

Small or ill-defined samples of galaxy spin measurements may therefore mask any positive effect by statistical noise. This may be the reason for the current absence of a convincing detection of significant galaxy spin alignments, and the contradictory conclusions reached by a variety of observational attempts to address the issue. While some claim alignments do indeed exist (e.g. Yuan et al. 1997), be it a weak one, other studies do not find any significant evidence (Han, Gould & Sackett 1995, Cabanela & Dickey 1999). Given that most previous studies concentrated on areas where spin alignment tends to be weak, a substantial improvement may be accomplished by concentrating on those regions where we expect the strongest spin alignments, in the filamentary outliers branching out of clusters. If indeed detected, it would provide a tentalizing glimpse of the very dynamical processes underlying the shaping of the overall cosmic matter distribution into its salient foamlike pattern.

4.4. Anisotropic Collapse: the Zel'dovich Approximation

Evidently, in the world of reality there is no such thing as an isolated and homogeneous object, and this implies a considerably more complex and intricate evolution of cosmic structure. A full and self-consistent appreciation of the resulting emergence and morphology of cosmic structures has not yet properly settled. Often therefore we are confronted with mere qualitative descriptions of the intricate filamentary and foamlike patterns emerging in the cosmic matter distribution.

Yet, a large share of the outstanding and inherent tendencies of the evolving patterns in the cosmic matter distribution may indeed be readily identified, even for generic circumstances where the spatial density distribution is a stochastic fluctuation field. The Zel'dovich formalism, in essence a mere first-order Lagrangian approximation, which has played a major role in elucidating the qualititave aspects of the generic evolution of a random matter density field. Indeed, it may be argued that central role of the Zel'dovich formalism in structure formation studies stems from its ability to take any arbitrary initial random density field and mould it through a simple and direct operation into a reasonable approximation for the matter distribution at later nonlinear epochs.

As it takes into account the complete force field, comprising that induced by density perturbations inside and outside of a specific region ("patch"), the Zel'dovich formalism is basically suited for any complex spatial configuration, dealing fully and self-consistently with both internal and external influences. Of overriding importance is the one-to-one linear nature of the relation between displacement and primordial local gravitational force. This allows the Zel'dovich approximation to identify the location of emerging structures, the sites where the induced migration flows accumulate the displaced matter patches. As it takes into account the full vector force field, it leads to an insightful relationship between the anisotropy of the primordial peculiar force field and morphology of the emerging matter distribution. Its application within a variety of cosmological scenarios demonstrated that flattened and elongated features are generic features of the matter distribution at moderate quasi-linear phases of evolution. Moreover, the coherent flattened structures appear to arrange themselves into a global cellular skeleton permeating the cosmos.

The generic features of anisotropic collapse within generic media of cold matter distributions can be inferred by assessing the relation between a fluid element's density evolution and the eigenvalues of its deformation tensor, and hence the tidal force tensor (Eqn. 13, section 3.5.1).

Three instrumental observations concerning the collapse process can be readily made:

- Ultimate *fate*:
  Having one or more positive eigenvalues λ_i (i=1,2,3) is sufficient to guarantee collapse. Unless each individual $\lambda_m < 0$ (i=1,2,3), the fluid element, even if initially underdense, will undergo collapse along at least one of its axes at some stage during its evolution.

- *Collapse Configurations*:
  For fluid elements with at least one positive deformation eigenvalue, the ultimate collapse geometry of a fluid element can be one of 3 distinct configurations. Assuming that $\lambda_3 > \lambda_2 > \lambda_1$, a flattened *pancake* shape will be attained if only $\lambda_3 > 0$ and $\lambda_2 < 0$. While collapse has occurred along the corresponding axis, the element will expand along the 2 others. Likewise, if $\lambda_3 > \lambda_2 > 0$ and $\lambda_1 < 0$, the mass element will evolve into an elongated *spindle*. A state of full collapse along all three axes will only be reached if all $\lambda_i > 0$ (i=1,2,3).

- *Collapse Time Sequence*:
  The collapse will be anisotropic and, dependent on the sign of the deformation eigenvalues, proceeding along a sequence of one, two or three distinct stages. Firstly, collapse will happen along the direction of the largest positive eigenvalue at $a_{1c} = 1/\lambda_1$. It occurs upon the fluid element entering a flattened *pancake*. Subsequently, it will start contracting along a second direction, leading to collapse along a second axis at $a_{2c} = 1/\lambda_2$, corresponding to the presence in a *filament*. Ultimately, if also $\lambda_3 > 0$, the fluid element will undergo full collapse upon a singular point at $a_{3c} = 1/\lambda_3$.

Following these considerations, it is straightforward to sketch a qualitative picture of the gravitational evolution of the overall matter distribution. Starting from a field of minor (Gaussian) fluctuations, the first structures to undergo collapse are *pancakes*, composed of fluid elements that collapse along the first, largest eigenvalue, axis. Subsequently, we'll see the formation of elongated *filaments* once corresponding mass elements start contracting along the second direction. Finally, the emergence of dense compact clumps will be the result of the full collapse of fluid elements along all 3 collapse directions. The physical nature of the emerging object will depend on the scale of the corresponding deformation field, so that a *galaxy halo* will emerge through full collapse on a scale $< 1h^{-1}$Mpc, and a *galaxy cluster* from a similar collapse on a scale $\sim 4h^{-1}$Mpc.

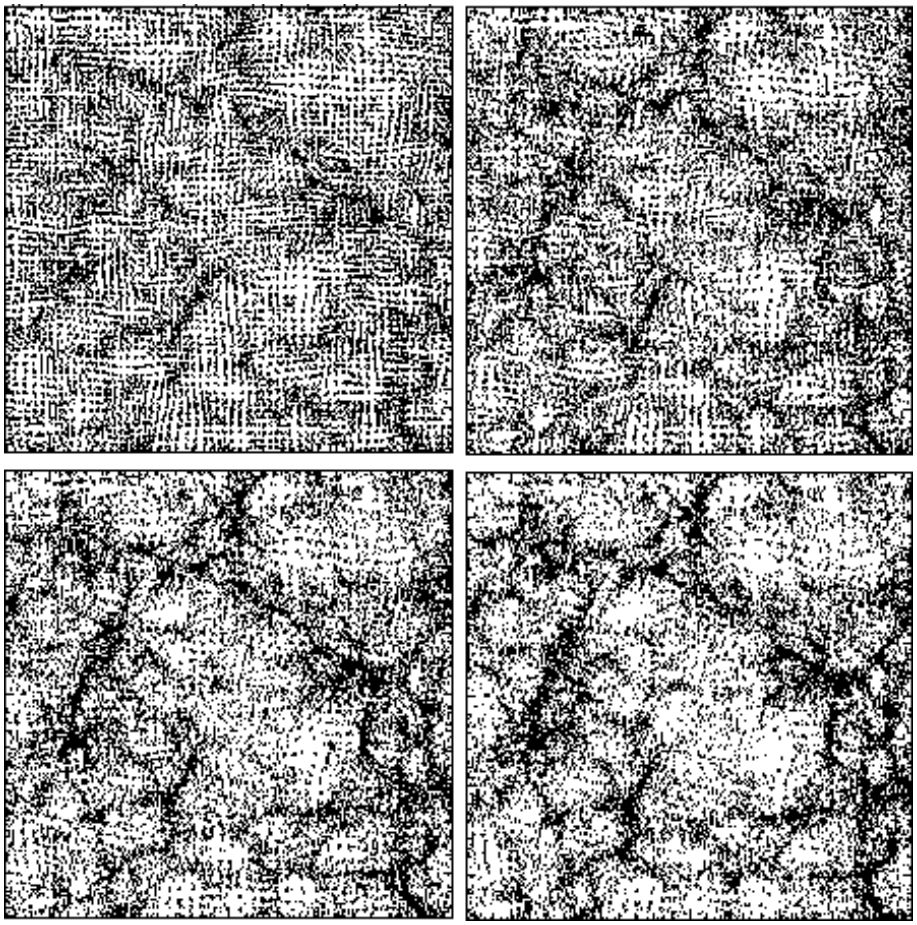

Figure 21. Zel'dovich displaced particle distributions inferred from a unconstrained random realization of a primordial matter distribution for a SCDM cosmological scenario in a $50h^{-1}$Mpc. Time sequence from top left to bottom right, frames corresponding to cosmic epochs $a = 0.10, 0.15, 0.20$ and 0.25.

The time sequence of four frames in Fig. 21 elucidates the success of the Zel'dovich scheme, as it does its obvious shortcomings. Portraying the Zel'dovich predictions for the cosmic matter distribution in a $50h^{-1}$Mpc box for a SCDM scenario, at cosmic epochs $a = 0.10, 0.15, 0.20$ and 0.25, the gradual morphological procession along "pancake" and "filamentary" stages can be readily observed. A comparison with the results of full-scale N-body simulations shows that in particular at early structure formation epochs the predicted Zel'dovich configurations are accurately rendering the full nonlinear matter distributions. On the basis of the four frames in Fig. 21 we can note that:

- A comparison of the last 3 frames with the very first stage indicates that the pattern of the resulting large scale matter distribution is already, be it faintly, imprinted in the primordial matter configuration.
- The essence of the Zel'dovich approximation is in the deformation tensor ψ_{mn}, directly related to the tidal field tensor T_{mn} (eqn. 14). It indicates the existence of the profound relation between the anisotropic force field as shaping agent and the resulting anisotropic matter concentrations, and the cosmic web of which these are the elementary constituents.
- The 1-1 Lagrangian-Eulerian mapping of the Zel'dovich approximation is only possible as long as a fluid element has not yet crossed the orbit of another fluid element.

Pursuing the latter, we see the approximation starts to fail after the occurrence of orbit crossing, which is clearly observed through the unrealistic "diffusion" of clumps, filaments and walls in the 4^{th} frame. Following orbit crossing, we will start to see thorough gravitationally induced orbit mixing and energy exchange proceeding towards a "quasi-equilibrium" state of complete virialization. The Zel'dovich approximation is fundamentally inadequate to describe these advanced nonlinear stages. In fact, its major limitation stems from its virtue of restriciting itself to the initial fluctuation field, so that it breaks down as soon as the self-gravity of the emerging structures becomes so strong that the initial "ballistic" motion of the fluid element gets seriously altered, redirected, slowed down, and possibly even brought to a halt. Full-scale gravitational N-body simulations, and/or more sophisticated approximations, are necessary to deal self consistently with these more advanced nonlinear stages.

From the Zel'dovich formalism we can readily infer that the overall morphology and spatial pattern of a cosmic density field at its "quasi-linear" development stage – i.e. the prominence of flattened structures, denser elongated filaments and dense compact clumps as well as their interconnectedness – is sensitively dependent on the statistical distribution of the values of the eigenvalues λ_i. For the case of a Gaussian random density fluctuation field, Doroshkevich (1970) computed the probability distribution for the eigenvalues λ_1, λ_2, and λ_3,

$$\begin{aligned} P(\lambda_1,\lambda_2,\lambda_3) \quad &\sim \quad (\lambda_1-\lambda_2)(\lambda_1-\lambda_3)(\lambda_2-\lambda_3) \\ &\times \quad \exp\left\{-\frac{15}{2\sigma^2}\left[\lambda_1^2+\lambda_2^2+\lambda_3^2-\frac{1}{2}(\lambda_1\lambda_2+\lambda_1\lambda_3+\lambda_2\lambda_3)\right]\right\} \end{aligned} \tag{54}$$

This yields a probability of 8% that all of the eigenvalues are negative, $\lambda_3 < \lambda_2 < \lambda_1 < 0$, while 92% of the matter has one or more positive eigenvalues. From a detailed assessment of the deformation eigenvalue distribution (eqn. 15) for scenarios with relatively strong perturbations on large scales, a distinct wall- and filament-dominated weblike configuration during the moderate quasi-linear evolution phase is the natural outcome. Vast coherent wall-like and filamentary features characterize the matter distribution. On the other hand, when small-scale perturbations are so prominent that full collapse has taken place on small scales even before any noticeable anisotropic contraction on larger scales has occurred, orbit crossing and virialization have been so ubiquitous that the Zel'dovich description will be seriously challenged, rendering the validity of its predictions more than dubious.

The essential role of the anisotropy in the force field – i.e. the tidal field – in shaping the cosmic matter distribution is evidently an essential element of the Zel'dovich approximation, which so emphatically invokes the deformation tensor, and by implication the initial tidal field configuration. Yet, the Zel'dovich approximation restricts itself to the linearly extrapolated tidal field configuration of the initial density field, and fails to react properly to the rapidly rising gravitational strength in and around emerging matter concentrations. While it indicates the proper context for understanding the dynamical mechanisms behind the formation of the cosmic foam, we need to extend our understanding of the evidently tight connection between the workings of the tidal force field and the moulding of a cosmic foam structure. Only by elucidating this relationship up to the fully nonlinear regime we may hope to get a full understanding of the dynamical evolution of the pervasive and enduring nature of the seemingly tenuous and fragile foamlike network permeating our observable Universe.

4.5. Foam Assembly and Tidal Dynamics: Tidal "Casting" of the Cosmic Web

First recognized in idealized approximations such as the Zel'dovich scheme – and its essence explained by the anisotropic collapse of homogeneous ellipsoids – the tendency of structures to evolve through a flattened and/or elongated phase has been found to be a universal phenomenon. It has proven to be a characteristic phenomenon for a gravitationally driven formation of structure, and has been recovered in a vast range of viable scenarios of gravitational cosmic structure formation.

A few recent studies (e.g. Bond, Kofman & Pogosyan 1996) have drawn attention to the close and causal link between the generically

anisotropic tidal force fields generated by typical cosmic matter distributions, their impact on the shape of an emerging and evolving structure, and the resulting cosmic foamlike structure. Indeed, if anything, the applicability of the Zel'dovich approximation far into the quasi-linear regime provides us with a rudimentary indication that there is a significant and possibly instrumental dynamical connection. Its remarkably long-lasting validity, by far surpassing the nominally valid linear regime, in combination with its basic affiliation to the primordial anisotropic force field (see Eqn. 14) provides a compelling indication for such a kinship. It warrants a considerably closer investigation of what may conceivably be an intimate and causal relationship between foam morphology of the cosmic matter distribution and the primordial cosmic force field. Such a study should involve the full range of evolutionary phases, including the late nonlinear stages at which the web features should actually condense out as (partially) virialized structures. With respect to the latter, it is important to realize that quasi-linear approaches like the Zel'dovich approximation cannot address the issue of whether filaments or walls will truely settle as genuine objects instead of dissolving, rendering them mere transient features.

4.5.1 *Cosmic Foam: Tidal Constraints and Connections.* Bond, Kofman & Pogosyan (1996) coined the word 'cosmic web' in their study of the physical content of the web, in which they drew attention to their finding that knowledge of the value of the tidal field at a few well-chosen cosmic locations in some region would determine the overall outline of the weblike pattern in that region. This relation may be traced back to a simple configuration, that of a "global" quadrupolar matter distribution and the resulting "local" tidal shear at its central site. Such a quadrupolar primordial matter distribution will almost by default evolve into the canonical cluster-filament-cluster configuration which appears so prominently in the cosmic foam. Indeed, this close connection between local force field and global matter distribution had been elucidated by means of a constrained field study by Van de Weygaert & Bertschinger (1996). They, amongst others, discussed the repercussion of a specified constraint on the value of the tidal shear at some specific location. From the expression of the tidal tensor in terms of the generating density distribution,

$$T_{ij}(\mathbf{r},t) \;=\; \frac{3\Omega H^2}{8\pi}\int \mathrm{d}\mathbf{r}'\,\delta(\mathbf{r}',t)\;\left\{\frac{3(r'_i-r_i)(r'_j-r_j)-|\mathbf{r}'-\mathbf{r}|^2\;\delta_{ij}}{|\mathbf{r}'-\mathbf{r}|^5}\right\}\;- \\ -\;\frac{1}{2}\Omega H^2\;\delta(\mathbf{r},t)\;\delta_{ij} \qquad (55)$$

we can immediately observe that any *local* value of T_{ij} has *global* repercussions for the generating density field. Such *global* constraints are in marked contrast to *local* constraints as the value of the density contrast δ itself, or the shape of the local matter distribution. One of the major virtues of their *constrained random field* construction technique (Bertschinger 1987, Hoffman & Ribak 1991) is that it offers the instrument for translating locally specified quantities into the corresponding implied global matter distributions for a given structure formation scenario. In principle, the choice of possible implied matter distribution configurations is limitless, yet it gets substantially curtailed by the statistical nature of its density fluctuations, the coherence scale of the matter distribution and hence of the generated force field as well as the noise characteristics over the various spatial scales, both set by the power spectrum of fluctuations.

The most straighforward example of a *global* constraint involves the local gravitational acceleration at one particular location. Such an acceleration has to be induced by a dipolar asymmetry in the matter distribution centered on that particular location. Such may be readily appreciated from the integral expression of **g** in Eqn. 1 (Van de Weygaert & Bertschinger 1996, Fig. 3). It is in a similar fashion that Eqn. 16 implies a quadrupolar pattern in the density field distribution, its particular realization determined by the orientation and strength of the local tidal shear. This can be readily observed from Fig. 22, which is an elaboration on a similar discussion in Van de Weygaert & Bertschinger (1996, Figs. 3 and 5). It provides a 3-D impression of the structure in the region immediately surrounding the location of the specified shear. Along each row we show maps in three mutually perpendicular cross-sections centered on the centre of the box.

In the purest, noise-free, implication of the specified constraints the *mean field* in the three top panels represents the clearest depiction of the average density field configuration inducing the specified tidal tensor. It is very clear that the constraint works out into a perfect global quadrupolar field (slightly alineated along the x-axis due to the extra specification of a central elongated small-scale peak). Superposing *residual* noise fluctuations, whose amplitude is modified by the local correlation with the specified constraints, results into a representative individual realization of a matter density distribution that would induce the specified constraint. The outcome is depicted in the second row of 3 panels. The close affiliation with a strong anisotropic force field, within the surrounding region, can then be directly observed from the lower row of corresponding x-, y- and z-slices. The contour maps (red) reveal the spatial configuration of full tidal field strength ($T = \sqrt{(}\sum_{k=1}^{3} T_k^2$), with

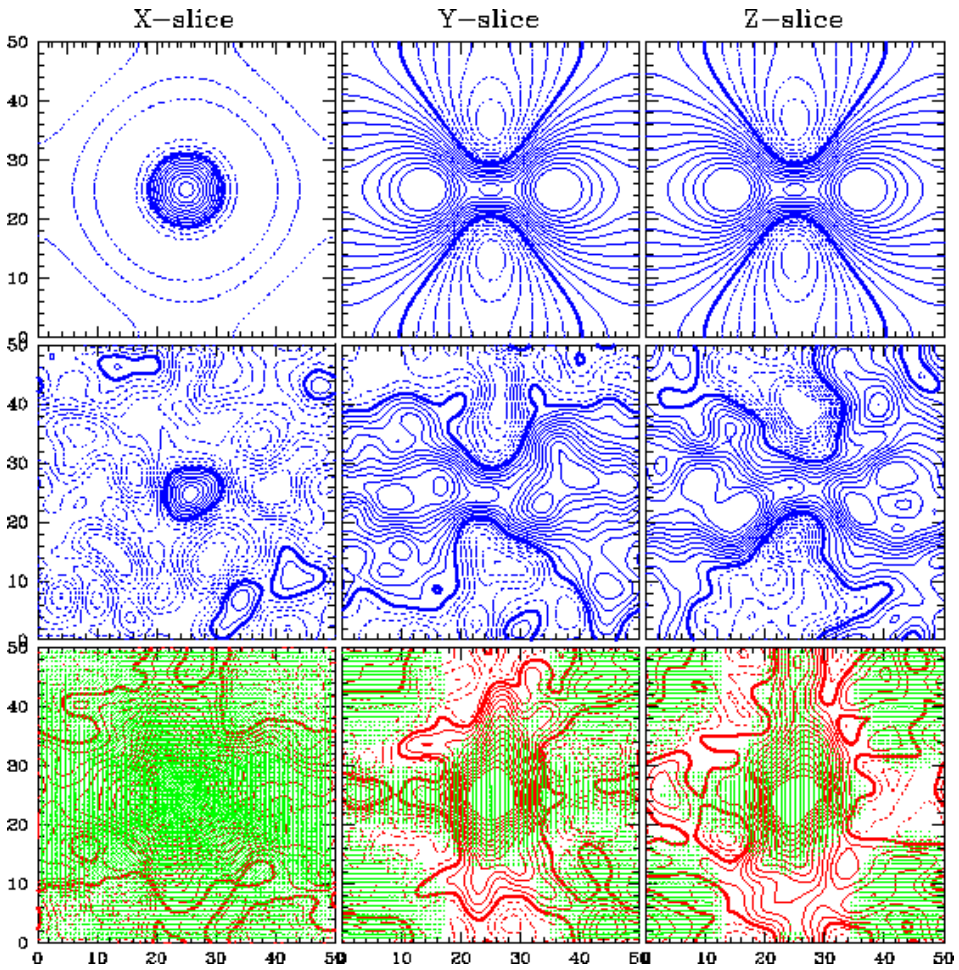

Figure 22. Constrained field construction of initial quadrupolar density pattern in a SCDM cosmological scenario, following the Hoffman-Ribak (1991) procedure in its field dynamical implementation by Van de Weygaert & Bertschinger (1996). The tidal shear constraint is specified at the box centre location, issued on a Gaussian scale of $R_G = 2h^{-1}$Mpc and includes a stretching tidal component along the x- and y-axis acting on a small density peak at the centre. Its ramifications are illustrated by means of three mutually perpendicular slices through the centre. Top row: the "mean" field density pattern, the pure signal implied by the specified constraint. Notice the clear quadrupolar pattern in the y- and z-slice,directed along the x- and y-axis, and the corresponding compact circular density contours in the x-slice: the precursor of a filament. Central row: the full constrained field realization, including a realization of appropriately added SCDM density perturbations. Bottom row: the corresponding tidal field pattern in the same three slices. The (red) contours depict the run of the tidal field strenght $|T|$, while the (green) tidal bars represent direction and magnitude of the "compressional" tidal component in each slice (scale: $R_G = 2h^{-1}$Mpc).

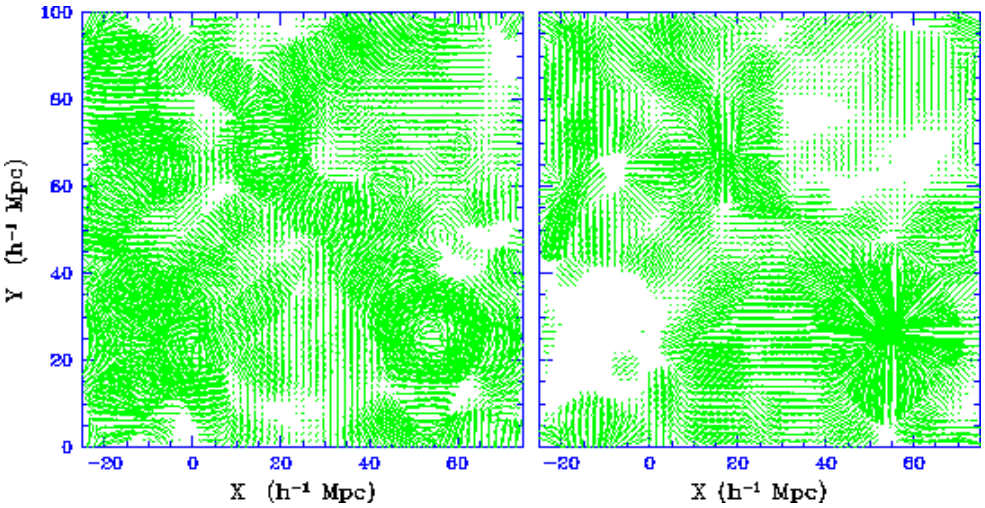

Figure 23. Decomposition of the tidal field components within a slice through a simulation of structure formation in an $\Omega_\circ = 0.3$ CDM Universe ($z \approx 1.5$, cf. fig. 18). Left: the "compressional" tidal component. Right: the "dilational" (stretching) tidal component). The scale of the tidal field is $R_G = 2h^{-1}$Mpc (roughly rendering "external" tidal contributions). See footnote for further explanation.

T_k a tidal tensor eigenvalue) in this central region. Note that we e have crudely included the concept of "external" by (spherically) filtering the field on a (rather arbitrary) scale of $2h^{-1}$Mpc. It amply illustrates the fact that the specified constraints work out into a maximum in the tidal field strength at the box centre. As is clearly borne out by the Y- and Z-slices (central and righthand frame), the tidal field strength contours are noticeably elongated along the Z-axis, culminating in a maximum at the constraint centre. Notice that this elongation is oriented roughly perpendicular to the stretching direction of the tidal shear, and along the axes along which a compressing force is acting (see footnote). A totally different configuration is seen in the x-slice. Around the centre no distinct orientation can be identified. A much more strongly peaked pattern is shown in this plane, concentrated on the box centre.

Further elucidating the patterns in the suggestive tidal strength contour maps are the superimposed "compressional" tidal bars (green), indicating orientation and magnitude of the compressional tidal components within each of the 3 mutually perpendicular planes slicing through the centre of the box[3]. It shows that the central region wherein the tidal

[3]on the basis of the effect of a tidal field, we may distinguish at any one location between "compressional" and "dilational" components. Along the direction of a "compressional" tidal component T_c (for which $T_c < 0.0$) the resulting force field will lead to contraction, pulling

field strength assumes its maximum value, is showing up conspicuously when dissecting the field into its physically active components. The central region is clearly the one where the tidal bars have their largest size. Even more interesting is their corresponding orientation, coherently directed perpendicular to the x- and y-axis and along the z-axis. Thus, in the central and righthand frame we see a pattern of bars directed in parallel to the Z-axis, while the lefthand x-slice frame reveals a pattern of radially directed bars.

The depicted tidal configurations seem to suggest that from the onset of the structure formation process on, the force field comprises a pattern of force anisotropies that will ultimately to strongly moulded, and folded, patterns in the matter distribution.

4.5.2 *Tidal Connections: filaments.* A telling illustration of the correlation between the anisotropy in the cosmic force field and the presence of strongly anisotropic features is provided by the multi-faceted impression in Fig. 24 of a conspicuous filamentary structure which emerged in an (128^3 particle) N-body simulation of structure formation in a SCDM scenario ($\Omega_\circ = 1.0$, $H_\circ = 50$ km/s/Mpc). The depicted particle distribution corresponds to a cosmic epoch at which $\sigma_8 \approx 0.7$ for the matter distribution, roughly corresponding to the present, and is shown in three mutually perpendicular planes passing through the box centre. The filament, elongated along the x-direction and oriented perpendicular to the $y - z$, appears as a dominant feature in the particle distribution (top row frames). Note the two massive cluster concentrations on either side of the filament, to the left and right end of the x-axis. These matter assemblies, in conjunction with the correspondingly large underdense volumes surrounding the filament perpendicular to its spinal axis, define a roughly quadrupolar density field. Naturally, this translates directly into a tidal force field with a strong compressional component perpendicular to the filament. A striking demonstration of this intimate relationship between tidal field and the presence of a salient anisotropic structure like the depicted filament is presented in the corresponding lower row of frames in Fig. 24. The contour maps reveal how the maximum in tidal strength is reached in and immediately around the filament, and forms a plateau that appears to follow its spine along the full elongated extent, cut off near the position of the cluster complexes

---

together the matter currents. The "dilational" (or "stretching") tidal component T_d, on the other hand, represents the direction along which matter currents tend to get stretched as $T_d > 0$. Note that within a plane, cutting through the 3-D tidal "ellipsoid", the tidal field can consist of two compressional components, two dilational ones or – the most frequently encountered situation – of one dilational and one compressional component. Also see fig. 14

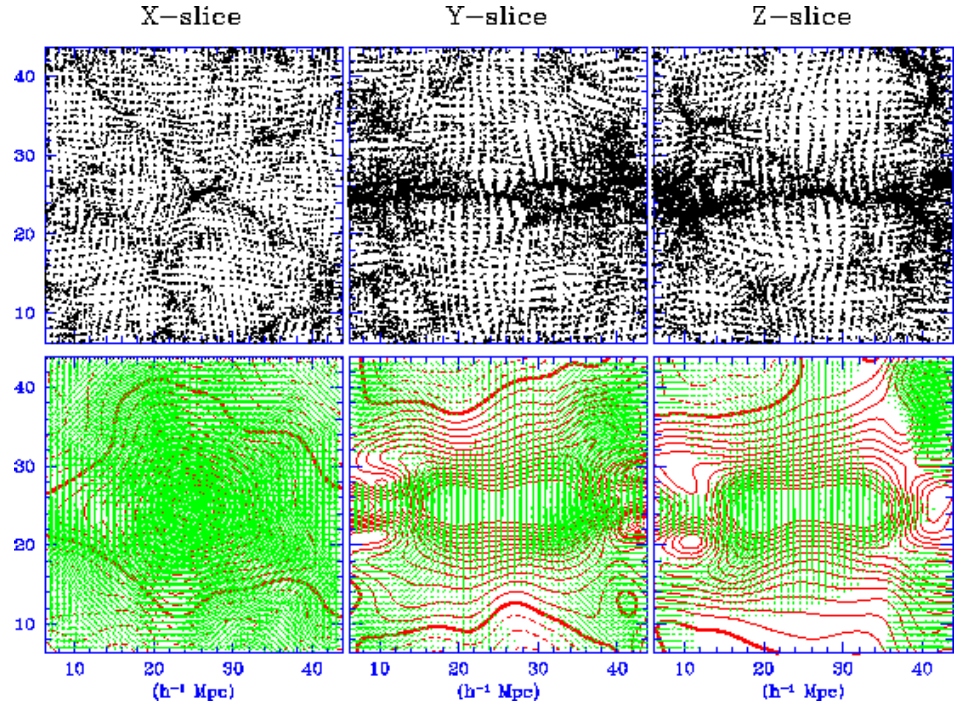

Figure 24. Illustration of connection between mass distribution in and around a filament and the corresponding tidal field (scale: $R_G = 2h^{-1}$Mpc). The filament has formed in a N-body simulation of structure formation in a SCDM cosmological scenario. Top row: the particle distribution in the mutually perpendicular x-, y- and z-slices through the centre of the box. Bottom row: the tidal field configuration, both tidal strength contours (red) and compressional tidal field bars (green) in the same slices. The similar patterns along in the y- and z-slices clearly reflect the striking tidal pattern along the spine of the filament. They are in marked contrast with the almost circularly symmetric and highly concentrated pattern in the x-slice, illustrative of the dynamical impact of the filament perpendicular to its spine.

located on either side. The contours in the plane perpendicular to the filament complements this impression superbly, revealing the strongly centrally peaked and compact force strength field centered on its spinal column.

Even more evocative are the superimposed "compressional" tidal bars (green). It shows that the filaments not only delineate regions of considerable tidal strength, as we can infer from the plateau in the map of total tidal strength and from the large size of the compressional bars in and immediately around the filament, but also appear to stand out when directing attention to the coherence of the field configuration. The filament is delineated by a region with an impressive coherence in both strength and orientation of the tidal bars along the full extent of the filament.

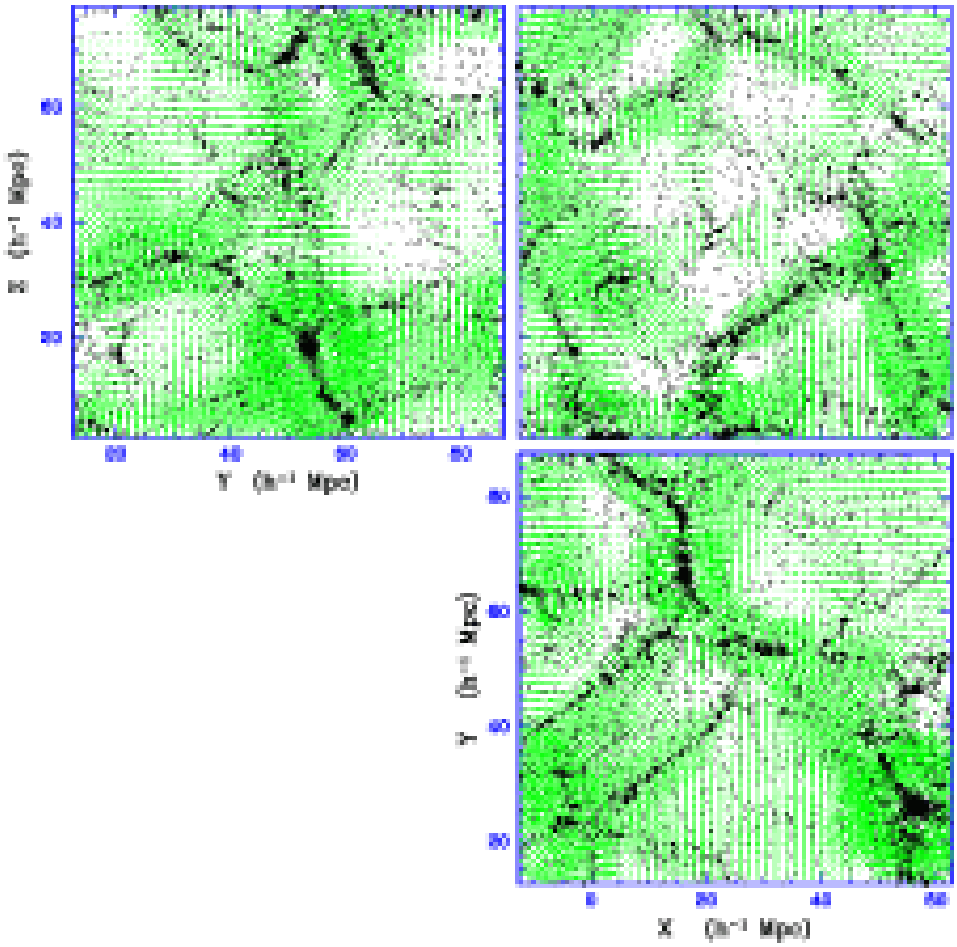

Figure 25. The compressional tidal field pattern in three mutually perpendicular slices through a simulation box containing a realization of cosmic structure formed in an open, $\Omega_\circ = 0.3$, Universe for a CDM structure formation scenario (scale: $R_G = 2h^{-1}$Mpc). The matter distribution corresponds to the present cosmic epoch. Each frame contains the corresponding particle distribution within a $5h^{-1}$Mpc thin region centering on the slice, on which the related tidal bar configuration (green) is superimposed. The matter distribution, displaying a pronounced weblike geometry, is clearly intimately linked with a characteristic coherent and correlated compressional tidal bar pattern. Note the specific arrangement of the planar slices. Along the top row the x- and y-slice share the same vertical z-axis, while in the righthand column the z- and y-slice share the same horizontal x-axis.

4.5.3 *Tidal connections: the unified web.* Having established the strong correlation between a filament and its surrounding tidal field, the issue of how to interpret this within the generic context of a pattern

of interconnected filaments – and walls – will further clarify the special correspondence and possible causal connection with the tidal field configurations.

To that end, we adressed the web pattern in an N-body simulation of a CDM structure formation scenario in an open Universe, $\Omega_\circ = 0.3$. In an open Universe a pronounced weblike pattern gets established relatively fast, after which further growth and development stops as soon as the expansion of the Universe starts to dominate over the gravitational influence of the cosmic matter distribution. It leads to the final fruition of cosmic structure at a redshift of around $z \approx (1/\Omega_\circ - 1)$ (also see Fig. 27). One well-known consequence is the implication of a virtually unchanging population of rich clusters of galaxies over a large redshift range from $z = 0$, and thus the presence of clusters at high redshift (see e.g. Eke, Cole & Frenk 1996; Bahcall, Fan & Cen 1997). As clusters reflect the underlying cosmic foam and form a particular aspect of its geometrical structure, an unchanging cluster population implies a virtually unchanging pattern in the cosmic matter distribution.

Figure 25 contains an illustration of the resulting cosmic web formed at a redshift $z \approx 2$. A set of the three mutually perpendicular (x-, y- and z-) plane slices centered on a specified position in the box, each with a size of $80h^{-1}$Mpc, evoke an impression of the three-dimensional foam pattern in the particle distribution (dots). Superimposed (green) are the compressional tidal bars. A rich amount of information is yielded by this cosmic snapshot. Notice the special grouping of the three frames, such that the top two (x- and y-) planes share the z-axis as the vertical axis while, with y-slice in its top righthand position, the two righthand (z- and y-) planes share the x-axis as horizontal axis.

The most striking aspect of the three frames is the surprisingly *strong* correlation between the particle distribution in conspicuous – massive yet compact and thin – filaments and the spatial configurations outlined by the corresponding compressional tidal field bars (the correspondence with the dilational tidal component is considerably less compelling, see Fig. 23). All through the cosmic foam we can delineate the filaments as the sites where the compressional tidal forces are both strong (large tidal bars) as well as particularly strong, coherently and mutually parallel oriented, perpendicular to the spine of the filaments.

Another outstanding feature of the compressional tidal field configuration concerns the location of the massive rich clusters in the matter distribution. Literally, these clumps in the particle distribution stand out as genuine "nodes" within the global compressional tidal bar pattern. It is no surprise to see them marking the maxima in the strengh of the tidal field, as can be straightforwardly discerned from the size of

the tidal bars in their immediate environment. In this respect, it is most instructive to focus on the cluster in the lower lefthand corner of the z-slice. Around that cluster the field strength is so strong that the bars seem to weave a genuine "bird's nest" of overlapping and intersecting bars. To our idea, however, it is the contrasting topology of the bar pattern in their immediate environment which forms the true distinctive mark of the rich clusters within the overall cosmic tidal pattern. With a coherent lining up of the compressional field perpendicular to their spine is characteristic for filaments, clusters appear to direct the compressional tidal force into a closed loop of laterally oriented field bars.
As a final note we wish to point out the readily apparent close relation between the tidal field configuration shown in Fig. 25 and the pattern of inflicted distortions of background galaxy images through weak lensing by the large scale matter distribution, and in particular by massive rich clusters (see e.g. Blandford et al. 1991, Jain, Seljak & White 2000). While the maps of weak lensing distortion numerically comprise a weighted projection over the full three-dimensional tidal shear pattern, it is in essence a slice through the latter which is shown in the figures illustrated in this contribution. In fact, based on the full 3-D tidal field, Couchman, Barber & Thomas (1999), devised a computational scheme to predict the resulting weak lensing distortion pattern. Immediately evident from the tidal bar maps in Fig. 25 is the reason why clusters have been the main focus of studies employing the observed weak lensing image deformation configurations to infer the mass of the enclosed cluster mass (based in particular on work of Tyson, Wenk & Valdes, 1990 and Kaiser & Squires 1993). Only in their immediate surroundings the tidal field strength is substantial enough, and the pattern appropriately well-behaved, that a reconstruction from the observed galaxy images yields a gravitational matter distribution with a sufficiently high signal/noise level. The more moderate to weak field values pertaining throughout the general cosmic field, and as yet even around filaments, have not yet produced reconstructions that would represent unequivocal significant mass distributions. On the other hand, comparing the relative tidal strengths, we may expect that cluster mass estimates on the basis of the observed shear pattern will to some extent be influenced by the surrounding structures (for a thorough study see Hoekstra 2001). Promising is that in recent years advances in detector sensitivity have surged to such extent that the presence of significant image distortions by the general field of large scale structures – the detection of *"cosmic shear"* – has been demonstrated beyond doubt on the basis of intricate statistical analysis (Van Waerbeke et al. 2000). However, maps of the

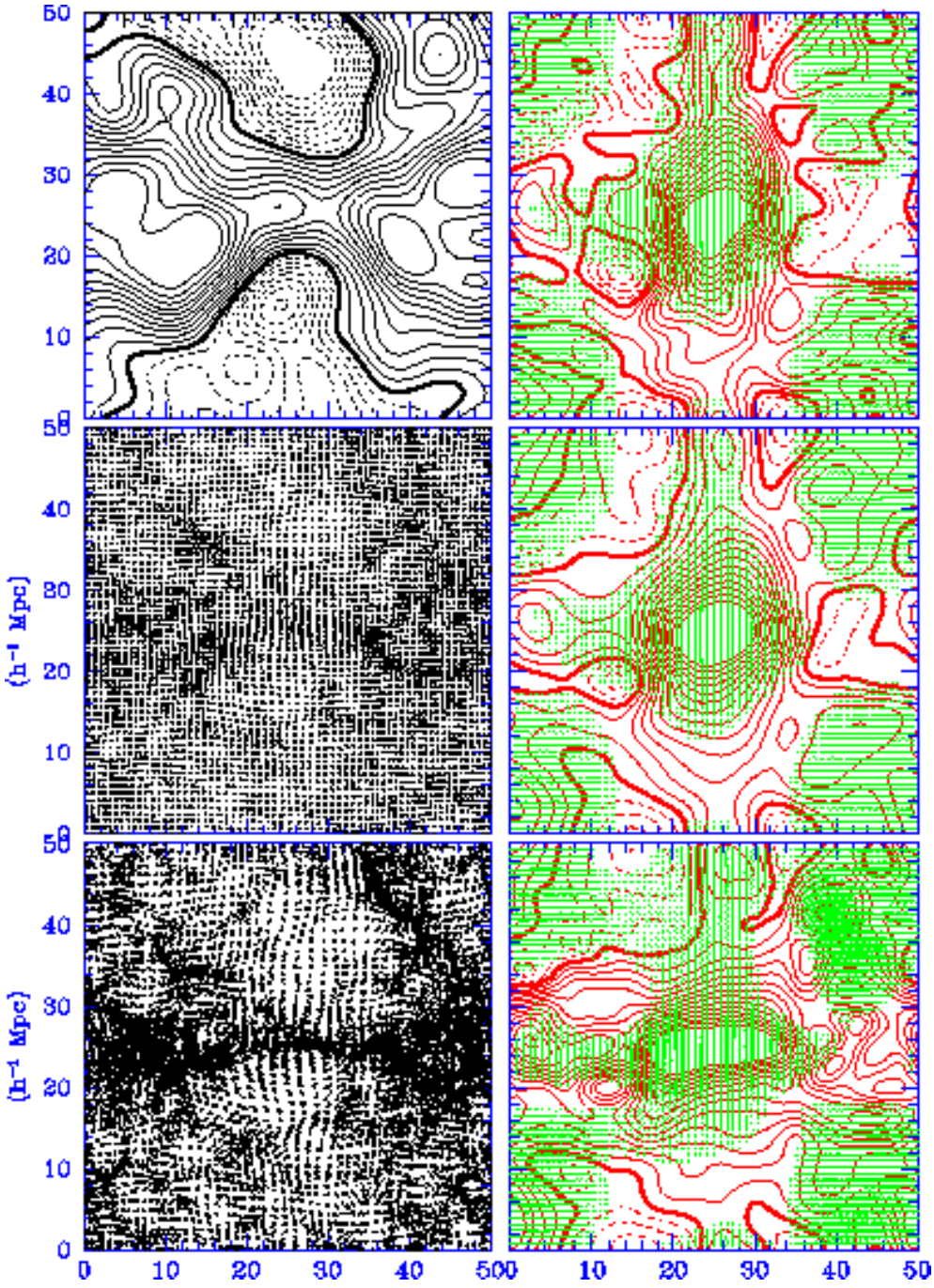
50
40
30
20
10
0
(h⁻¹ Mpc)
0
10
20
30
40
50

Figure 26. The emergence of a filament in an SCDM structure formation scenario. Based on the basis of a $N-body$ simulation of a particular (constrained) realization. Lefthand column: density/particle distribution in z-slice through the centre of the simulation box. Righthand column: the corresponding tidal field configurations, represented through the full tidal field strength $|T$ contour maps (red), as well as the corresponding compressional tidal bars (scale: $R_G = 2h^{-1}$Mpc). Top row: primordial cosmic conditions (primordial density field and tidal field). Centre row: $a = 0.2$, the first onset of an emerging filament. Bottom row: the filament at the present epoch (for this realization: $a = 0.8$. Note the formation of the filament at the site where the tidal forces peaked in strength from the onset onward, with a tidal pattern whose topology remains roughly similar, although the flattening of the tidal contours along the spine od the ultimately contracted filament is readily apparent.

cosmic matter distribution in the general field still seem to be just beyond grasp of current technology.

4.5.4 *Tidal Moulding: Shaping a Filament, a History.* The strong correlation between the compressional components of the tidal field and the presence of a dense filamentary feature (or, similarly yet less pronounced, wall-like patterns) conjures up the question of the nature of a possible causal link between these two physical aspects. For investigating such a causal link, we in particular wish to assess whether the presence of a strong tidal field presages the in situ "condensation" of a wall, filament or related structure. The emergence of the cosmic web pattern could then be described as a process of casting the affiliated cosmic matter flows into a primordially shaped mould, which would have been outlined at the onset by the tidal field induced by the tiny matter density fluctuations in the pristine Universe.

Indeed, preliminary systematic investigations of such a causal connection do indicate the formation of the web pattern following the directions outlined by the primordial tidal field, specifically of its compressional components. Figure 26 is displaying the development of the filamentary structure of Fig. 24. In a sequel of three timesteps, from top to bottom rows, it displays the corresponding primordial density field ($a(t) = 0.0$, top row), and the gradual emergence through a moderate quasi-linear phase ($a = 0.5$, central row) to the final assembly into the salient nonlinear filament ($a_\circ = 1$, the present epoch). While we see a drastic evolution in the configurations of the matter distribution (the left column frames depict the matter distribution in the central $x - z$ plane for the 3 timesteps), the configuration in the corresponding tidal field contour maps (frames in the righthand column, contours in red) display a considerably more moderate development. Qualitatively, they appear to retain their primordial signature quite well, be it that the later more anisotropic stages naturally involve a correspondingly elongated tidal field. Yet, we also clearly see the formation of the filament

precisely there where the primordial compressional field is very strong and coherent. We therefore argue that a *mapping of the compressional tidal component represents a prediction for the locus of the main cosmic web features.*

4.5.5 *Tidal Moulding: Weaving the Cosmic Tapestry, a History.* With the gradual emergence of one particular filament seemingly predestinated by the tidal field configuration, it is rather logical to expect this to reflect a global process in which the complete cosmic foam is being cast by the overall tidal field pattern. This indeed is what the evolution of the cosmic web pattern in an open $\Omega_\circ = 0.3$ FRW Universe dominated by CDM evidently shows in Figure 27. The particle distribution at three consecutive cosmic epochs ($a = 0.2$, $a = 0.4$ and $a = 0.6$) shows the emerging cosmic foam, whose outlines have been marked at a relatively early time. The development of the cosmic foam essentially consists of a rapid increase of its density contrast as matter flows into its skeleton, a growth which ceases at around $a = 0.3 - 0.4$. Evidently, the evolution between top, $a = 0.2$, and centre panel, $a = 0.4$, is substantial. This is hardly so between centre, $a = 0.4$, and lower panel ($a = 0.6$).

The evolution and structure in the particle distribution is clearly reflected in the (compressional) tidal field pattern (panels right column). The tidal bars in the top panel already appear to outline most of the web from the onset onward. Note for intance the beautiful correlation between the particle content and tidal bar configuration of the two filaments running diagonally upward and roughly parallel from the lefthand lower corner of each panel. Another prominent example is the large assembly of filaments – with clusters acting as nodal joints – that runs from roughly halfway the top of the panel towards its righthand lower corner. It stands out clearly at all three consecutive timesteps. Interestingly, the filaments do indeed appear to be outlined from very early cosmic epochs onward while the clusters do not. They only show up as dominating "tidal loops" at later epochs, once the web is reaching fruition. This appears to suggest cluster locations to be determined by the cosmic foam or, rather, its tidal cast. In conclusion, this teaches us how intimately the cosmic web and the population of clusters are linked as accessories of the full cosmic foam machinery.

4.6. Hierarchical Assembly: Web Granularity

Having identified the principal mechanism behind the foamlike geometry of the large scale matter distribution, it is important to point out

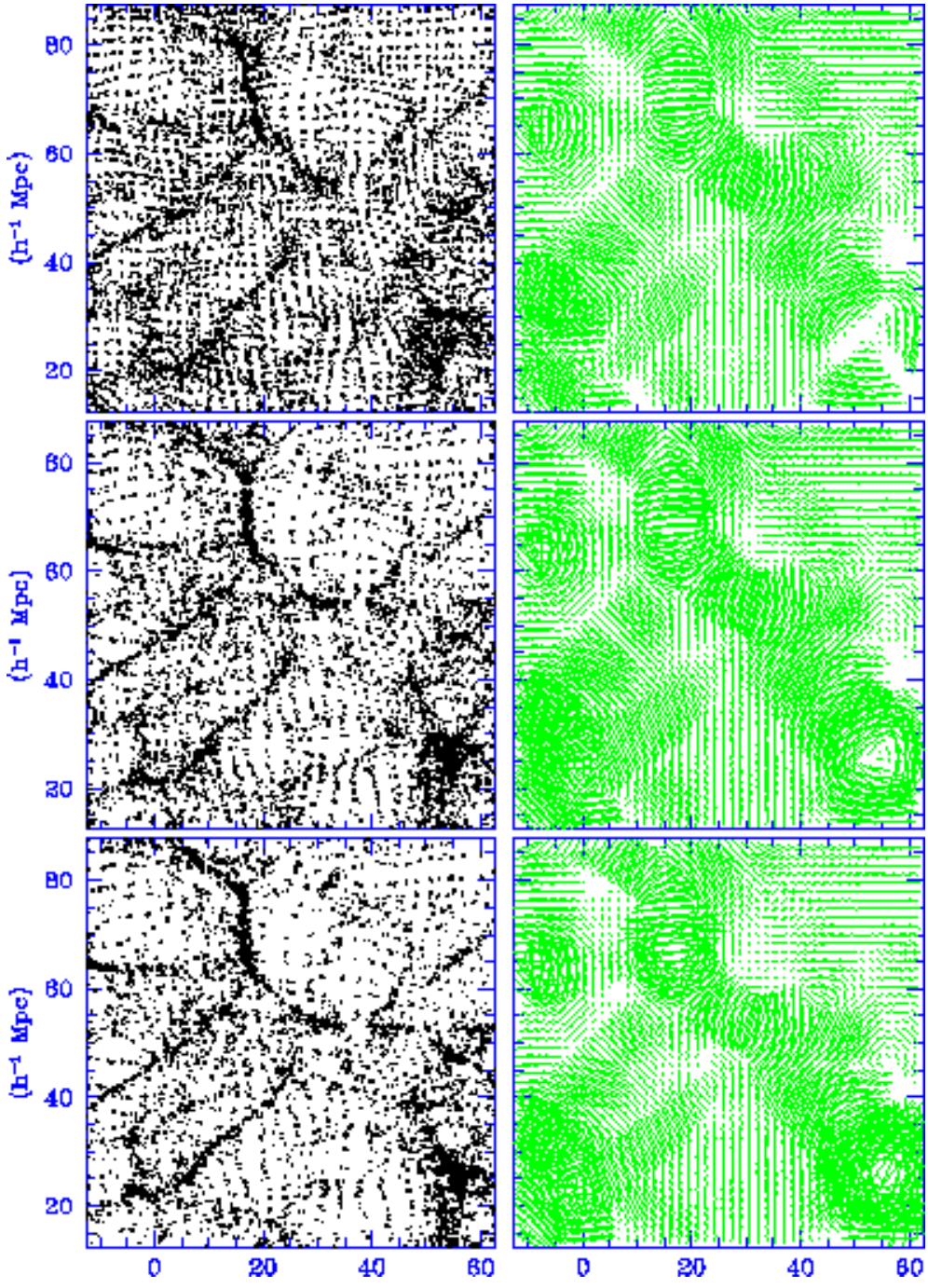
80
60
40
20
(h^{-1} Mpc)
0
20
40
60

Figure 27. Evolution of a cosmic foam pattern in an open $\Omega_\circ$ CDM Universe. For three consecutive timesteps with expansion factors $a = 0.2$, $a = 0.4$ and $a = 0.6$, each row shows the particle distribution in the central z-slice through a corresponding N-body simulation realization (lefthand frame) in conjunction with the compressional tidal bar configuration in the same slice (righthand frame). The geometry of the weblike matter distribution does not involve substantial qualitative changes. The process of structure formation appears to consist of a gradual inflow of matter into the web channels. These channels, sites where filaments appear to emerge, can be traced back to the primordial tidal field pattern.

that the full assembly of cosmic structure is considerably more complicated than a single monologous collapse into a global superstructure.

On the contrary, the observed cosmic matter distribution is a stochastic superposition of a great many different fluctuations, covering a wide range of scales and dynamical states. Although all perturbations evolve simultaneously through their mutually effected cosmic gravity field, they do so by their own individual rate, chiefly determined by scale and physical configuration. The decisive quantity is their primordial amplitude, setting the dynamical timescale and evolution rate. Hence, the key significance of the fluctuation power spectrum, the function specifying the expected perturbation amplitudes at each spatial scale.

What emerges is a picture of cosmic structure consisting of a complex of structures and features, moulded into ever larger entities, ultimately grouping into an encompassing foamlike Megaparsec structure. The individual substructures will have reached different evolutionary stages and hence display a diverse range of morphological geometries. Compact and dense clumps have emerged at highly advanced stages. More moderate quasi-linear phases have been reached by the features displaying the most pronounced anisotropic – elongated or flattened – geometries. On the very largest scales only some mild density depressions or enhancements can be discerned, being fluctuations still residing in the very early linear regime of growth.

4.6.1 *Hierarchical Assembly: Clump formation.* In hierarchical formation scenarios small-scale fluctuations have a higher primordial amplitudes as the larger scale ones in which they are embedded. These small sized perturbations will therefore have passed through the full itinerary of evolutionary phases at a substantially faster rate than the ones on a larger scale. We will therefore observe the small scale clumps to be the first ones to emerge as genuine recognizable cosmic objects. The larger scale perturbation will not yet have matured as fully yet. Instead, we will observe the gradual development of the encompassing perturbation through merging and accretion of the smaller scale clumps, a process which may be readily appreciated from the computer simulation shown

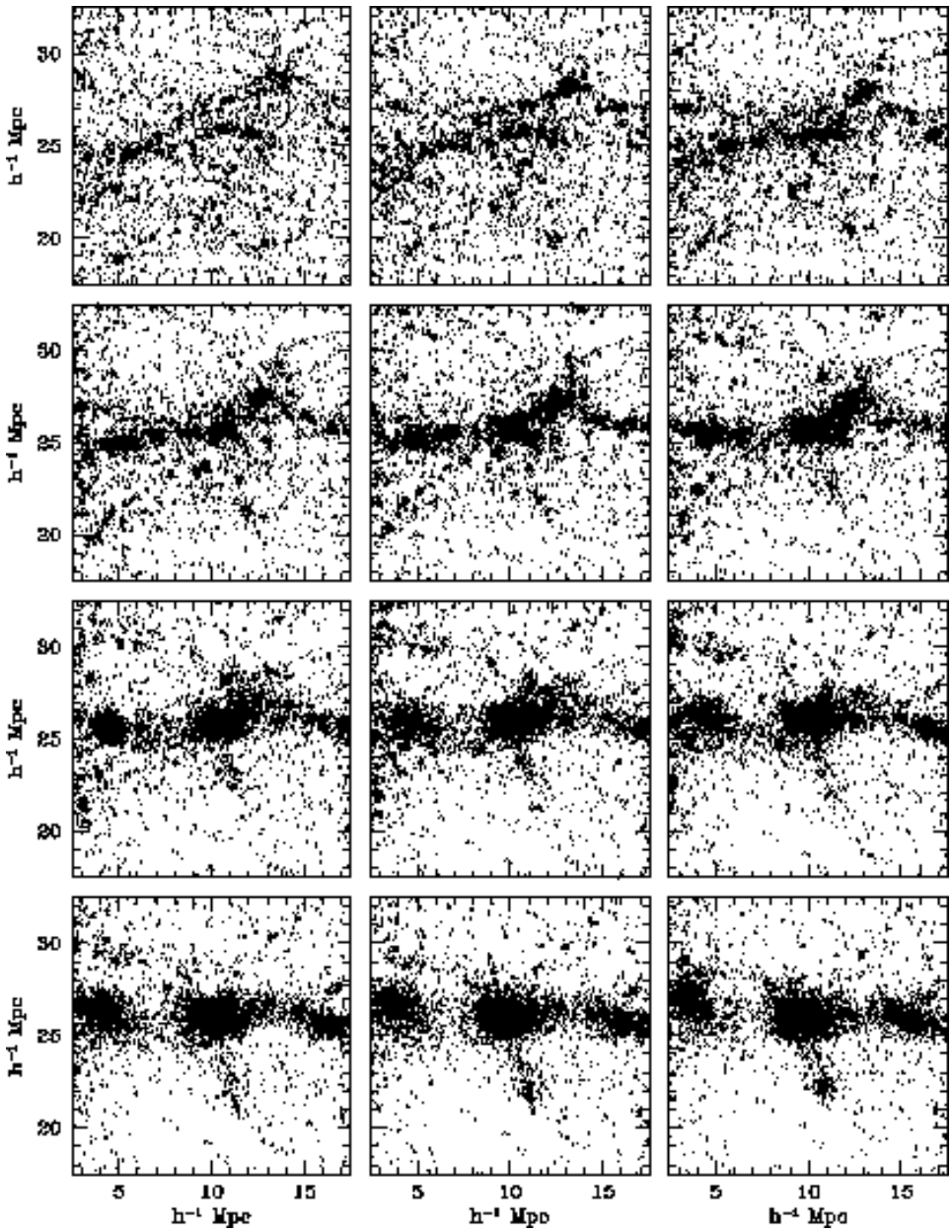

Figure 28. Gravitational Instability: hierarchical assembly of a filamentary structure. Focussing in on a small $15 \times 15 \times 15 h^{-1}$Mpc region of a P^3M N-body simulation of structure formation in a SCDM scenario ($\Omega_0 = 1.0, H_0 = 50\,$km/s/Mpc), from the $100h^{-1}$Mpc box 128^3 simulation shown in Fig. 12. Time is running from top left to bottom right, from $a = 0.1$ to $a = 1.0$. Notice how small-scale clumps aggregate into ever larger haloes, all arranged along a roughly filamentary configuration (oriented horizontally).

in Fig. 28. Aptly described by the concept of *merger tree* (see e.g. Kauffman & White 1993), the precise path that an encompassing perturbation follows towards final collapse and virialization may be highly diverse. Both accretion onto a small-scale core as well as merging of more comparable substructures are viable evolutionary tracks. The precise historic track that will be followed will be determined by scale and specific physical circumstances.

At a typical galaxy scale ($\sim 0.5h^{-1}Mpc$), perturbations underwent gravitational collapse, virialization and – as at these scale gas and radiative processes do play a dominating role – further dissipative contraction of its baryonic matter content within the dark matter potential well. Ultimately, this yields the gaseous and luminous basic constituents of our Universe, the galaxies.

Encompassing a larger primordial region, rich galaxy clusters are generically considered to represent the most massive and most recent (nearly) fully collapsed and virialized structures in our Universe. Their inner and most compact regions have certainly fully matured. Often they form the core of a wider vigorously evolving complex, while substantial amounts of surrounding material continuously accrete while the encompassing perturbation is approaching a comparable stage of development.

4.6.2 *Hierarchical Assembly: Linear Power Law Excursions.* Turning attention to the quasi-linear structures within these hierarchical scenarios – at a present-day scale in the order of $\sim 10h^{-1}$Mpc – we still find the development of a foamlike geometry. However, its assembly will not have been the result of a simple monologous anisotropic contraction. Instead, it will have emerged through a preferential gravitational clumping of substructures along the principal directions of the corresponding large-scale anisotropic collapse. Hence, walls and filaments will not be uniform and coherent structures, but instead resemble a grouping of beads on a rod.

In fact, nearly all viable formation scenarios may be regarded specific versions of the same hierarchical theme. The major differences in coherence of structures and other physical characteristics between the various hierarchical scenarios can ultimately (mostly) be traced back to differences in *power spectrum slope*,

$$n \;=\; \frac{d\ln P(k)}{d\ln k}\;. \tag{56}$$

The latter determines the relative dynamical state of substructures by the time they combine into a larger encompassing structure. If they

are fully virialized objects a "grainy" configuration will emerge, while a roughly similar dynamical timescale over a wide range of scales – i.e. a spectral slope $n \sim -3$ – will yield a rather coherent structure. This can be readily appreciated by considering the relative timescales in which structures on various mass scales M will form within hierarchical formation scenarios. To retain lucidity, let us restrict to a scenario with a pure power spectrum,

$$P(k) \;=\; A\; k^n \;. \tag{57}$$

We follow a description on the basis the excursion set formalism (Bond et al. 1991) which extended the Press-Schechter formalism (Press & Schechter 1974), putting it on a more robust physical footing. This analytical formalism has proven to yield remarkably good predictions on the sample average characteristics of an emerging population of nonlinear objects evolving from a linear field of density fluctuations in the primordial cosmos.

The pure Press-Schechter treatment makes the assumption of nonlinear objects evolving from initial fluctuation peaks whose shape is perfectly spherically symmetric. Then, the fully analytically tractable spherical model (Gunn & Gott 1972) can be invoked to find relatively simple expressions for the dynamical timescales of the evolving density perturbation. As the analytical arguments are algebraically most tractable within the context of the Einstein-de Sitter Universe ($\Omega_0 = 1.0$), we will here restrict ourselves accordingly.

For any spherical initial (linear) overdensity Δ_i we may then identify the epoch a_{turn} at which its initial expanding motion turns around into contraction, the epoch a_{vir} at which it will have contracted towards its virial radius, and in the academically interesting yet physically less relevant collapse time a_{coll} at which it will have collapsed onto a singular point. Relating the dynamics of the spherically contracting cloud to the (hypothetical) linear evolution of the initial density field, the observation can be made that these dynamically characteristic (nonlinear) epochs can be simply related to the corresponding linearly extrapolated density excess, $\Delta_{lin}(t)$ of the same perturbation,

$$\Delta_{lin}(t) \;=\; \frac{D(t)}{D(t_i)}\;\Delta_i \;>\; \delta_c, \tag{58}$$

in which $D(t)$ is the density perturbation growth factor according to linear gravitational instability theory (Peebles 1980). Hence, once the linearly extrapolated $\Delta_{lin}(t)$ exceeds the proper critical (excursion) value, δ_c, we will observe the nonlinearly evolving spherical density perturbation itself to reach the the corresponding characteristic phase. The

value of the (excursion) values δ_c appear to be universal for the specific spherical case, and for an Einstein-de Sitter Universe are given by the values:

$$\delta_{c,turn} \;=\; 1.08 \;; \quad \delta_{c,vir} \;=\; 1.59 \;; \quad \delta_{c,coll} \;=\; 1.69 \;, \qquad (59)$$

where we presumed the fluctuation to start its evolution on the basis of the growing mode solution of perturbation theory (Peebles 1980). These values will be slightly modified if e.g. the perturbation sets off without an initial corresponding velocity perturbation.

The *excursion set* description thus readily identifies the characteristic stages of its full nonlinear evolution – turnaround time, virialization time and ultimate collapse time – with that of reaching a critical linearly extrapolated density value, we may simply turn to the far simple Gaussian nature of the initial density fluctuation field to predict the full history of the emergence of objects from those initial conditions. As the formalism treats fluctuations over all scales on an equal footing, it deals with the collapse of density excesses over a large range of scales. This translates into an impressively insightful and surprisingly accurate description. The ongoing process of fully collapsed objects merging is the process contributing to the growth of the larger-scale density fluctuations. Gradually, the encompassing large scale entity will then reach a collapse phase where its linear (extrapolated) density excess passes through the critical *excursion* value. By working out the history of emerging objects according to this formulation in terms of the Press-Schechter philosophy, we are able to construct for any given realization of the primordial density field the resulting *merger tree* history of the hierarchical process (Bower 1991, Kauffman & White 1993).

By reducing the nonlinear formation history to one in which we can focus on the initial fluctuation field, the problem has been simplified to one in which we deal with simple Gaussian statistics. This then leads to a situation in which we can readily compute at each cosmic epoch t the fraction $F(M,t)$ of matter fluctuations on a given mass scale M that will have fully collapsed. Its time dependence is fully incorporated through the evolving value of the density field dispersion value $\sigma(M,t)$,

$$\sigma(M,t) \;=\; \frac{D(t)}{D(t_i)}\,\sigma(M,t_i)\;. \qquad (60)$$

Then, the fraction of linearly extrapolated density fluctuations in excess of the critical value δ_c,

$$F(M,t) \quad = \quad \frac{1}{\sqrt{2\pi}\;\sigma(M,t)}\;\int_{\delta_c}^{\infty}\;\exp\left\{-\frac{\delta^2}{2\sigma^2(M,t)}\right\}\;d\delta$$

$$= \quad \frac{1}{2}\left[1 \; - \mathrm{erf}\left\{\frac{\delta_c}{\sqrt{2}\sigma(M,t)}\right\}\right] , \tag{61}$$

in which erf(x) is the conventional error function. Notice that by this definition of $F(M)$ we deal with the full range of density values, thereby delimiting a mere 50% to overdense fluctuations. Instead of computing the fraction $F(M,t)$ for a given value of the $\sigma(M,t)$, we may invert this by computing the cosmic epoch t at which a particular fixed fraction F_c of the density fluctuations on mass scale M have collapsed (or, equivalently, have turned around or collapsed to the virial radius), and hence the time at which $\sigma(M,t)$ has reached a corresponding critical value σ_c.

$$\sigma(M,t) \; = \; \sigma_c \; \equiv \; \frac{\delta_c}{\sqrt{2}} \, \mathrm{erfinv}\left\{1 - 2F_c\right\} \; , \tag{62}$$

with erfinv(x) the inverse error function. By comparing the corresponding $\sigma(M,t)$ on two mass scales M_1 and M_2 we find the ratio between the density growth factors $D(t(M_1)) \equiv D_t(M_1)$ and $D(t(M_2) \equiv D_t(M_2)$ at which the density field at both scales has reached the same level of "fruition". For linearly evolving fluctuations, $\sigma_c = (D_t(M)/D_\circ)\sigma_\circ$, and thus

$$\frac{D_t(M_1)}{D_t(M_2)} \; = \; \frac{\sigma_\circ(M_2)}{\sigma_\circ(M_1)} \; . \tag{63}$$

where the linear density fluctuations on the scale M are normalized to their present day values $\sigma_\circ$. These are directly related to the power spectrum $P(k)(\propto k^n)$ of the density field via the corresponding length scale,

$$\sigma^2(M) \; = \; \left\langle \left(\frac{\delta\rho}{\rho}\right)^2 \right\rangle \quad \propto \quad M^{-(n+3)} \; . \tag{64}$$

We therefore see that the characteristic dynamical times on different mass scales M, specified in terms of the linear growth factor D_t of matter fluctuations, can be straightforwardly related to the spectrum of primordial density fluctuations,

$$\frac{D_t(M_1)}{D_t(M_2)} \; = \; \left(\frac{M_2}{M_1}\right)^{(n+3)/2} \; . \tag{65}$$

On the basis of the above we find major differences in the qualitative progression of the hierarchical evolution process for fluctuation spectra with different spectral slopes n. Proceeding from a pure white noise spectrum with $n = 0$ to spectra with ever more negative values of n

$(0 > n > -3)$, we notice a diminishing ratio of characteristic timescales. Hence, in a scenario with $n = 0$ we will see the full collapse and virialization of small-scale M_1 clumps before fluctuations on an order of magnitude larger scale M_2 start to approach a similar stage. By contrast, such M_1 fluctuations will hardly get the time to fully virialize before the encompassing larger scale M_2 fluctuations reach a similar dynamic state.

4.6.3 *Hierarchical Assembly: Granulated Filaments.* Taking the specific example of an emerging filament, its formation will consist of the gradual assembly of earlier virialized small-scale clumps. A rather grainy feature will be the result. In an $n = -2$ scenario, on the other hand, the contracting filament will be collapsing while its contents in smaller scale clumps have not yet had the opportunity to fully settle. Often these have not yet even reached a stage of full virialization, and perhaps still reside in a stage with a pronounced anisotropic geometry (i.e. only one or two of its principal axes have passed on to full collapse). Such scenarios will produce coherent large-scale filaments in which the internal small-scale structure is only moderately visible, if at all once they get fully merged with the encompassing superstructure. Most dramatic will be the $n = -3$ scenario, which is the asymptotic situation in which fluctuations over the full range of scales undergo contraction and collapse at the same time. It marks the fundamental limit for genuine hierarchical clustering. In other words, we have identified a sliding scale of morphological constituency and appearance within the context of possible hierarchical structure formation scenarios.

4.6.4 *Hierarchical Assembly: Shaping Up.* Unlike the basic Press-Schechter formulation followed above, based on spherical configurations, a realistic formalism should take into account the intrinsically anisotropic shape of (primordial) density peaks. From the statistics of linear Gaussian random fields (e.g. Bardeen et al. 1986) we know that spherical density peaks do not exist, all peaks have at least some degree of primordial flattening, be it never extreme. Referring to the growing anisotropy of homogeneous ellipsoidal overdensities, it is evident that this will involve considerable repercussions for the evolution of each individual peak. Indeed, merely correcting for this by means of an approximate idealized (isolated) homogenous ellipsoidal model has already proven to yield a significant improvement on quantitative aspects and details such as the predicted mass function of collapsed clumps (Sheth, Mo & Tormen 2001).

For the purpose of our focus on the morphology of filaments, a major consequence is the corresponding diffusion in collapse time scales.

Collpase times will no longer only be set by the value of the initial overdensity, its primordial shape will modify this to a considerabel extent. It may lead to situations in which clumps with a higher amplitude initial overdensity may reach ultimate collapse later than a more moderate overdensity, in the case of its primordail shape being sufficiently more elongated.

For our considerations concerning flattened and filamentary features these modifications will be even more relevant. We are interested in exactly those scales at which the large-scale object is still residing in one of its intermediate anisotropic phases. Unlike issues of final halo mass spectrum, here collapse has not yet progressed through the full itinerary of the ultimate 3-D collapse unto a compact clump. One property of anisotropic collapse is the differentiation in collapse times along each of the principal directions of the object, inducing a diffusion in relative collapse timescales (see the axis evolution of a homogeneous ellipsoid, Fig. 20). The issue of comparative *dynamical timescales* at different spatial scales of hierarchically embedded structures will therefore be even more contrived than in the simple approximate scheme presented above.

For instance, in a strongly elongated case the longest axis may not yet have reached the contraction phase while along the shortest axis the object is well on the way towards full collapse, reaching this stage on a much shorter timescale than it would have done in the equivalent spherical case. At some given scale a structure may therefore not yet have evolved to an evolutionary state as advanced as its peer would have done in the purely spherical case (because its final collapse direction, along the longest axis, has evolved more slowly). On the other hand, the encompassing overdensity on a larger scale may have advanced up to a stage of contraction along the shortest axis at a considerably faster rate than it would have done in the equivalent spherical situation. With respect to a purely spherical formalism, it would involve a convergence of evolutionary timescales of structure at different spatial scales.

Nonetheless, we may consider expression (65) as a useful guiding principle. It represents a robust lower limit to an effect that may get aggravated by the diffusion of timescales resulting from the modifications on the basis of peak anisotropy. These would amplify the effect and therefore, if anything, underline the presented analytical arguments even more strongly.

In summary, in a scenario with a higher value of spectral slope $n \uparrow 0$ (towards white noise) the interscale difference in dynamical timescales is sufficient large that we will still be able to distinctly identify between the subsequent evolutionary phases at various scales. In such a scenario, the typical "granular" character will be retained. On the other hand, as

the slope n of power law scenarios tends more and more towards lower values, $n \downarrow -3$, the emerging coherent superstructures will assume an increasingly dominating stature over their substructure. The contrast of the latter will diminish as n decreases, while the filamentary and/or wall-like nature of the superstructure will stand out stronger and stronger.

Even further complications are awaiting us when focussing on the detailed nonlinear gravitational effects occurring in the interior of the web structures. "Interscale" nonlinear gravitational interactions will be linking up features at different scales, producing an additional amplification of their alignments.

4.6.5 *Hierarchical Assembly: Nonlinear Aggravation.* The "Press-Schechter" type linear arguments presented above in essence involve a simple "isolated nonlinear" extrapolation of features identified in the primordial density field. It does not take into account the nonlinear interactions between the features forming at various scales. In fact, the hierarchical congregation of filamentary structures is considerably complicated by a variety of such nonlinear effects.

A systematic alignment of flattened peaks with respect to their surroundings is a generic property in any Gaussian linear initial density field (e.g. Bardeen et al., Van de Weygaert & Bertschinger 1996). These primordial alignments get significantly amplified by the subsequent infall of clumps from the surroundings, in which several extra nonlinear effects may be discerned.

Subclumps rain in along directions set out the large-scale configurations. The hierarchical buildup of a filament makes the impression of a process of a gradual and continuous inflow of small clumps alon the direction of the filament towards the highly dense connecting clusters. It's as if filaments act like migration channels of the emerging cosmic web.

Earlier, we have seen that the location of these channels can be traced back to the primordial tidal field pattern. The morphology and nature of filaments – strong, dominating, large and coherent or bearing the character of short, weak and erratic hairlike extensions connected to nearby peaks – will be of decisive influence over aspects like the angular distribution of clumps infalling towards a cluster. An interesting nonlinear alignment amplification is involved with this process.

Van Haarlem & Van de Weygaert (1993, HW) focussed on the infall pattern of clumps as they are channelled through the filament towards heavy clusters (see Fig. 29 and Fig. 30, from HW). As expected, the infall pattern is heavily influenced by the strength, contrast and multitude of the filamentary connections of the cluster towards the cosmic

surroundings. In Fig. 29 and Fig. 30 we see the difference between the infall towards a cluster arising in a SCDM formation scenario and that towards a cluster in a pure white noise ($P(k) \propto k^0$) scenario, lacking any substantial large-scale power. In the case of the SCDM scenario (Fig. 30, with a slope $n \approx -1$ on the relevant cluster scale) we observe a pronounced and dominating filament. It induces a pattern of continuously infalling subclumps, all entering along the one outstanding direction defined by the filament. In the other set of frames (Fig. 29), we see the effects of a typical "white noise" ($P(k) \propto k^0$) scenario, with small scale clumps having fully settled before one can even start to notice the presence of features on a larger spatial scale. Upon the cluster-like core

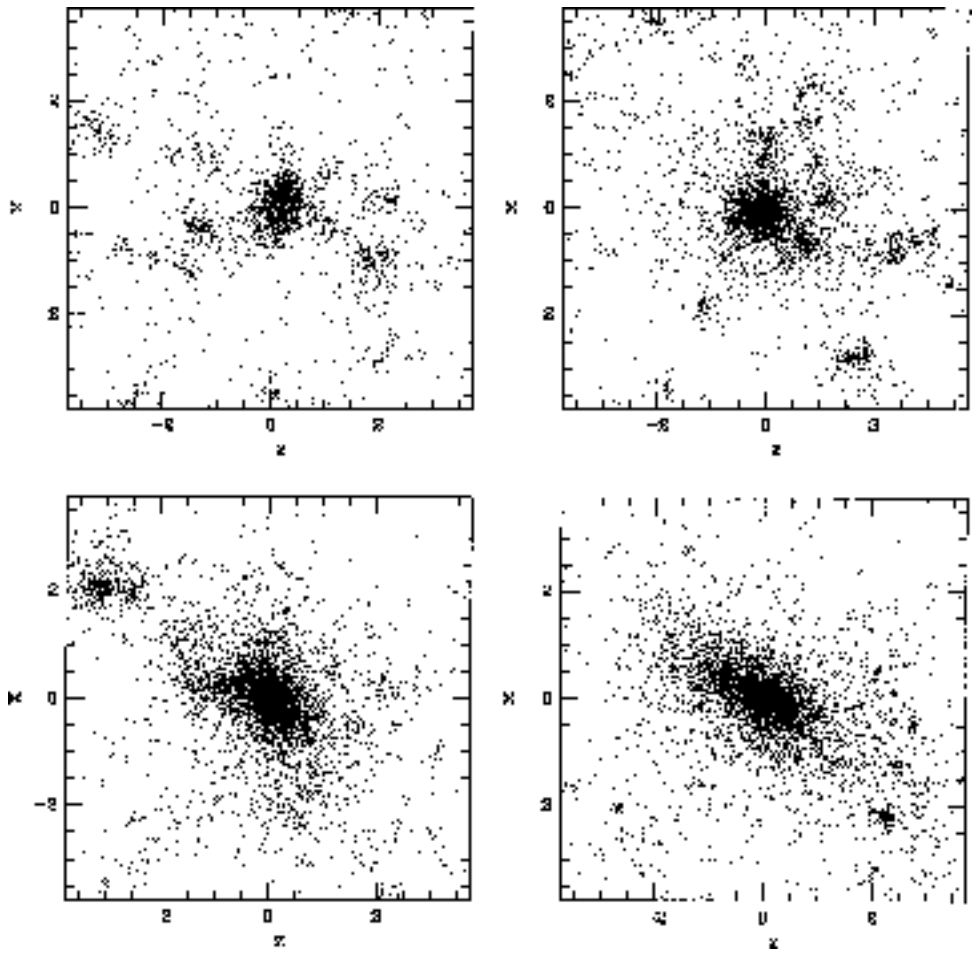

Figure 29. Infall onto forming cluster: infall from arbitrary directions, typical for a $P(k) \propto k^0$ white noise structure formation scenario (Einstein-de Sitter Universe, $\Omega_0 = 1$. From Van Haarlem & Van de Weygaert 1993. Reproduced by permission of the AAS.

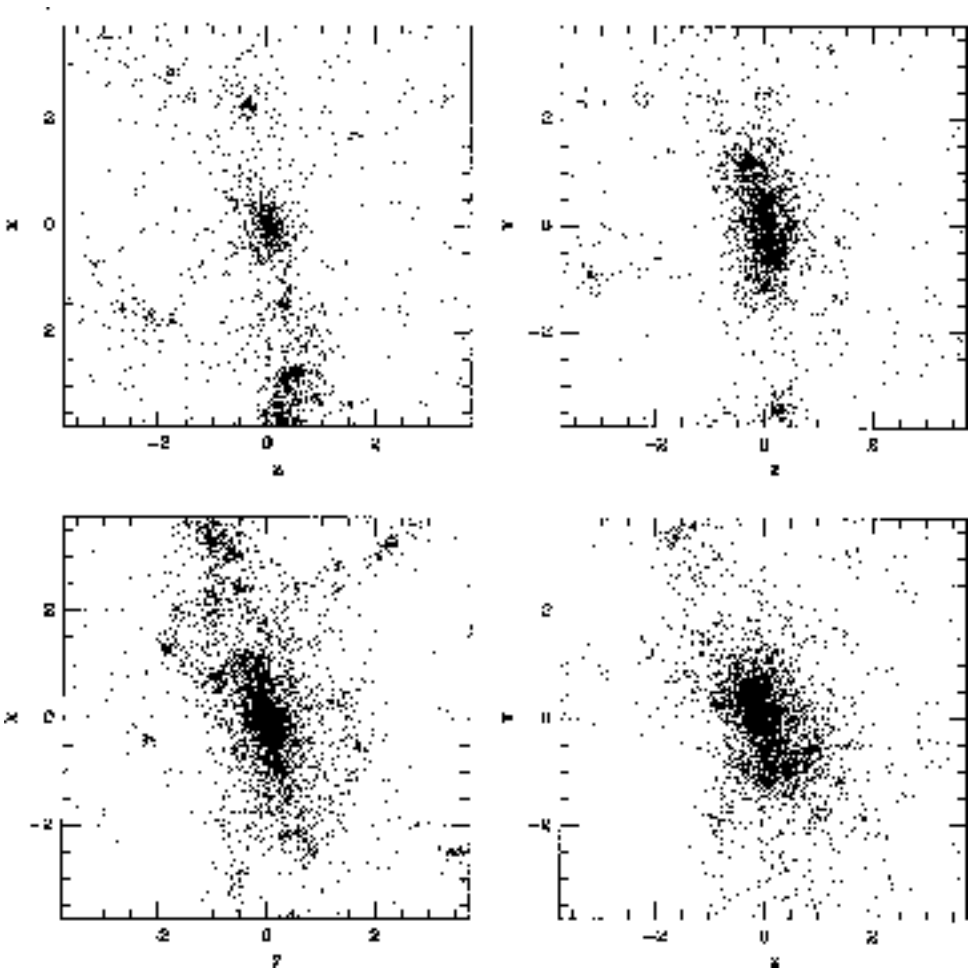

Figure 30. Infall onto forming cluster: channelling of infalling clumps via a filament connecting to the cluster, typical in a CDM structure formation scenario in a Einstein-de Sitter Universe ($\Omega_0 = 1$). From Van Haarlem & Van de Weygaert 1993. Reproduced by permission of the AAS.

finally having arrived at a stage of contraction, it is accompanied by an isotropic pattern of small clumps continuously raining in from all over the "sky"

Interestingly, a cluster appears to orient itself towards the direction along which the last substantial subclump came falling in (HW). This is a pure nonlinear gravitational effect, involving the equipartition and virialization of the energy and momentum contained in the "particles" of the infalling clump. The preferential direction defined by the infall direction of the clump, and hence of the major share of the linear momenta

of its constituent "particles", then leads to an anisotropic redistribution in the phase space of the resulting merger.

As a consequence of the cluster orienting itself towards the last infalling clump the angular distributions of the infalling objects assume an even more significant influence. In the $P(k) \propto k^0$ scenario, the orientation of clusters will hardly have any systematic correlation with the surrounding matter distribution. This stands in marked contrast to the situation in the presence of a pronounced filament. The exclusive and continuous infall of clumps along the spine of the dominating filament (see Fig. 30, from HW) indueces a strong aligment of cluster orientation, its substructure and the cosmic surroundings. This was most manifestly depicted in the sky distribution of infall directions of clumps onto the evolving cluster complexes. In the white noise $n = 0$ situation, the "sky" pattern did not reveal any preferred direction. On the other hand, an outstanding and stable infall angle could easily be identified in the case of the CDM cluster (see HW, Fig. 30).

In summary, in hierarchical scenarios with a relatively high level of large scale power we can discern a variety of mutually amplifying factors contributing to the development of pronounced morphologies. Partially, this had already be predestined by their primordial shape. Due to the spatial correlations in primordial density fields, matter fluctuations are intrinsically aligned. Adding to to such linear primordial circumstances, and occasionally dominating over them, are the various nonlinear couplings between surrounding and embedding structures within the matter distribution.

The implied alignment of clusters with surrounding large scale structure has been adressed in a variety of observational studies. Conclusive evidence is hard to unveil due to a plethora of disturbing physical influences and processes. A few studies tried to find indications through the presence of a significant cluster-cluster alignment (Binggeli 1982, Rhee & Katgert 1987). Other analyses seek to investigate possible vestiges of the cluster infall process on the remaining substructures. One related interesting effect may be that the inflow rate of subclumps becomes a significantly more efficient process through the presence of filaments. A strong indication for the reality of such an effect is the recent work by Plionis & Basilakos (2001), who disclosed a tight link between alignment of clusters with respect to their surroundings and the presence of substructure. Other tantalizing consequences may be a possible trace left in the morphology of infalling galaxies, which will certainly be effected by the influences to which they get subjected upon their arrival in the clusters. Indications for such morphological tendencies have been found by Thomas & Katgert (personal communication, see Thomas 2002).

4.7. Voids holding Sway

It is with some justification that most observational attention is directed to regions where most matter in the Universe has accumulated. Almost by definition they are the sites of most observational studies, and the ones that are most outstanding in appearance. However, inspired by early computer calculations, Icke (1984) pointed out that for the understanding of the formation of the large coherent patterns pervading the Universe it may be more worthwhile to direct attention to the complementary evolution of underdense regions, the progenitors of the observed voids.

4.7.1 *The Bubble Theorem.* Icke (1984) made the interesting observation that the arguments presented for the anisotropic collapse of overdensities, when approximated by that of homogenous ellipsoids, are equally valid when considering the evolution of *low*-density regions. These low-density regions are the progenitors of the observed voids. Note that although uniform ellipsoids at first appear to be a rather artificial configuration, they do represent proper second-order approximations to the density field in the immediate vicinity around a peak or dip, a fact that may be easily appreciated from the fact that the smallest closed contours in any topographical map are ellipses. While for underdensities the same equations are used for this approximation, the *quintessential* observation is that the sense of the final effect is reversed. Because a void is effectively a region of negative density in a uniform background:

- *Expansion*
  Voids expand as overdense regions collapse
- *Spherical shape*
  slight asphericities decrease as the voids become larger.
- *Velocity field*
  The (peculiar) velocity field has a Hubble-type character, linear in position: super-Hubble expansion.

The second point can be simply deduced from the observation that with respect to an equally deep spherical underdensity, an ellipsoidal void has a decreased rate of expansion along the longest axis of the ellipsoid and an increased rate of expansion along the shortest axis. Moreover, one may readily appreciate that the uniform density of homogeneous ellipsoids corresponds to a velocity field that will be a linear function of position, so that in the interior of such a void we will observe a Hubble-type velocity field. In summary, voids will behave like low-density 'super-

Hubble' expanding patches in the Universe. To describe this behaviour the term "Bubble Theorem" (Icke 1984) was coined.

Evidently, we have to be aware of the serious limitations of the ellipsoidal model. It disregards important aspects like the presence of substructure. More serious is the neglect of any external influence, whether secondary infall, "collision" with surrounding matter, or the role of nonlocal tidal fields. Yet, comparison with the evolution of voids in realistic clustering scenarios shows that in the case of voids, it tends to become a better description as time proceeds, in particular for the very inner regions. N-body simulations clearly bear out that the density fields in the central region of the (proto)void will flatten out while the voids expand and get drained (Fig. 31, from Van de Weygaert & Van Kampen 1993). Hence, voids develop into regions of a nearly uniform density and the region of validity of the approximation grows accordingly.

4.7.2 *Soapsud of Expanding Voids.* By contrast to the overdense features, the low-density regions start to take up a larger and larger part of the volume of the Universe. Upon their discovery, the independent dynamical role of underdense regions was not immediately appreciated, many considering them mere byproducts in the form of space evacuated by contracting high density clumps. Once it got realized that also dips and valleys in the pristine density field may develop a distinct dynamical evolution of their own (e.g. Hoffman & Shaham 1982), it was straightforward to see that such underdense regions must play an essential and independent dynamical role in the formation of cosmic structure. Even though the value of their underdensity cannot surpass the natural value of -1.0 – nothing can be emptier than empty – their growing size may compensate to achieve a dynamical influence akin to that of a considerably compacter high-density clump, as long as their coherence scale is such that their effective mass is comparable. While they grow to occupy a larger and larger fraction of the Universe, it will be as if matter in the intervening high-density domains will gradually be swept up in the wall-like and filamentary interstices, yielding a natural explanation for the resulting coherence of the cosmic foam. In realistic circumstances, expanding voids will sooner or later encounter their peers or run into dense surroundings. The volume of space available to a void for expansion is therefore restricted. Voids will also be influenced by the external cosmic mass distribution, and substructure may represent an additional non-negligible factor within the void's history. In general, we deal with a complex situation of a field of expanding voids and collapsing peaks, of voids and peaks over a whole range of sizes and masses, expanding at different rates and at various stages of dynamical development. For the

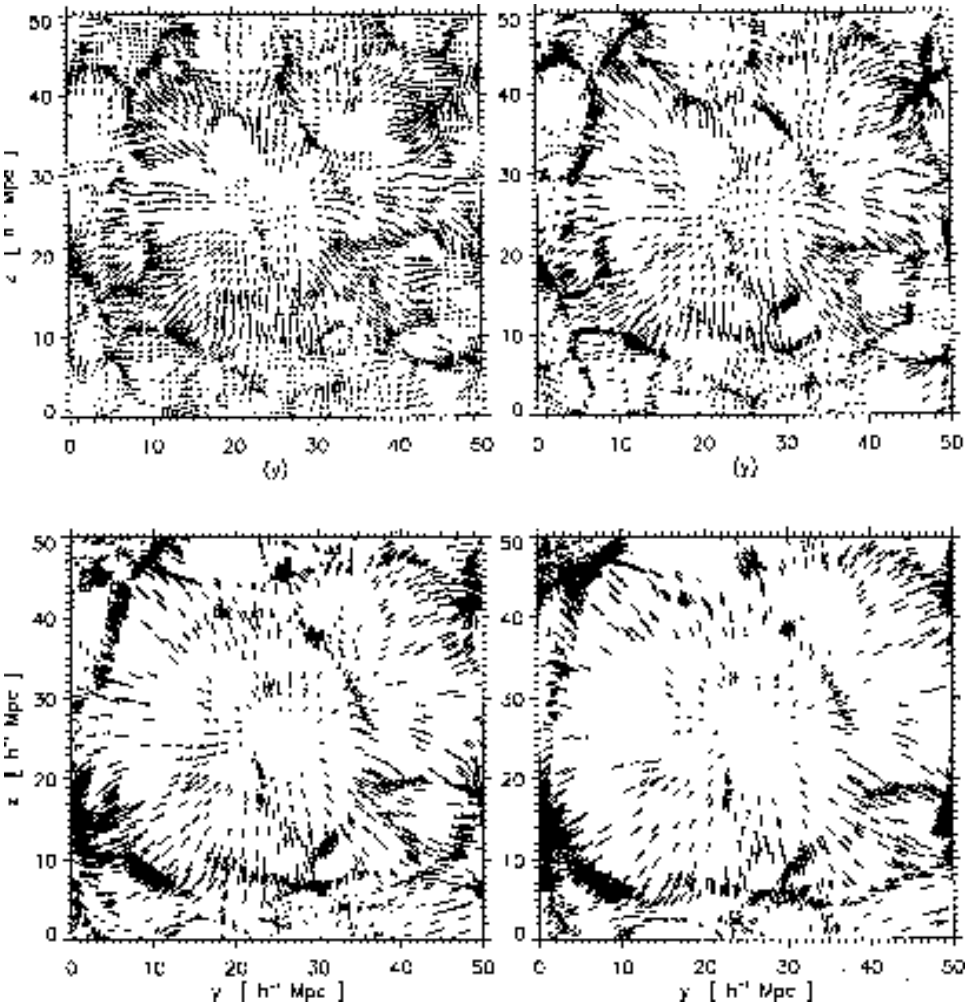

Figure 31. The evolution of a void in a constrained SCDM N-body simulation of a $3\sigma_0(4h^{-1}\mathrm{Mpc})$ void. Shown are particle distributions at expansion factors $a = 0.2, 0.4, 0.7$ and 1.0. The particle position is indicated by a dot, forming the base of the corresponding velocity vector within the slice. From van de Weygaert & van Kampen 1993. Reproduced by permission of the Royal Astronomical Society.

purpose of our geometric viewpoint, the crucial question is whether it is possible to identify some characteristic and simplifying elements within such a complex. Indeed, simulations of void evolution (e.g. Dubinski et al. 1993) represent a suggestive illustration of a hierarchical process akin to the *void hierarchy* seen in realistic simulations (e.g. Van de Weygaert 1991b). It shows the maturing of small-scale voids until their boundaries would reach a shell-crossing catastrophe, after which they merge

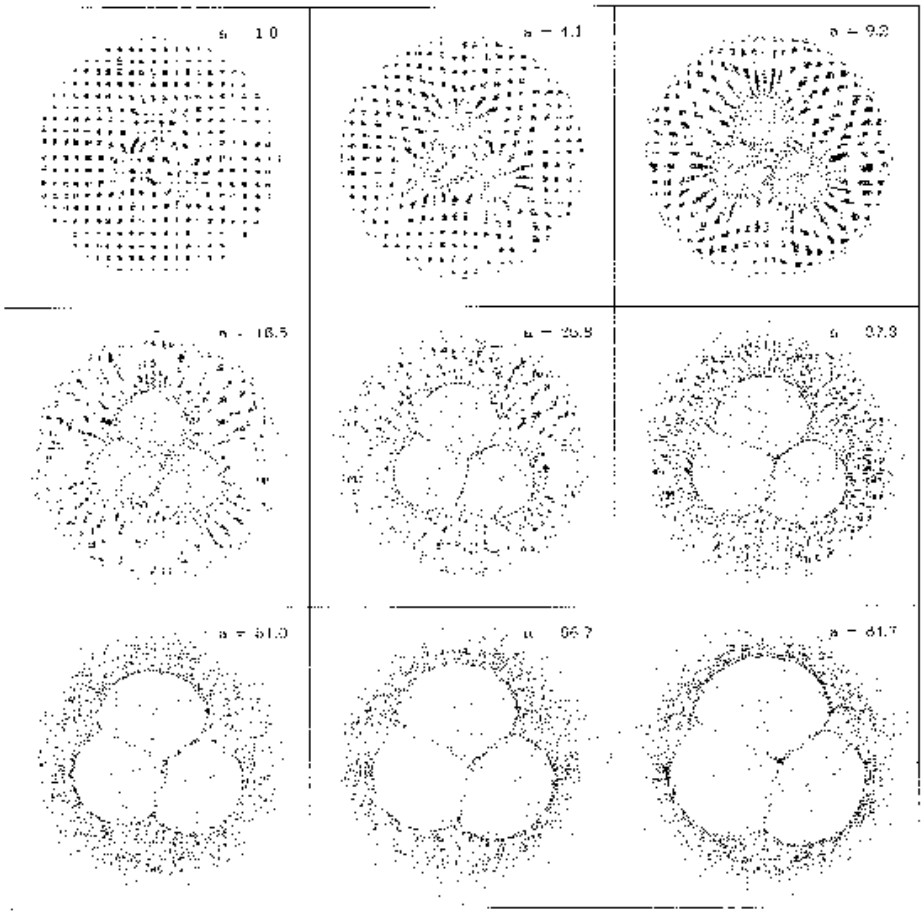

Figure 32. Evolving void hierarchy. Illustration from Dubinski etal. 1993. A nested set of a large spherical tophat void filled with 3 smaller yet deeper ones, each of them in turn filled with another set of 3 even deeper and smaller voids. Illustrated are the comoving poisition for one slice through the centre of the sphere at different cosmic epochs. At different epochs, different void scales emerge based on their initial depths. As the evolution proceeds, substructure freezes in a network of walls. Courtesy: John Dubinski. Reproduced by permission of the AAS.

and dissolve into a larger embedding void. This process gets continuously repeated as the larger parent voids in turn dissolve into yet larger voids. At any one cosmic epoch there appears to be a characteristic void size, the one corresponding to the typical tophat void shell-crossing scale (see Fig. 32, from Dubinski et al. 1993). Interestingly, a crude estimate shows that for a large range of primordial spectra voids of such size would approximately constitute a volume-filling network.

4.7.3 *Void Hierarchy.* Indeed, a detailed assessment of the void hierarchy as it evolves from a primordial Gaussian density field (Sheth & Van de Weygaert 2002) suggests the gradual disappearance of small voids as they merge and get absorbed into the encompassing underdensities, while colossal and large voids would be rare by virtue of the fluctuation field statistics, the mainstay of voids would have sizes within a rather restricted range. Corresponding calculations yield a void size distribution (broadly) peaked around a characteristic void size.

4.7.4 *Voids: Fragmenting the Universe.* A bold leap then brings us to a geometrically interesting situation. Taking the voids as the dominant structure-shaping component of the Universe, and following the "Bubble Theorem", we may think of the large scale structure as a close packing of spherically expanding regions. Then, approximating a peaked void distribution by one of a single scale, we end up with a situation in which the matter distribution in the large scale Universe is set up by matter being swept up in the bisecting interstices between spheres of equal expansion rate. This *ASYMPTOTIC* description of the cosmic clustering process leads to a geometrical configuration that is one of the main concepts in the field of stochastic geometry: VORONOI TESSELLATIONS.

4.8. The Cosmic Foam:

Pulling together the Strings

The preceding sections compel us to conclude that one of the most *prominent manifestations* of structure formation driven by the *force of gravity* is a strong and persistent tendency of matter to aggregate into weblike networks of filaments and walls.

4.8.1 *The Cosmic Foam: Dynamic Essence.* The basic mechanism behind this tendency can be most straightforwardly illuminated on the basis of the dynamical evolution of the simplified asymptotic configuration of isolated homogenous ellipsoidal overdensities. A subsequent elaboration towards the generic context of a general field of stochastic density fluctuations is worked out by the first-order Lagrangian formalism of the Zel'dovich approximation, comprising quasi-linear displacements which have proven to retain such surprising validity over a long cosmic time. From these two idealizations focussing on the relevant core issues, we have come to learn that the continuously increasing tendency towards matter migration flows into ever more flattened and, ultimately, elongated structures is ultimately stemming from the accompanying

generic anisotropies in the gravitational force field. In first instance, these anisotropies are a natural complement of the spatially stochastic, random, nature of the primordial density field. However, once the emerging matter features have developed pronounced anisotropic shapes, the tendency gets strongly reinforced, which leads to a cosmic pattern with pronounced features of high contrast, connecting into the cosmic foam.

4.8.2 *The Cosmic Foam: Dynamic Elaborations.* Subsequent elaborations of more detailed and careful considerations of the processes involved with the gravitational clustering allow us to appreciate important correlated issues. Failing to deal with the growing selfgravity of emerging structures, and therefore not being able to explain the apparent solidity, cohesion and temporal persistency of e.g. filamentary structures, the Zel'dovich approximation needs to be supplemented by more elaborate schemes. Indeed, a variety of analytical approximation schemes and descriptions have attempted to assimilate the selfgravity of structures, usually enhancing the solidity and cohesion of massive structures by design. Analytical non-linear approximation schemes which sought to extend the Zel'dovich scheme – like the adhesion model, the frozen flow approximation and the truncated Zel'dovich approximation (see Sahni & Coles 1995, for an extensive and balanced review) – without exception produce pronounced and compact weblike structures.

Less through the insight of an analytical approximation, based on some well-chosen and balanced assumptions, than through their capacity to reproduce the real world as good as possible in as much detail as technically feasible, elaborate and sophisticated full-scale gravitational N-body computer simulations have presented the most convincing evidence for the overall prominence of foamlike patterns. These N-body simulation, handling ever more complex and sophisticated situations, have made clear that overdensities – on any scale and in any scenario – indeed tend to collapse such that they become increasingly anisotropic. At first they turn into a flattened 'pancake', possibly followed by contraction into an elongated filament. Note that such structures may still expand along one direction, even while having collapsed along any of the other !

4.8.3 *The Cosmic Foam: Relaxation and Cosmic Amnesia.* Ultimately, the evolutionary phase marked by the pronounced geometrical pattern of the cosmic web will give way to yet more advanced stages wherein virialization starts to assume a dominant role. The object finally settles down into a quasi-equilibrium virialized state of its internal structure and kinematics. Galaxies and clusters are evident examples

of objects that have reached this stage. Even though highly nonlinear objects will retain some memory of past flattened and elongated geometries, in the virialization process a substantial fraction gets evened out. Hence, we encounter the most pronounced anisotropies in stages of moderate quasi-linear dynamical evolution, that in which the object has contracted along one or two dimensions, but not yet reached full nonlinear collapse.

4.8.4 *The Cosmic Foam: Fossils in Space.* Regardless of their internal morphology, we have therefore arrived at the point at which we can fully appreciate the unique position of the cosmic web within the overall scheme of cosmic organization.

The cosmic web and its constituting structural elements form marked and characteristic features within the spatial cosmic distribution of matter, structures with dimensions in the 10-500 Mpc regime that still reside at a unique stage of their dynamical development. On these intermediate Megaparsec scales features have as yet only evolved mildly since the recombination epoch. While sufficiently pronounced to analyze and scrutinize their structure and dynamics, they have not yet passed through the more complex nonlinear phases wherein orbit mixing of the accompanying migration flows and virialization of the matter content have upset causal relationships and rendered orbit inversion a nontrivial and cumbersome procedure.

Partially related is the fact that on these scales it suffices to use a simple "dust" equation of state. In most formation scenarios nonbaryonic dark matter is the dominant gravitational component, essentially setting the gravititional potential wells, while for all possible scenarios dissipative gas and radiative processes may be conveniently set aside at these large scales. Also beneficial is the fact that on these scales we can also circumvent the complexities of a full General Relativistic description of the gravitational forces involved, simple Newtonian gravitational instability provides a more than appropriate accurate description.

Hence, the Megaparsec structures joining into the cosmic web may be justifiably portrayed as genuine "cosmological fossils". It is them who contain, more directly tangible than any other object in our Cosmos, the keys for unlocking the enigma to the emergence of the Universe's infrastructure !!!

4.8.5 *The Cosmic Foam: Unravelling the Cosmic Pattern.* All in all, we conclude that the cosmos has been supplied with a dominant force of gravity which not only determines its global development and fate, but also takes care of a truely enticing internal matter distribution. It is

the *generic anisotropic nature of gravitational contraction and collapse* that acts as the *principal cause responsible* for the characteristic *foamlike appearance* of the cosmic matter distribution.

Direction closer attention to its ensuing dynamical evolution, we have come to realize that the scale of the presently observed cosmic foam is exactly the one corresponding to a stage of mild nonlinearity, the stage at which structures tend to acquire their most pronounced stage. Therefore, more so even then through the sheer intrinsic beauty of the complex geometric patterns themselves, we have come to appreciate why in the study of structure formation it is the *the cosmic foam* which should be branded as its most *fundamental manifestation* !

Also, we have come to appreciate the existence of major technical obstacles towards unravelling the cosmic secrets contained within the cosmic foam. The absence of any informative instrument for analyzing and exploiting the characteristic, intrinsically geometric, properties of the cosmos' interior matter arrangement implies us to accept a disregard for and squandering of highly relevant information. Hence, following the alternative and complementary track of adressing the stochastic geometric nature of the cosmic web, we seek to define a path towards a more fundamental understanding of its geometric aspects. Such insight will pave the way towards a better and more meaningful exploitation of the treasure trove of information on the process of structure formation contained in the salient frothy patterns we have found to permeate our Universe.

5. CELESTIAL POLYHEDRA:... Tessellating the Universe

Following the philosophy delineated above, and continuing the arguments leading to the concept of Voronoi tessellations, we proceed by construct the "skeleton" of the mass distribution by considering the locus of points towards which the matter streams out of voids. The premise is that some primordial cosmic process generated a density fluctuation field. In this random density field we can identify a collection of regions where the density is slightly less than average or, rather, the peaks in the primordial gravitational potential perturbation field. As we have seen, these regions are the seeds of the voids. These underdense patches become "expansion centres" from which matter flows away until it runs into its surroundings and encounters similar material flowing out of adjacent void, as indeed is observed with the CDM void in Fig. 31. Notice also that the dependence on the specific structure formation scenario at hand is entering via the spatial distribution of the sites of the density

dips in the primordial density field, whose statistical properites are fully determined by the spectrum of primordial density fluctuations.

Matter will collect at the interstices between the expanding voids. In the asymptotic limit of the corresponding excess Hubble parameter being the same in all voids, these interstices are the bisecting planes, perpendiculary bisecting the axes connecting the expansion centres. For any given set of expansion centres, or *nuclei*, the arrangement of these planes define a unique process for the partitioning of space, a *Voronoi tessellation* (Voronoi 1908). A particular realisation of this process (i.e. a specific subdivision of N-space according to the Voronoi tessellation) may be called a *Voronoi foam* (Icke & Van de Weygaert 1987).

5.1. Voronoi Tessellations: the Geometric Concept

A Voronoi tessellation of a set of spatially distributed nuclei is a space-filling network of polyhedral cells (see Fig. 34), each of which delimits that part of spacethat is closer to its nucleus than to any of the other nuclei. Hence, each Voronoi region Π_i is the set of points which is nearer to nucleus i than to any of the other nuclei j in a set Φ of nuclei $\{x_i\}$ in d-dimensional space $\Re^d$, or a finite region thereof,

$$\Pi_i = \{\vec{x} | d(\vec{x}, \vec{x}_i) < d(\vec{x}, \vec{x}_j) \ , \ \forall \ j \neq i\} \ , \tag{66}$$

where $\vec{x}_j$ are the position vectors of the nuclei in Φ, and $d(\vec{x}, \vec{y})$ the Euclidian distance between $\vec{x}$ and $\vec{y}$ (evidently, one can extend the concept to any arbitrary distance measure). From this basic definition, we can directly infer that each Voronoi region Π_i is the intersection of the open half-spaces bounded by the perpendicular bisectors (bisecting planes in 3-D) of the line segments joining the nucleus i and any of the the other nuclei. This implies a Voronoi region Π_i to be a convex polyhedron (or polygon when in 2-D), a *Voronoi polyhedron*.

The complete set of Voronoi polyhedra constitute a space-filling tessellation of mutually disjunct cells, the *Voronoi tessellation*. A good impression of the morphology of a complete Voronoi tessellation can be seen in figure 22, a tessellation of 1000 cells generated by a Poisson distribution of 1000 nuclei in a cubic box.

Figure 34 shows how in three dimensions a Voronoi foam forms a packing of Voronoi cells, each cell being a convex polyhedron enclosed by the bisecting planes between the nuclei and their neighbours. A Voronoi foam consists of four geometrically distinct elements: the polyhedral cells (*voids*), their walls (*pancakes*), edges (*filaments*) where three walls intersect, and nodes (*clusters*) where four filaments come together.

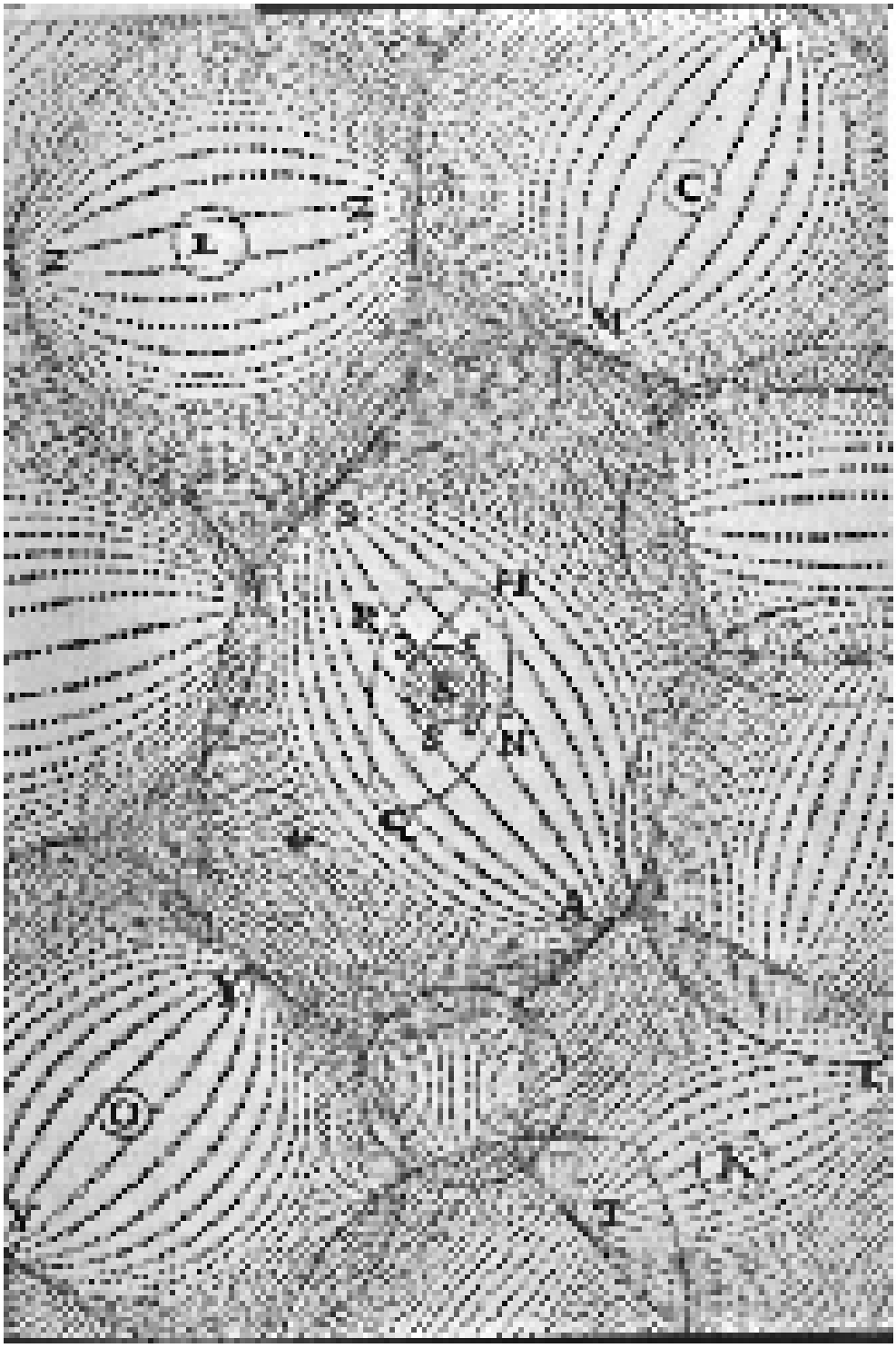

Figure 33. R. Descartes; Le Monde, Ou Traité de la Lumière, &c., Paris, MDCLXIV

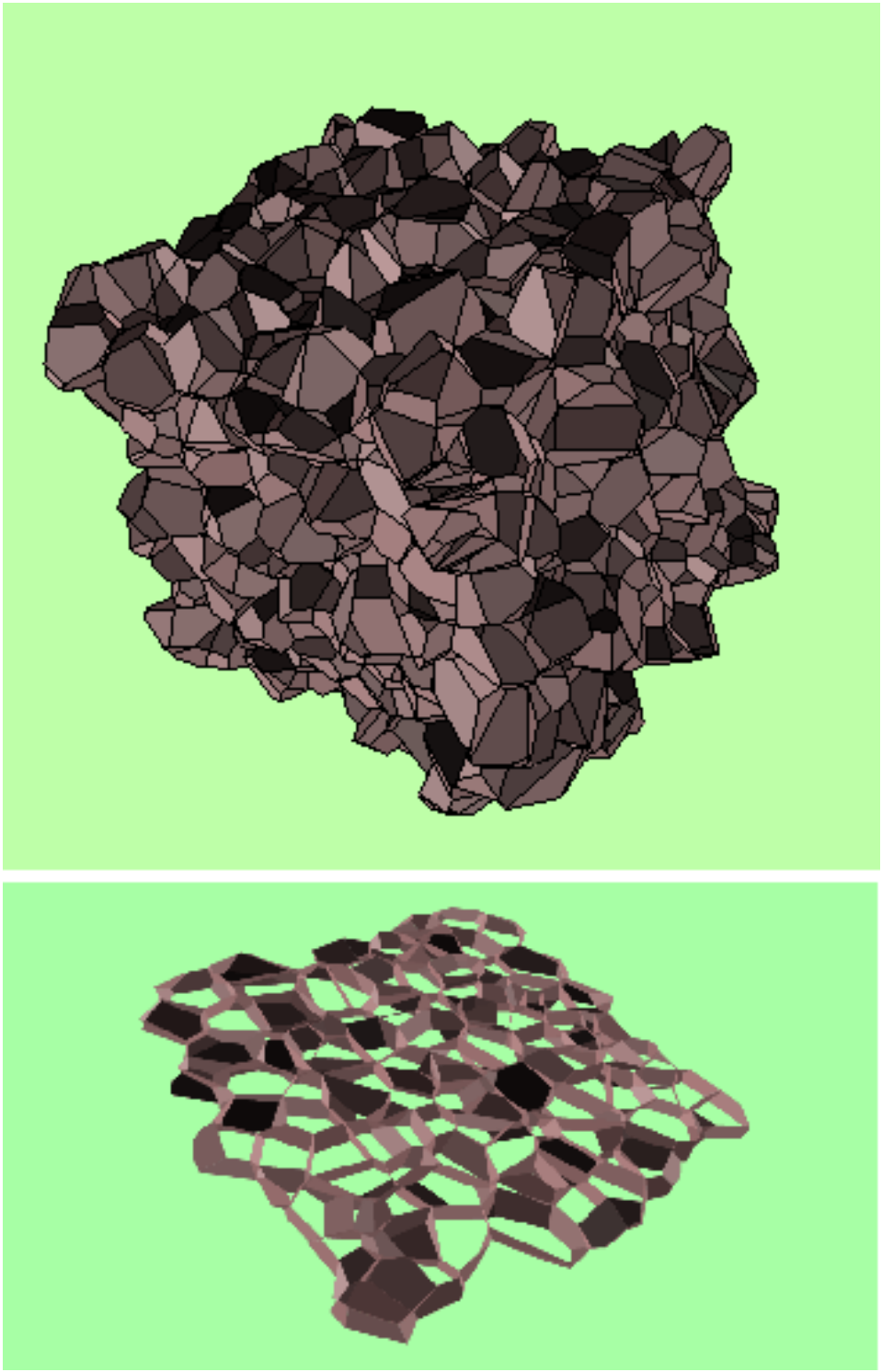

Figure 34. A full 3-D tessellation comprising 1000 Voronoi cells/polyhedra generated by 1000 Poissonian distributed nuclei. Courtesy: Jacco Dankers

Taking the three-dimensional tessellation as the archetypical representation of structures in the physical world, we can identify four constituent *elements* in the tessellation, intimately related aspects of the full Voronoi tessellation. In addition to (1) the polyhedral *Voronoi cells* Π_i these are (2) the polygonal *Voronoi walls* outlining the surface of the Voronoi cells, (3) the one-dimensional *Voronoi edges* defining the rim of both the Voronoi walls and the Voronoi cells, and finally (4) the *Voronoi vertices* which mark the limits of edges, walls and cells. To appreciate the interrelation between these different geometric aspects, figure 23 lifts out one particular Voronoi cell from a clump of a dozen Voronoi cells. The central cell is the one with its polygonal Voronoi walls surface-shaded, while the wire-frame representation of the surrounding Voronoi cells reveals the Voronoi edges defining their outline and the corresponding vertices as red dots.

While each Voronoi cell is defined by one individual nucleus in the complete set of nuclei Φ, each of the polygonal Voronoi walls Σ_{ij} is defined by two nuclei i and j, consisting of points $\vec{x}$ having equal distance to i and j. Evidently, the Voronoi wall Σ_{ij} is a subregion of the full bisecting plane of i and j, the subregion consisting of all points $\vec{x}$ closer to both i and j than other nuclei in Φ. The number of walls constituting the surface of each cell Π_i is a stochastic quantity. In fact, in three dimensions even the average number of walls per cell in a specific finite Voronoi tessellation is a stochastic quantity, with an expectation value of 7.768 for a Poisson-Voronoi tessellation (ie. a tessellation generated by Poisson distributed nuclei). In analogy to the definition of a Voronoi wall, a Voronoi edge Λ_{ijk} is a subregion of the equidistant line defined by three nuclei i, j and k, the subregion consisting of all points $\vec{x}$ closer to i, j and k than to any of the other nuclei in Φ. Moreover, in analogy to the definition of Voronoi walls the Voronoi edge Λ_{ijk} is a part of the – surface of – three Voronoi cells, Π_i, Π_j and Π_k. Evidently, it is part of the perimeter of three walls as well, Σ_{ij}, Σ_{ik} and Σ_{jk}, the first of which is a segment of the surface of Π_i and Π_j, the second one of Π_i and Π_k and the third one of Π_j and Π_k. Pursuing this enumeration, Voronoi vertices V_{ijkl} are defined by four nuclei, i, j, k and l, being the one point equidistant to them and closer to them than to any of the other nuclei belonging to Π_i. In other words, the vertex is the circumsphere of the tetrahedron defined by the four nuclei. In other words, each set of nuclei i, j, k and l corresponding to a Voronoi vertex defines a unique tetrahedron, which is known as Delaunay tetrahedron (Delone 1934), with the defining characteristisc that no other nucleus can be inside their circumsphere. It also implies that from the set of Voronoi

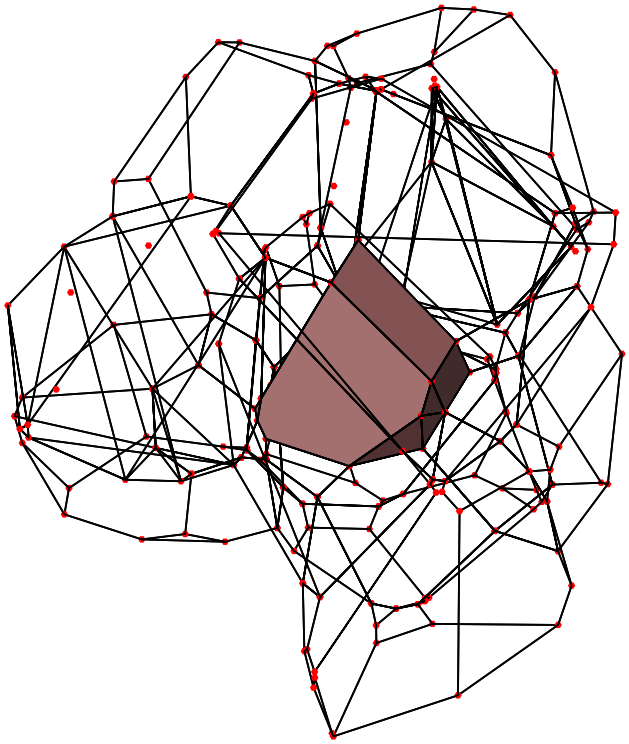

Figure 35. Wireframe illustration of interrelation between various Voronoi tessellation elements. The central "Voronoi cell" is surrounded by its wire-frame depicted "contiguous" Voronoi neighbours. The boundaries of the cells are the polygonal "Voronoi walls". The wire edges represent the Voronoi edges. The "Voronoi vertices", indicated by red dots, are located at each of the 2 tips of a Voronoi edge, each of them located at the centre of the circumsphere of a corresponding set of four nuclei. Courtesy: Jacco Dankers.

vertices we can define an additional "dual" space-filling tessellation, the *DELAUNAY TESSELLATION*.

To appreciate the geometric definitions and relationships it is instructive to turn to Fig. 35, showing a wire-frame network of all Voronoi edges belonging to the contiguous (neighbouring) Voronoi cells touching one particular central Voronoi cell (solid). It indicates the sites, by means heavy red dots, of the corresponding Voronoi vertices (and Delaunay circumcentres). Notice then, that the stochastic point process of nuclei brings forth a new and uniquely defined, that of the *vertices* !!!

5.2. Voronoi Tessellations: the Cosmological Context

In the cosmological context *Voronoi Tessellations* represent the *Asymptotic Frame* for the ultimate matter distribution distribution in any cosmic structure formation scenario, the skeleton delineating the destination of the matter migration streams involved in the gradual buildup of cosmic structures. Within such a cellular framework the interior of each "*VORONOI CELL*" is considered to be a void region. The planes forming the surfaces of the cells are identified with the "*WALLS*" in the galaxy distribution (see e.g. Geller & Huchra 1989). The "*EDGES*" delineating the rim of each wall are to be identified with the filaments in the galaxy distribution. In general, what is usually denoted as a flattened "supercluster" or cosmic "wall" will comprise an assembly of various connecting walls in the Voronoi foam, as the elongated "superclusters" or "filaments" will usually consist of a few coupled edges (Fig. 41 and 42 clearly illustrate this for the Voronoi kinematic model). Finally, the most outstanding structural elements are the "*VERTICES*", tracing the surface of each wall, outlining the polygonal structure of each wall and limiting the ends of each edge. They correspond to the very dense compact nodes within the cosmic network, amongst which the rich virialised Abell clusters form the most massive representatives. In a way, the Voronoi foam outlines the "skeleton" of the cosmic matter distribution. It identifies the structural frame around which matter will gradually assemble in the course of the development of cosmic structure. In this view the process of cosmic structure formation is one in which we see a gradually unfolding of the cellular pattern in the matter distribution as matter is set to migrate away from the primordial location towards the high-density features in the cosmic foam.

Although the idea of tessellations in an astronomical context dates back centuries (see Fig. 33), the first actual application of Voronoi tessellations to astrophysics is of a more recent date. Kiang (1966) invoked them to obtain a mass spectrum for the fragmentation of interstellar molecular clouds, be it without success in reproducing the Initial Mass Function of stars. It were Matsuda & Shima (1984) who noticed the similarity between 2-D Voronoi tessellations and the outcome of the first computer experiments of cosmic structure formation (Melott 1983), a similarity which found a solid foundation when Icke & van de Weygaert (1987) independently stuck upon the concept of Voronoi tessellations pursuing the physical argument that expanding density depressions play a dominating and regulating role in the formation of cosmic structure (Icke 1984).

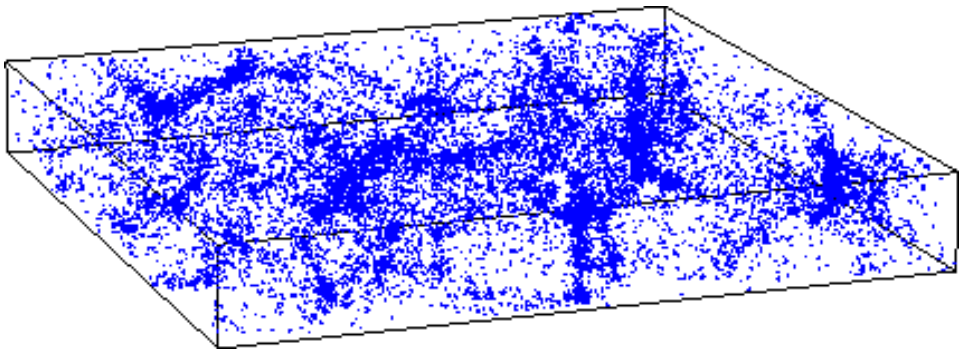

Figure 36. Voronoi Galaxy Distribution: an example of a galaxy distribution whose geometrical pattern is defined through a Voronoi network. Also see Fig. 41 & 42

5.3. Voronoi Galaxy Distributions

Cosmologically, the great virtue of the Voronoi foam is that it provides a conceptually simple model for a cellular or foamlike distribution of galaxies, whose ease and versatility of construction makes it an ideal tool for statistical studies. The stochastic, non-Poissonian and geometric nature of the spatial distribution of walls, filaments and clusters framing the cosmic web is responsible for large-scale spatial clustering in the matter distribution, and the related galaxy populations. The Voronoi model hands us a flexible template for studying galaxy distributions around geometrical features that themselves have some distinct and well-defined stochastic spatial distribution, represented by the corresponding components in the Voronoi tessellations.

To study the specific properties of such weblike galaxy distributions, geometrically constructed models offer a variety of advantages. Its great virtue is its realistic rendering and representation of the spatial distribution of walls and filaments defining the overall distribution. In its focus on these geometric components, it provides a laboratory for studying a variety of different cellular distributions. It may therefore fulfil a key role in dissecting the fundamental spatial characteristics of such geometries, and potentially is a very useful instrument for understanding and interpreting the observed galaxy distribution. An additional virtue is that the model distributions will be far less restricted in resolution and number of particles than conventional N-body experiments, as cellular structure can be generated over a part of space beyond the reach of any N-body experiment. The Voronoi model will therefore also be particularly suited

for studying the properties of galaxy clustering in cellular structures on very large scales, for example in very deep pencil beam surveys, as well as for studying the clustering of clusters in these models.

A mere qualitative assessment of such three-dimensional geometries already yields the interesting and important observation that the non-Poissonian distribution of the Voronoi walls, edges and vertices is a stochastic process characterized by strong spatial correlations. This is readily apparent from e.g. Fig 35, and even more obvious from the lower frame slice in Fig. 34. The important repercussion is that the geometric Voronoi components themselves are grouping into coherent "super"structures, inducing intrinsic spatial correlations over scales substantially superseding the basic cell scale (see Van de Weygaert 2002a,b). Also note that the nontrivial morphology of spatially clustered geometrical elements not only determines the overall clustering properties of its galaxy population but that it also forms a stark contrast to less physically motivated and less realistic stochastic toy models as e.g. the double Poisson process.

The obvious shortcoming of the model is the fact that it does not and cannot addres the galaxy distribution on small scales, i.e. the distribution within the various components of the cosmic skeleton. This will involve the complicated details of highly nonlinear small-scale interactions of the gravitating matter. N-body simulations are by far the most reliable for treating that problem in the highly nonlinear clustering stages.

For our purposes, we take the route of complementing the large-scale cellular distribution induced by Voronoi patterns by a user-specified small-scale distribution of galaxies. On the one hand, it would be ideal to use well-defined and elaborate physical models to fill in this aspect. On the other hand, it would remove the essence of the charm and flexibility of the Voronoi concept. Far more beneficial is to set up tailor-made and user-defined spatial model distributions. In this, we distinguish two different yet complementary approaches. One is the fully heuristic approach of *"Voronoi element models"*, genuine tools for the systematic investigation of very specific individual details of the full cellular structure. The second, supplementary, approach is that of the "Voronoi kinematic distributions", which attempt to "simulate" foamlike galaxy distributions in the true meaning of the word.

5.3.1 *Voronoi galaxy distributions: Voronoi Element Models.* A more practical alternative approch involves the generation of tailor-made purely heuristic "galaxy" distributions in and around the various elements of a Voronoi tessellation, "Voronoi Element Models". Such mod-

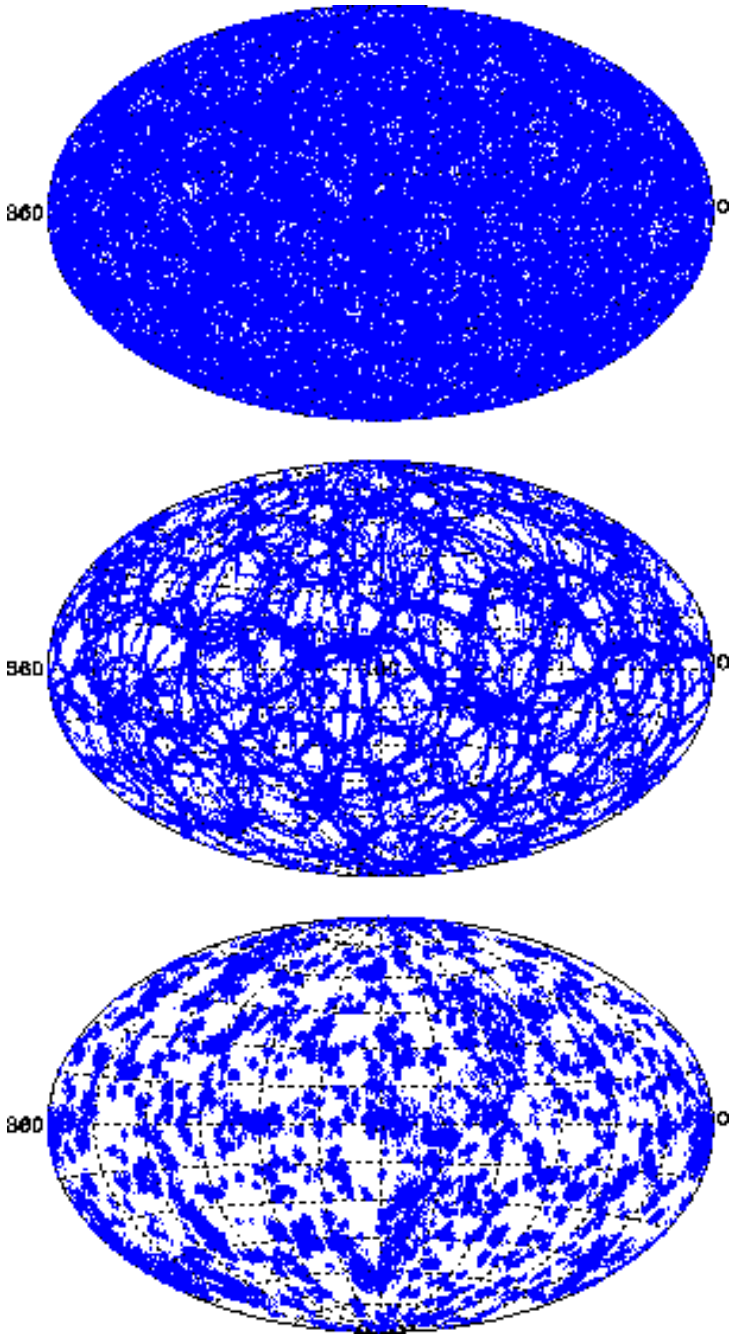
360
0
360
0
360
0

Figure 37. Sky distributions for three different patterns of Voronoi galaxy distributions, depicted by means of an Aitoff projection. The depicted skies correspond to a wall-dominated Voronoi Universe (top), a filamentary Voronoi Universe (centre) and a cluster-dominated Voronoi Universe (bottom). The observer has been mapping all galaxies in a magnitude-limited survey ($m_{lim} = 15.5$) comprising a surrounding $250h^{-1}$Mpc spherical region lifted out of a world in which the mean size of the void (cell) regions is $\approx 25h^{-1}$Mpc. The number of galaxies corresponds to the number density set the Schechter luminosity function of Efstathiou, Ellis & Peterson, for galaxies brighter than $M_{gal} = -17$. From: Van de Weygaert 2002b.

els are particularly apt for fathoming profound systematic properties of spatial galaxy distributions confined to one or more structural elements of nontrivial geometric spatial patterns.

Telling examples are the ones represented by means of the Aitoff projected sky distributions depicted in Fig. 37. These yield a impression of what the observed galaxy distribution on the sky would be for a fictitious observer within such a model Universe, assuming ideal and uniform observational conditions. The resulting processed model sky distributions are a lucid means of conveying the impression one would obtain if one were living in such a model world and observe the surrounding world. Figure 37 shows the full sky distribution in Aitoff projection of all galaxies brighter than $m_{lim} = 16.5$ out to a maximum depth of $100h^{-1}$Mpc, if the observer were to reside in a Universe with an interior foamlike pattern consisting of only walls (top), filaments (centre) or cluster clumps (bottom).

5.3.2 *Voronoi galaxy distributions: Web Pattern Dynamics.* An illustrative example of potential applications of such heuristic Voronoi models is the study of dynamics of matter distributions confined to one or more structural elements. For instance, the gravitational force field corresponding to a wall-dominated matter distribution would be resembling the gravity vector field shown in Fig. 38, being 3 perpendicular planes centered on one specific location. It shows that the gravitational influence of the matter content in the walls is particularly strong in the direct environment of the walls. The interior of the voids are remarkably less pronounced, partly due to the evening out of the conflicting gravitational attractions exerted by the various individual walls. Extending such considerations, a comparison between the gravity field configurations effected by a wall-dominated, filamentary or cluster-dominated matter distribution (Fig. 39) reveals a rising contrast in gravitational strength between empty void regions and ever more compact and denser high-density regions (notice that in all cases, the matter density within each individaul wall is uniform, be it with a surface density different

for each wall, determined as it is by its immediate environment). In the wall-dominated world (Fig. 39, lefthand frames), gravitatitional forces are particularly strong near the densest vertices (clusters), yet also have a noticeable strength immediately in and around nearly every wall. The walls can be readily identified from the spatial pattern of the gravity field itself, delineating dynamical boundaries between low-density voids. The topology of the gravity field changes drastically as

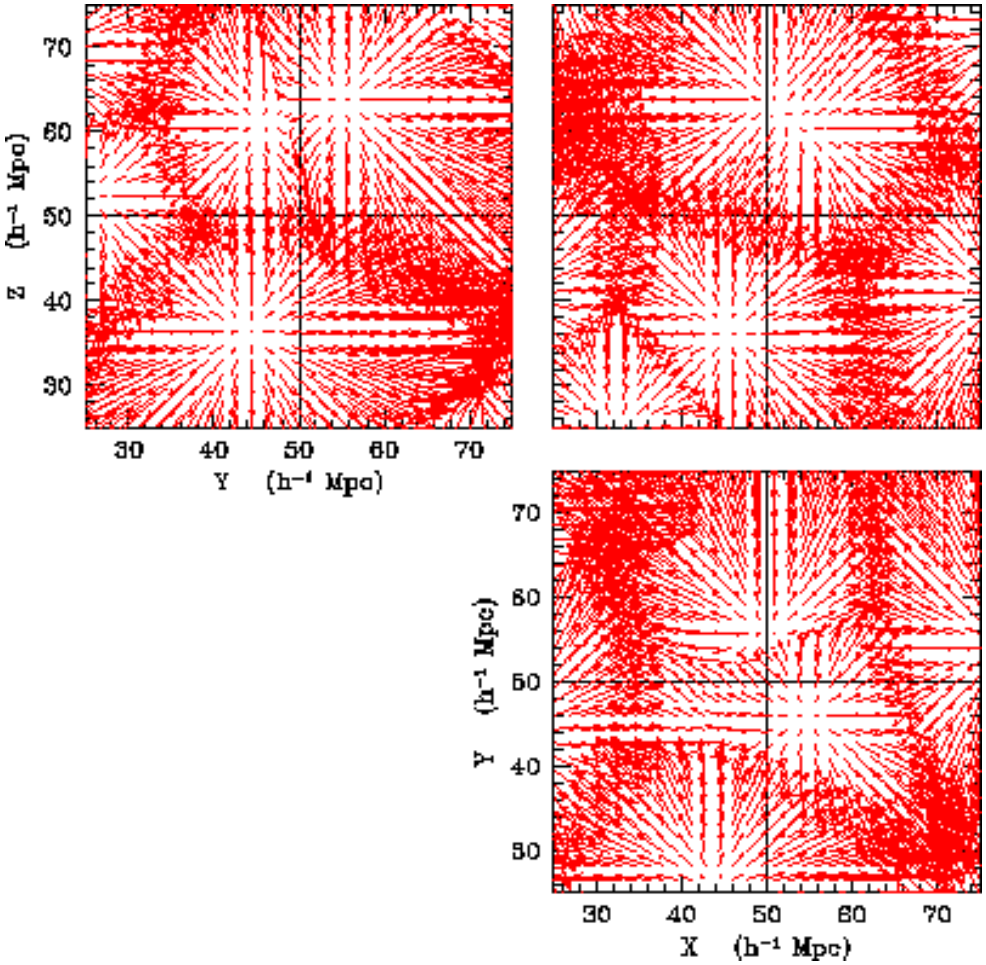

Figure 38. The gravity field around one particular location in a wall-dominated (Voronoi) matter distribution, illustrated by grid vector maps of the gravity component in three mutually perpendicular planes passing through the central location. The length of each vector is proportional to the strength of the gravity and its direction pointing in the direction of the gravitational acceleration at the grid location represented by the base of the vector.

the matter distribution assumes a more filamentary character (Fig. 39, central frames). The walls get more tenuous and command less and less dynamical weight, gradually dissolving into the background. The low-density voids, on the other hand, appear to merge into large regions characterized by a low and divergent gravity field. Dynamically more pronounced are the high-density cluster regions near the interstices of the densest filaments. They represent regions of considerably stronger gravity than in the corresponding case of a wall-dominated matter distribution. Also notice that the occasional "isolated" filament – located at the boundary between large voids – is characterized by a pronounced and concentrated gravity field, rapidly falling off into the void region. This trend of strongly concentrated gravity fields is continued towards configurations with compact cluster clumps. Very strong gravitational

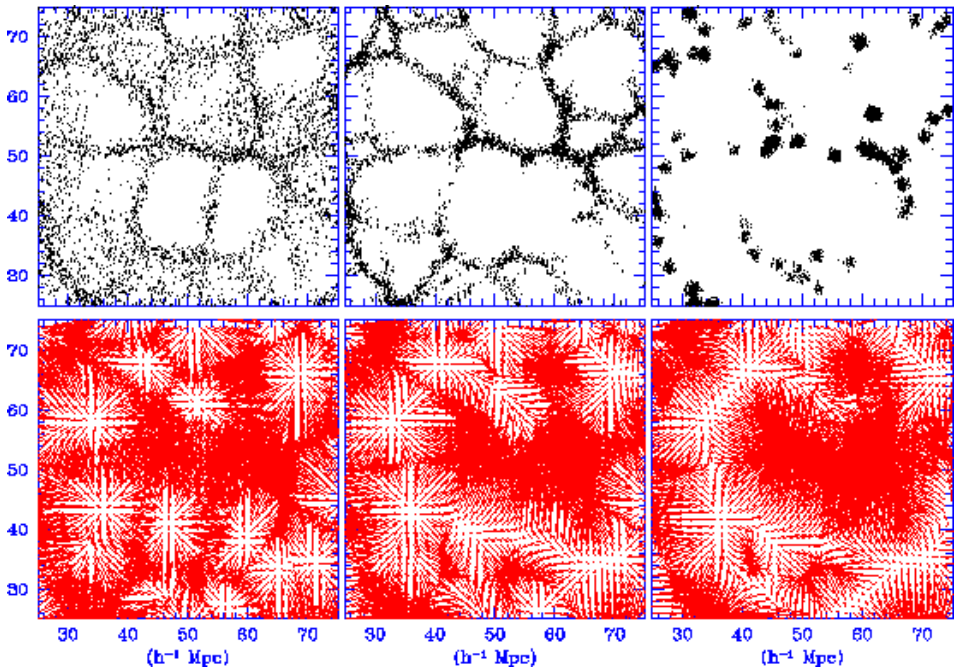

Figure 39. Gravity fields of 3 specific cellular (Voronoi) matter distributions. The top row of 3 panels depicts the particle distribution in a central slice through the box of the Voronoi model realizations, while the bottom row involves the corresponding gravity vector fields in the same central slice of the box. In the bottom row, the arrows indicate the direction and strength of the gravity force component in the shown slice. All particle distributions correspond to a uniform density in each individual element, wall, filament or cluster. Left: a Voronoi wall distribution. Centre: a filamentary Voronoi distribution. Right: a Voronoi cluster distribution. From: Van de Weygaert 2002b.

forces are felt near the complexes of such (clustered) clumps, with a weak gravity pertaining in the remaining low density regions.

Armed with the insight provided by the nature, patterns and behaviour of such artificial gravity fields – induced by specific asymptotic cellular matter distributions – we get equipped with a necessary toolbox for a far more systematic and meaningful assessment of the dynamics of the more complex and realistic matter distributions usually encountered in N-body computer simulations. It will pave the way for a far more systematic study of the typical characteristics of the dynamics involved with cellular matter concentrations.

5.3.3 *Voronoi galaxy distributions: the Kinematic Model.* Alternatively, we can generate distributions that more closely resemble the outcome of dynamical simulations, and represent an idealized and asymptotic description thereof. Such a model is the *kinematic model* defined by Van de Weygaert & Icke (1989).

The kinematic Voronoi model is based on the notion that when matter streams out of the voids towards the Voronoi skeleton, cell walls form when material from one void encounters that from an adjacent one. In the original "pancake picture" of Zel'dovich and collaborators, it was gaseous dissipation fixating the pancakes (walls), automatically leading to a cellular galaxy distribution. But also when the matter is collisionless, the walls may be hold together by their own self-gravity. Accordingly, the structure formation scenario of the kinematic model proceeds as follows. Within a void, the mean distance between galaxies

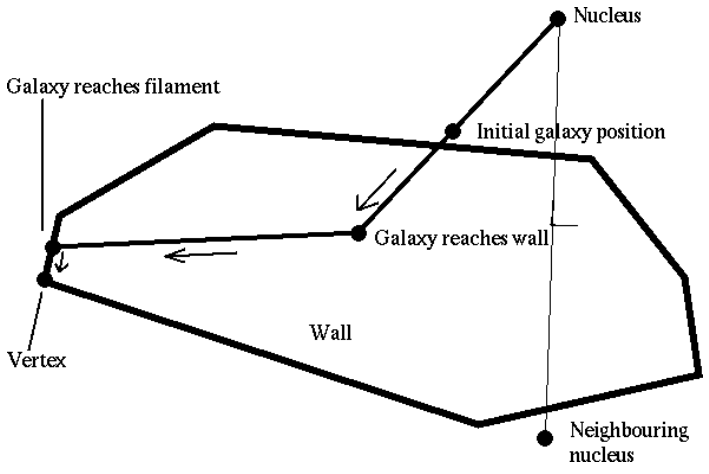

Figure 40. Schematic illustration of the Voronoi kinematic model. Courtesy: Jacco Dankers.

increases uniformly in the course of time. When a galaxy tries to enter an adjacent cell, the gravity of the wall, aided and abetted by dissipational processes, will slow down its motion. On the average, this amounts to the disappearance of its velocity component perpendicular to the cell wall. Thereafter, the galaxy continues to move within the wall, until it tries to enter the next cell; it then loses its velocity component towards that cell, so that the galaxy continues along a filament. Finally, it comes to rest in a node, as soon as it tries to enter a fourth neighbouring void. In a Voronoi foam, there are exactly four cells adjoining each node, and the above process is unique. An immediate consequence of this kinematic behaviour is that the density in the walls quickly becomes smaller than in the filaments which, in turn, remain less dense than the nodes, where all matter eventually congregates. This is the main reason why we identify the nodes with the rich Abell clusters. The evolutionary progression of an almost featureless random distribution, via a wall-like and filamentary morphology towards a distribution in which matter ultimately aggregates into conspicuous compact cluster-like clumps can be immediately appreciated from the sequence of 9 cubic 3-D particle distributions in Figure 41. Proceeding from the top left, left to right, and from top to bottom, it depicts a sequel of consecutive timesteps within the kinematic Voronoi cell formation process. The depicted boxes have a size of $100h^{-1}$Mpc. Within these cubic volumes some 64 Voronoi cells with a typical size of $25h^{-1}$Mpc delineate the cosmic framework around which some 32000 galaxies have aggregated[4].

The steadily increasing contrast of the various structural features is accompanied by a gradual shift in topological nature of the distribution. The virtually uniform particle distribution at the beginning (upper left-hand frame) ultimately unfolds into the highly clumped distribution in the lower righthand frame.

At first only a faint imprint of density enhancements and depressions can be discerned. In the subsequent first stage of nonlinear evolution we see a development of the matter distribution towards a wall-dominated foam. The contrast of the walls with respect to the general field population is rather moderate (see e.g. second frame), and most obviously discernable by tracing the sites where the walls intersect and the galaxy density is slightly enhanced. The ensuing frames depict the gradual progression via a wall-like through a filamentary towards an ultimate

[4]corresponding roughly to the number density of galaxies yielded by a Schechter luminosity function with parameters according to Efstathiou, Ellis & Peterson (1988): $\phi_* = 1.56\,10^{-1}\,(h^{-1}\mathrm{Mpc})^{-3}$, $\alpha = -1.07$ and $M_* = -19.68 + 5log h$, where we restricted ourselves to galaxies brighter than $M_{gal} = -17.0$. In the full "simulation box" of $200h^{-1}$Mpc, this amounts to 268,235 galaxies.

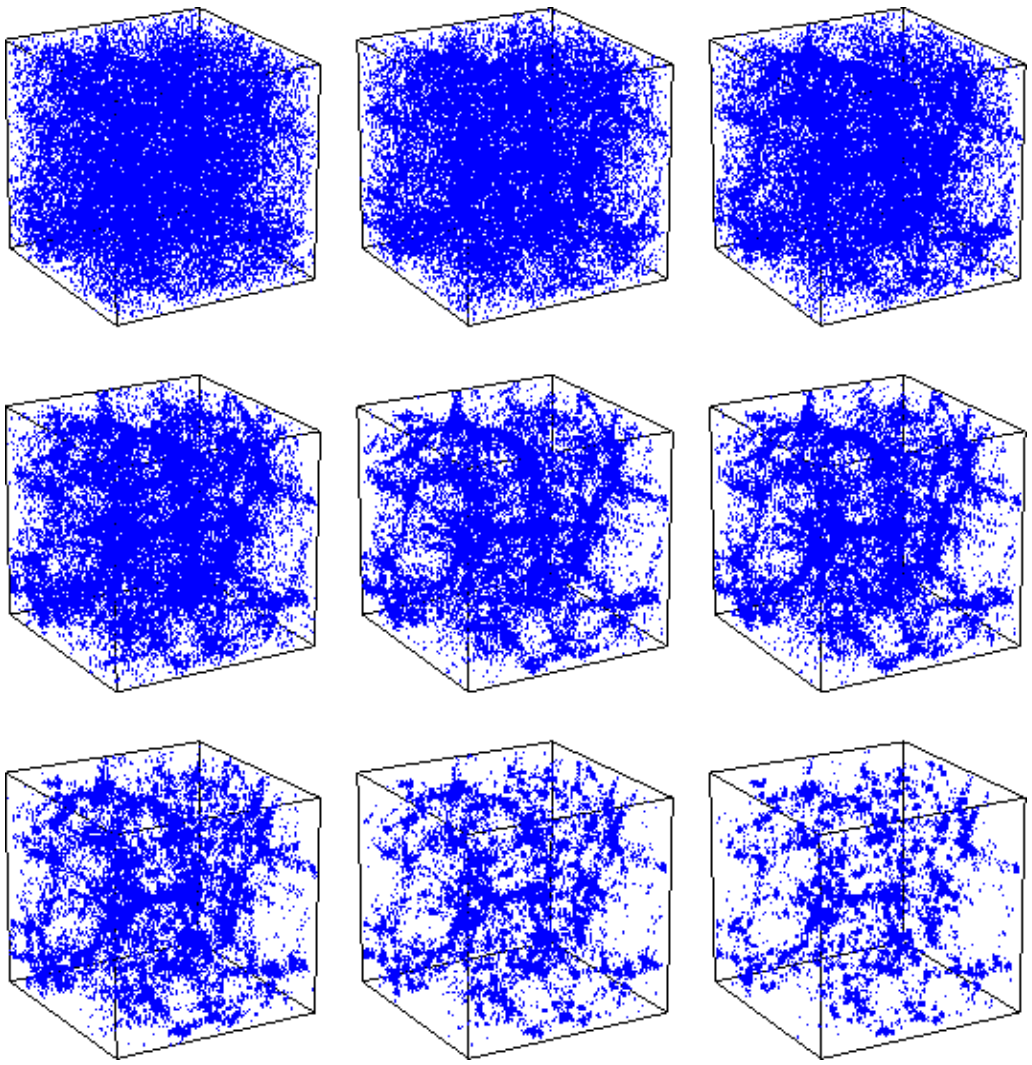

Figure 41. Evolution of galaxy distribution in the Voronoi kinematic model. A sequel of 9 consecutive timesteps within the kinematic Voronoi cell formation process, proceeding from left to right, and from top to bottom. The depicted boxes have a size of $100h^{-1}$Mpc. Within these cubic volumes some 64 Voronoi cells with a typical size of $25h^{-1}$Mpc delineate the cosmic framework around which some 32000 galaxies have aggregated. Taken from a total (periodic) cubic "simulation" volume of $200h^{-1}$Mpc containing 268,235 "galaxies".

cluster-dominated matter distribution. By then nearly all matter has streamed into the nodal sites of the cellular network. The initially al-

most hesitant rise of the clusters quickly turns into a strong and incessant growth towards their appearance as dense and compact features which ultimately stand out as the sole dominating element in the cosmic matter distribution (bottom righthand frame).

A particularly transparent view of the way in which the various morphological elements connect into the cosmic foam is shown by a set of cross-sections through the simulation boxes. A progressive evolutionary sequence of 6 such slices is shown in Figure 42, corresponding to the same realization as the cubic distributions in Fig. 41. On purpose the slicewidth of $20h^{-1}$Mpc was chosen to be slightly smaller than the characteristic cellsize of $25h^{-1}$Mpc. The cross-sections give a good impression of the way in which the various filaments, each of varying orientation, link up with their peers into a seemingly undulating and space pervading network, sprinkled with a population of dense and compact clusters delineating the interstices of the network. The semblance of of the slice distributions to that of galaxies in the slice redshift surveys released since the first one by De Lapparent, Geller, & Huchra (1986) is indeed striking

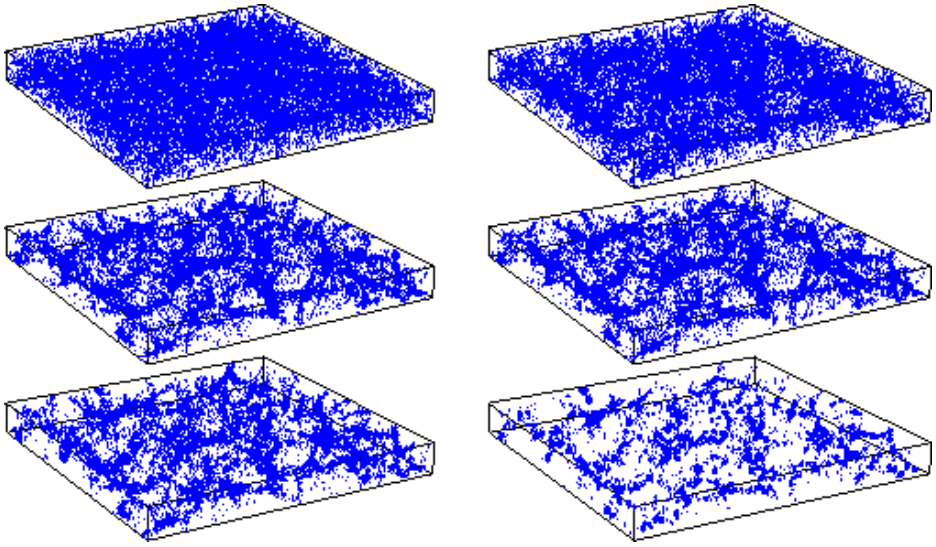

Figure 42. A sequel of six slices from a kinematic Voronoi model realization. Frames represent successive cosmic snapshots, taken the same "simulation" volume as in Fig. 41. Each slice has a slicewidth of $20h^{-1}$Mpc and full boxsize of $200h^{-1}$Mpc.

5.3.4 *Voronoi galaxy distributions: Observing the World of Voronoi.*

Most often observational samples represent a non-uniform sampling of the full spatial galaxy distribution. The resulting selection function

makes it almost impossible to obtain an objective and complete reconstruction of the true spatial distribution. This is in particular true when highly nonlinear and anisotropic features, so characteristic for foamlike patterns, are involved. Comparison of observational samples with model distributions processed through a typical observational setup are therefore often a good way for evaluating the model's validity. Besides the telling examples in Fig 36 of three additonal sky galaxy distributions observed by a fictituous observer, we present two other typical observational strategies.

Slice redshift surveys through a kinematic Voronoi distribution were simulated. A typical example is shown in Figure 43. It concerns a "redshift" survey with a limiting magnitude of $m_{lim} = 16.5$, out to a depth of $100h^{-1}$Mpc within a 12° wide slice of 150° length. The resemblance to published survey results is indeed striking. Notice for instance the "Great Wall" running laterally along the slice, consisting

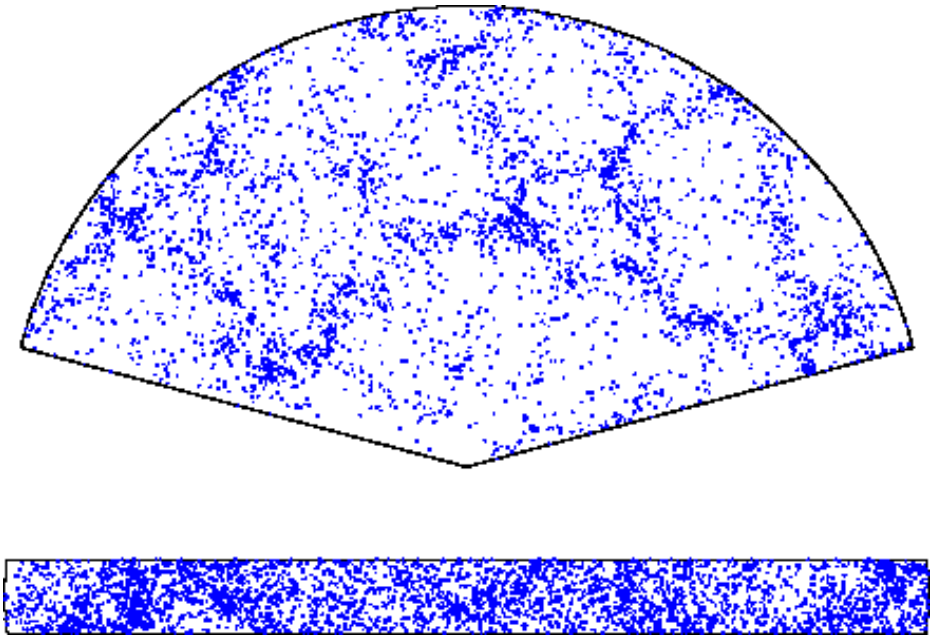

Figure 43. Top: A simulated redshift slice through a kinematic Voronoi distribution of galaxies. Galaxies distributed within the Voronoi foam, in which walls and filaments were having a proper width. The galaxies were given a luminosity, randomly drawn from a proper (Schechter) galaxy luminosity function (parameters: Efstathiou, Ellis & Peterson 1988. The apparent magnitude limit of the survey is $m_{lim} = 16.5$, confined to a slice with angular width and length of 12° by 150°, going out to a depth of $100h^{-1}$Mpc. Bottom: the sky galaxy distribution of the galaxies depicted in the slice.

of a series of connected individual Voronoi walls. In addition, we can discern various outstanding high-density "clusters". The corresponding sky projection of the slice galaxies in the lower frame reinforces the realistic impression.

The Voronoi model has been in particularly succesfull in explaining and interpreting the spiky pencil-beam redshift surveys (as shown in Fig. 44). It is rather easy to understand that the typical spiky pattern in these narrow redshift beams is due to the passing of the lines of sight through walls, and occasionally filaments, of the frothy galaxy distribution. Van de Weygaert (1991a,b) and Subbarao & Szalay (1992) invoked the Voronoi model to show that such a spiky pattern in the redshift distribution can be understood quite naturally with a cellular pattern extending out to high redshifts, a fact that had been pointed out on the basis of an analytical evaluation of Voronoi statistics by Coles (1991). To this end, Van de Weygaert (1991a,b) simulated and analyzed pencil-beam patterns in Voronoi 'universes', some suggestively similar to the observational results (see Fig. 44). In particular, it was pointed out while the wall distribution is not intrinsically regular a certain fraction (some 15%) of the beams would yield a 'quasi-periodic' galaxy distribution, offering a non-contrived explanation for the puzzling regularity in the Broadhurst et al. (1990) results.

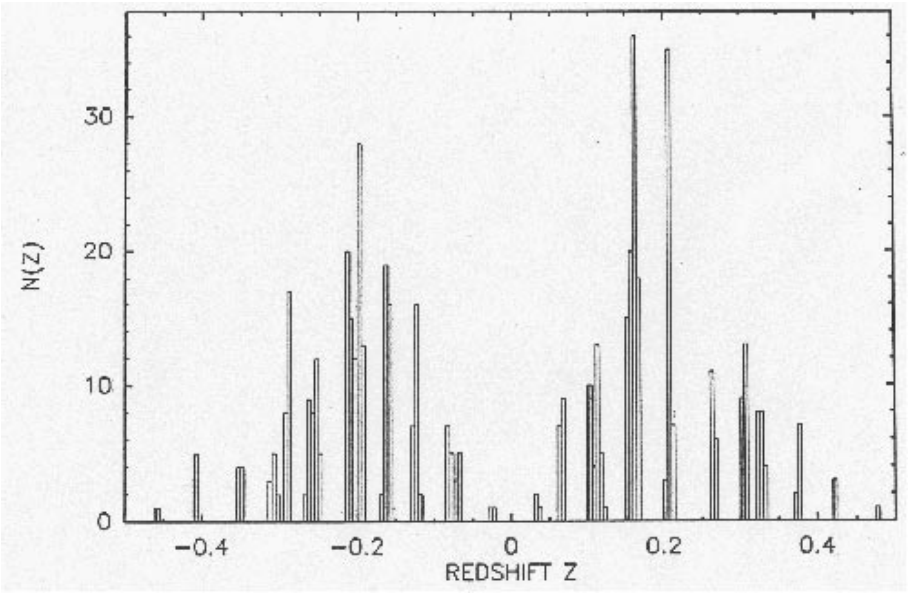

Figure 44. A simulated pencil beam survey through a deep Voronoi web. From Van de Weygaert 1991a,b. Reproduced by permission of the Royal Astronomical Society.

5.3.5 *Voronoi galaxy distributions: Quantification of Galaxy Clustering.* To be of more than illustrative use, Voronoi tessellations should supersede the status of a pure qualitative sketch and be able to reproduce quantitative aspects of the observed galaxy and mass distribution.

A full quantitative description of any point distribution in principle consists of the full hierarchy of M-point correlation functions ξ_M. They are defined along the lines set by that of the 2-point function $\xi(r)$, quantifiying the excess probability of finding a pair of points in volume elements dV_1 and dV_2 separated by a distance r in a point sample of average number density $\bar{n}$, the two-point function $\xi(r)$ is defined by

$$dP(r) \;=\; \bar{n}^2\;(1+\xi(r))\;dV_1 dV_2\;. \tag{67}$$

Conventional cosmological terminology expresses the amplitude of $\xi(r)$ in terms of the scale $r_{\rm o}$,

$$\xi(r_{\rm o}) \;=\; 1\;. \tag{68}$$

Conventionally denoted by the name "correlation length", we prefer the more correct name of "clustering length". Rather than a characteristic geometric scale, $r_{\rm o}$ is a measure for the "compactness" of the spatial clustering. A more significant scale within the context of the geometry of the spatial patterns in the density distribution is the scale at which

$$\xi(r_{\rm a}) \;=\; 0\;. \tag{69}$$

As a genuine scale of coherence it is a highly informative measure for the morphology of nontrivial spatial structures, so that we reserve the name "correlation length" for this scale.

In many cosmological studies the two-point correlation function $\xi(r)$ figures predominantly and often exclusively. This is partially based on historical development, $\xi(r)$ being the obvious first step in characterizing deviations from uniform point distributions. Other, substantial, cosmological considerations are of a more profound nature. The Gaussianity of the matter field perturbations in early linear phases of evolution implies a full description by $\xi(r)$. In more advanced nonlinear phases, ξ figures in the close link between the kinematics of associated matter flows and the matter distribution and forms the basic element in a a hierarchical correlation function series. And, more straightforward, is the practical consideration of the limited measurability of higher order functions as noisy samples of objects imply an incessant error increase with order M.

As for the real world, the most solid estimate of the spatial two-point correlation function of galaxies is inferred on the basis of the millions of objects in sky catalogues, through deprojection of the angular two-point

correlation $\omega(\theta)$. On scales $\leq 5h^{-1}$Mpc this is very well approximated by a power law, which implies a power-law spatial correlation function $\xi(r)$ (see e.g. Efstathiou 1996),

$$\xi_{gg}(r) \;=\; \left(\frac{r_{\rm o}}{r}\right)^{\gamma}\,; \qquad\qquad \gamma \approx 1.8, \quad r_{\rm o} \approx 5h^{-1}{\rm Mpc}\,. \qquad (70)$$

Although direct estimates from 3-D redshift survey samples are complicated by discreteness noise, sampling and selection effects and redshift distortions, overall they tend to corroborate this power-law behaviour, also wrt. the parameter values (e.g. Davis & Peebles 1983).

5.3.6 *Voronoi galaxy distributions: Point correlation analysis.* The two-point correlation for a representative "Voronoi kinematic" galaxy distributions is depicted in Fig. 45. It shows a kinematic galaxy distribution for a distribution optimally resembling the observed galaxy distibution. The two bottom frames depict the value of $\xi(r)$ as a function of the distance r between the "galaxies", expressed in units of the typical cell size λ_c. The figure contains both a log-log plot (lefthand), highlighting the small-scale clustering behaviour, and a lin-lin plot (righthand). The lin-lin plot is particularly apt in disclosing large-scale correlations in the spatial galaxy distribution, in particular also over distances considerably extending beyond the first zero-crossing of ξ, which typically is of the order of one cellsize. To be able to trace ξ over such a large spatial range, including ones where the amplitude of correlations is miniscule, a specially designed algorithm was implemented (Van de Weygaert 2002a,b). Note that the levelling off of $xi(r)$ at the radii $r \lesssim 0.5\lambda_c$ is an artefact. It is a consequence of the prescription for setting up the cellular galaxy samples, which slightly smears out the galaxy distribution in and around the walls, filaments and vertices. A striking aspect of the lin-lin ξ plot is the beating pattern (righthand frame). Such a pattern of oscillating function values, alternating between positive and negative values, together with a gradually dimishing oscillation amplitude is very characteristic for cellular geometries. At sub-cellular scales $\xi(r)$ has very high positive values, seemingly diverging for $r \rightarrow 0$. Falling off like a power-law at these small distances (lefthand frame), it reaches a zero value at a correlation distance $r_{\rm a} \approx 0.6\lambda_c$. Subsequently, it becomes anticorrelated before reaching again a spatial range with positive correlations as $r > 1.65\lambda_c$, be it with very small correlation values. Our code was able to follow non-zero correlation values over distances $r > 2-2.5\lambda_c$, beyond which the progressive damping of the correlation amplitude renders any non-zero correlation practically indetectable.

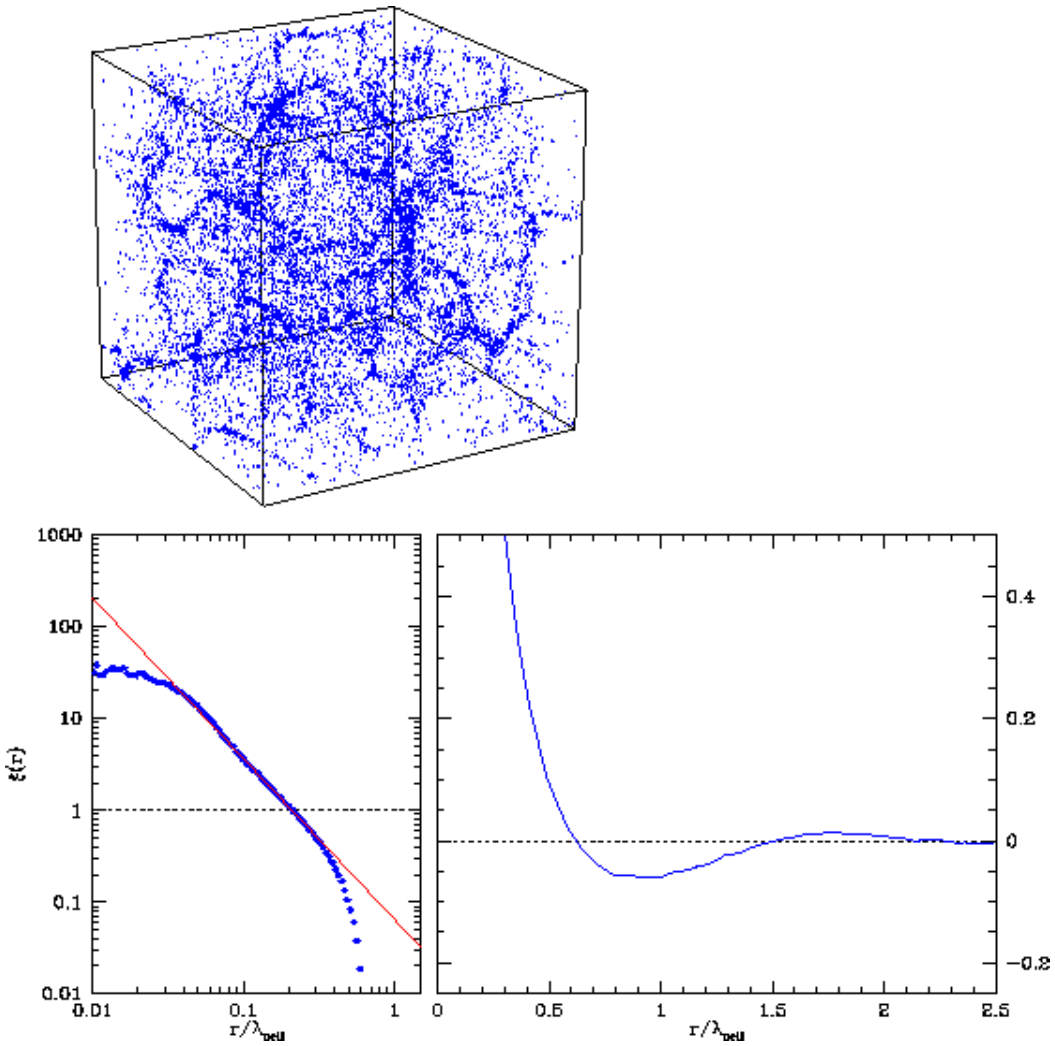

Figure 45. Two-point correlation function analysis of a selection of galaxies in a Voronoi kinematic model realization. Top frame: a spatial 3-D depiction of a full galaxy sample in a box of size $150h^{-1}$Mpc, at a stage corresponding to the present cosmic epoch $\sigma(8h^{-1}\text{Mpc} \approx 1$. The cellular morphology with walls and filaments forms a marked pattern throughout the box, with sites of a few conspicuously dense cluster "nodes" standing out. Bottom left: a log-log plot of the $\xi(r)$, with distance r in units of the basic cellsize $\lambda_{\rm cell}$. The power-law character of ξ up to $r \sim 0.5\lambda_c$ is evident. Bottom right: a lin-lin plot of ξ. The beautiful ringing behaviour out to scales $r \sim 2\lambda_{\rm cell}$ has been amply recovered. From: Van de Weygaert 2002b.

Turning to the log-log plot, only evaluated for $r < r_{\rm a} \lesssim \lambda_c$, we encounter some interesting behaviour. Most enticing is the power-law be-

haviour of $\xi(r)$ over almost the complete subcellular range. For the distribution shown the power-law slope is $\gamma \approx 1.85$ (!!!), while $r_{\rm o} \approx 0.23\lambda_c$. When considering the development of $\xi(r)$ over the gradual progress of the kinematic model we find a correlation function whose shape is similar to the one shown in Fig. 45, though with a constantly increasing amplitude. The "correlation" scale $r_{\rm a}$ does not shift (the cellular pattern in the Voronoi model is static) as the coherence scale of the galaxy distribution does not evolve. On the other hand, the increasing level of clustering finds its expression in a steadily growing "clustering length" $r_{\rm o}$ as well as a continuously increasing power-law slope. For instance, the first box in Fig. 41 corresponds to a $(r_{\rm o}/\lambda_c, \gamma) \approx (0.06, 1.3)$ versus the values of $(0.23, 1.85)$ that we quoted for the final stage.

Intriguing is the finding that a value of $r_{\rm o} \approx 5h^{-1}$Mpc, the current value for the observed galaxy distribution, would suggest a cellular scale $\lambda_c \approx 20 - 25h^{-1}$Mpc when we take the timesteps with $r_{\rm o}/\lambda_c \approx 0.2 - 2.25$ as best match to the observed galaxy distribution. Such a size $\lambda_c \approx 25h^{-1}$Mpc is teasingly close to the quoted values for the size of typical voids. In fact, the suggested intimate relation between cellsize and clustering length $r_{\rm o}$ had already been pointed out by Heavens (1985) for the simple – and highly artificial – configuration of an infinite network of cubic cells. If interesting, an even more intriguing thought may be that this is not contradictory to the conventional explanation within the context of nonlinear gravitational clustering starting from a field of Gaussian random density perturbations, but should rather be seen as complementary manifestations. Both the clustering length $r_{\rm o}$ and the cellular pattern are then intimately related, both being a product of the underlying process of gravitational clustering.

The discussed kinematic Voronoi distribution represents a teasingly good agreement with that in the observed galaxy distribution. Naturally, the versatility of the Voronoi model allows it to be used as a template for a range of significantly different distributions. For example, we tested the correlation behaviour for pure wall-like, pure filamentary, and pure cluster galaxy distributions. Restricting the galaxy locations to uniform distributions within these structural features, we found that all three yield a power-law ξ at sub-cellular scales, with a filamentary distribution corresponding to a substantially higher clustering amplitude $r_{\rm o} \approx 0.23\lambda_c$ and steeper slope of $\gamma \approx 1.9$, while a wall-like distribution has a more moderate $r_{\rm o} \approx 0.14\lambda_c$ and a shallow slope $\gamma \approx 1.4$ (Van de Weygaert 1991b, 2002b).

5.3.7 *Voronoi galaxy distributions: Words of Prudence.* Of course the detailed and full physical picture underlying the cosmic galaxy dis-

tribution is expected to differ from that encapsulated in the Voronoi model, considerably so in the very dense, highly nonlinear regions of the network, around the filaments and clusters. Nonetheless, the success of the Voronoi kinematic model in reproducing and describing the structural morphology and relevant characteristics of the cosmic foam, both the one seen in large redshift surveys as well as the one found in the many computer model N-body simulations, indicates its significance for the goal of defining a proper geometric model which may hope to succeed in modelling its essentials.

5.4. Superclustering

Within the context of the identification of the Voronoi framework with the large-scale matter distribution, a special role is assumed by the *Voronoi vertices*. They are the tentative sites of the most pronounced components in the large scale galaxy distribution, the clusters of galaxies, located at the interstices in the cosmic framework. This can be clearly discerned from the evolving structure in Figure 41.

It is with respect to the identification of Voronoi vertices with the clusters of galaxies that the most telling and intriguing successes of the Voronoi model have been registered. Of instrumental significance in this context is the fact that the identification of vertices with clusters is straightforward, fully and exclusively defined by the geometry of the Voronoi tessellation realization. A primary assessment of the clustering of these vertices is fully set by the geometry of the tessellation and can therefore be done without further assumptions. When doing this, we basically use the fact that *the Voronoi node distribution is a topological invariant* in co-moving coordinates, and does not depend on the way in which the walls, filaments, and nodes are populated with galaxies. The statistics of the nodes should therefore provide a robust measure of the Voronoi properties. By contrast, for the modelling of related galaxy distributions additional specification for the fine small-scale details is very necessary.

5.4.1 *Superclustering: Cluster Clustering.* As borne out by Fig. 7/8, clusters display a significant degree of clustering. An important issue is whether their clustering is merely a randomly sampled and diluted reflection of the underlying mass distribution or whether there are some clearly distinguishing characteristics to it. A comparison with the galaxy distribution have revealed three distinct aspects in the clustering of clusters.

- The first aspect is the finding that the clustering of clusters is considerably more pronounced than that of galaxies. The two-point correlation function $\xi_{cc}(r)$ of clusters appears to be a scaled version of the power-law galaxy-galaxy correlation function, $\xi(r) = (r_o/r)^\gamma$. Most studies agree on the same slope $\gamma \approx 1.8$ while all yield a significantly higher amplitude. The estimates of the latter differ considerably from a factor $\simeq 10 - 25$. The original value found for the "clustering length" $r_{\rm o}$ for rich $R \geq 1$ Abell clusters was $r_{\rm o} \approx 25 h^{-1}$Mpc (Bahcall & Soneira 1983),

$$\xi_{cc}(r) \;=\; \left(\frac{r_{\rm o}}{r}\right)^\gamma \;; \qquad\qquad \gamma = 1.8{\pm}0.2; \quad r_{\rm o} = 26{\pm}4\, h^{-1}{\rm Mpc}\,, \tag{71}$$

  up to a scale of $100h^{-1}$ Mpc (Bahcall 1988). Later work favoured more moderate values in the order of $15 - 20h^{-1}$Mpc (e.g. Sutherland 1988, Dalton et al. 1992, Peacock & West 1992). In terms of statistical significance, the recent clustering analysis of the cleanly defined REFLEX cluster sample has produced the currently most significant and elucidating determination of cluster-cluster correlation function (see Fig. 46, from Borgani & Guzzo 2001) and its corresponding power spectrum (Borgani & Guzzo 2001, Collins et al. 2001, Schuecker et al. 2001). As can be clearly discerned from Fig. 46, it strongly endorses the amplified cluster clustering wrt. the galaxy distribution (from the LCRS survey, Tucker et al. 1997).

- A related second property of cluster clustering is that the differences in estimates of $r_{\rm o}$ are at least partly related to the specific selection of clusters. There appears to be a trend of an increasing clustering strength as the clusters in the sample become more rich ($\approx$ massive). On the basis of the first related studies, Szalay & Schramm (1985) even put forward the (daring) suggestion that samples of clusters selected on richness would display a 'fractal' clustering behaviour, in which the clustering scale $r_{\rm o}$ would scale linearly with the typical scale L of the cluster catalogue,

$$\xi_{cc}(r) \;=\; \beta \left(\frac{L(r)}{r}\right)^\gamma \;; \qquad L(R) \;=\; n^{-1/3}\;. \tag{72}$$

  The typical scale $L(R)$ is then the mean separation between the clusters of richness higher than R. Although the exact scaling of $L(r)$ with mean number density n is questionable, observations seem to follow the qualitative trend of a monotonously increasing $L(R)$. It also appears to be reflected to some extent in a similar

increase in clustering strength encountered in selections of model clusters in large-scope N-body simulations (e.g. Colberg 1998).

- A final and third aspect of cluster clustering, is the issue of the spatial range over which clusters show positive correlations, the "coherence" scale of cluster clustering. Usually it is an aspect that escapes proper attention, yet may be of crucial significance. There is ample evidence that $\xi_{cc}(r)$ extends out considerably further than the galaxy-galaxy correlation ξ_{gg}, possibly out to $50h^{-1}-100h^{-1}$Mpc. This is not in line with conventional presumption that the stronger level of cluster clustering is due to the more clustered locations of the (proto)cluster peaks in the primordial density field with respect to those of (proto)galaxy peaks. According to this conventional "peak bias" scheme we should not find significant non-zero cluster-cluster correlations on scales where the galaxies no longer show any significant clustering. If indeed ξ_{gg} is negligible on these large scales, explaining the large scale cluster-cluster clustering may be posing more complications than a simple interpretation would suggest.

5.4.2 *Superclustering: Voronoi Vertices.* An inspection of the spatial distribution of Voronoi vertices (Fig. 47, righthand frame) immediately reveals that it is not a simple random Poisson distribution. The full spatial distribution of Voronoi vertices in the $250h^{-1}$Mpc cubic volume of figure 30 involves a substantial degree of clustering, a clustering which is even more strongly borne out by the distribution of vertices in a thin slice through the box (bottom lefthand frame) and equally well reflected in the sky distribution (bottom righthand frame). The impression of strong clustering, on scales smaller than or of the order of the cellsize $\lambda_{\rm C}$, is most evidently expressed by the corresponding two-point correlation function $\xi(r)$ (Fig. 48, left: log-log, right: lin-lin). Not only can we discern a clear positive signal, but out to a distance of at least $r \approx 1/4\,\lambda_{\rm c}$ the vertex-vertex correlation function is indeed an almost perfect power-law,

$$\xi_{vv}(r) = \left(\frac{r_{\rm o}}{r}\right)^{\gamma}\,; \qquad\qquad \gamma = 1.95; \quad r_{\rm o} \approx 0.3\,\lambda_{\rm c}\,. \qquad (73)$$

with a slope $\gamma \approx 1.95$ and "clustering length" $r_{\rm o} \approx 0.3\,\lambda_{\rm c}$. Beyond this range, the power-law behaviour breaks down and following a gradual decline the correlation function rapidly falls off to a zero value once distances are of the order of (half) the cellsize. A value of $r_{\rm a} \approx 0.5\lambda_c$ for the zeropoint "correlation length" may be established most clearly

Figure 46. The two-point correlation functions ξ of galaxies (squares) and X-ray clusters of galaxies (circles), plotted as a function of (redshift space) separation r_s, computed from the Las Campanas galaxy redshift survey (Tucker et al. 1997) and the REFLEX X-ray cluster survey (Collins et al. 2001). The two curves are the predictions for 2 CDM models, both in spatially flat universes ($\Omega_m + \Omega_\lambda = 1$), one with $\Omega_m = 0.3, h = 0.7$ (solid line), the other with $\Omega_m = 0.5, h = 0.6$ (dashed line). Courtesy: Borgani & Guzzo 2001. Reproduced by permission of Nature.

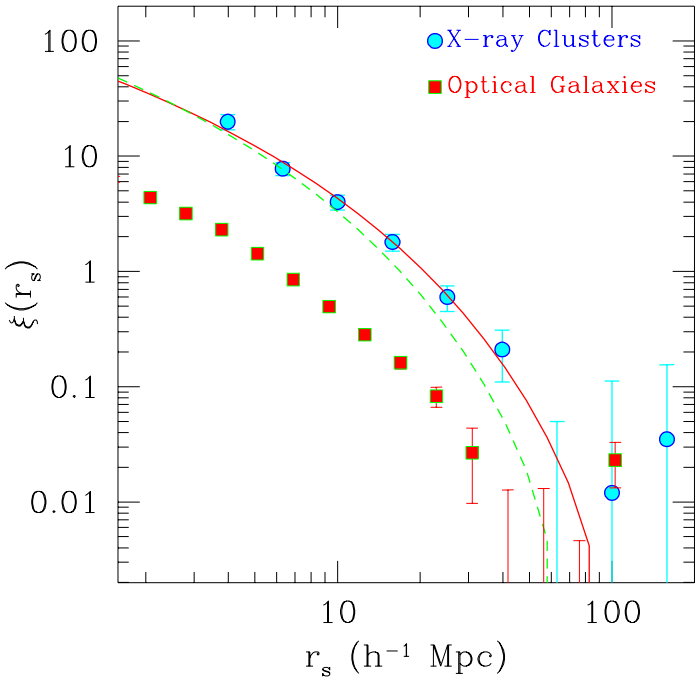

from a linear-linear diagram of $\xi(r)$, while beyond r_a the distribution of Voronoi vertices appears to be practically uniform. Its only noteworthy behaviour is the gradually declining and alternating quasi-periodic ringing between positive and negative values similar to that we also recognized in the "galaxy" distribution, a vague echo of the cellular patterns which the vertices trace out. Ultimately, beyond $r \approx 2\lambda_c$ any noticeable trace of clustering seems to be absent. The power-law behaviour of ξ_{vv} is in remarkable agreement with that of the cluster distribution. It may hint at a geometrical origin for the power law slope $\gamma \approx 2$ of the cluster distribution. Also, its amplitude is in accordance with the observed cluster clustering length $r_\mathrm{o} \approx 20h^{-1}\,\mathrm{Mpc}$, i.e. if we assume a basic cosmic foam cellsize of $\lambda_\mathrm{c} \approx 70h^{-1}\,\mathrm{Mpc}$. The latter might actually be a complication, be it for the most simplistic interpretation assuming that every vertex would indeed represent a cluster.

5.4.3 *"Geometric Biasing": Cluster Selections.* The vertex correlation function in eqn. (18) does not take into account possible selection effects for the vertices. In reality, not every vertex will represent sufficient mass, or a sufficiently deep potential well, to be identified with a true compact galaxy cluster. If we take the Voronoi model as an asymptotic approximation to the true galaxy distribution, its vertices will comprise a range of "masses". Upon closer attention, the time sequence of evolving galaxy distributions in Fig. 41 indicates a continuously widening difference in the concentration of particles in and near vertices. Dependent on the specific geometrical setting of each vertex

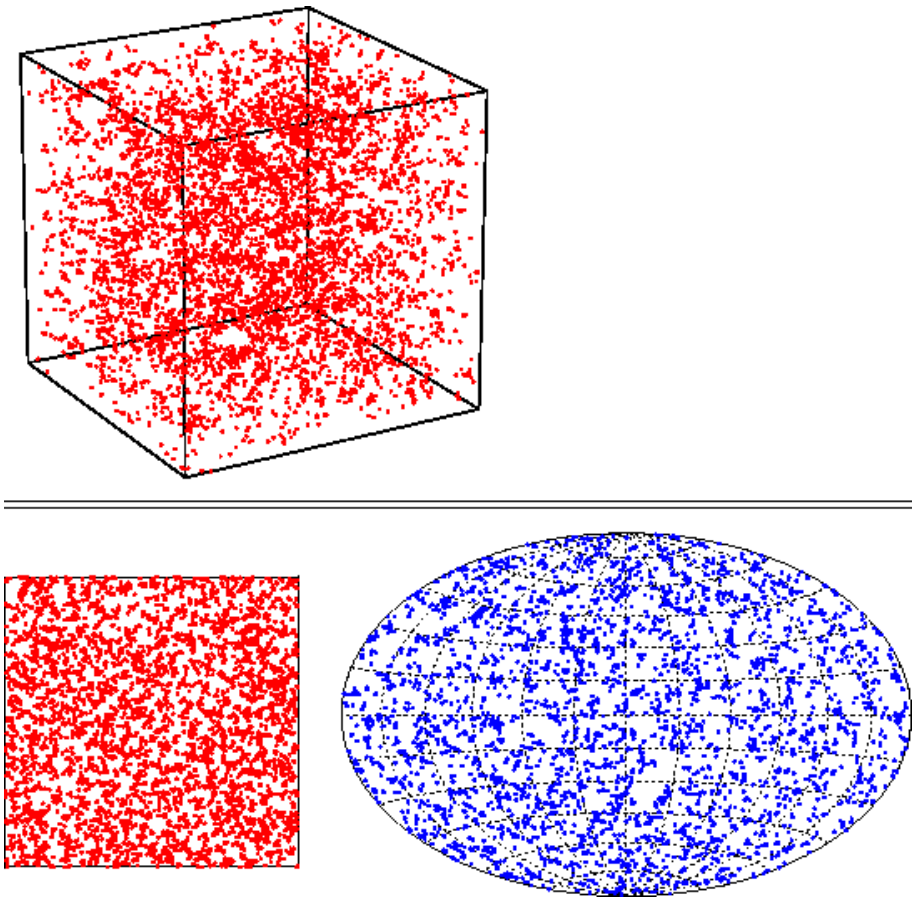

Figure 47. The spatial distribution of a full sample of Voronoi vertices. Top frame; the 3-D distribution in a $250h^{-1}$Mpc box containing 1000 Voronoi cells ($\sim$ 6725 vertices). Notice the hint for vertices grouping in superstructures. Bottom left: the vertex distribution in a $25h^{-1}$Mpc wide slice through box. Bottom right: an (Aitoff) sky projection of vertices out to a distance of $125h^{-1}$Mpc from the box centre.

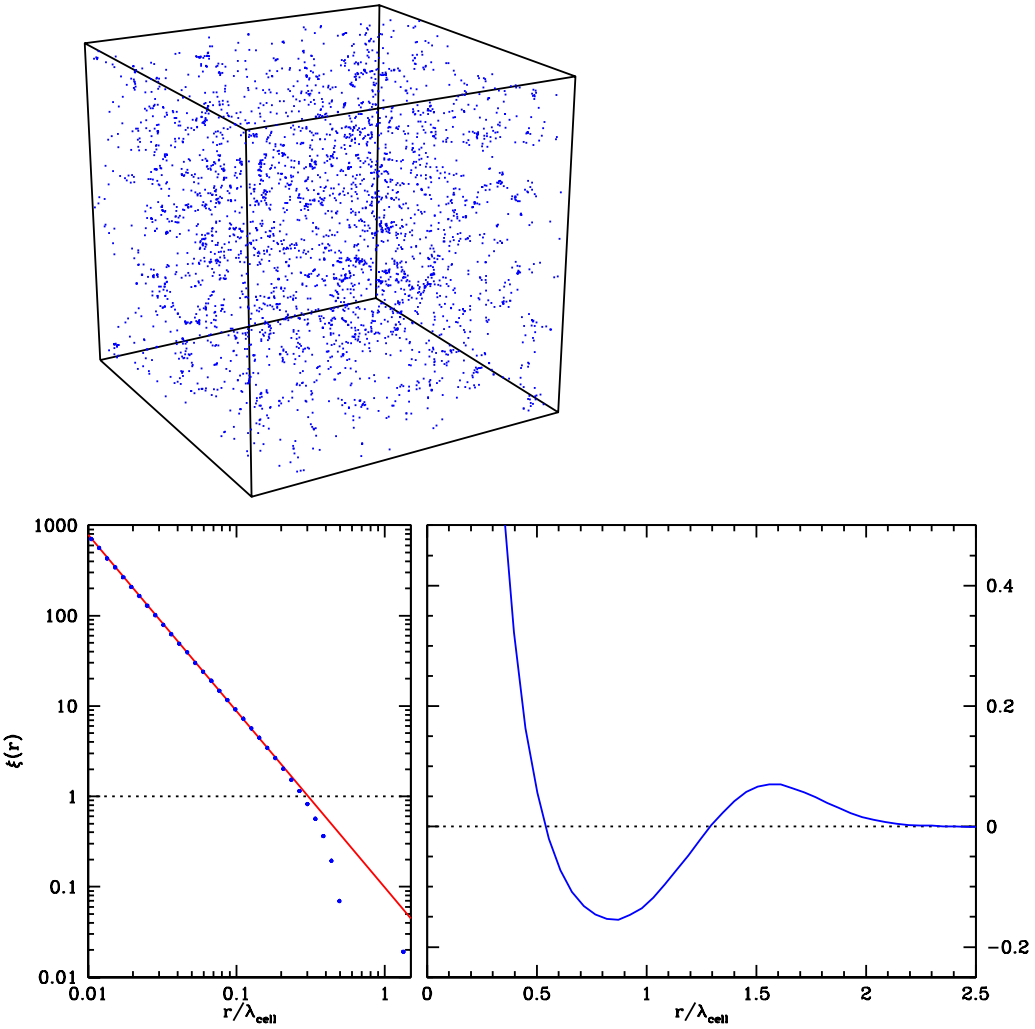

Figure 48. Two-point correlation function analysis of a (full, non-selected) set of Voronoi vertices. Top frame: a spatial 3-D depiction of Voronoi vertex distribution. Upon close attention, the underlying cellular geometry may be discerned. Bottom left: a log-log plot of the $\xi(r)$, with distance r in units of the basic cellsize $\lambda_{\rm cell}$. The power-law character of ξ up to $r \sim 0.3\lambda_c$ is evident. Bottom right: a lin-lin plot of ξ. The beautiful ringing behaviour out to scales $r \sim 2\lambda_{\rm cell}$ has been amply recovered. From: Van de Weygaert 2002a.

– the size of the corresponding cells, walls and edges, the proximity of nearby vertices, etc. – the total mass acquired by a vertex will span a wide range of values.

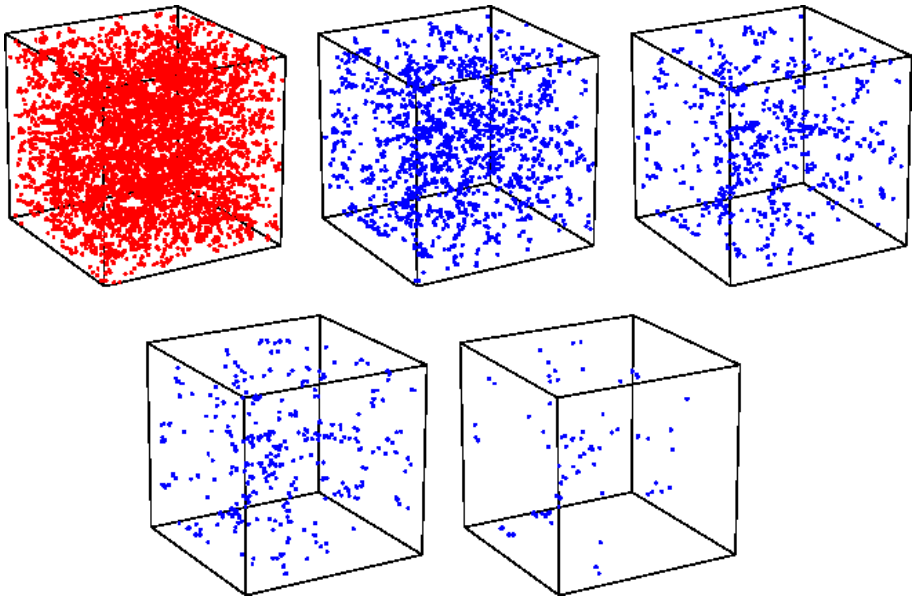

Figure 49. Selections of vertices from a full sample of vertices. Depicted are the (100%) full sample (top left), and subsamples of the 25%, 10%, 5% and 1% most massive vertices (top centre, top right, bottom left, bottom right). Note how the richer vertices appear to highlight ever more pronounced a filamentary superstructure running from the left box wall to the box centre. From: Van de Weygaert 2002a.

Brushing crudely over the details of the temporal evolution, we may assign each Voronoi vertex a "mass" estimate by equating that to the total amount of matter ultimately will flow towards that vertex. Invoking the "Voronoi streaming model" as a reasonable description of the clustering process, it is reasonably straightforward if cumbersome to compute the "mass" or "richness" $\mathcal{M}_{\rm V}$ of each Voronoi vertex by pure geometric means (Van de Weygaert 2002a). The geometric computation far more efficient than Monte Carlo "particle-based" evaluations, yet also challenging and cumbersome in its implementation. In essence, the computation of the final mass consists of the evaluation of the Lagrangian volume of the mass content of the vertex. This Lagrangian volume is a non-convex polyhedron centered on the Voronoi vertex. The connected Voronoi nuclei, in the "streaming model" supplying the Voronoi vertex with inflowing matter, define the polyhedral vertices.

To get an impression of the resulting selected vertex sets, Figure 49 shows 5 times the same box of $250h^{-1}$Mpc size, each with a specific subset of the full vertex distribution (top lefthand cube). In the box we set up a realization of a Voronoi foam comprising 1000 cels with an average size of $25h^{-1}$Mpc. From the full vertex distribution we selected the ones whose "richness" $\mathcal{M}_{\rm V}$ exceeds some specified lower limit. The

depicted vertex subsets correspond to progressively higher lower mass limits, such that 100%, 25%, 10%, 5% and 1% most massive vertices are included (from top lefthand to bottom righthand). The impression is not the one we would get if the subsamples would be mere random diluted subsamples from the full vertex sample. On the contrary, we get the definite impression of a growing coherence scale !!! For instance, it is as if the 1% subsample subtends a single huge filament running the extent of the full box, even though this would be suggesting a single feature of $200 - 250h^{-1}$Mpc size, an order of magnitude larger than the basic Voronoi cellsize.

5.4.4 *"Geometric Biasing": Transforming Clustering Patterns.* The observed tendency of more massive vertex subsamples to display a stronger level of clustering which extends out to large distances has been scrutinized. After all, the human eye has a great talent for picking up patterns, thereby regularly exaggerating their reality or even imagining them while they do not even exist. To correct for possible diluted

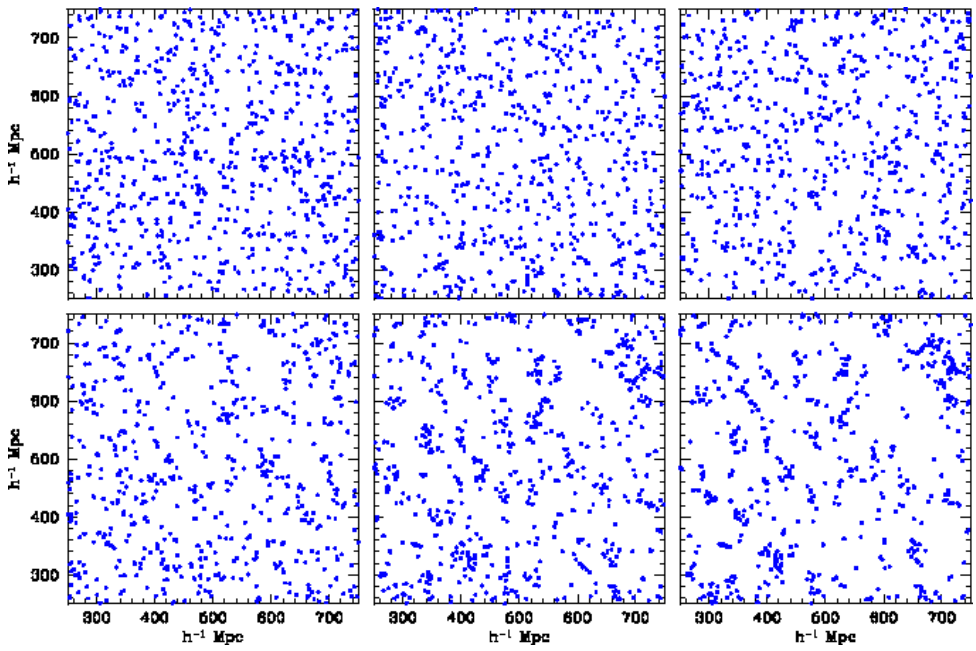

Figure 50. Selections of Voronoi vertices. Each subsample consists of the same number of vertices, randomly selected from samples of ever richer vertices from top left to bottom right. Top left: random selection from complete sample of vertices. Bottom right: 0.25% richest vertices. Notice the continuous increase in clustering strength, and the stark contrast between the mild clustering of the full sample and that amongst the richest vertices. From: Van de Weygaert 2002a.

sampling effects provoking an exaggerated impression of an intrinsically moderate or even non-existent clustered distribution, we calibrated all point samples to the same number density, thereby assuring that their spatial statistics would be retained. This is accomplished by pure random sampling of the same number of points from each subsample.

For a huge cubic volume of $800h^{-1}$Mpc, containing 64^3 cells of $25h^{-1}$Mpc size, Figure 50 shows the enticing result. Beyond any doubt it confirms the impression of a intrinsic significantly stronger clustering for the more massive vertices. There is a salient contrast between the rather moderate level of clustering in the top lefthand frame (100% level) and the striking point patterns in the sample of bottom righthand frame (0.25% level) is remarkable.

At least three aspects concerning the more pronounced clustering of the more massive cluster samples may be discerned:

- *Stronger clustering*
  The clustering itself is stronger, expressing itself in tighter and more compact point concentrations.

- *Increased clustering scale*
  The clustering extends over a substantially larger spatial range. Structures, clumps and huge voids, subtending several elementary cell scales are clearly visible (see in particular centre and right bottom frames Fig. 50).

- *Anisotropic extensions*
  The subtended large scale features appear to become more distinctly anisotropic, wall-like or filamentary, for more massive samples (note the huge filamentary complexes in lower righthand frame Fig. 50).

These visual impressions seem to reveal a striking "superclustering" tendency hidden within the basic cosmic foam pattern – modelled by the basic Voronoi foam – and disclosing itself only through the distribution of its most prominent elements, the most massive clusters. The supercluster complexes – huge filaments and walls – form by linking several (Voronoi) edges and walls.

Note that linking a set of randomly oriented filaments or walls generically would not subtend such stretched superstructures. Instrumental in understanding the presence of such features is their embedding within the underlying "cellular" geometry of the matter distribution, the significance of which has usually escaped proper appreciation, if any at all. A key aspect of cellular geometries is the rigid embedding of walls and edges into a distinct connected network. As is easily inferred from geo-

metrical modelling, walls and edges will not be oriented randomly and isotropically with respect to each other. On the contrary, their mutual orientation is typically centering around values of obtuse angles. The Voronoi geometry presents us with a telling illustration of this fact (see Fig. 51, and Van de Weygaert 1991b, 1994): walls and edges do indeed connect to their neighbouring peers with angles whose statistical distribution peaks around obtuse angles $\sim 120^\circ$. The distribution function for both walls and edges is indeed a peaked distribution, with the minor part of angles below $\sim 100^\circ$, and the majority subtending obtuse angles larger than $\sim 120^\circ$.

Thus, large coherent filaments are a direct consequence of an underlying cellular geometry. They get assembled by virtue of the implicit obtuse intra-wall and intra-filament angles.

We have therefore found that richer objects not only cluster more strongly, but also out to a larger range. Hence, our audacious claim that it is the geometry of foamlike networks which is responsible for observed supercluster patterns in the distribution of the rich clusters and rare cosmic powerhouses of the AGNs. Also note that such geometries would induce a distinct flattening in the distribution of clusters and AGNs at scales where we would not be able to trace any such anisotropy in the galaxy distribution itself. The seeming contrast between these large scale concentrations, out to beyond $100h^{-1}$Mpc, and the smaller scales on which detectable galaxy clustering is encountered, is likely to find its origin in the very nontrivial geometry of the galaxy distribution itself !

5.4.5 *"Geometric Biasing": Correlation Scaling.* The qualitative impression of a gradually stronger, more pronounced and richer pattern

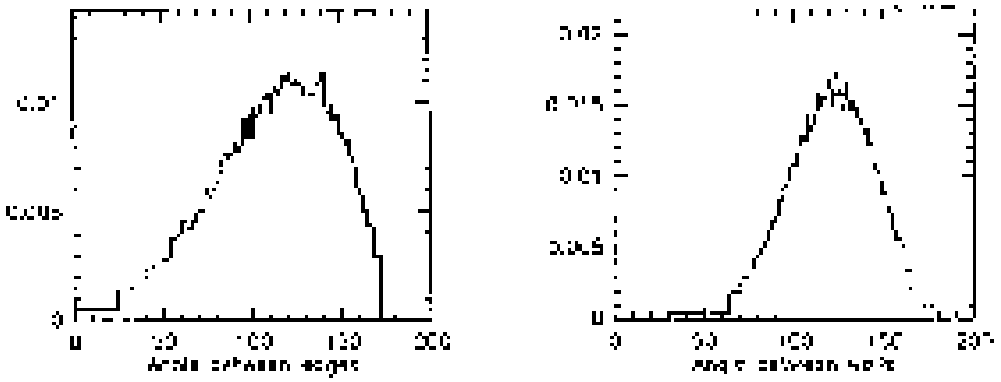

Figure 51. Angles between neighbouring Voronoi walls (left) and Voronoi edges (right) in a Poisson Voronoi tessellation (tessellation resulting from Poisson distributed nuclei). Notice that both distribution functions are peaked around the obtuse angle of $\sim 120^\circ$. From Van de Weygaert 1991b, 1994.

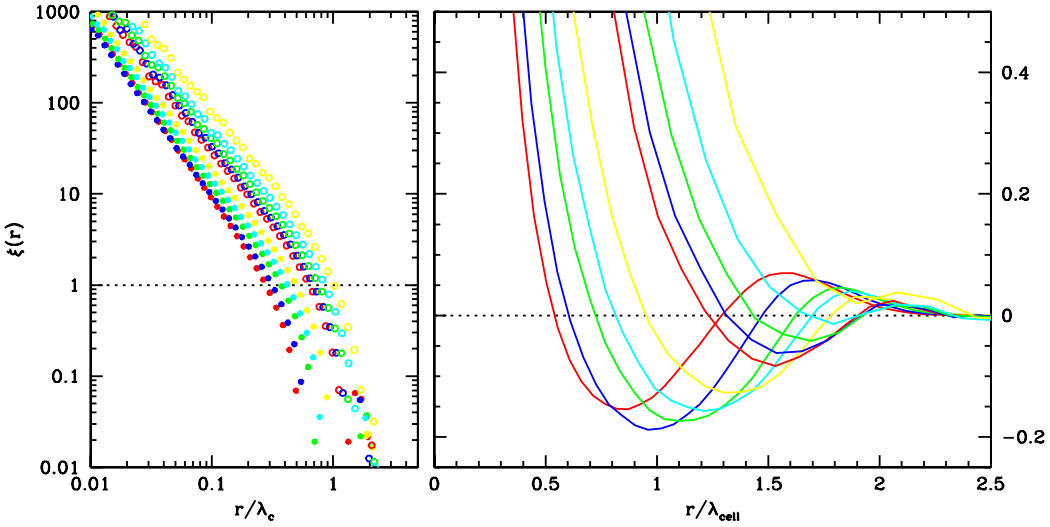

Figure 52. Scaling of the two-point correlation function of Voronoi vertices, for a variety of subsamples selected on the basis of "richness", ranging from samples with the complete population of vertices down to subsamples containing the 2.5% most massive vertices. Left: log-log plot of $\xi(r)$ against r/λ_c, with λ_c the basic tessellation cellsize ($\equiv$ intranucleus distance). Notice the upward shift of $\xi(r)$ for subsamples with more massive vertices. Right: lin-lin plot of $\xi(r)$ against r/λ_c. Notice the striking rightward shift of the "beating" pattern as richness of the sample increases. From: Van de Weygaert 2002a.

of clustering becomes even more striking upon quantitatively analyzing correlation function systematics (Fig. 52, Van de Weygaert 2002a). A thorough numerical study of vertex clustering patterns disclosed an unexpected and surprising "self-similarity".

The impression of stronger clustering is indeed confirmed through a systematic, linear, increase in the value of the "clustering length" r_o. Possibly more surprising is the equally systematic increase of the "correlation length" r_a, the quantitative expression for the observed impression of point clustering noticeably extending over larger regions of space. Especially noteworthy are the following aspects of clustering scaling (see Fig. 52 & 53):

- *Two-point correlation function*
  The two-point correlation functions of selected massive cluster samples display a behaviour similar to that found for unbiased samples (Fig. 52): an almost perfect power-law at short range which beyond its coherence scale changes gradually into a oscillating behaviour between positive and negative correlations, swiftly decaying within a few "ringings" to zero level.

- *Parameters $\xi(r)$*
  The parameters characterizing the generic behaviour of ξ – amplitude, coherence scale and power-law slope – are subject to systematic scaling behaviour.

- *Correlation amplitude*
  The amplitude of the correlation functions increases with rising vertex sample richness. The "clustering length" $r_{\rm o}$ increases almost perfectly linear as a function of the characteristic intra-vertex distance $\lambda_{\rm v}$ of the particular richness selected vertex sample.

- *Correlation extent*
  The large-scale (lin-lin) behaviour of ξ_{vv} extends out to larger and larger distances with increasing sample richness. As in the case of $r_{\rm o}$ the "correlation (coherence) scale" $r_{\rm a}$ possesses an almost perfectly linear relation as function of the average sample vertex distance λ_v.

- *Clustering and coherence scaling*
  Therefore, combining the behaviour of $r_{\rm o}$ and $r_{\rm a}$ a striking "self-similar" scaling behaviour is revealed: the ratio of correlation versus clustering length is virtually constant for all vertex samples, $r_{\rm a}/r_{\rm o} \approx 1.86$ (for Poisson Voronoi tessellations).

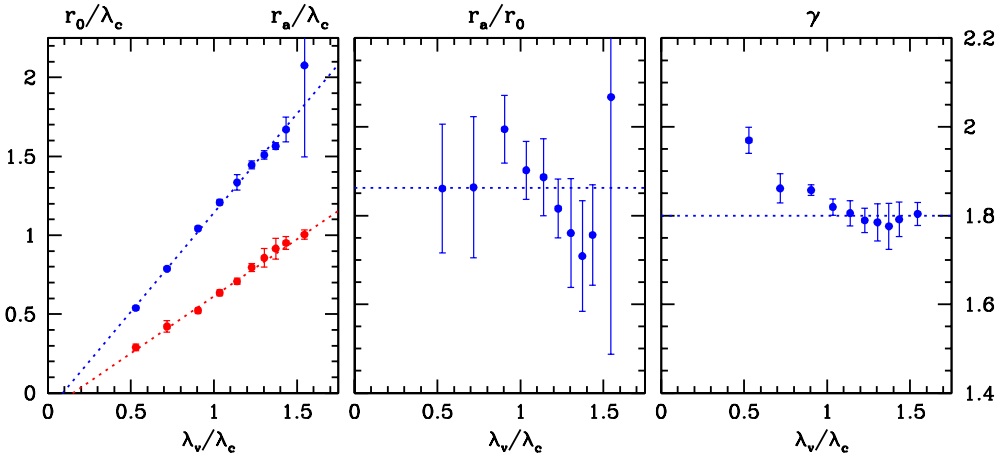

Figure 53. Scaling of Voronoi vertex two-point correlation function parameters for vertex subsamples over a range of "richness"/"mass". Left: the clustering length r_0 (red, $\xi(r_0) \equiv 1.0$) and the correlation (coherence) length r_a (blue, $\xi(r_a) \equiv 0$) as a function of average spatial separation between vertices in (mass) selected subsample, λ_v/λ_c. Centre: the ratio between clustering length r_0 and coherence length r_a as function of subsample intravertex distance λ_v/λ_c. Right: the power-law slope γ as function of λ_v/λ_c.

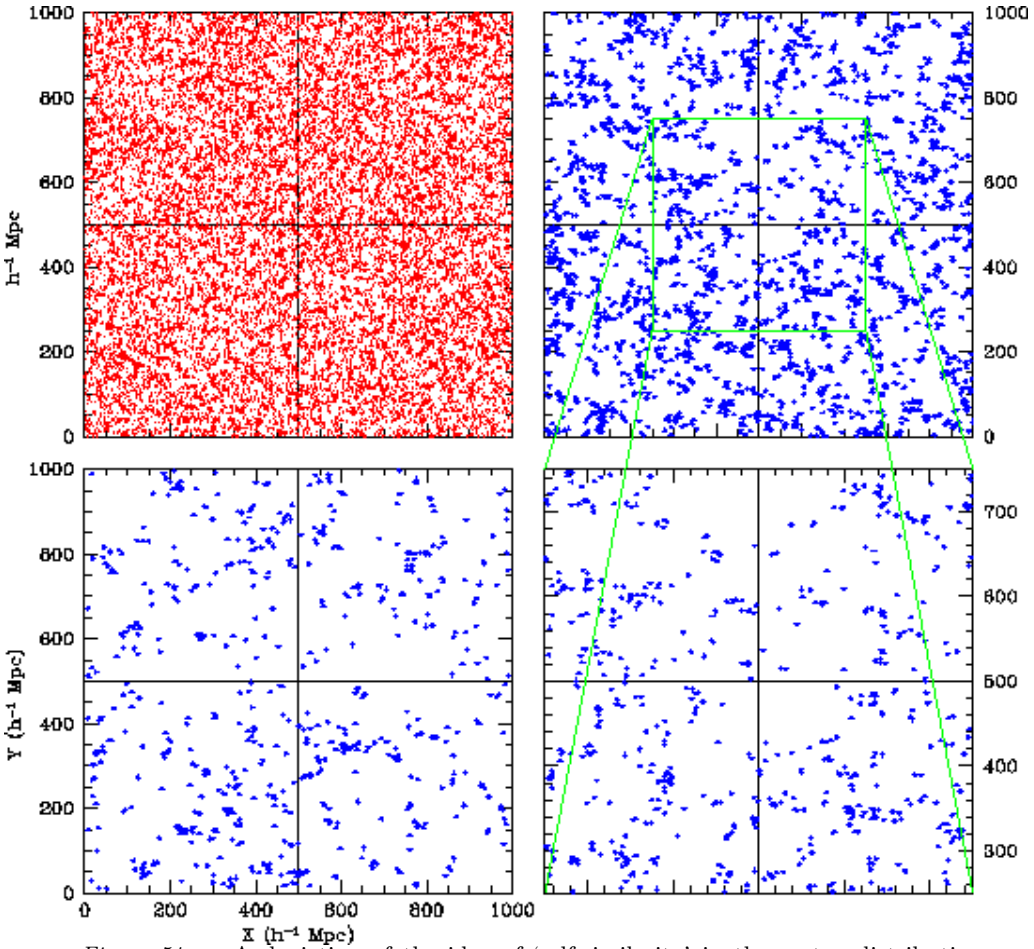

Figure 54. A depiction of the idea of 'self-similarity' in the vertex distribution. Out of a full sample of vertices (top left) in a central slice, (top right) the 20.0% richest vertices. Similarly, (bottom left) the 2.5% richest vertices. When lifting the central $1/8^{th}$ region out of the 20% vertex subsample in the (top righthand) frame and sizing it up to the same scale as the full box, we observe the similarity in point process between the resulting (bottom righthand) distribution and that of the 2.5% subsample (bottom lefthand). Self-similarity in pure form !

- *Correlation function slope*
  At the short power-law range, the correlation functions have rather similar slopes. Nonetheless, a slight and significant trend in the power-law slope has been found, involving an gradually increasing tilt. Interestingly, we see a gradual change from a slope $\gamma \approx 1.95$ for the full sample to a robust (and suggestive) $\gamma \approx 1.8$ for the selected samples.

All in all, these intrinsically geometrical properties hint at a scaling behaviour which may befittedly be called "geometrical biasing". It is be

qualitatively different from the more conventional "peak biasing" picture (Kaiser 1984) in that it involves an effect of spatial extending clustering, yet equivalent in its ramifications for offering an explanatio for the more pronounced level of clustering displayed by galaxy clusters.

5.4.6 *"Geometric Biasing": Self-Similarity and the Cosmic Foam.* Arguably most enticing in the scaling behaviour of the correlation functions has been the finding that the vertex clustering patterns display an intriguing intrinsic *self-similarity.* The correlation functions of the various richness selected samples all appear to constitute, within reasonable limits, a scaled version of correlation function. The full correlation function $\xi_s(r)$ of the various richness selected subsamples s, not just the part in the power-law range, consistute self-similar mappings of an elementary function $\xi_{\rm el}$, scaled by means of a characteristic lengthscale parameter L_s.,

$$\xi_s(r) \,=\, \frac{1}{A_s}\,\xi_{\rm el}\Big(r/L_s\Big)\,. \tag{74}$$

In other words, in terms of point statistical behaviour, each selected vertex sample behaves like a spatially scaled version of a basic point distribution. This is tellingly illustrated in Fig. 54 through a realization of such a vertex distribution, in comparison with a few selected subsets. A central slice through the full sample of Voronoi vertices in a box of a $1000h^{-1}$Mpc is shown in the top lefthand frame (all vertices in red). From these the 20% richest are selected and shown in the top righthand frame, while the 2.5% richest are shown in the lower lefthand frame. Notice the impression of vast coherent linear structures !!! Then, sizing up the central half-size part of the "20%" sample and comparing the resulting point process to the full sample of the "2.5%" sample we indeed do find point distributions whose spatial statistics is practically equivalent. In other words, a pure illustration of a genuine self-similar point process !

Figure 55. Observing in the Atacama Desert: a world filling tessellation. Courtesy: Dave Watson (CSIRO, Div. Exploring and Mining, Perth, Australia).

6. HORA EST:...

The World, A Foam

We have explored the background behind the uncovered foamlike geometry of the cosmic galaxy distribution. Over the past decades gradually a new paradigm for the cosmic matter distribution has been established, that of a Megaparsec scale cosmic foam, in which walls, filaments – with scales up to over $100h^{-1}$Mpc – and galaxy clusters link up into a vast cosmos pervading network, meandering in between huge empty void regions with sizes up to tens of Megaparsec.

We have indicated that such foamlike geometries are manifestations of the process of structure formation under the influence of gravity. Acting in a Universe evolving from a primordial distribution which is nearly uniform but for a sea of tiny density ripples, it is the cosmic force field which is ultimately responsible for the emergence of structure in the Universe. Not only the final fate of the forming individual matter concentrations is a consequence of its workings. Its sway extends sofar that it as well controls the intricate morphology and geometry in which the cosmos' matter content settles itself. It is the intrinsically anisotropic character

of the cosmic force field which transforms gravity into the sculptor of the salient patterns in the cosmic matter distribution. We extensively discussed the way in which gravity from the onset onward moulds the matter distribution into the salient filamentary and wall-like structures that form such distinctive elements of the observed and mapped galaxy and matter distribution. In particular, by means of the simple asymptotic *ellipsoidal model* we indicated why on scales where gravity has started to decouple these perturbations from the cosmic background, while not yet having proceeded to a stage full collapse an intrinsic anisotropic shape is a natural configuration. The discussion continued with the indication of how such features assemble into the nontrivial and astonishing complexity of the *cosmic foam*.

Isolating within this cosmic foam assembly the void, underdense regions, we argued how we can understand the formation of the cosmic web in an equivalent, seemingly alternative yet complementary, approximation. Starting from the premise of the intrinsically simpler dynamics of underdense regions we find a Universe in which we will observe the rise of perpetually expanding "void sectors", whose continuous and proliferating drainage and unceasing tendency towards a spherical shape must be seen as one of the major symptoms of the gravitational structure growth process. On the basis of such a view, we are led to an asymptotic description ultimately yielding a geometrical model for the cellular distribution of matter. *Voronoi Tessellations* represent a central concept in the mathematical branch of *Stochastic Geometry*.

Voronoi tessellations represent a versatile and flexible mathematical model for foamlike patterns. Based on a seemingly simple definition, Voronoi tessellations define a wealthy stochastic network of interconnected anisotropic components, each of which can be identified with the various structural elements of the cosmic galaxy distribution. On the basis of this concept we have been able to investigate the ramifications of nontrivial foamlike patterns for a variety of characteristics of the spatial organization of matter in our Universe.

On the basis of the geometry of Voronoi tessellations we have seemingly uncovered a surprising yet fundamental kinship between the cosmic foam and the large scale cluster distribution. Plainly tentalizing is the finding – within the context of cellular geometries so characacteristic for the cosmic matter distribution – that a geometry as that of the cosmic foam holds the implication of an effect which may be denoted as a "geometrical biasing". In this contribution, we describe the existence of the underlying self-similar clustering behaviour in such cellular or foamlike geometries. It suggests a tantalizing and intimate relationship between the cosmic foamlike geometry and a variety of aspects of the spatial

distribution of galaxies and clusters. It would explain why the level of clustering amongst massive galaxy clusters is so much stronger than that between their more moderate brethren. As significant is the finding of positive spatial cluster-cluster correlations over scales substantially exceeding the "elementary" scale of voids and other cosmic foam elements.

Indeed, it appears that our Universe in more than one way resembles Plato's Academia, that venerable institution devoted to learning, seeking to uncover the secrets of the world and our existence, over whose door it was said to be written:

"Let no one unversed in geometry enter here. "

Acknowledgments

In preparing this manuscript, I wish to thank John Peacock for his permission to use the 2dF image in Fig. 1 and Fig. 5, Michael Strauss for providing me with the Sloan redshift survey impression in Fig. 1, Luiz da Costa for providing the CfA2/SSRS survey map in Fig. 1, and to the LCRS team for the Las Campanas redshift map in Fig. 1, and S. Maddox for Fig. 2. Also grateful I am to Martha Haynes for supplying me with Fig. 5, to Stefano Borgani for his permission to use Fig. 7, 8, and 46, to Alex Szalay for issueing Fig. 11, to V. de Lapparent for the permission to use Fig. 3, to B. Kirshner for using Fig. 9, to H. Quintana for Fig. 10, to G. Bothun for Fig. 13 and to John Dubinski for Fig. 32. Dave Watson provided the beautiful Atacama desert impression. In particular I am grateful to Jacco Dankers for helping to prepare the Geomview package graphs of Fig. 34, 35 & 40. In particular acknowledged are W. Schaap and E. Romano-Díaz for useful and inspiring discussions, and for preparing Figs. 14 & 15 and Figs. 17 & 18, and allowing me to use these prior to publication.

Fond memories and gratitude characterize these days in the cradle of western civilization.

First and foremost, the author wishes to thank Manolis Plionis for the kind invitation for this wonderful workshop, for his caring hospitality and even more for the almost infinite and greatly appreciated patience and coöperation in preparing this contribution, beset as it was by an unacceptable delay in submission. Yet, ultimately, the contribution is not nearly as large as the gratitude for the joys of Archaion Gefseis and the late night sounds and dances of rebetiko ... it was like Zorba spelling out the essentials of true living !

Moving these days was the heartwarming hospitality of the Papadopoulos family; Padelis, his parents and brother made us feel like family by indulging us to the intoxicating delights of traditional Greek gastronomy, feasting and sirtaki !

Then, in the quest for the origin and workings of our world, it was no more than proper to pay due respect to the two Athenians who were so crucial in moulding the human mind into its prime instrument of inquiry ... inciting a pilgrimage to the cell where Socrates' showed the ultimate resolve for principle and moral, and a visit to the foundations of western knowledge and learning, there where Plato's Academia assembled ...

Profoundly awe-inspiring it was to witness Zeus himself descending, amidst his thunderclouds over the Acropolis he came to pay tribute to a special Greek friend, namesake and descendant of the legendary queen of Greece, the woman who launched a thousand ships, Helena ...

"... Each time I climbed the Acropolis again, the Parthenon seemed to be swaying slightly, as in a motionless dance – swaying and breathing. ..."

cont'd beyond next page

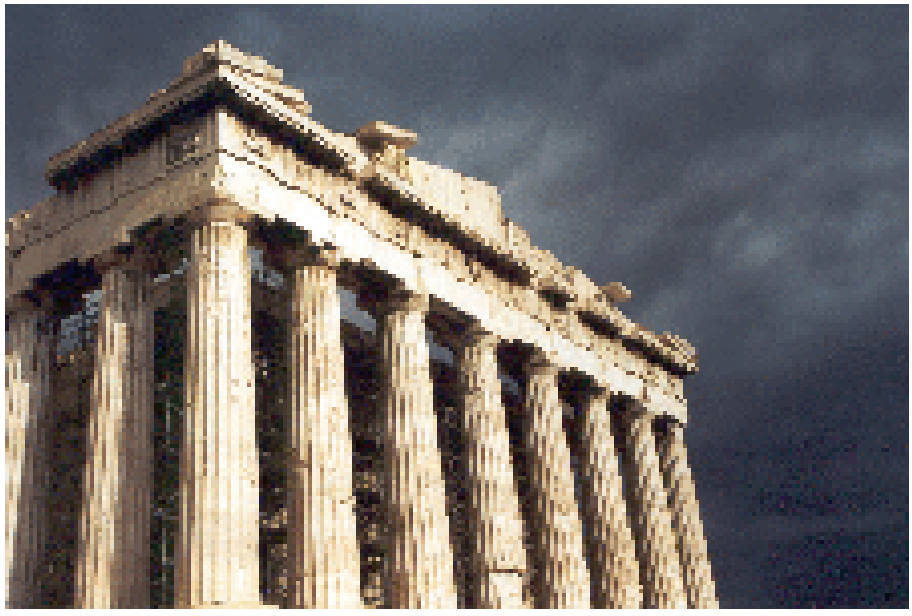

"[..] This temple that towered before me, what a trophy it was, what a collaboration between mind and heart, what a supreme fruit of human effort ! Space had been conquered; distinctions between large and small had largely vanished. Infinity entered this narrow, magical parallelogram carved out by man, entered leisurely and took its repose there. Time had been conquered as well; the lofty moment had been transformed into eternity."

Nikos Kazantzakis, Report to Greco, 1961

References

Abell G., 1958, ApJS, 3, 211
Abell G.O., Corwin H.G., Olowin R.P., 1989, ApJS, 70, 1
Baffa C., Chincarini G., Henry R.B.C., Manousoyanaki J., 1993, A&A, 280, 20
Bahcall N.A., 1988, ARA&A, 26, 631
Bahcall N.A., Soneira R., 1983, ApJ, 270, 20
Bahcall N.A., Fan X., Cen R., 1997, ApJ, 485, L53
Balbus S.A., Hawley J.F., 1998, Revs. Mod. Phys., 70, 1
Banday A.J., Zaroubi S., Górski, K.M., 2000, ApJ, 533, 575
Bardeen J.M., Bond J.R., Kaiser N., Szalay A.S., 1986, ApJ, 304, 15 (BBKS)
Bardelli S., Zucca E., Zamorani G., Moscardini L., Scaramella R., 2000, MNRAS, 312, 540
Barnes J., Efstathiou G., 1987, ApJ, 319, 575
Batuski D.J., Miller C.J., Slinglend K.A., Balkowski C., Maurogordata S., Cayatte V., Felenbok P., Olowin R., 1999, ApJ, 520, 491
Bernardeau F., van de Weygaert R., 1996, MNRAS, 279, 693
Bernardeau F., Colombi S., Gaztañaga E., Scoccimarro R., 2002, Phys. Rep., subm.
Bertschinger E., 1987, ApJ, 323, L103
Bertschinger E., Dekel A, Faber S.M., Dressler A., Burstein D., 1990, ApJ, 364, 370
Bertschinger E., Jain, B., 1994, ApJ, 431, 486
Blandford R. D., Saust A.B., Brainerd T.G., Villumsen J.V., 1991, MNRAS, 251, 600
Böhringer H., Schuecker P., Guzzo L., Collins C., Voges W., Schindler S., Neumann D.M., Cruddace R.G., DeGrandi S., Chincarini G., Edge A.C., MacGillivray H.T., Shaver P. , 2001, A&A, 369, 826
Bond J.R., Myers S.T., 1996a, ApJS, 103, 1
Bond J.R., Myers S.T., 1996b, ApJS, 103, 41
Bond J.R., Myers S.T., 1996c, ApJS, 103, 63
Bond J.R., Cole S., Efstathiou G., Kaiser N., 1991, ApJ, 379, 440
Bond J.R., Kofman L., Pogosyan D. Yu., 1996, Nature, 380, 603
Borgani S., Guzzo L., 2001, Nature, 409, 39
Bothun G.D., Geller M.J., Kurtz M.J., Huchra J.P., Schild R.E., 1992, ApJ, 395, 347
Bower R.G., 1991, MNRAS, 248, 332
Brainerd T.G., Scherrer R.J., Villumsen J.V., 1993, ApJ, 418, 570
Branchini E., Plionis M., 1996, ApJ, 569
Branchini E., Zehavi I., Plionis M., Dekel A., 2001, MNRAS, 313, 491

Broadhurst T.J., Ellis R.S., Koo D.C., Szalay A.S., 1990, Nature, 343, 726
Cabanela J.E., Dickey J.M., 1999, AJ, 118, 46
Catelan P., Theuns T., 1996a, MNRAS, 282, 436
Catelan P., Theuns T., 1996b, MNRAS, 282, 455
Colberg J., 1998, Parallel Supercomputer Simulations of Cosmic Evolution, Ph.D. thesis, Ludwig-Maximilian Univ. München
Coles P., 1990, Nature, 346, 446
Coles P., Melott A., Shandarin S.F., 1993, MNRAS, 260, 765
Collins C., Guzzo L., Böhringer H., Schuecker P., Chincarini G., Cruddace R., DeGrandi S., MacGillivray H.T., Neumann D.M., Schindler S., Shaver P., Voges W., 2001, MNRAS, 319, 939
Couchman H.M.P., Barber A.J., Thomas P.A., 1999, 308, 180
Dalton G.B., Efstathiou G., Maddox S.J., Sutherland W.J., 1992, ApJ, 390, L1
Davis M., Peebles P.J.E., 1983, ApJ, 267, 465
Dekel A., 1994, ARAA, 32, 371
Dekel A., Bertschinger E., Faber S.M., 1990, ApJ, 364, 349
Dekel A., Rees M.J., 1994, ApJ, 422, L1
De Lapparent V., Geller M.J., Huchra J.P., 1986, ApJ, 302, L1
Delone B.V., 1934, Bull. Acad. Sci. (VII) Classe Sci. Mat., 793
Descartes, R., 1664, Le Monde, Ou Traité de la Lumière, &c., Paris
Doroshkevich A.G., 1970, Afz, 6, 581 [1973, Astrophys., 6, 320]
Dubinski J. 1992, ApJ, 401, 441
Dubinski J., Carlberg R., 1991, ApJ, 378, 496
Dubinski J., Da Costa L.N., Goldwirth D.S., Lecar M., Piran T., 1993, ApJ, 410, 458
Dunn A.M., Laflamme R., 1993, MNRAS, 264, 865
Efstathiou G., Jones B.J.T., 1979, MNRAS, 186, 133
Efstathiou G., Frenk C.S., White S.D.M., Davis M., 1988, MNRAS, 235, 715
Efstathiou G., Ellis R.S., Peterson, B.A., 1988, MNRAS, 232, 431
Efstathiou, G., 1996, in *Cosmology and Large Scale Structure*, Proc. Les Houches summerschool XV, eds. R. Schaeffer, J. Silk, M. Spiro, J. Zinn-Justin, NATO ASI series
Eisenstein D., Loeb A., 1995, ApJ, 439, 520
Eke V.R., Cole S., Frenk C.S., 1996, MNRAS, 282, 263
Ettori, S., Fabian, A.C., White, D.A., 1997, MNRAS, 289, 787
Ferreira P. G., Magueijo J., Gorski, K.M., 1998, ApJ, 503, L1
Geller M.J., Huchra J., 1989, Science, 246, 897
Giavalisco M., Mancinelli P.J., Mancinelli P.J., Yahil A., 1993, ApJ, 411, 9
Giovanelli R., Haynes M., 1991, ARA&A, 29, 499
Giovanelli R., Haynes M., 1996, private communication
Gunn J.E., Gott J.R., 1972, ApJ, 176, 1
Han C., Gould A., Sackett P.D., 1995, ApJ, 445, 46
Heavens A., 1985, MNRAS, 213, 143
Heavens A., Peacock J., 1988, MNRAS, 232, 339
Hoekstra H., 2001, A&A, 370, 743
Hoffman Y. 1986, ApJ, 301, 65
Hoffman Y. 1988, ApJ, 329, 8
Hoffman Y., Shaham J., 1982, ApJ, 262, L23
Hoffman Y., Ribak E., 1991, ApJ, 380, 5
Hoffman Y., Eldar A., Zaroubi S., Dekel A., 2001, ApJ, astro-ph/0102190

Hoyle F., 1949, in Problems of Cosmical Aerodynamics, eds. Burgers, J.M. & van de Hulst, H.C., Central Air Documents. Dayton, Ohio, p. 195
Hui, Bertschinger E., 1996, ApJ 471, 1
Icke V., 1972, Formation of Galaxies Inside Clusters, Ph.D. Thesis, University Leiden
Icke V., 1973, A&A, 27, 1
Icke V., 1984, MNRAS, 206, 1P
Jain B., 1997, MNRAS, 287, 687
Jain B., Seljak U., White S.D.M., 2000, ApJ, 530, 547
Jing Y.P., 2001, ApJ, 550, L125
Kaiser N., 1984, ApJ, 284, L9
Kaiser N., Squires G., 1993, ApJ, 404, 441
Kaiser N., Wilson G., Luppino G., Kofman L., Gioi I., Metzger M., Dahle H., 1998, astro-ph/9809268
Kauffmann G., White S.D.M., 1993, MNRAS, 261, 921
Kazantzakis N., Report to Greco, 1961 (Engl. ed. 1965, Faber and Faber, London)
Kiang, T., 1966, Zeitschr. f. Astrophys., 64, 433
Kirshner R.P., Oemler A., Schechter P.L., Shectman S.A., 1981, ApJ, 248, L57
Kirshner R.P., Oemler A., Schechter P.L., Shectman S.A., 1987, ApJ, 314, 493
Kofman L., Pogosyan D.Yu., Shandarin S.F., 1990, MNRAS, 242, 200
Kull A., Böhringer H., 1999, A&A, 341, 23
Lee J., Pen Ue-Li, 2000, ApJ, 532, L5
Lennon J., McCartney P., 1970, *Let it Be*. London: EMI
Lilje P.B., Yahil A., Jones B.J.T., 1986, ApJ, 307, 91
Lin C.C., Mestel L., Shu F.H., 1965, ApJ, 142, 1431
Lynden-Bell D., 1964, ApJ, 139, 1195
Lynden-Bell D., Faber S.M., Burstein D., Davies R.L., Dressler A., Terlevich R., Wegner G., 1988, ApJ, 326, 19
Lyttleton R.A., 1953, The stability of rotating liquid masses, Cambridge University Press
Matarrese S., Lucchin F., Moscardini L, Saez D., 1992, MNRAS, 259, 437
Maddox S.J., Sutherland W.J., Efstathiou G., Loveday J., 1990a, MNRAS, 243, 692
Maddox S.J., Efstathiou G., Sutherland W.J., 1990b, MNRAS, 246, 433.
Matsuda T., Shima, E., 1984, Prog. Theor. Phys., 71, 855
Melott A.L., 1983, MNRAS, 205, 637
Melott A.L., Buchert T., Weiss A., 1995, A&A, 294, 345
Melott A.L., Sathyaprakash B.S., Sahni V., 1996, ApJ, 456, 65
Mo H.J., White S.D.M., 1996, 282, 347
Moscardini L., Branchini E., Brunozzi P. Tini, Borgani S., Plionis M., Coles P., MNRAS, 1996, 282, 384
Nusser A., Dekel A., Bertschinger E., Blumenthal G.R., 1991, ApJ, 379, 6
Nusser A., Dekel A., 1992, ApJ, 391, 443
Nusser A., Branchini E., 2000, MNRAS, 313, 587
Peacock J.A., West M.J., 1992, 259, 494
Peebles P.J.E., 1969, ApJ, 155, 393
Peebles P.J.E., 1980, The Large-Scale Structure of the Universe, Princeton Univ. Press
Peebles P.J.E., 1987, ApJ, 317, 567
Peebles P.J.E., 1989, ApJ, 344, L53
Peebles P.J.E., 1990, ApJ, 362, 1
Plato, $\approx$ 355-350 B.C., Timaeus
Plionis M., Valdarnini R., 1991, MNRAS, 249, 46

Plionis M., Basilakos S., 2001, MNRAS, in the press
Polenta G., et al. 2001, ApJL, subm.
Porciani C., Dekel A., Hoffman Y., 2001a, MNRAS, subm.
Porciani C., Dekel A., Hoffman Y., 2001b, MNRAS, subm.
Press W.H., Schechter P., 1974, ApJ, 187, 425
Quinn T., Binney J., 1992, MNRAS, 255, 729
Quintana H., Carrasco E.R., Reisenegger A., 2000, AJ, 120, 511
Raychaudhury S., 1989, Nature, 342, 251
Reiprich T.H., Böhringer H., 1999, Astron. Nachr., 320, 296
Reisenegger A., Quintana H., Carrasco E., Maze J., 2000, AJ, 120, 523
Rhee G., Katgert P., 1987, A&A, 183, 217
Romano-Díaz E., Branchini E., van de Weygaert R., 2001, in "Where's the Matter? Tracing Dark and Bright Matter with the New Generation of Large Scale Surveys", eds. Treyer & Tresse, Edit. Frontièr, in press
Romano-Díaz E., Branchini E., van de Weygaert R., 2002, A&A, subm.
Ryden B.S., 1988, ApJ, 329, 589
Sahni V., Coles P., 1995, Phys. Rep., 262, 1
Scaramella R., Vettolani G., Zamorani G., 1991, ApJ, 376, L1
Schaap W., van de Weygaert R., 2000, A&A, 363, L29
Schaap W., van de Weygaert R., 2002a, A&A, in prep.
Schaap W., van de Weygaert R., 2002b, MNRAS, in prep.
Scherrer R.J., 1992, ApJ, 390, 330
Schuecker P., Böhringer H., Guzzo L., Collins C., Neumann D.M., Schindler S., Voges W., DeGrandi S., Chincarini G., Cruddace R., Müller V., Reiprich T.H., Retzlaff J., Shaver P., 2001, A&A, 368, 66
Shectman S. A., Landy S.D., Oemler A., Tucker D.L., Lin H., Kirshner R. P., Schechter P.L., 1996, ApJ, 470, 172
Shandarin S.F., Zel'dovich Ya.B., 1989, Rev. Mod. Phys., 61, 185.
Shapley H., 1930, Harvard Coll. Obs. Bull., 874, 9
Sheth R.K., Mo H.J., Tormen G., 2001, MNRAS, 323, 1
Sheth R.K., van de Weygaert R., 2002, in prep.
Smoot G. F., Tenorio L., Banday A.J., Kogut A., Wright E. L., Hinshaw G., Bennett C. L., 1994, ApJ., 437, 1
Strauss M., Willick J., 1995, Phys. Rep. 261, 271
SubbaRao, M.U., Szalay, A.S., 1992, ApJ, 391, 483
Sugerman B., Summers F.J., Kamionkowski M., 2000, MNRAS, 311, 762
Sutherland, W., 1988, MNRAS, 234, 159
Szalay A.S., Schramm D.N., 1985, Nature, 314, 718
Szomoru A. 1995, Ph.D. Thesis, University of Groningen
Thomas T., 2002, The influence of cluster environment on galaxies, Ph.D. Thesis, University Leiden
Tonry J.L., Blakeslee J.P., Ajhar E.A., Dressler A., 2000, ApJ, 530, 625
Tucker D.L., Oemler A. Jr., Kirshner R.P., Lin H., Shectman S.A., Landy S.D., Schechter P.L., Müller V., Gottloeber S., Einasto J., 1997, 285, L5
Tyson J.A., Wenk R.A., Valdes F., 1990, ApJ, 349, L1
van de Weygaert R., 1991a, MNRAS, 249, 159
van de Weygaert R., 1991b, Voids and the Large Scale Structure of the Universe, Ph.D. Thesis, University Leiden
van de Weygaert R., 1994, A&A, 283, 361
van de Weygaert R., 2002a, A&A, to be submitted

van de Weygaert R., 2002b, A&A, to be submitted
van de Weygaert R., Bertschinger, E., 1996, MNRAS, 281, 84
van de Weygaert R., Icke V., 2002, in Statistical Challenges in Modern Astronomy III, eds. E. Feigelson & G.J. Babu, in press
van de Weygaert R., van Kampen E., 1993, MNRAS, 263, 481
van Haarlem M., van de Weygaert R., 1993, ApJ, 418, 544 (HW)
Van Waerbeke L., Mellier Y., Erben T., Cuillandre J. C., Bernardeau F., Maoli R., Bertin E., Mc Cracken H. J., Le Fevre O., Fort B., Dantel-Fort M., Jain B., Schneider P., 2000, A&A, 358, 30
Voronoi G., 1908, J. reine angew. Math., 134, 198
Warren M.S., Quinn P.J., Salmon J.K., Zurek W.H., 1992, ApJ, 399, 405
White S.D.M., 1984, ApJ, 286, 38
Willick, J.A., Courteau, S., Faber, S.M., Burstein, D., Dekel, A., Strauss, M.A., 1997, ApJS, 109, 333
Wu J.H.P., Balbi A., Borrill J., Ferreira P.G., Hanany S., Jaffe A.H., Lee A.T., Rabii B., Richards P.L., Smoot G.F., Stompor R., Winant C.D., 2001, Phys. Rev. Lett. 87, in press
Yuan Q.R., Hu F.X., Su H.J., Huang K.L., 1997, AJ, 114, 1308
Zel'dovich Y.B., 1970, A&A, 5, 84

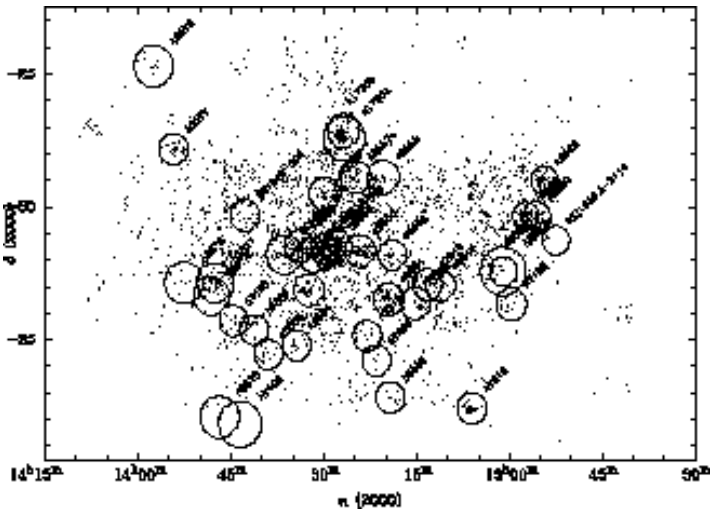
δ (2000)
α (2000)

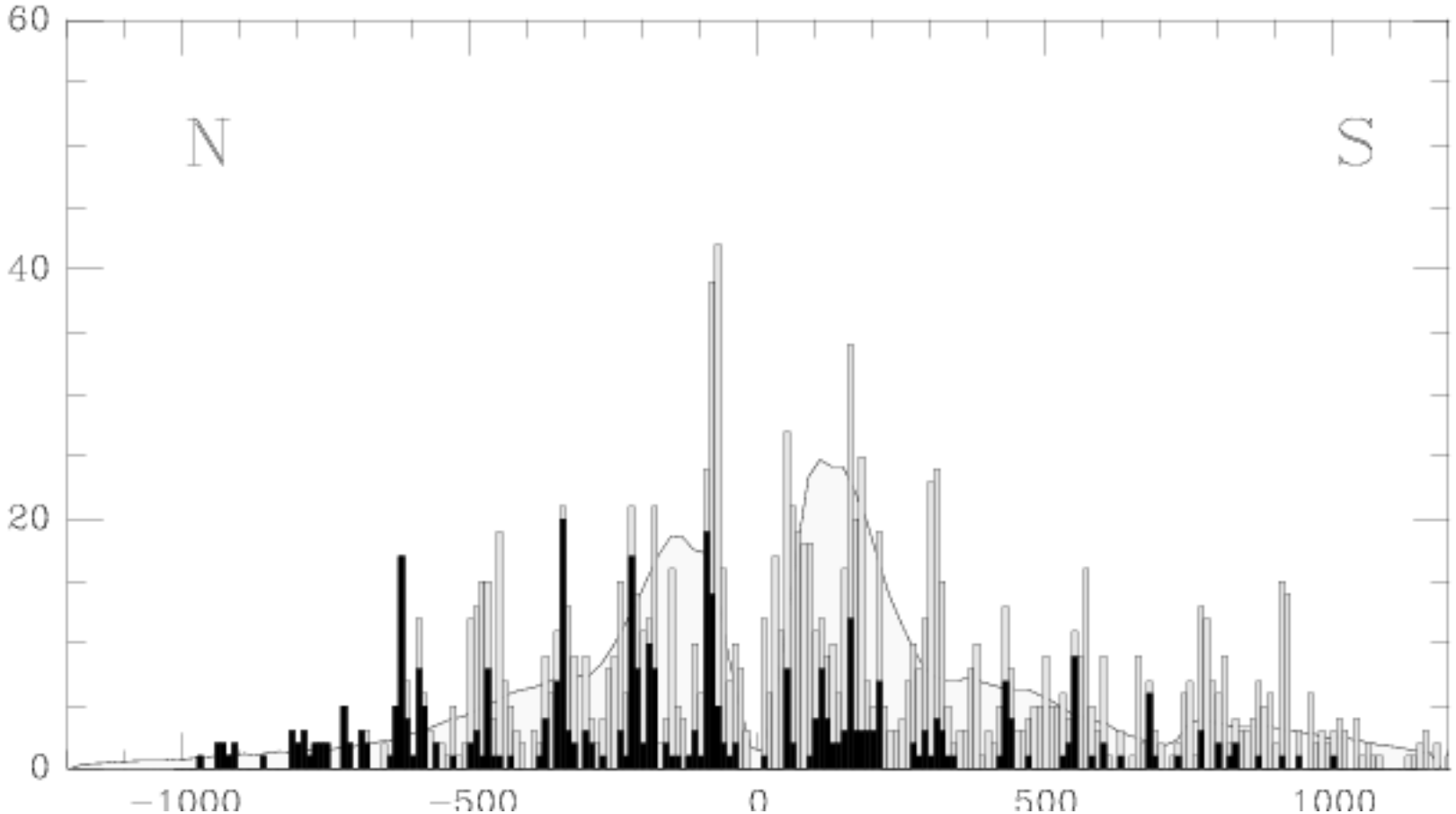
60
40
20
0
N
S
−1000
−500
0
500
1000

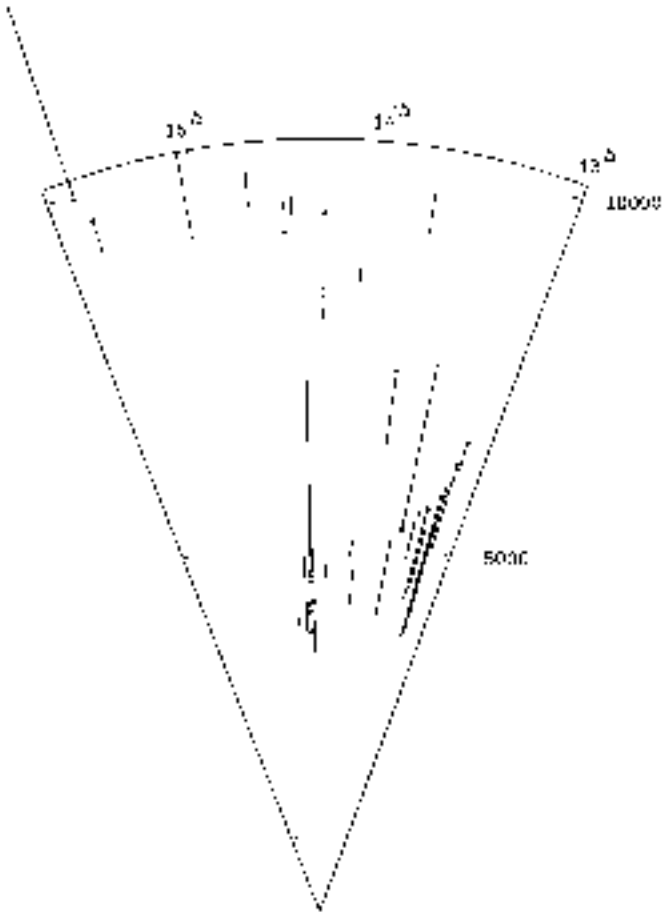

28.5 < δ < 33.5° cz (km/s)

(b) galaxies

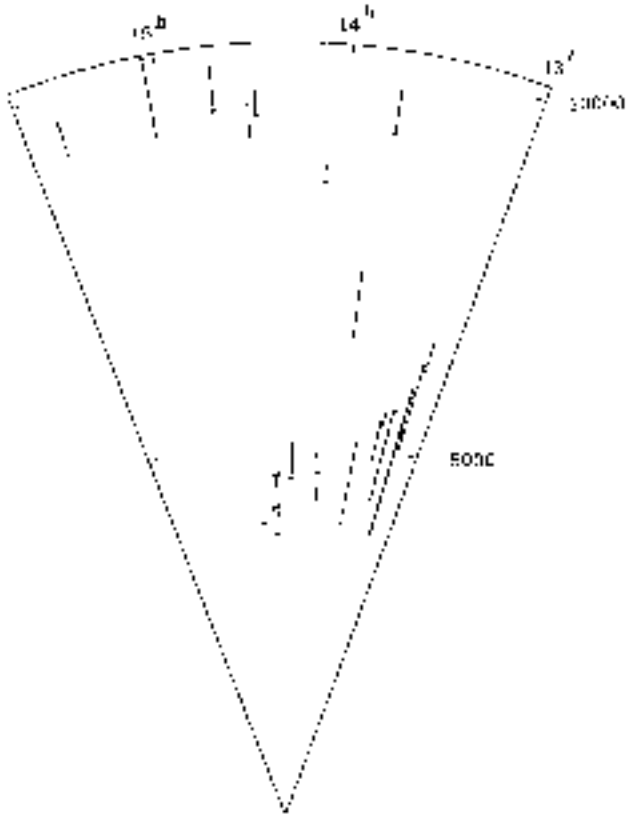

28.5 < δ < 33.5° cz (km/s)

(c) galaxies

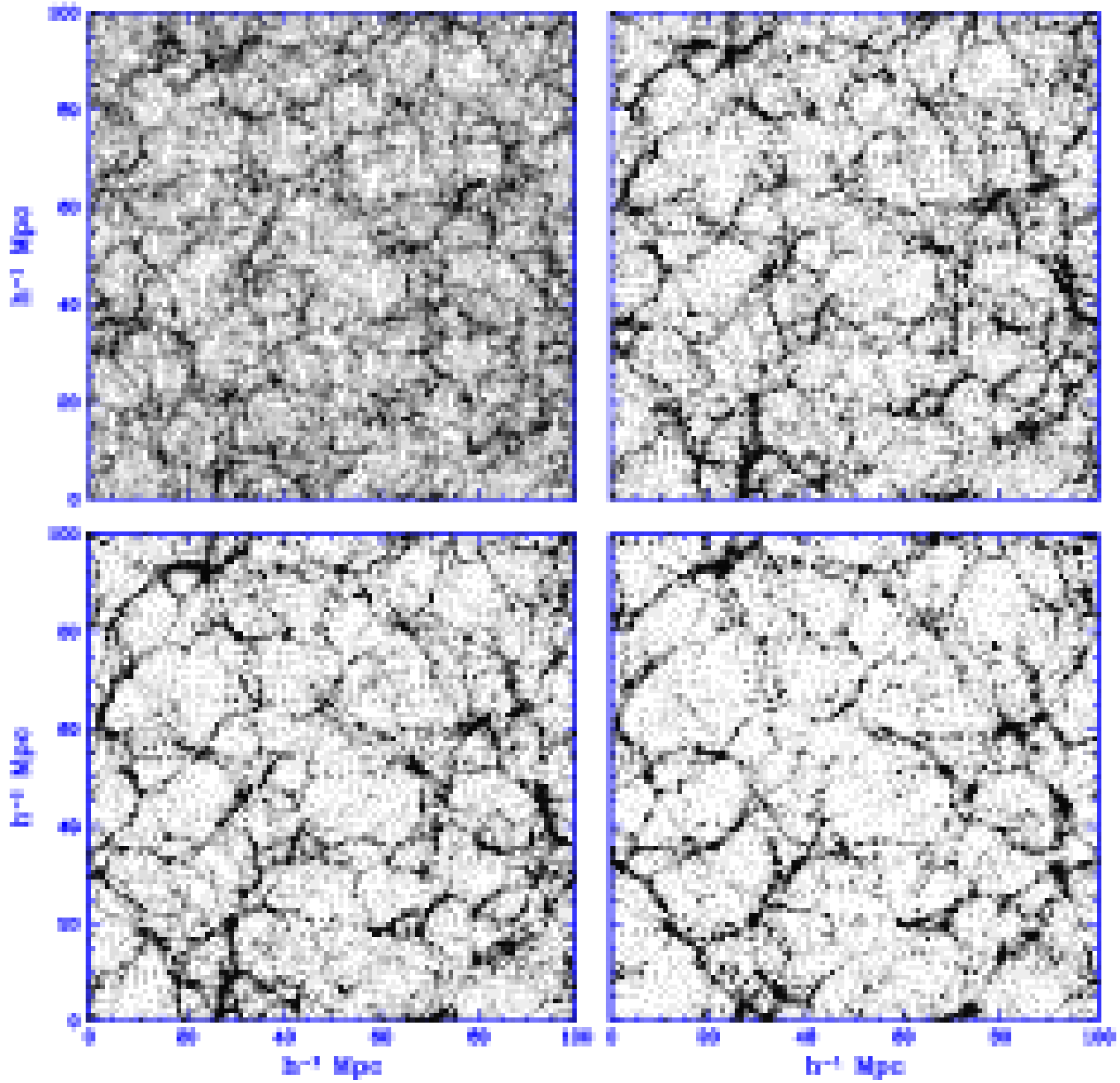
h^{-1} Mpc
h^{-1} Mpc
h^{-1} Mpc
h^{-1} Mpc

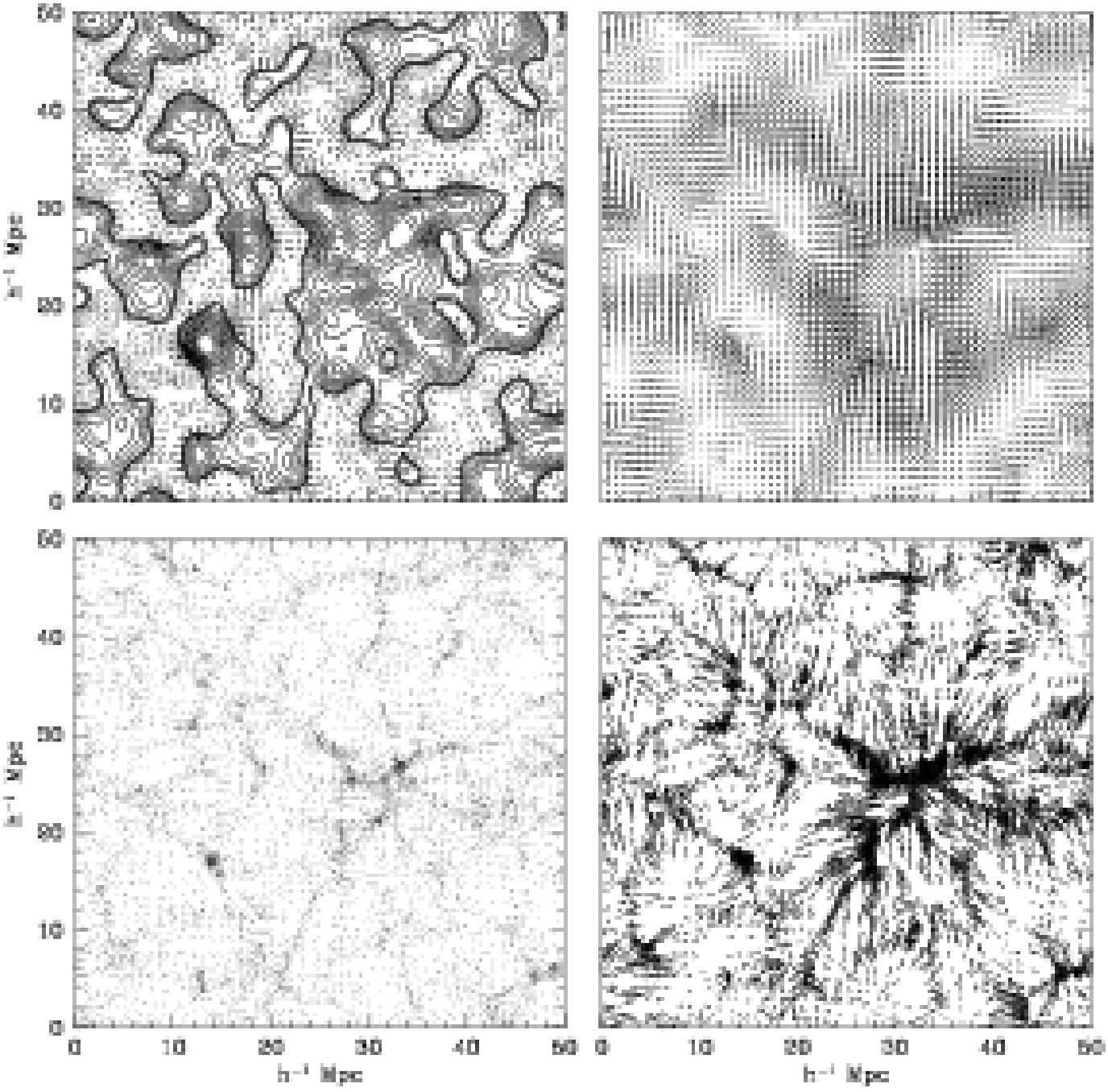
0
10
20
30
40
50
h⁻¹ Mpc
h⁻¹ Mpc

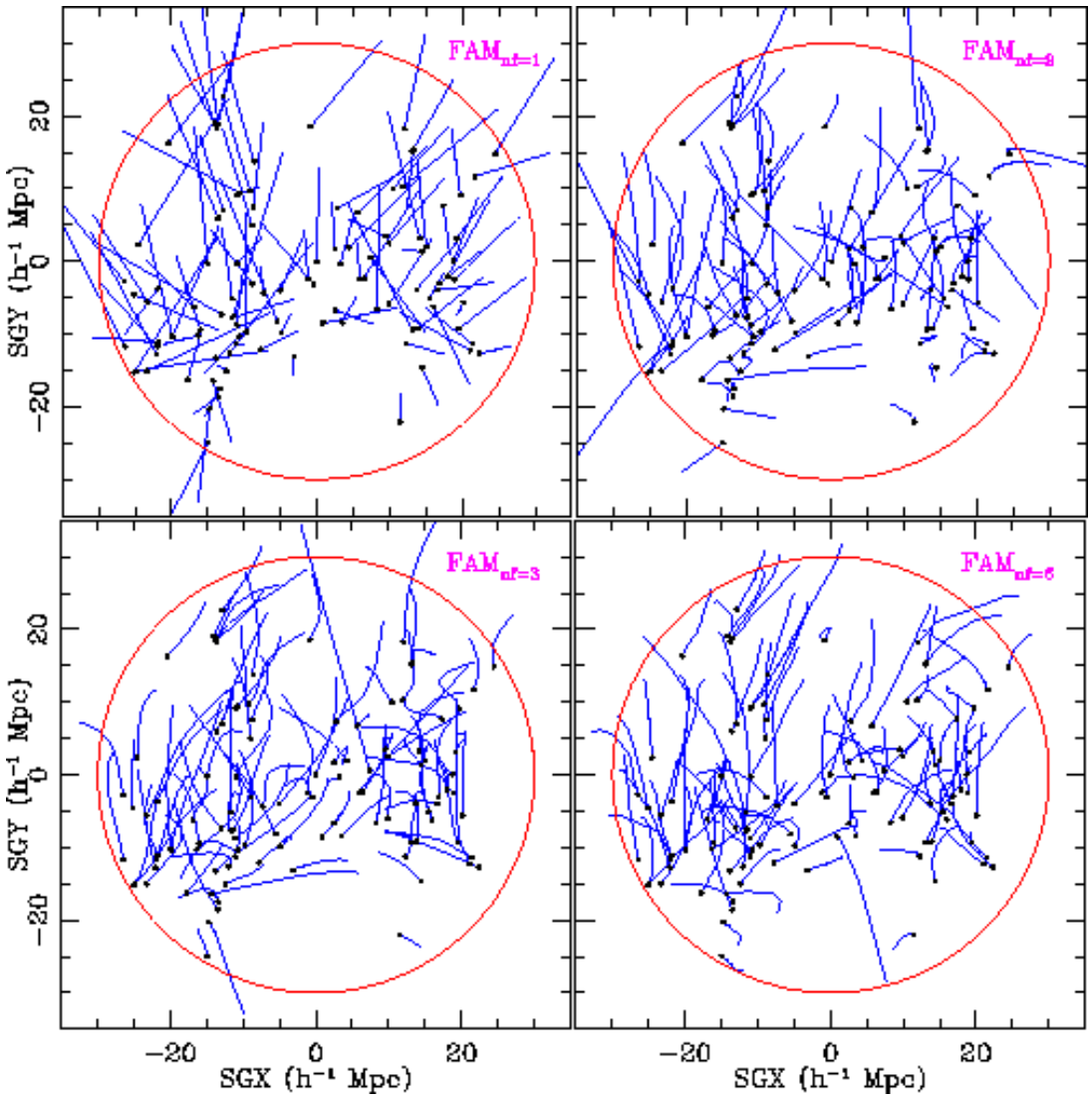
FAM$_{nf=1}$
FAM$_{nf=2}$
FAM$_{nf=3}$
FAM$_{nf=6}$
SGY (h^{-1} Mpc)
SGX (h^{-1} Mpc)
20
0
−20

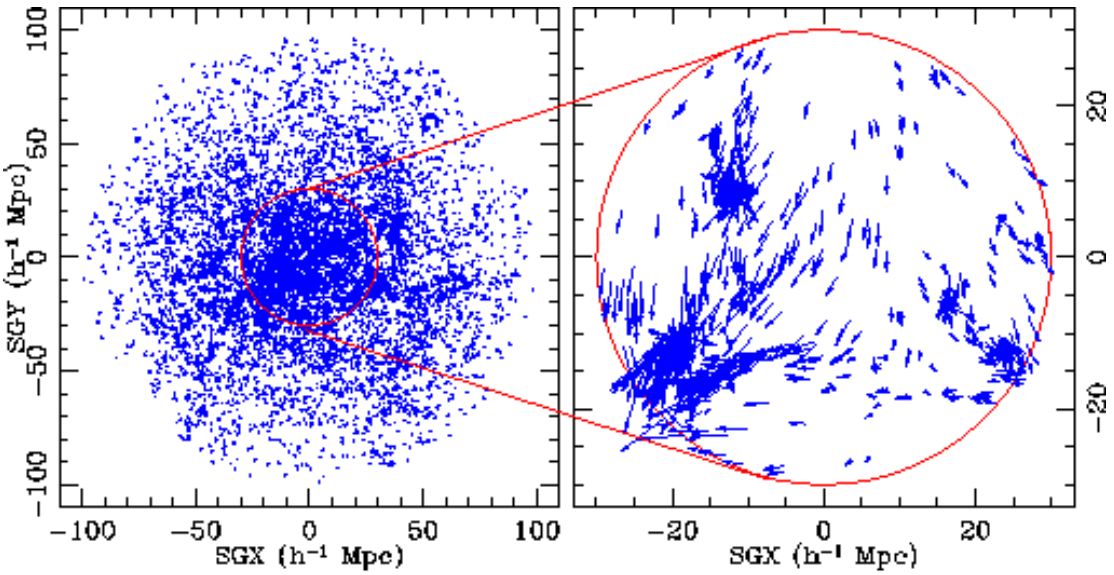
SGY (h^{-1} Mpc)
SGX (h^{-1} Mpc)
SGX (h^{-1} Mpc)

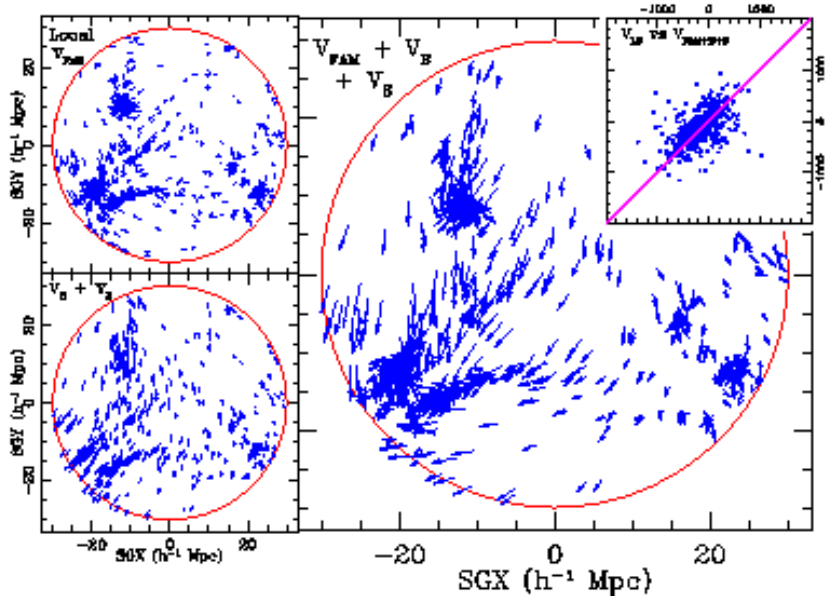
Local
V_{PAM}
V_{PAM} + V_E
+ V_S
SGX (h^{-1} Mpc)

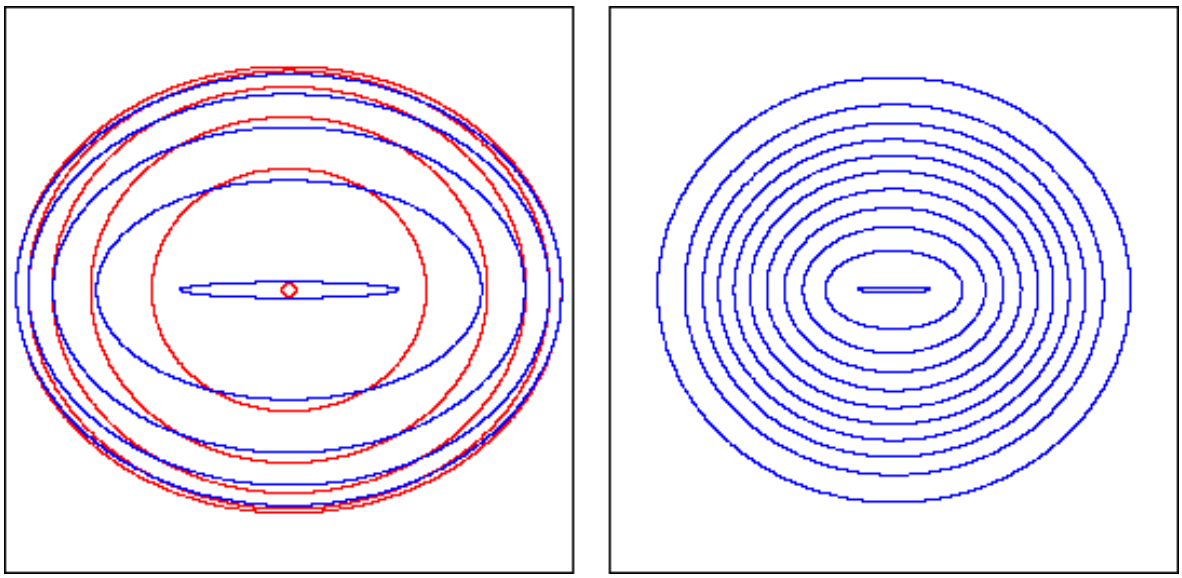

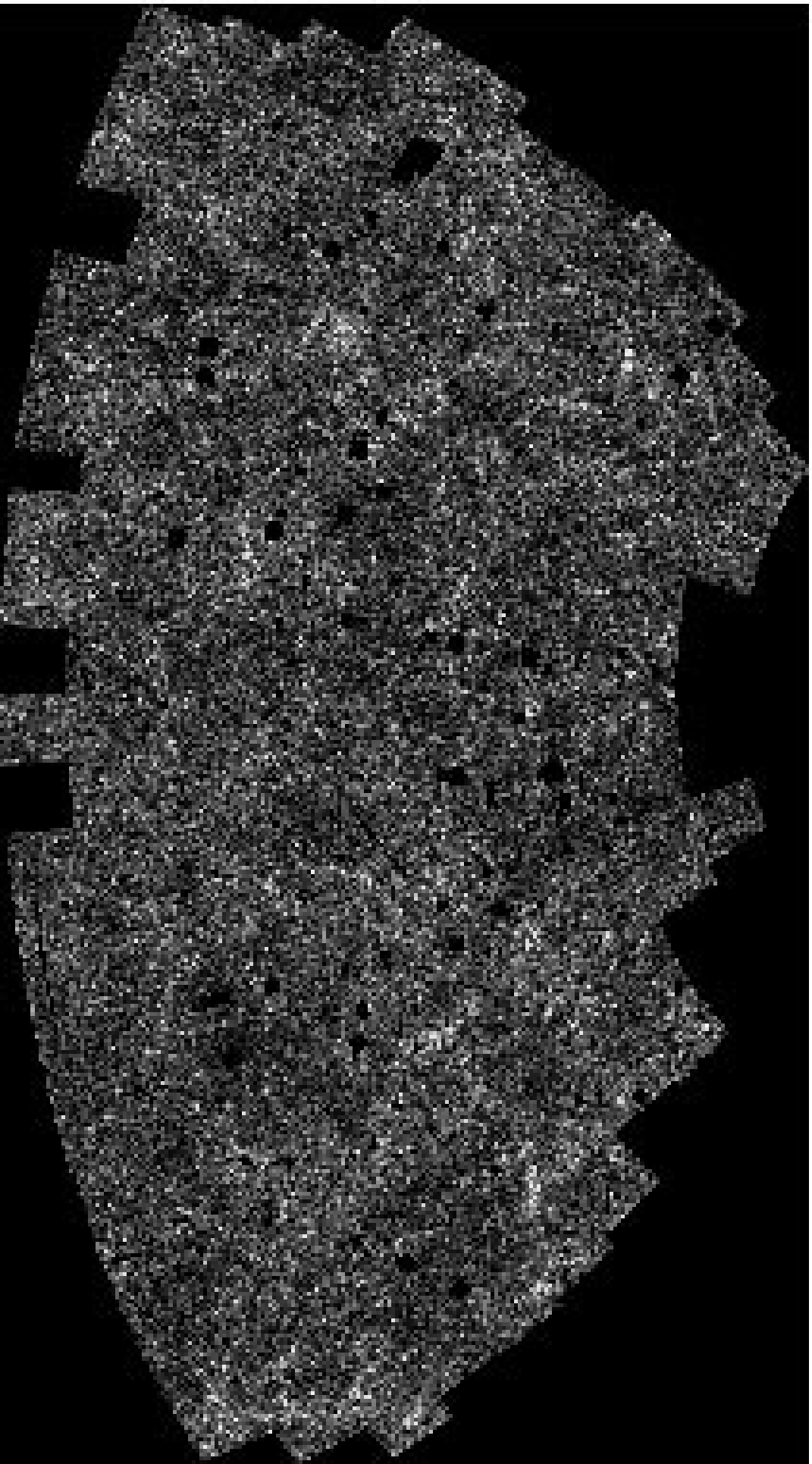

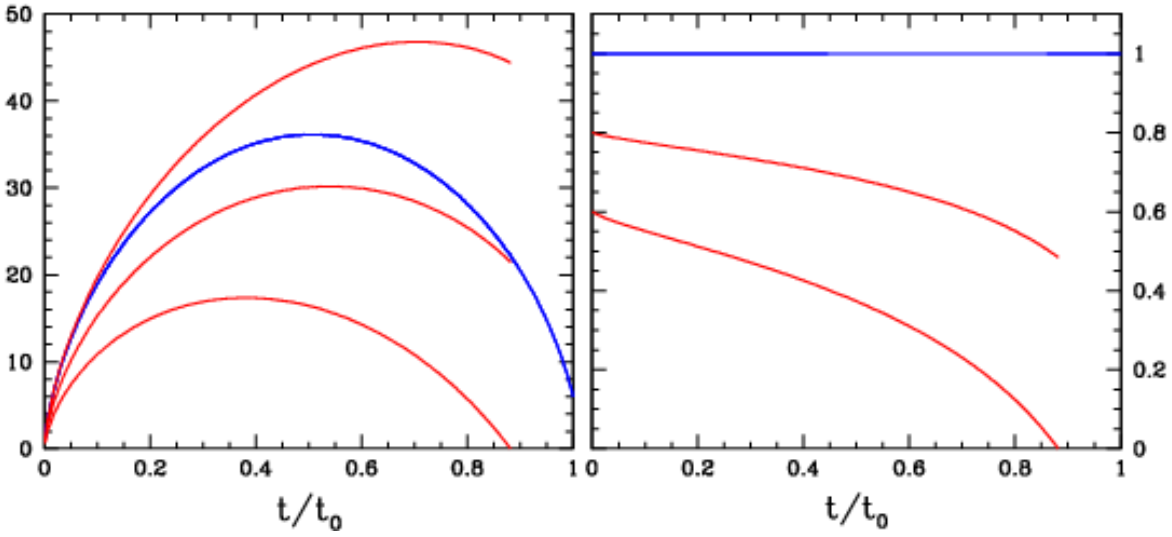
50
40
30
20
10
0
0
0.2
0.4
0.6
0.8
1
t/t0
1
0.8
0.6
0.4
0.2
0
0
0.2
0.4
0.6
0.8
1
t/t0

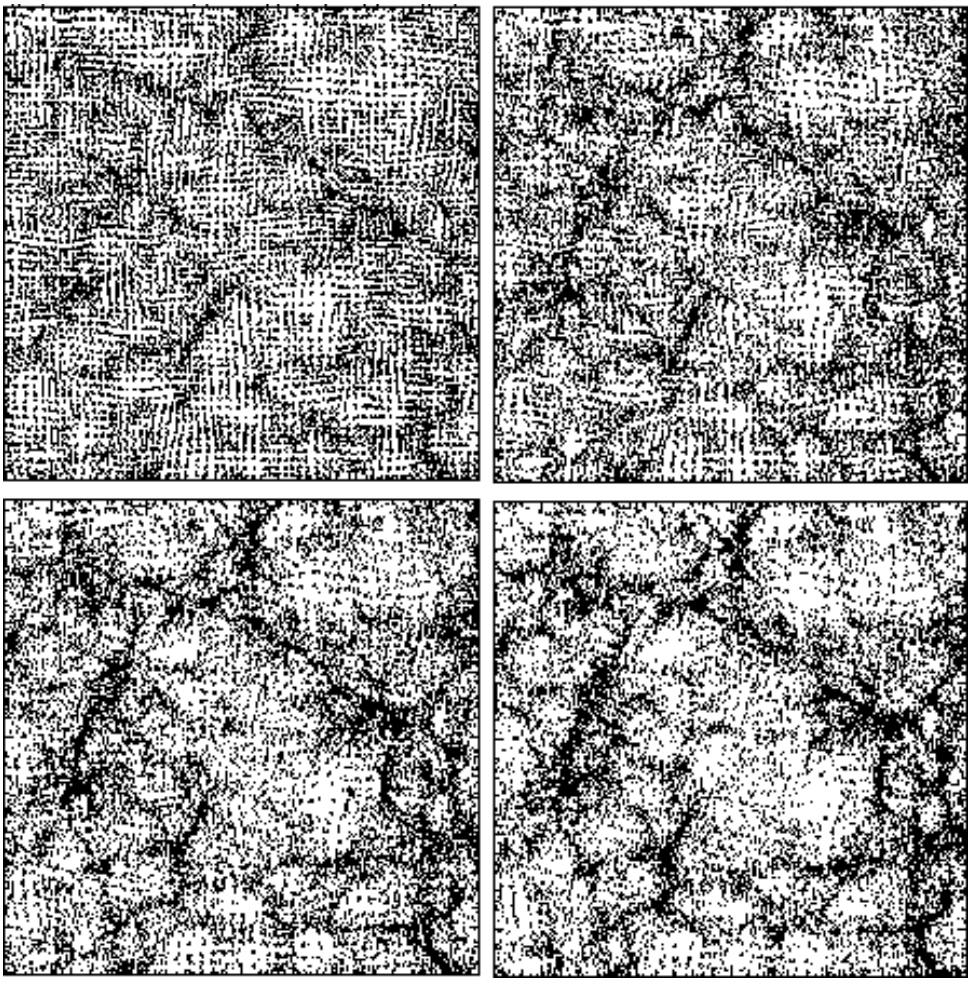

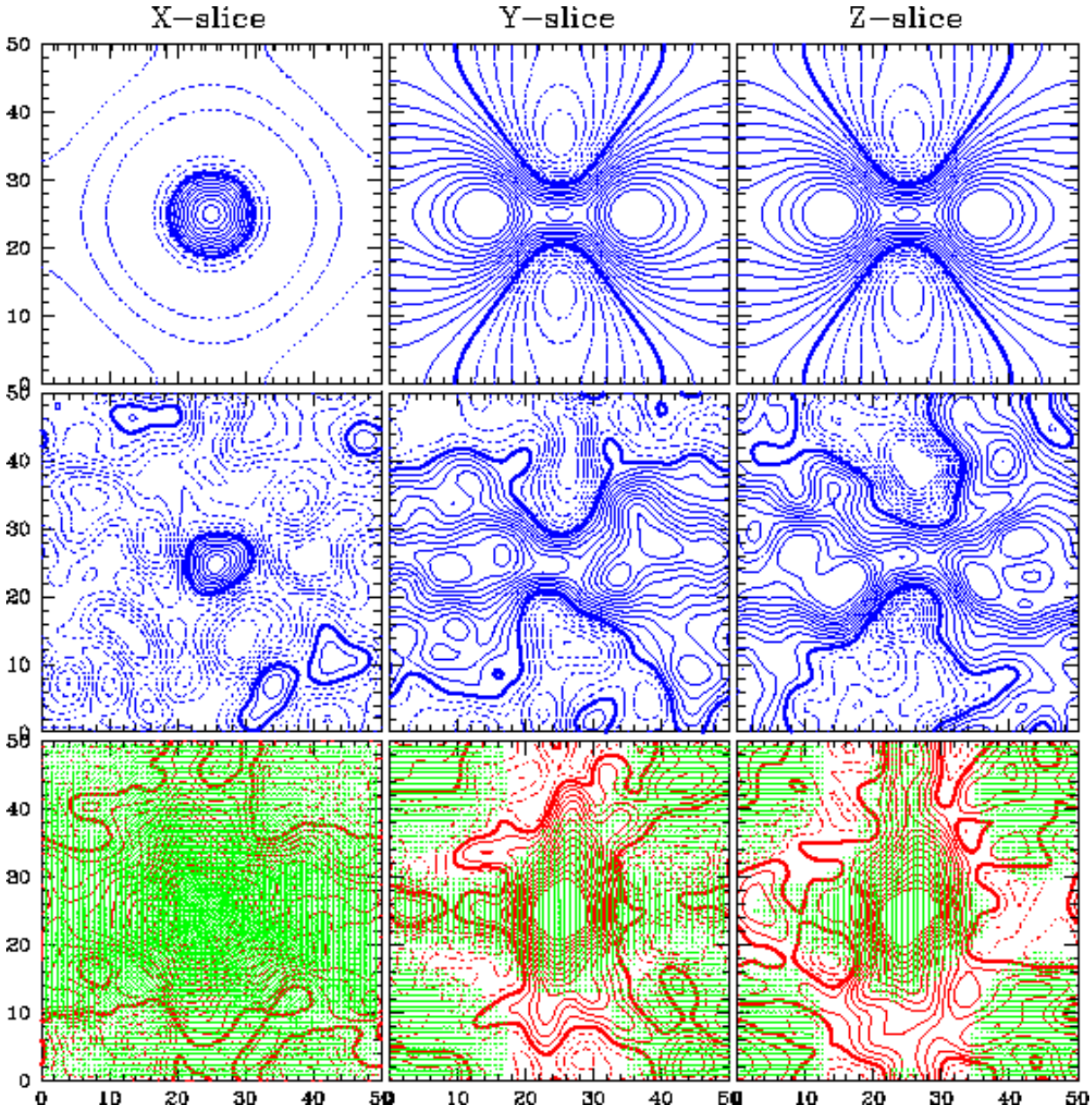
X−slice
Y−slice
Z−slice
0
10
20
30
40
50

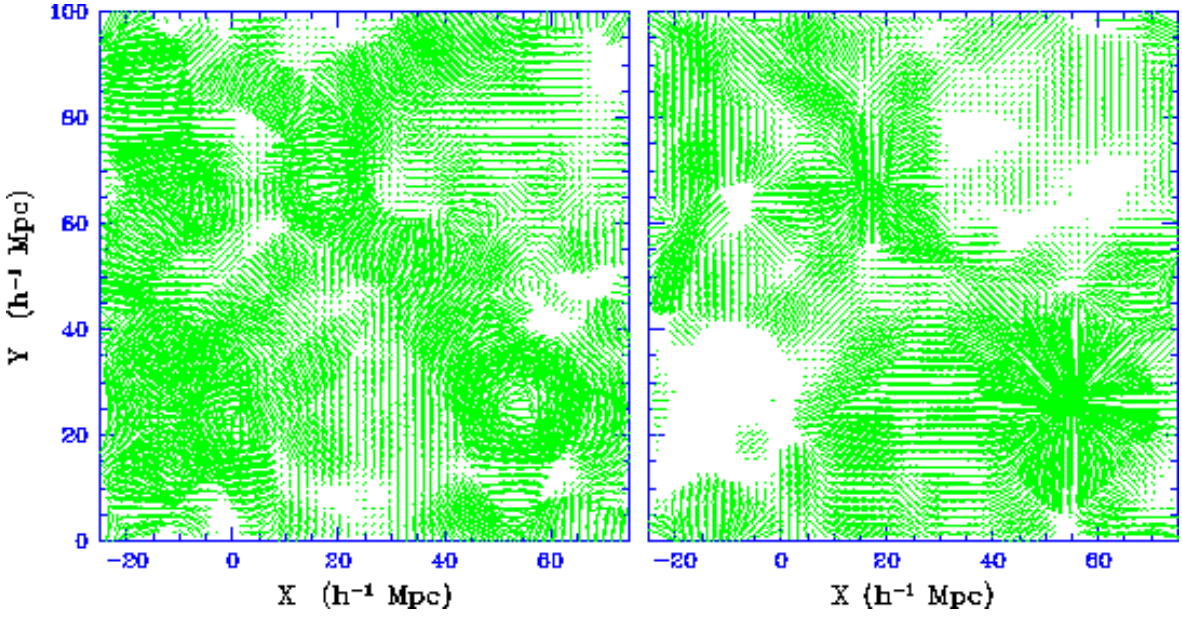
100
80
60
40
20
0
Y (h⁻¹ Mpc)
−20
0
20
40
60
X (h⁻¹ Mpc)
−20
0
20
40
60
X (h⁻¹ Mpc)

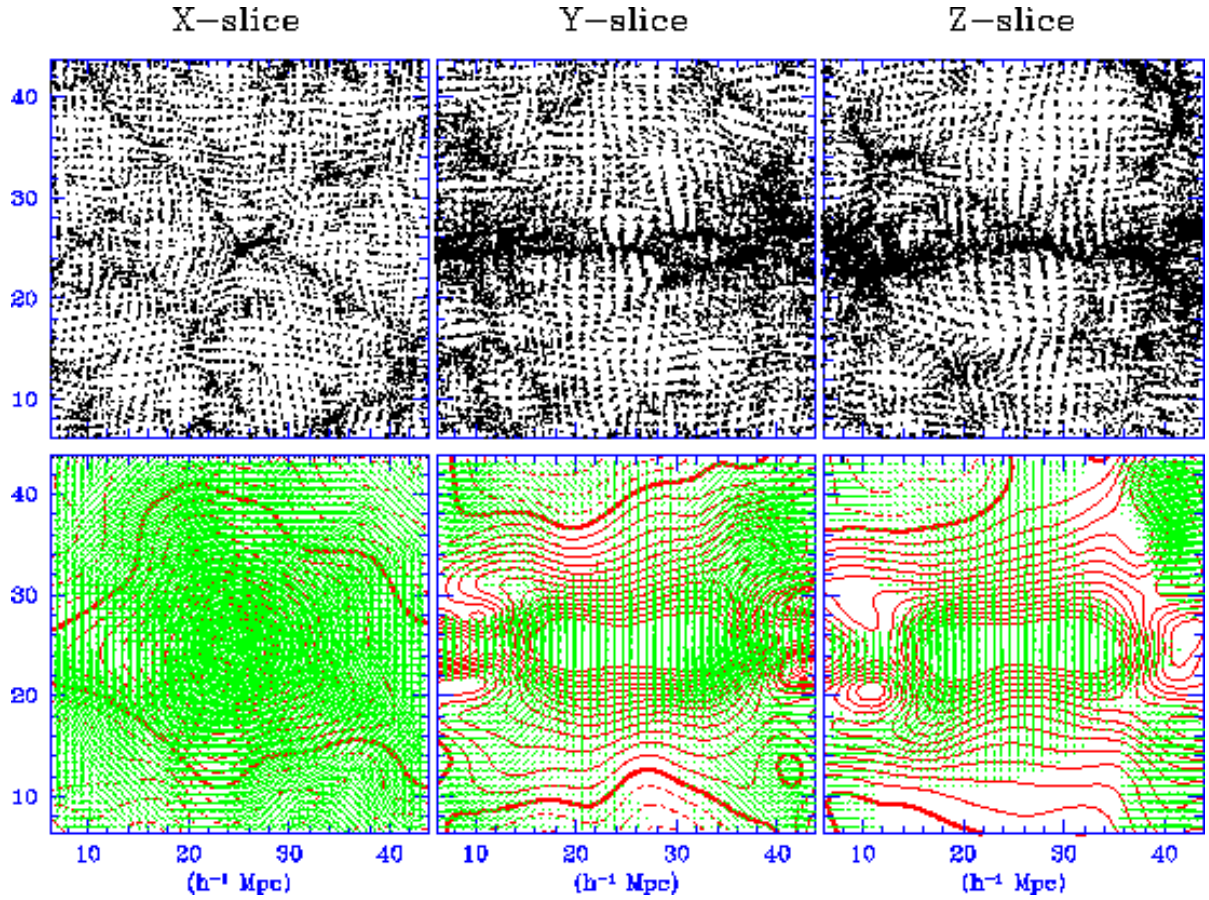
X−slice
Y−slice
Z−slice
40
30
20
10
10
20
30
40
(h⁻¹ Mpc)

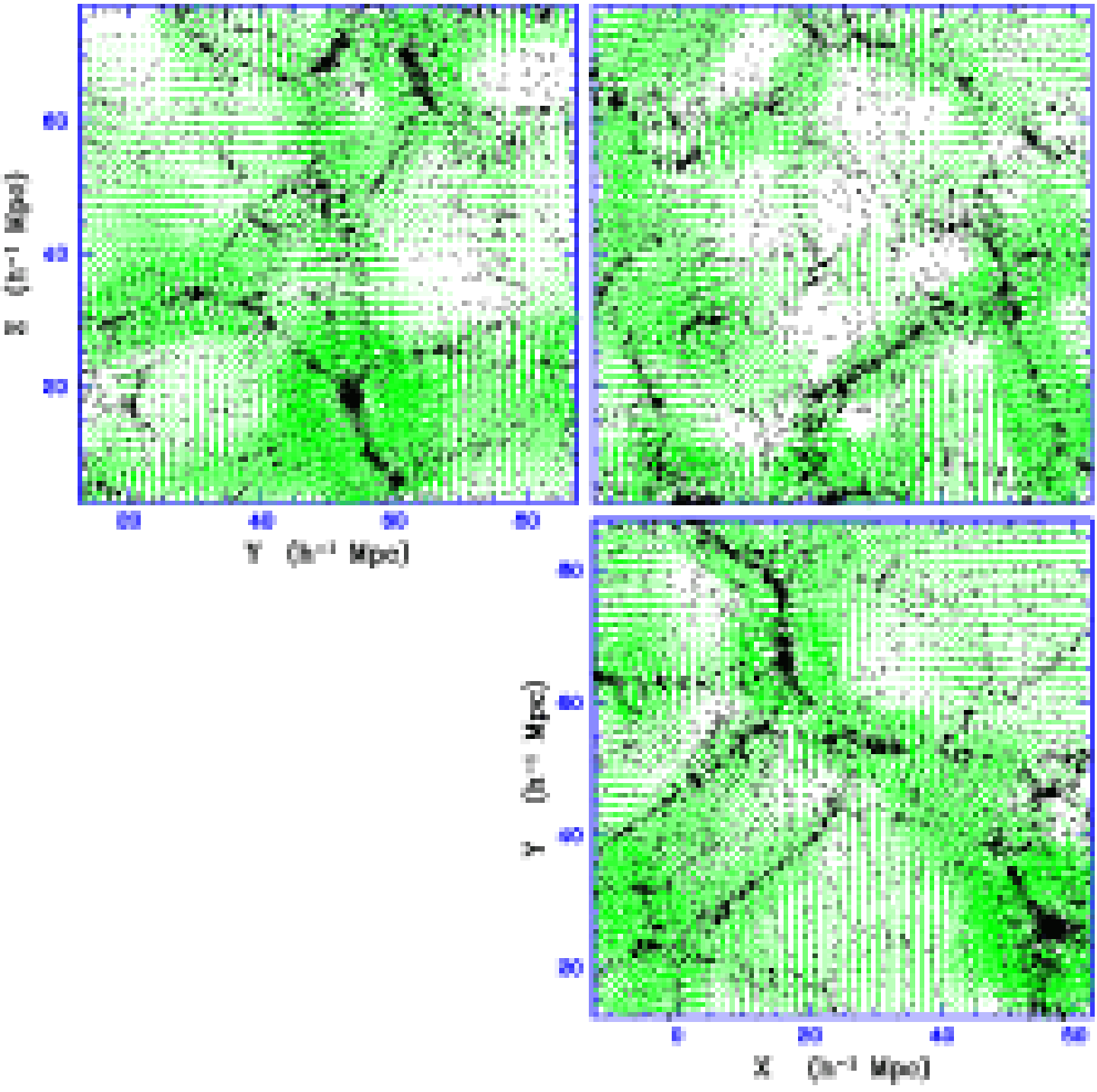
Z (h⁻¹ Mpc)
Y (h⁻¹ Mpc)
X (h⁻¹ Mpc)

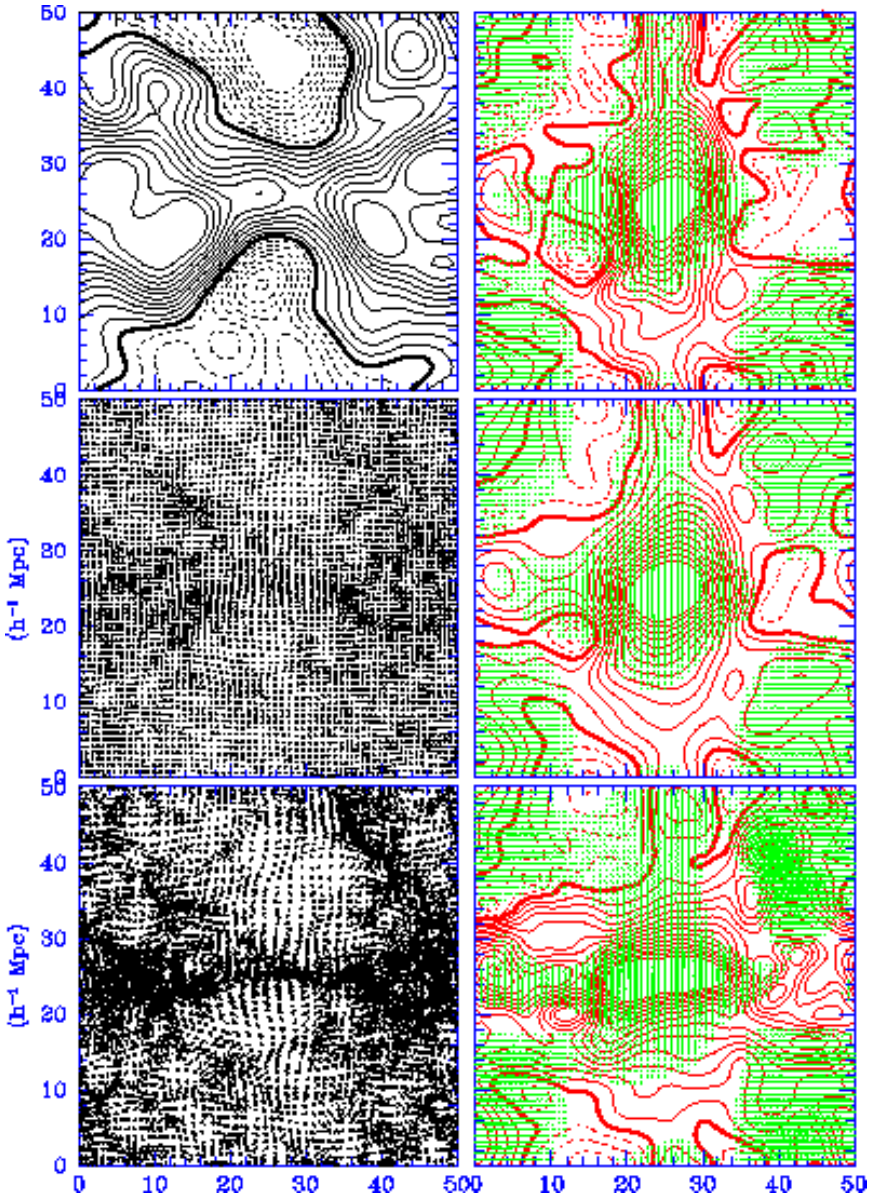
0
10
20
30
40
50
(h⁻¹ Mpc)
(h⁻¹ Mpc)

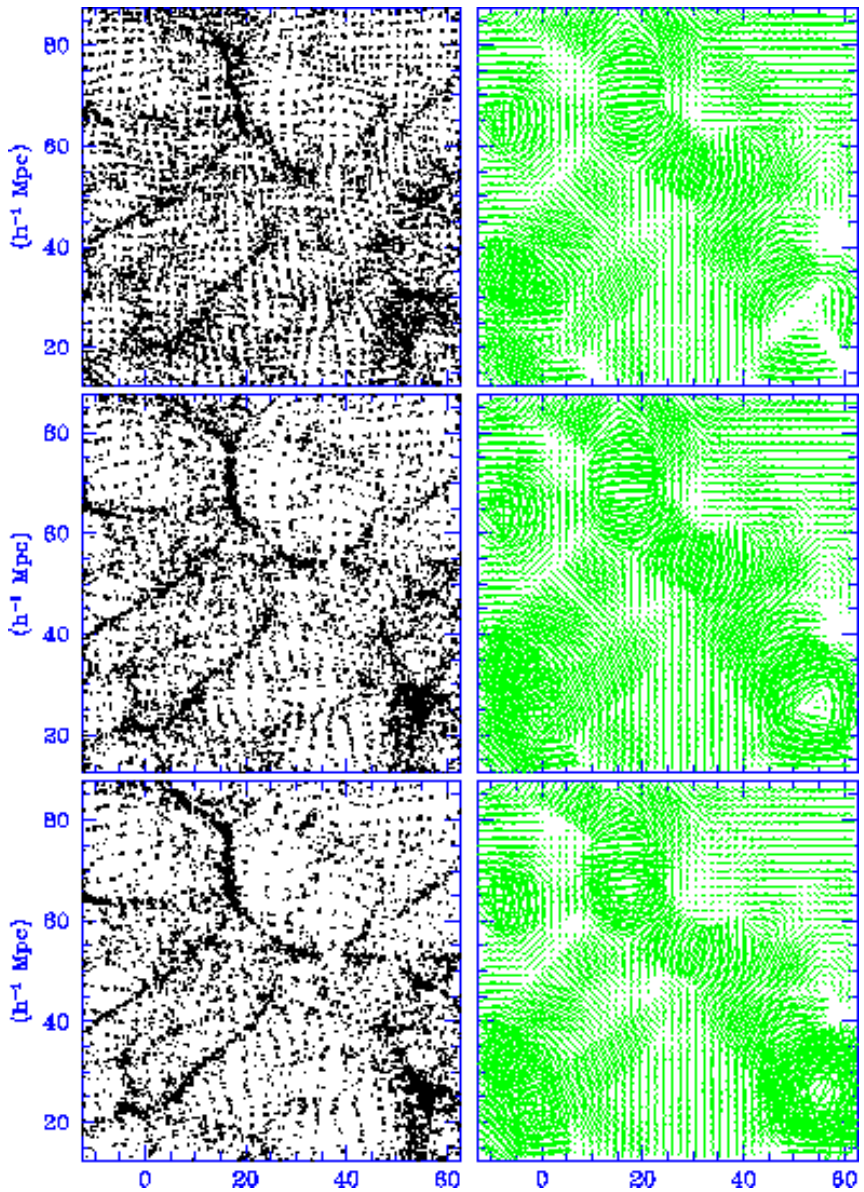
80
60
40
20
(h⁻¹ Mpc)
0
20
40
60

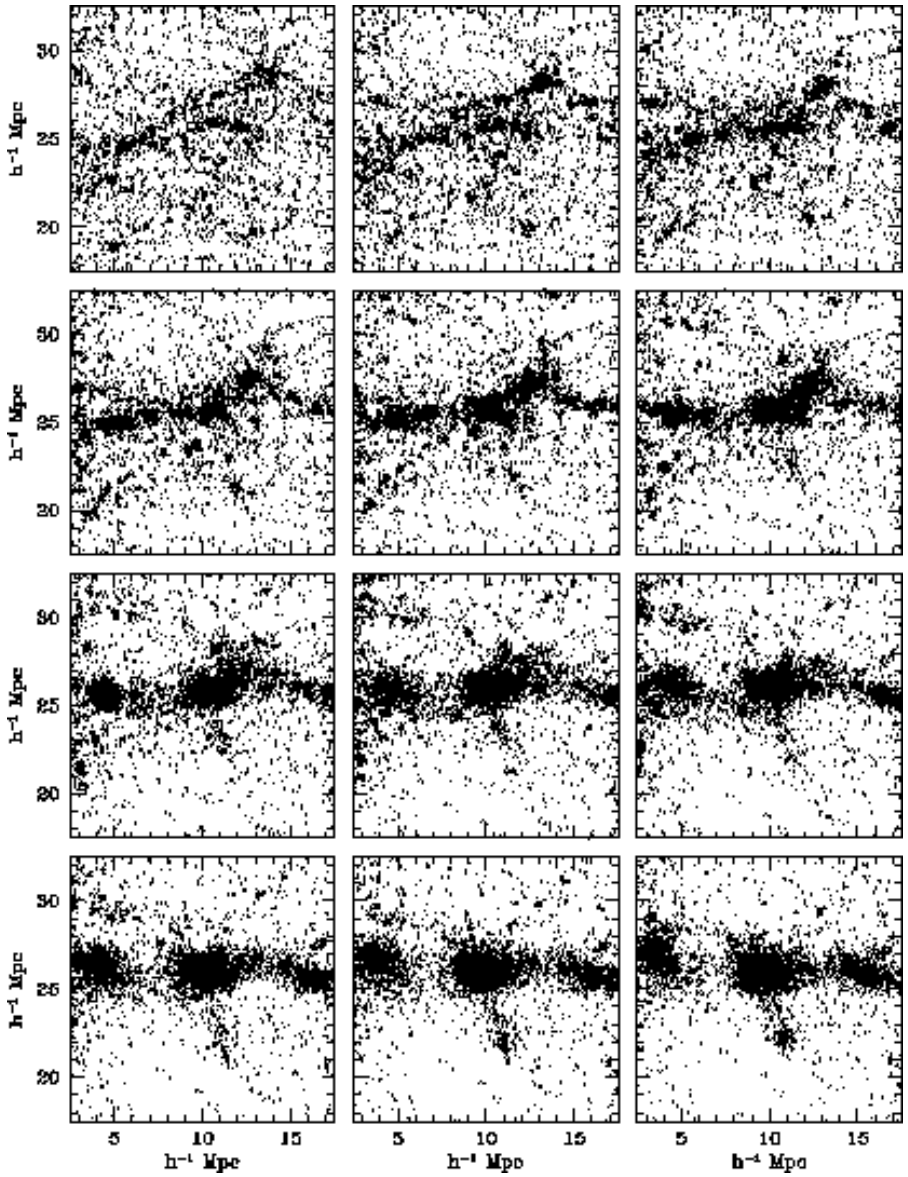
h⁻¹ Mpc
20
25
30
5
10
15
h⁻¹ Mpc

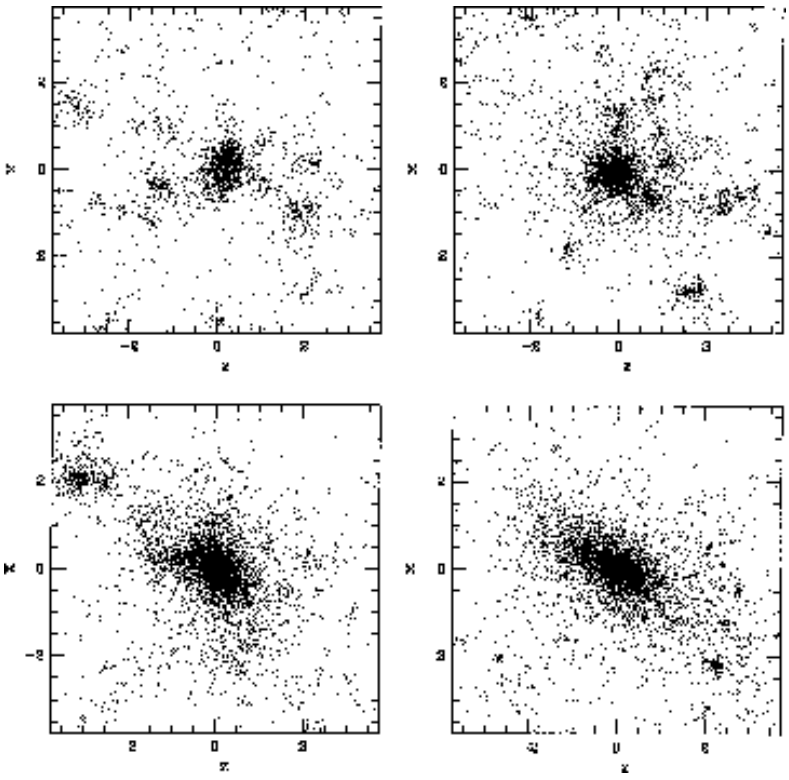

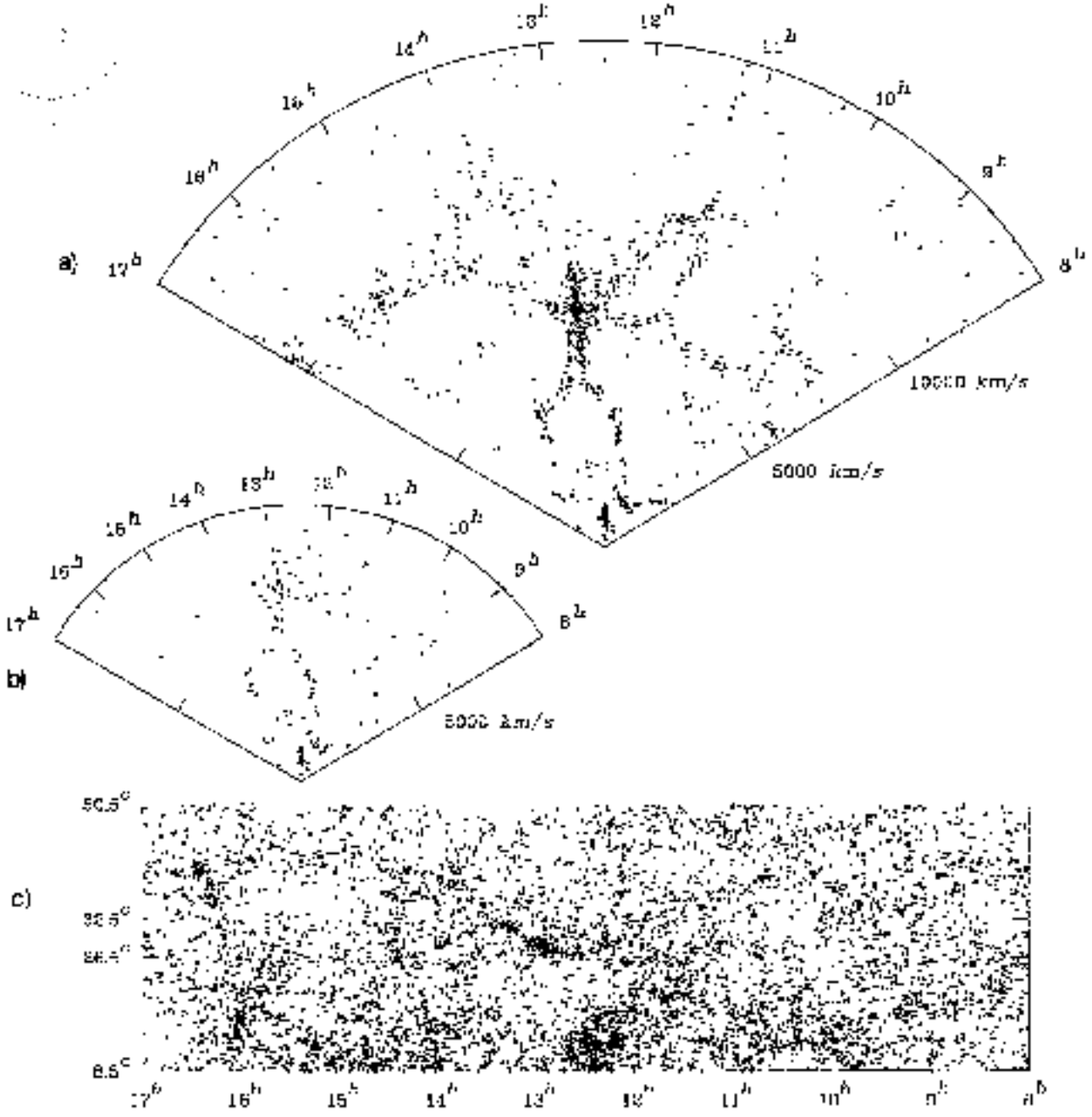
a)
b)
c)
10000 km/s
5000 km/s
5000 km/s

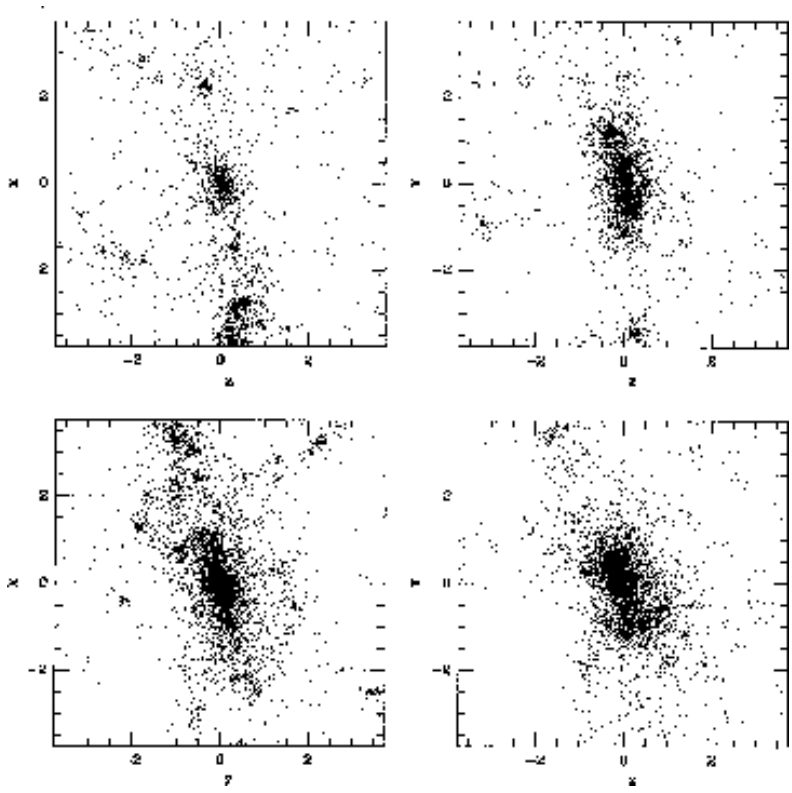
x
z
y
z
x
y

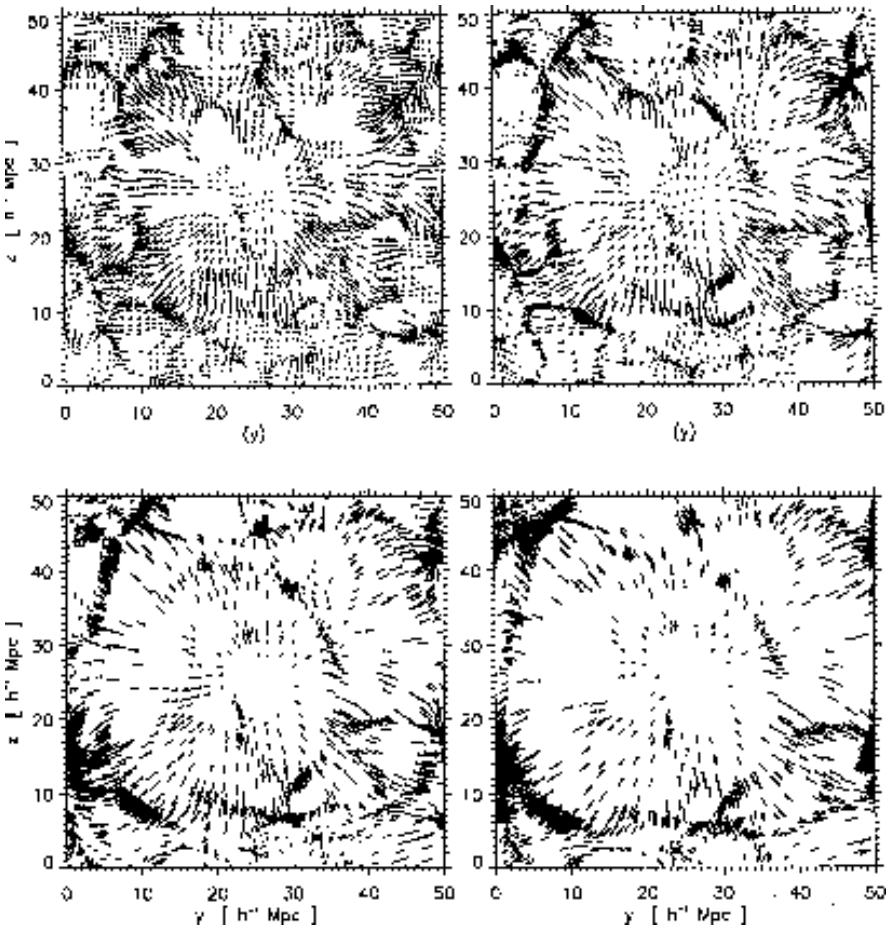
z [h⁻¹ Mpc]
(y)
(y)
z [h⁻¹ Mpc]
y [h⁻¹ Mpc]
y [h⁻¹ Mpc]

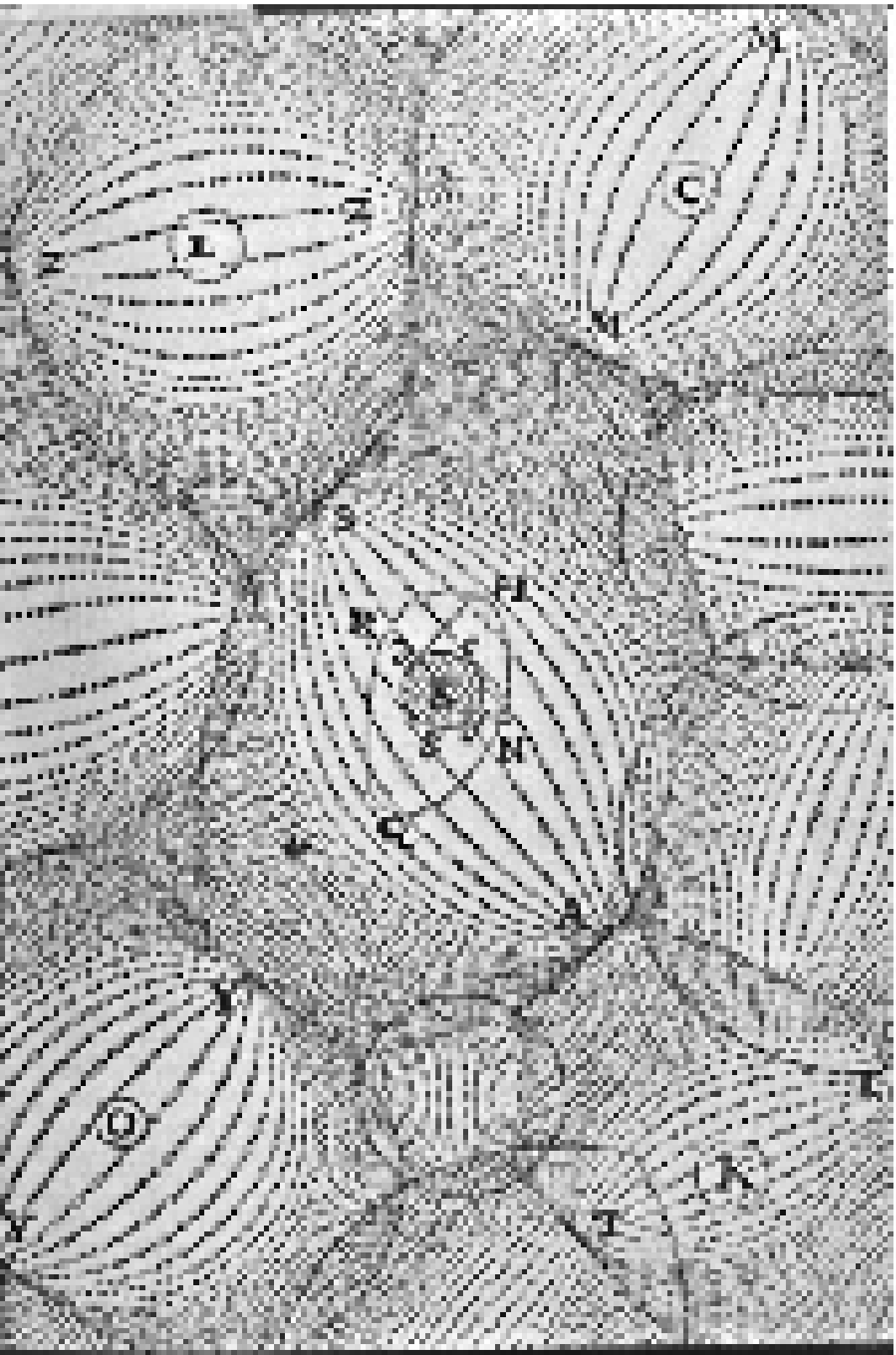
I
C
L
H
S
F
R
M
G
K
T

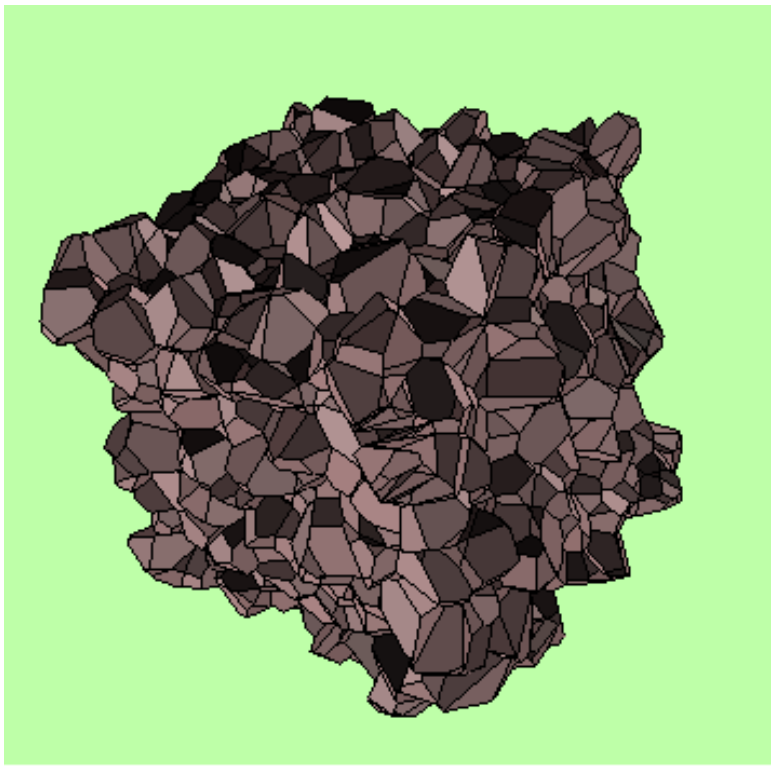

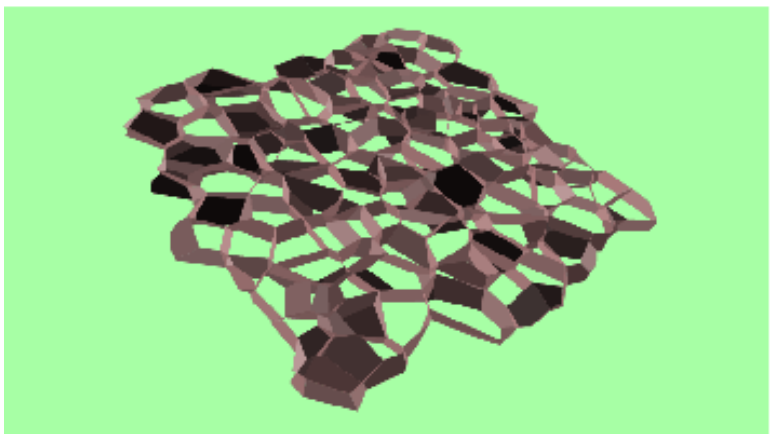

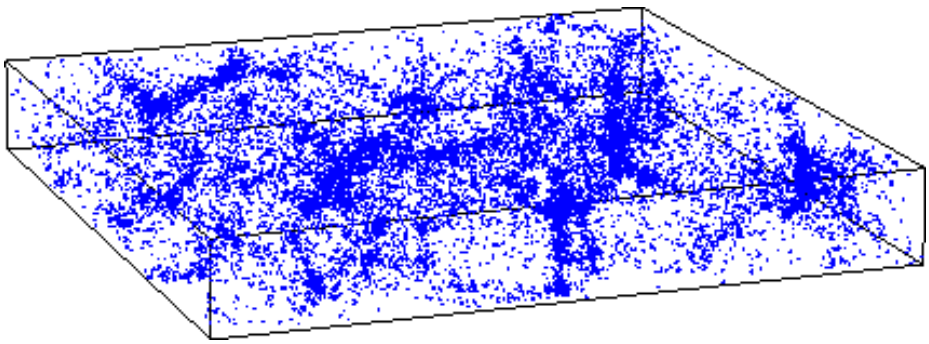

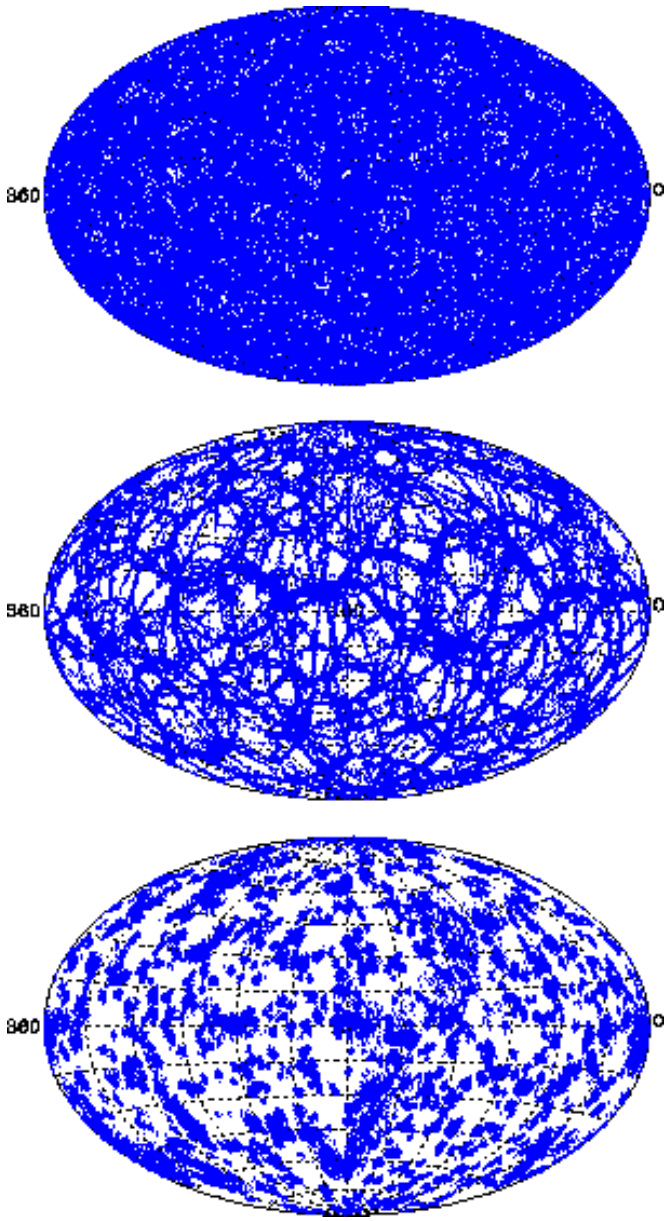
360
0
360
0
360
0

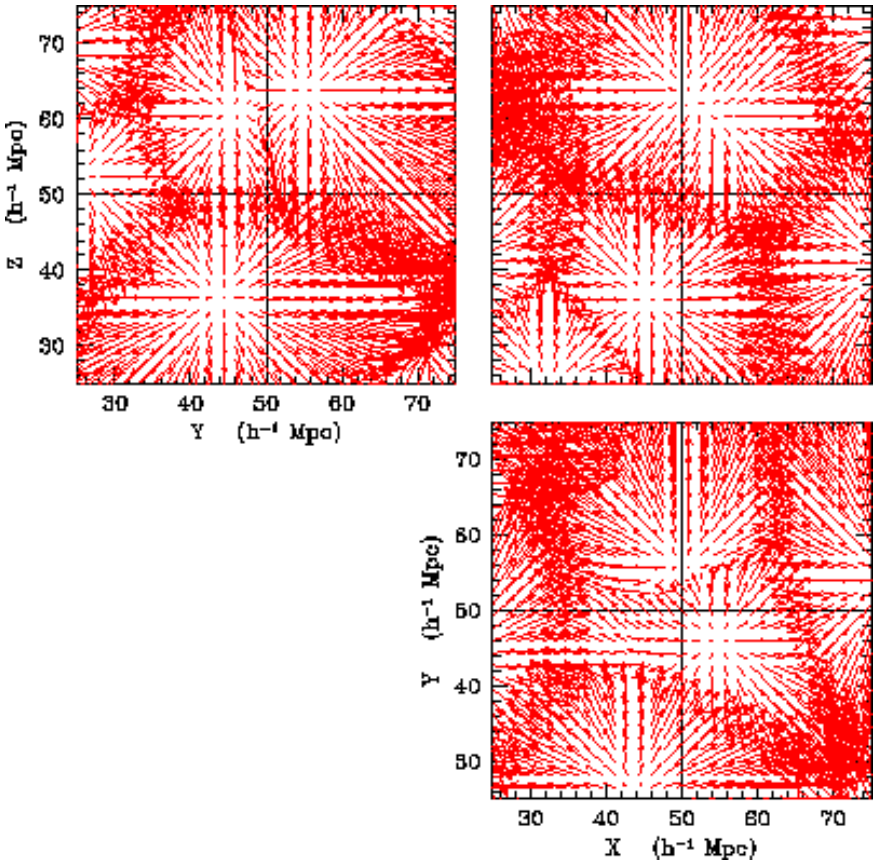
70
60
50
40
30
Z (h⁻¹ Mpc)
30
40
50
60
70
Y (h⁻¹ Mpc)
70
60
50
40
30
Y (h⁻¹ Mpc)
30
40
50
60
70
X (h⁻¹ Mpc)

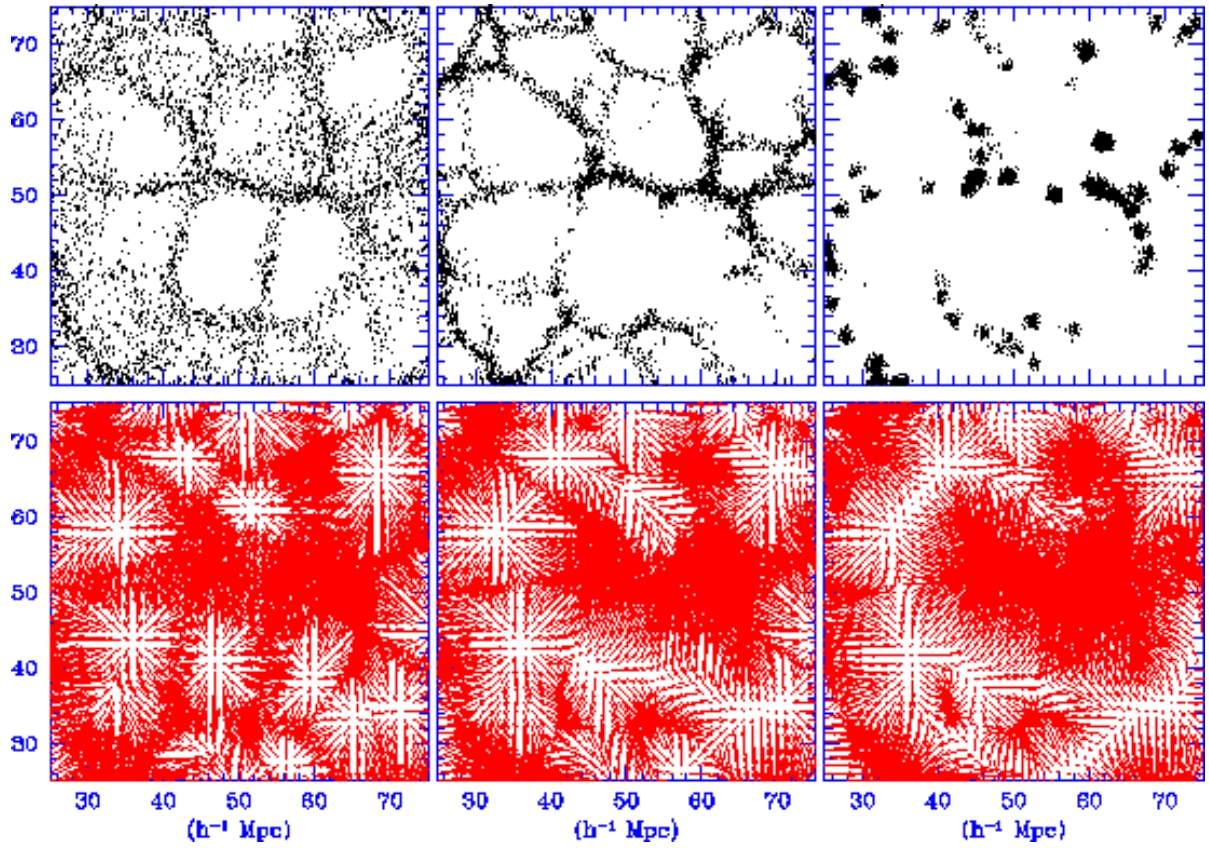
70
60
50
40
30
30
40
50
60
70
(h^{-1} Mpc)
(h^{-1} Mpc)
(h^{-1} Mpc)

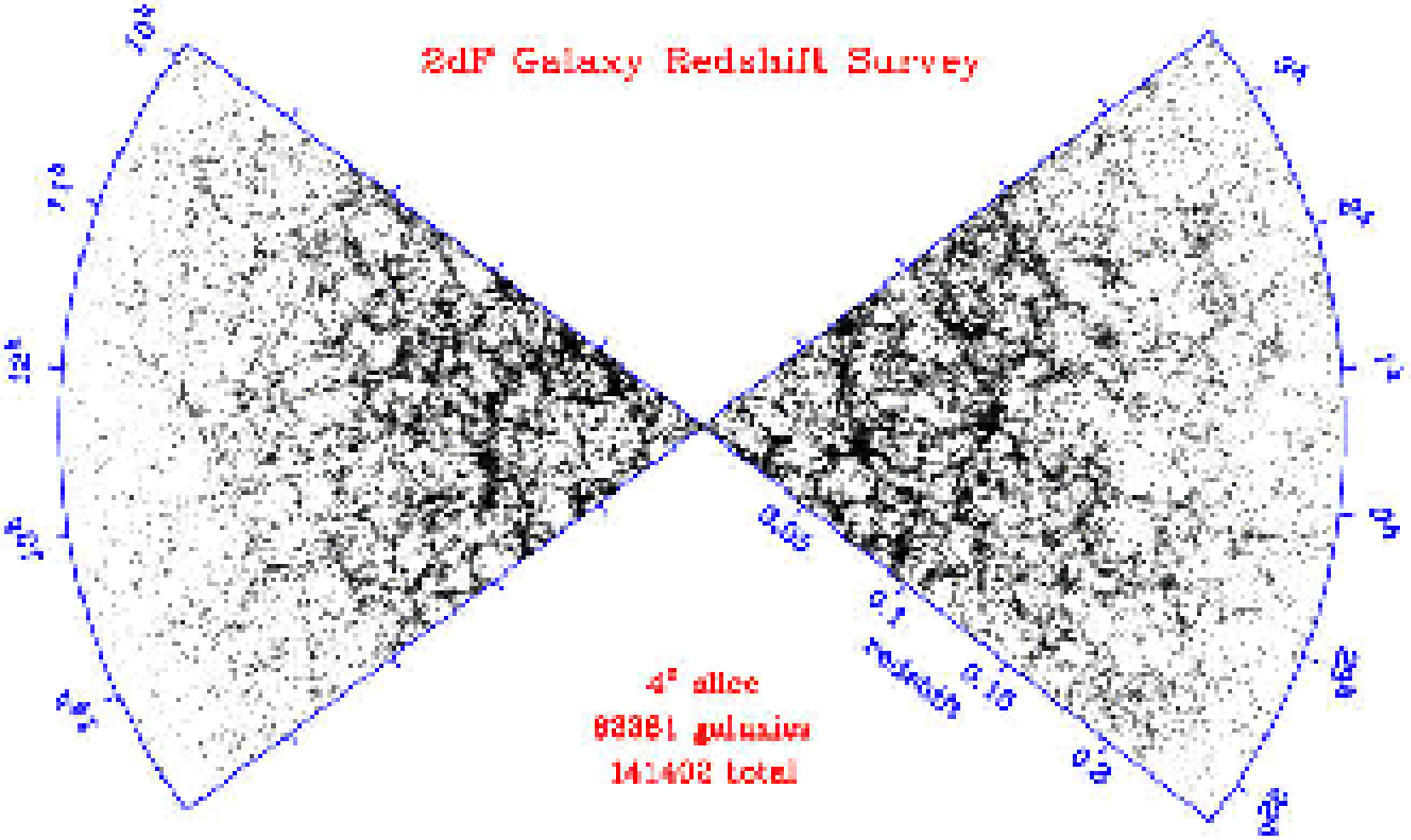
2dF Galaxy Redshift Survey
10h
8h
12h
4h
0.05
0.1
0.15
redshift
4° slice
93381 galaxies
141402 total

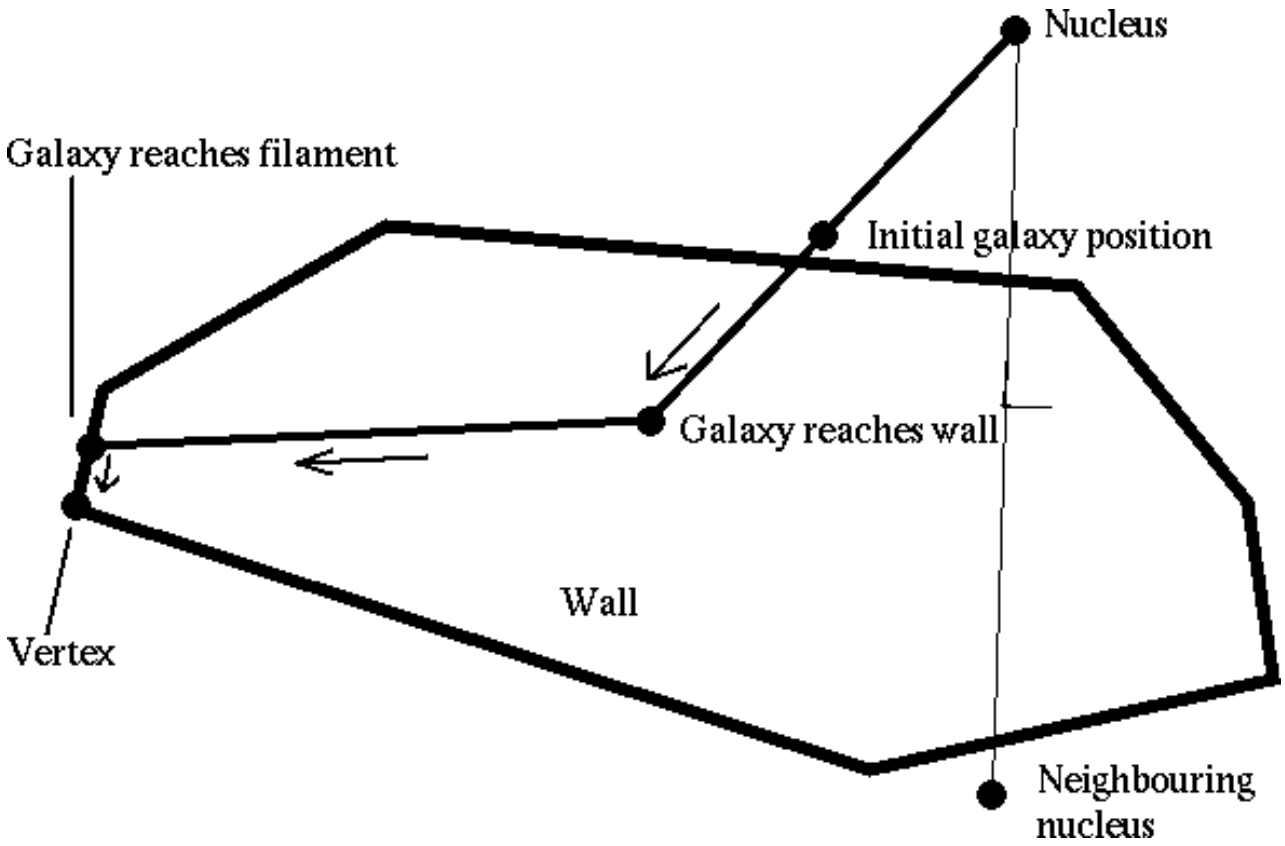
Nucleus
Galaxy reaches filament
Initial galaxy position
Galaxy reaches wall
Wall
Vertex
Neighbouring
nucleus

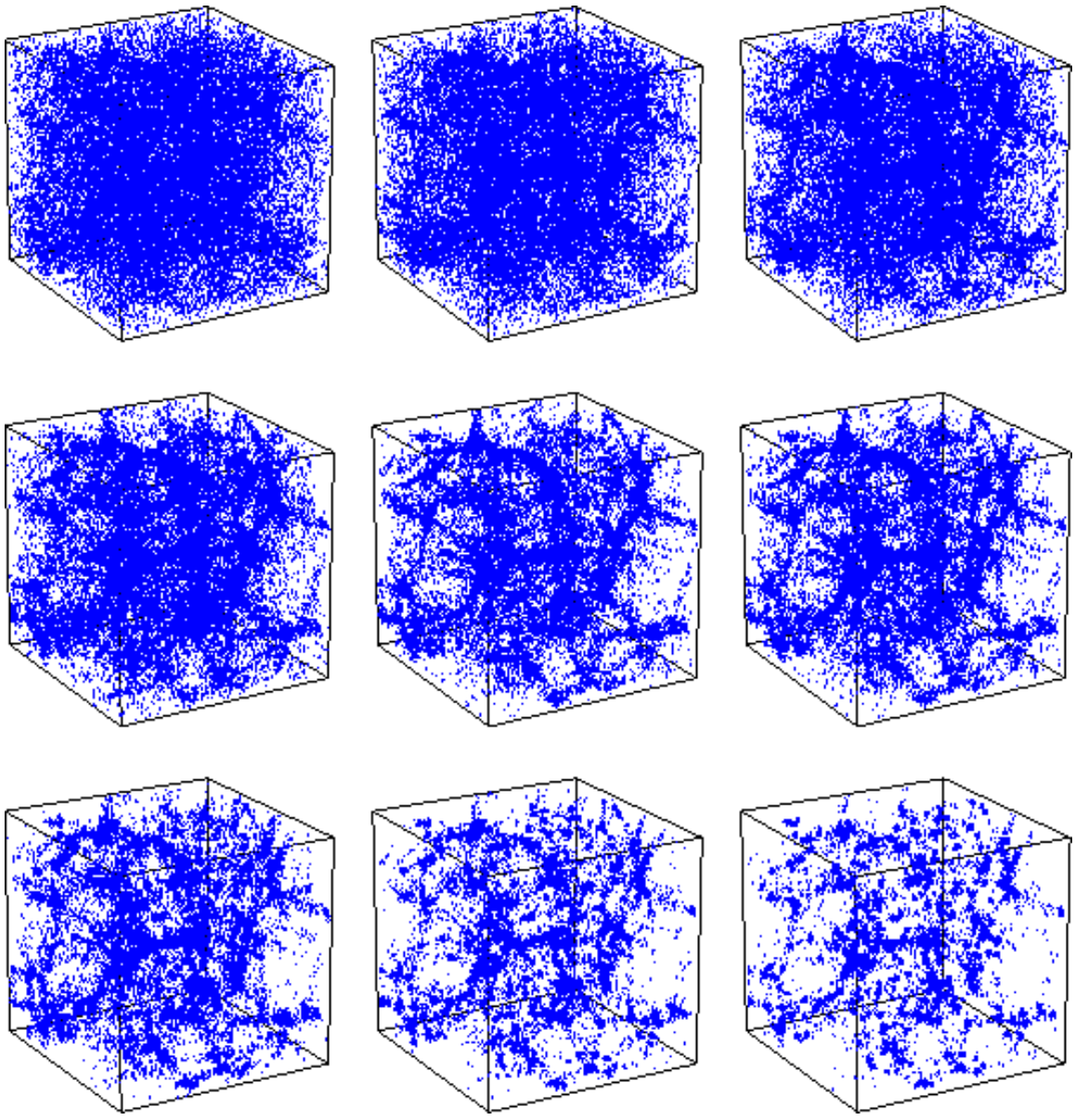

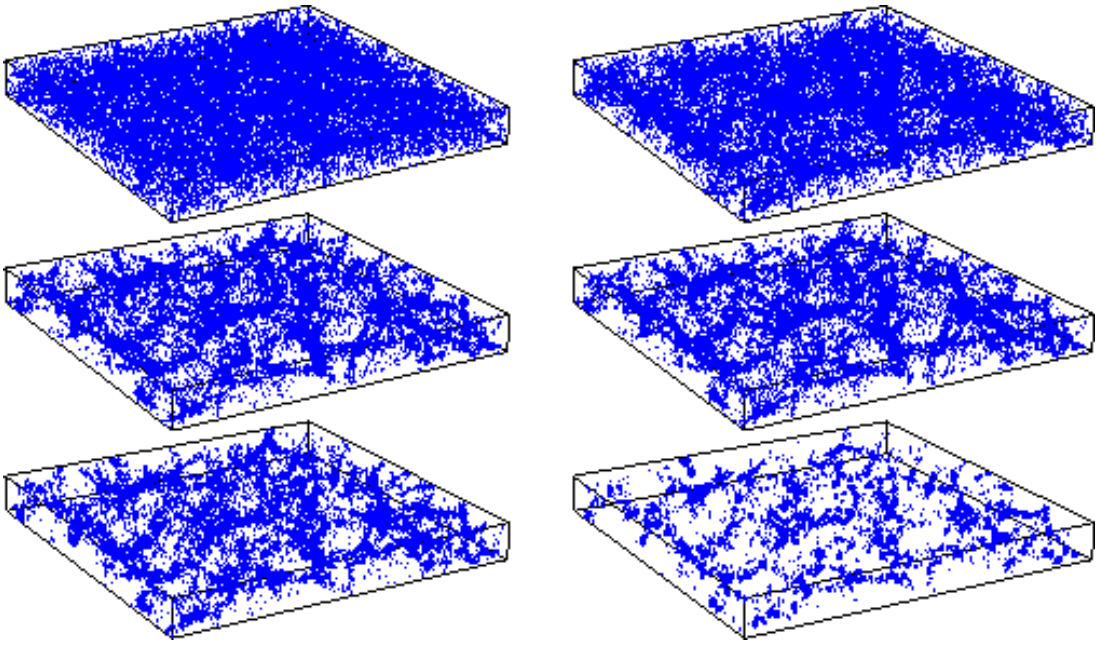

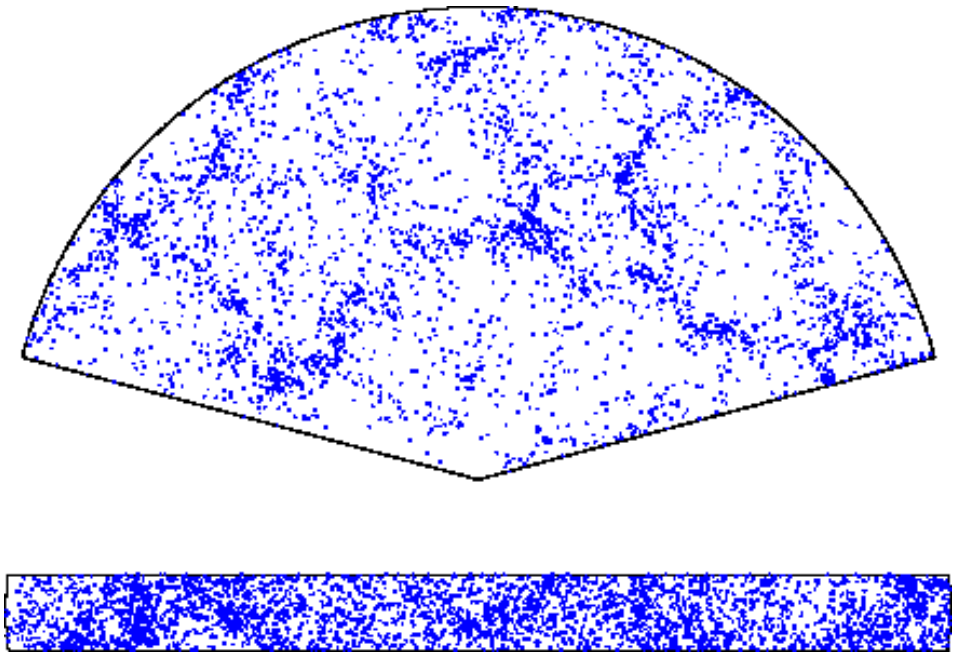

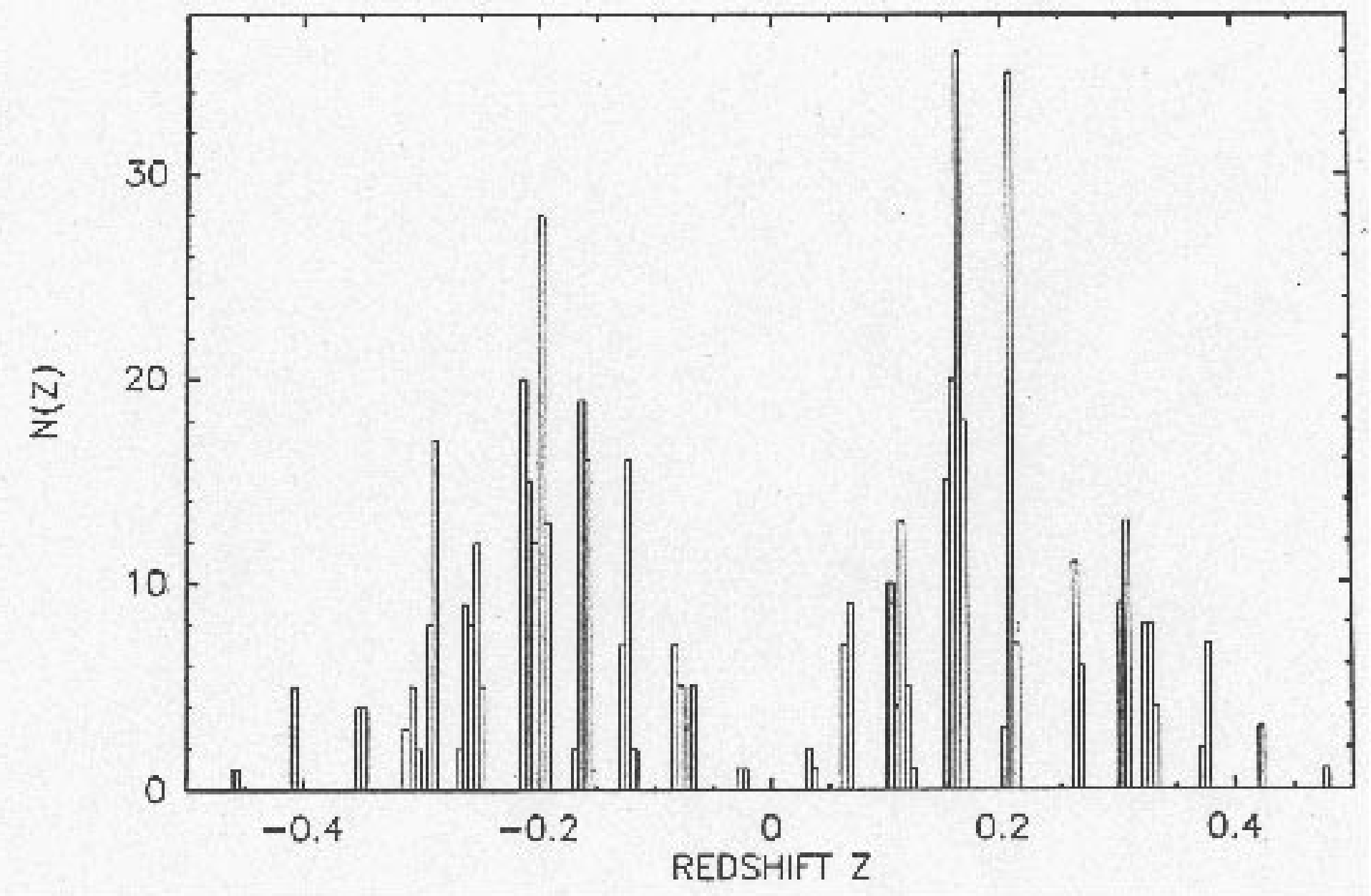
30
20
10
0
N(Z)
−0.4
−0.2
0
0.2
0.4
REDSHIFT Z

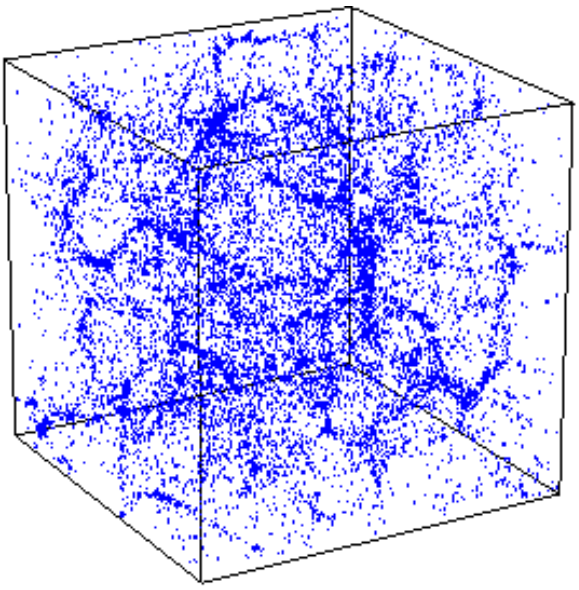

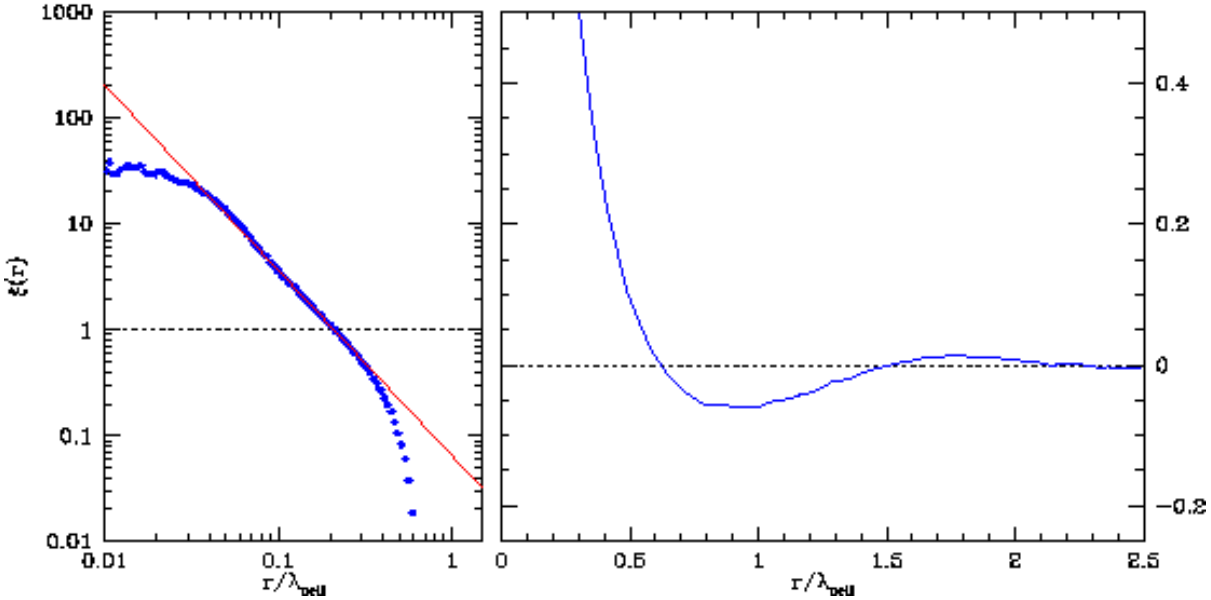
1000
100
10
1
0.1
0.01
ξ(r)
0.01
0.1
1
r/λ_pdl
0.4
0.2
0
−0.2
0
0.5
1
1.5
2
2.5
r/λ_pdl

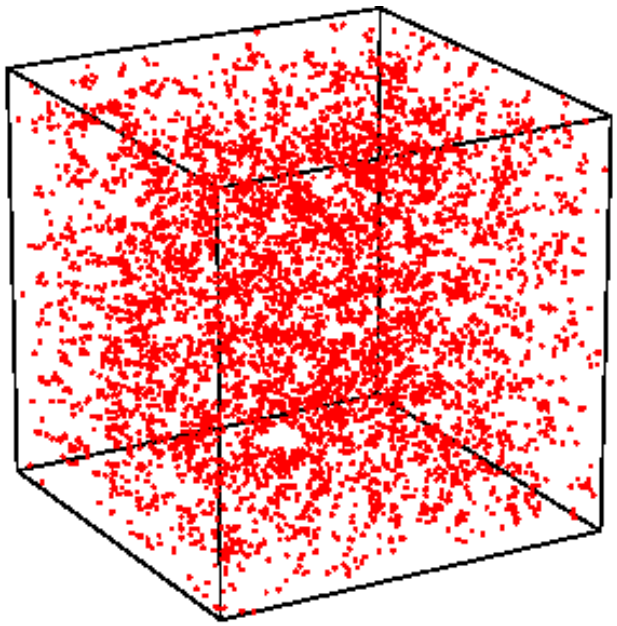

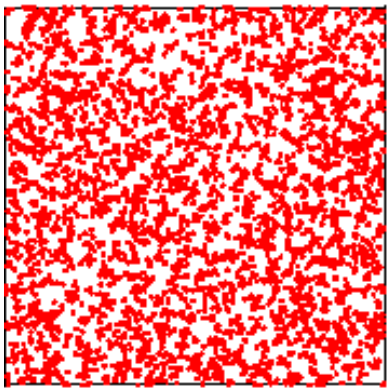

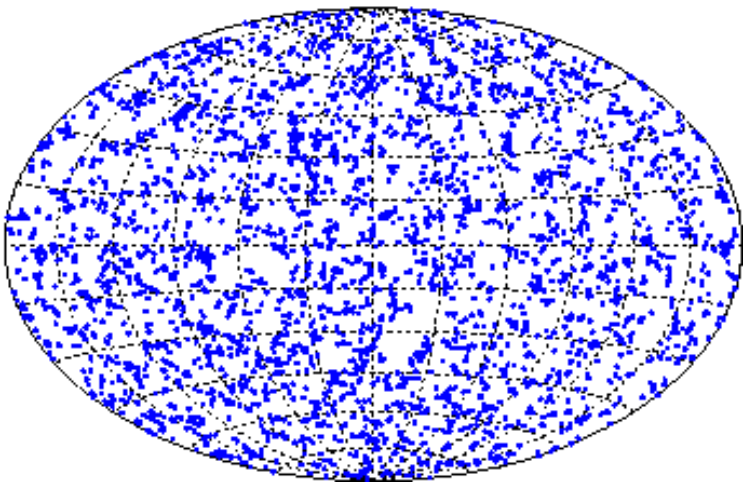

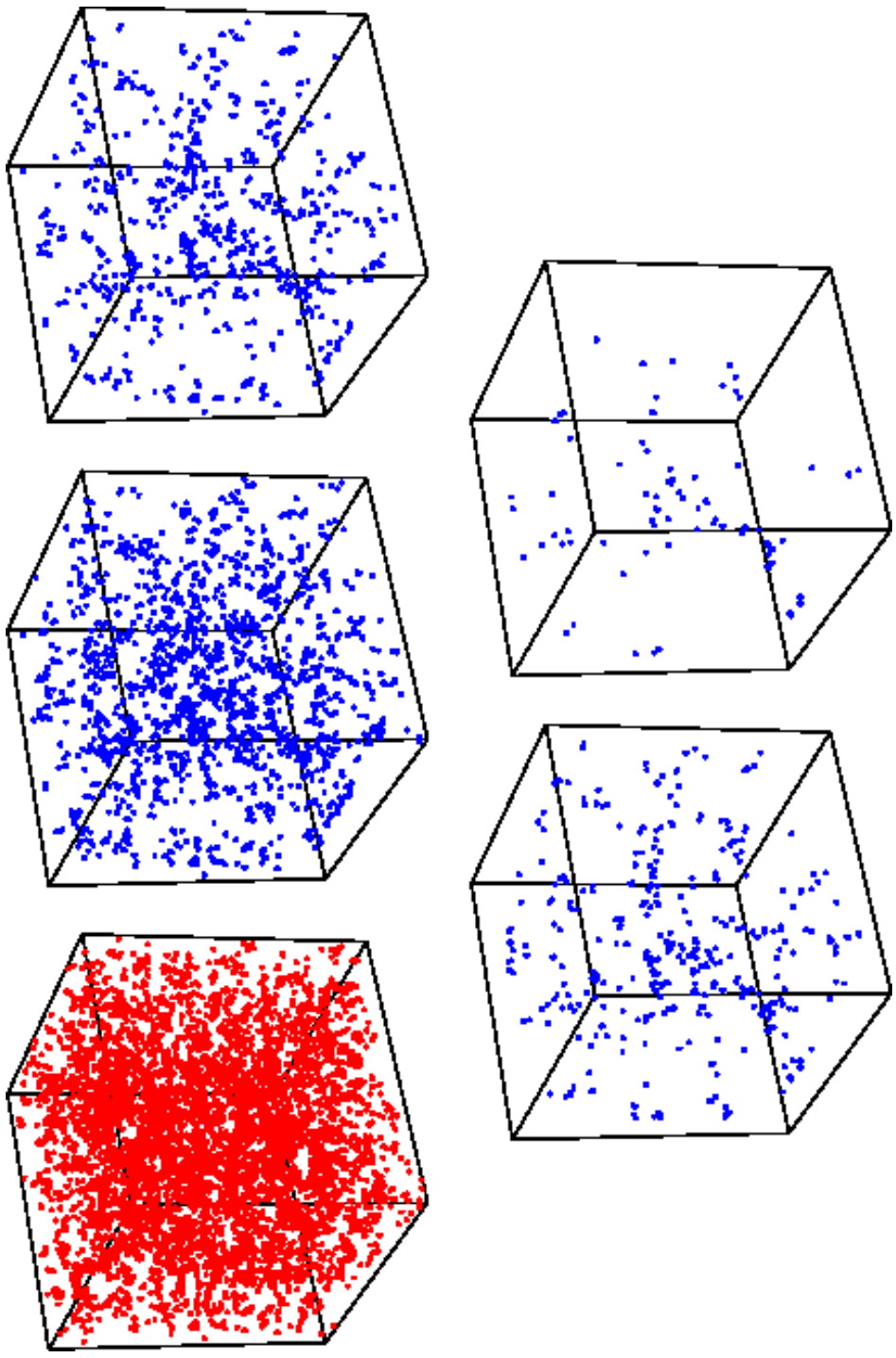

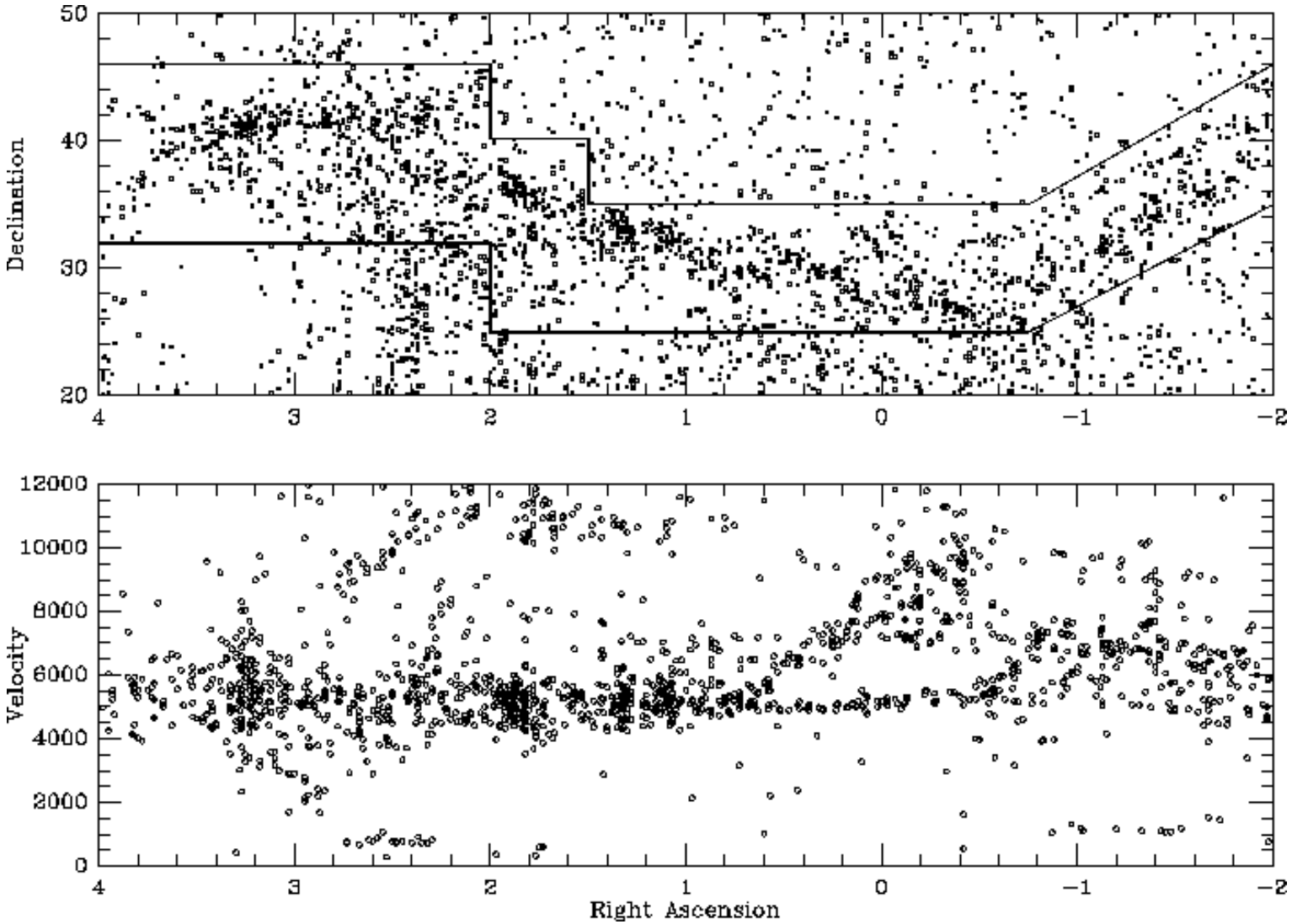
Declination
50
40
30
20
4
3
2
1
0
−1
−2
Velocity
12000
10000
8000
6000
4000
2000
0
Right Ascension

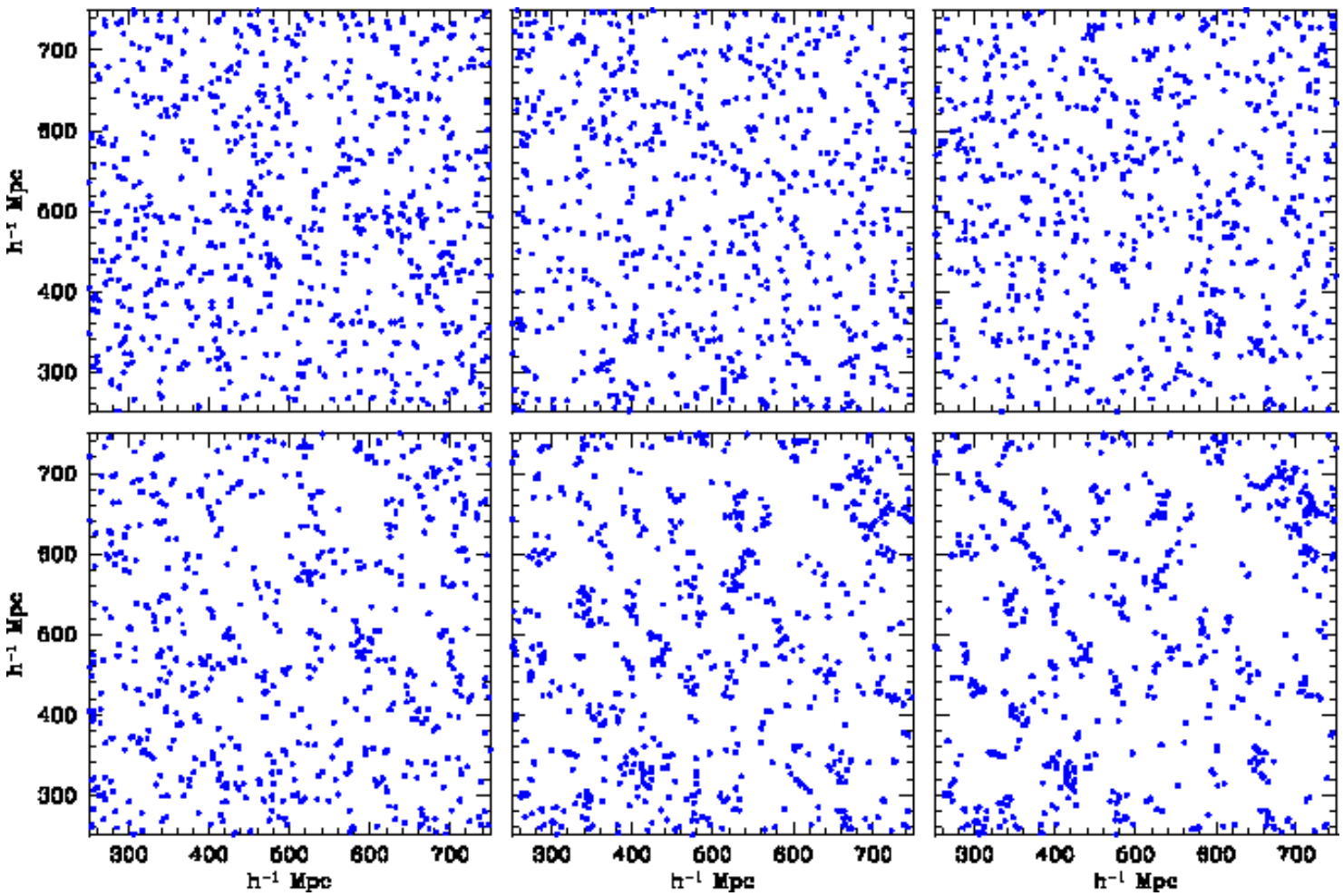
700
600
500
400
300
h⁻¹ Mpc
300
400
500
600
700
h⁻¹ Mpc

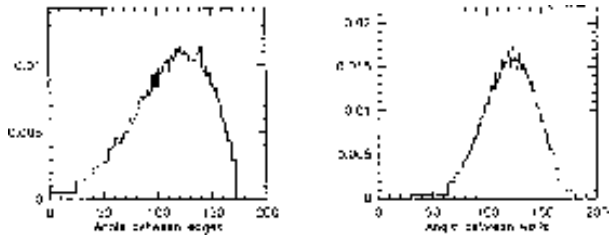
0.02
0.015
0.01
0.005
0
0
50
100
150
200
Angle between edges
0.02
0.015
0.01
0.005
0
0
50
100
150
200
Angle between edges

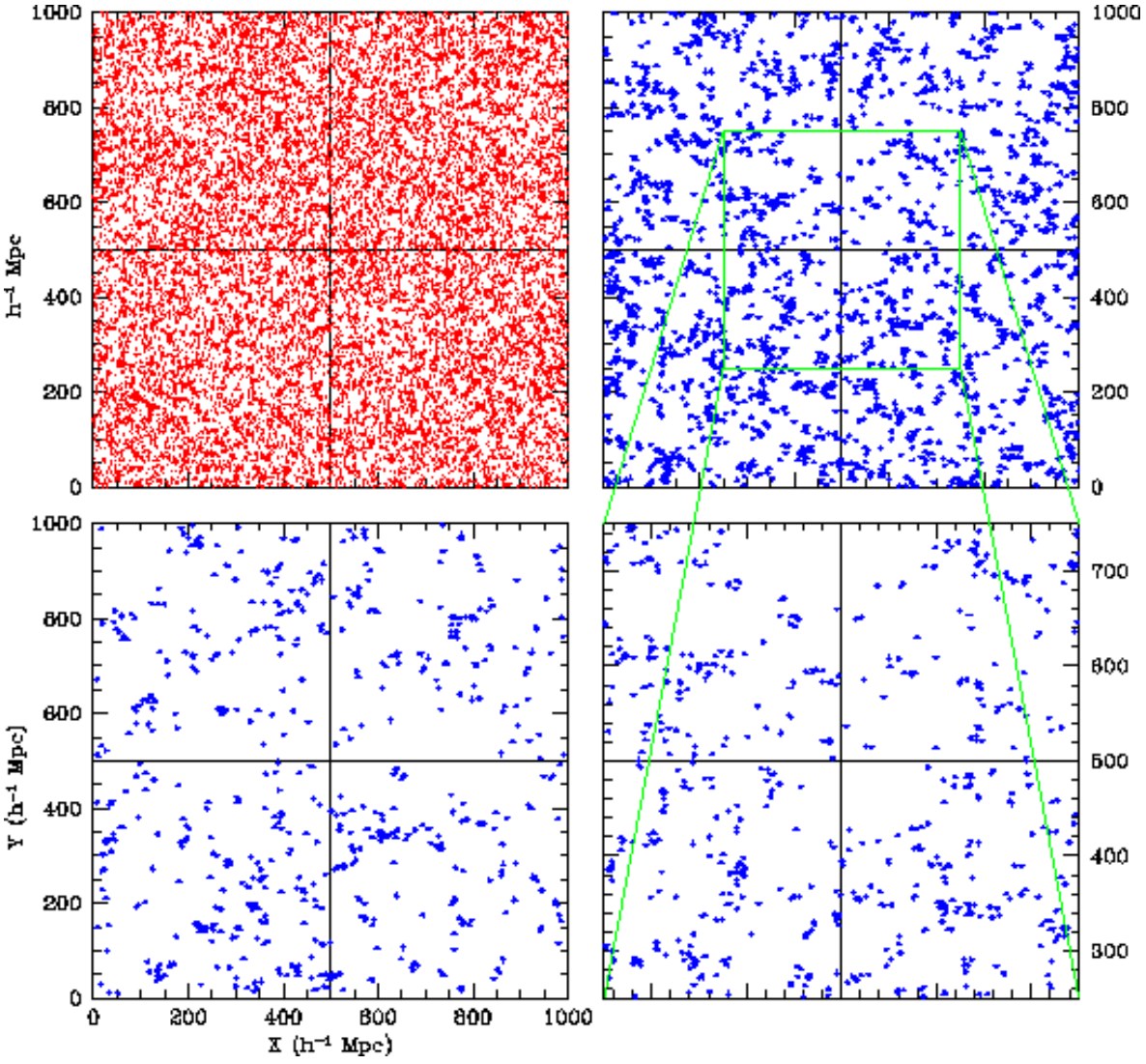
1000
800
600
400
200
0
h⁻¹ Mpc
1000
800
600
400
200
0
1000
800
600
400
200
0
Y (h⁻¹ Mpc)
0
200
400
600
800
1000
X (h⁻¹ Mpc)
1000
800
600
500
400
300

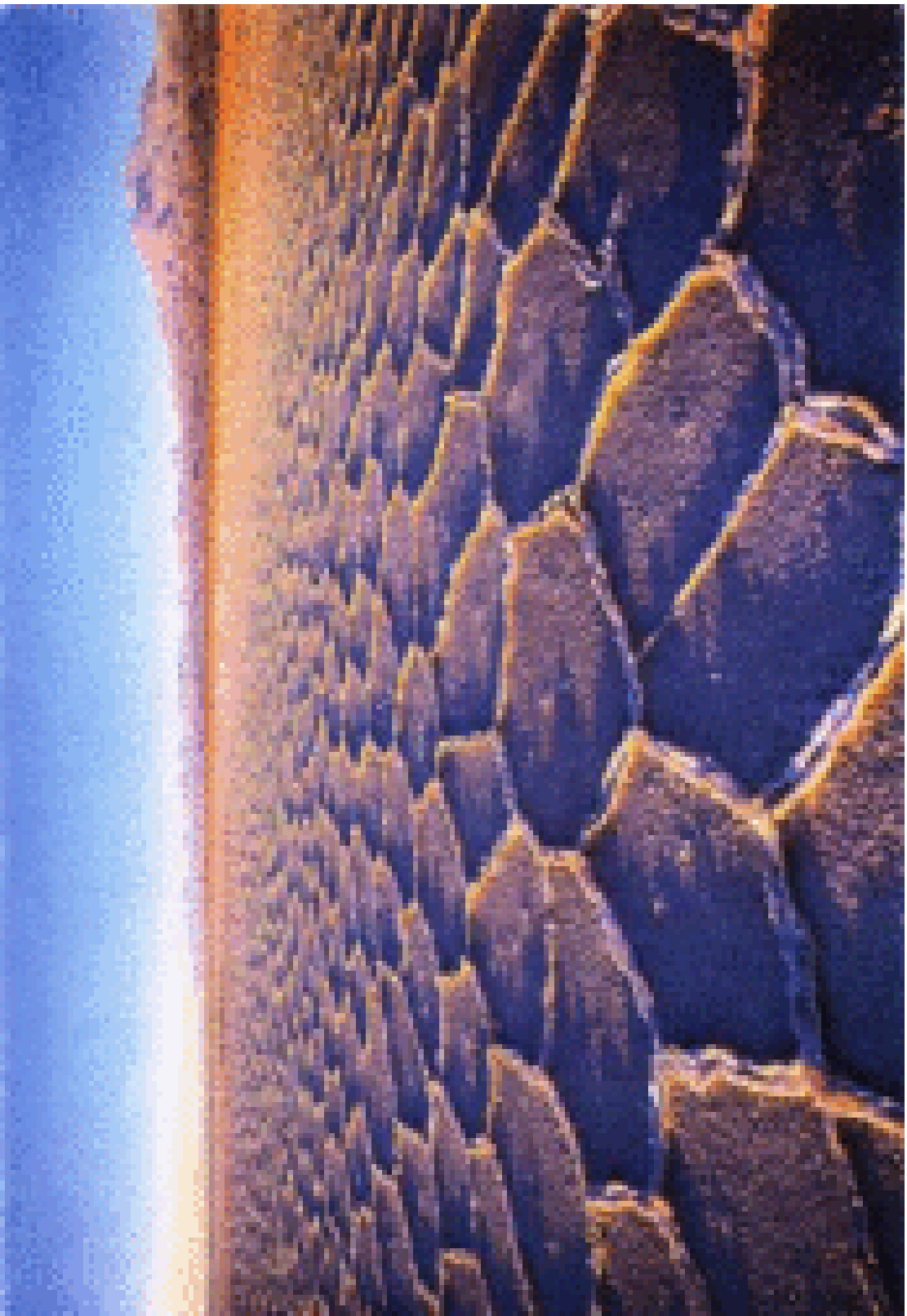

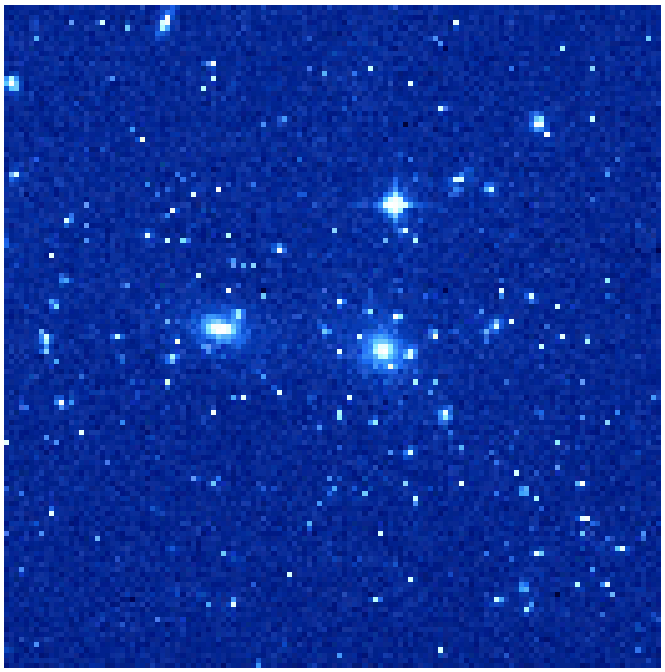

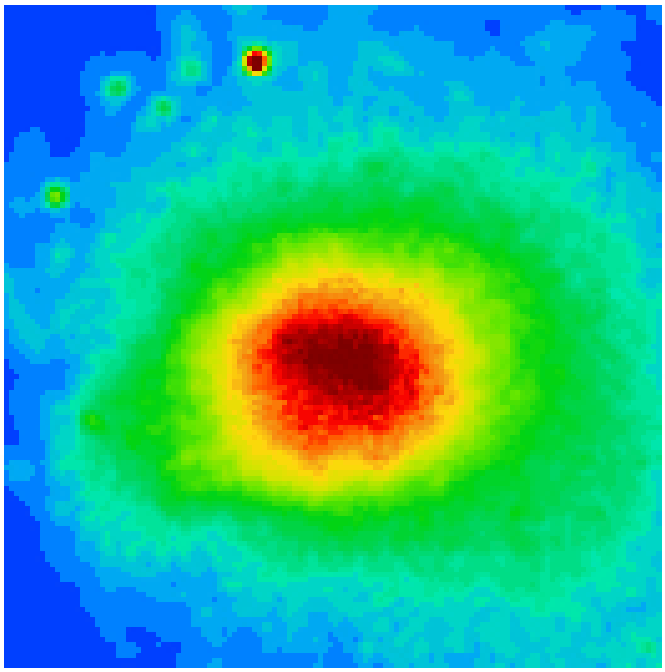

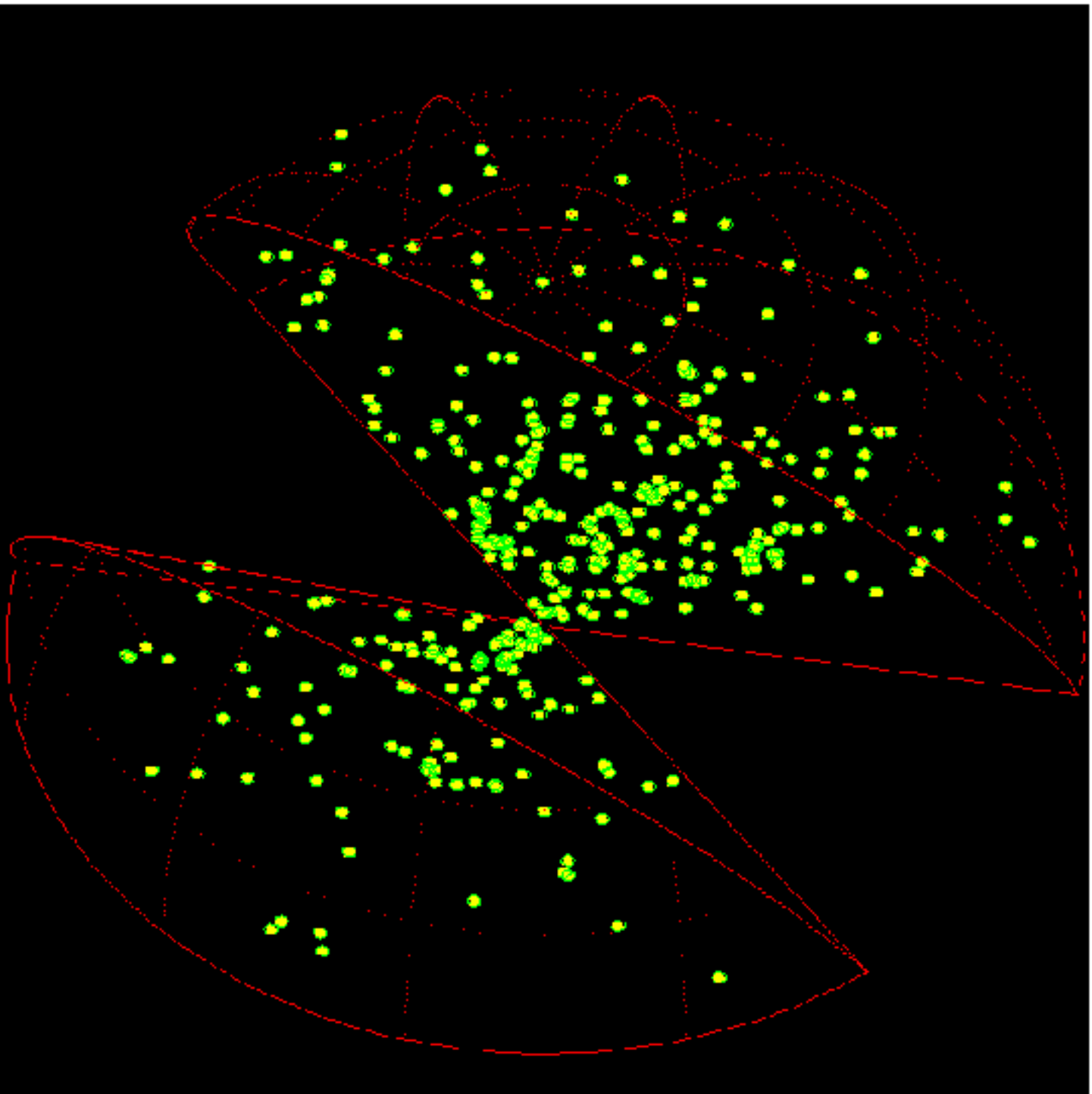

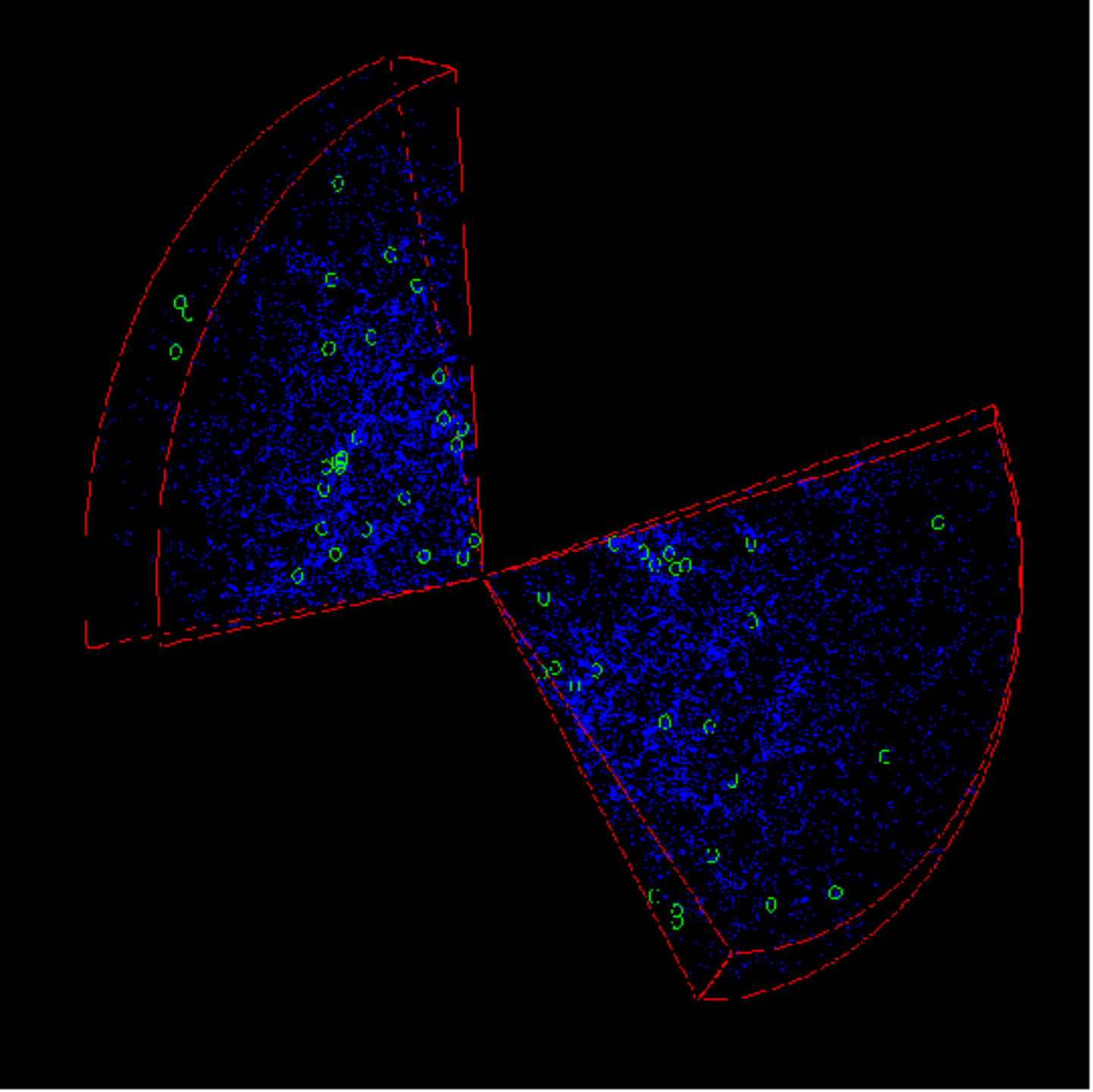

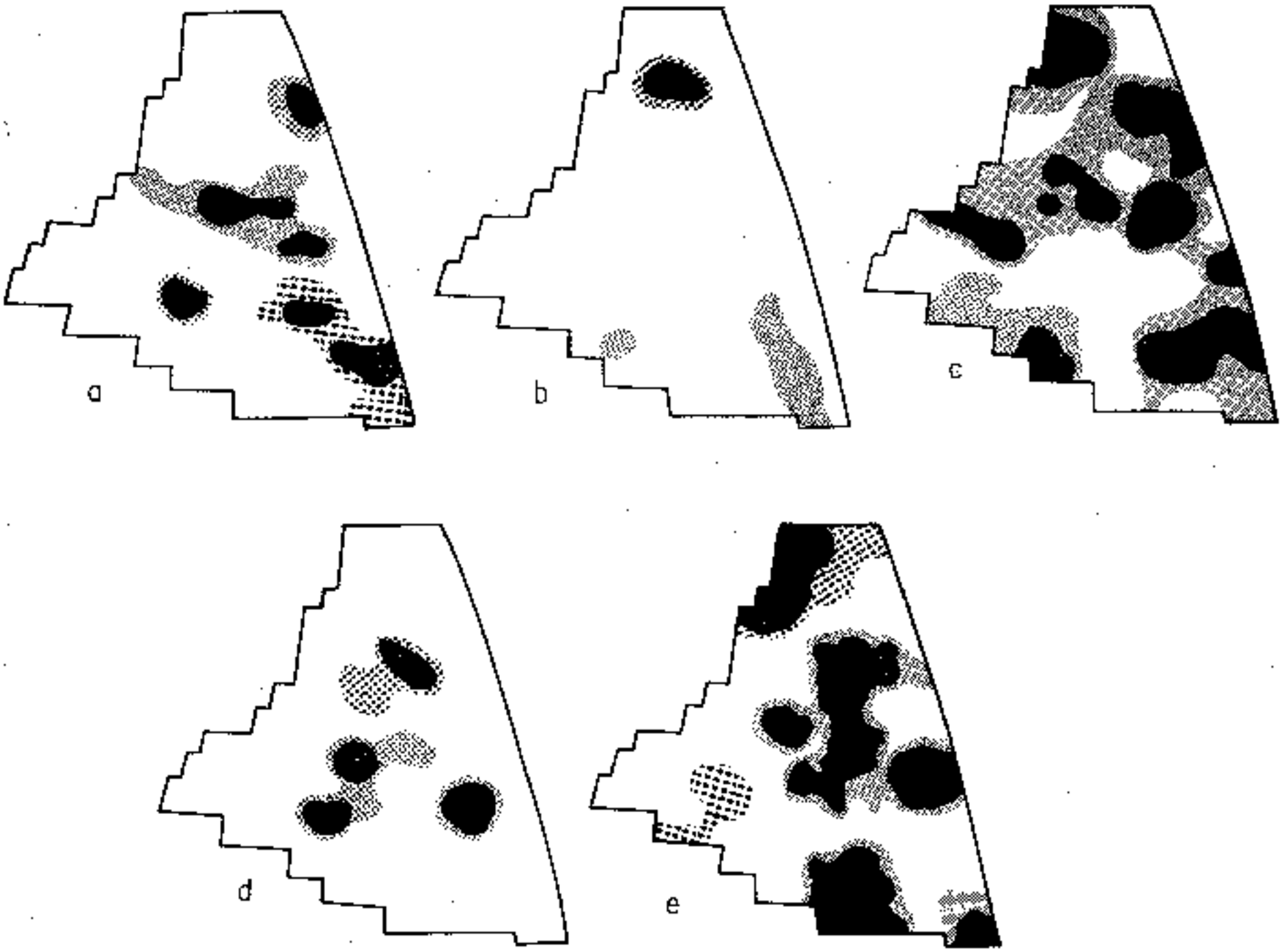
a
b
c
d
e